

**EUR 2842.e**

EUROPEAN ATOMIC ENERGY COMMUNITY - EURATOM

ON THE HYDRAULIC CHARACTERISTICS  
OF A BOILING WATER CHANNEL WITH  
NATURAL CIRCULATION

by

C.L. SPIGT  
(Technological University of Eindhoven)

1966



EURATOM/US Agreement for Cooperation

EURAEK Report No. 1644 prepared by the Technological University of  
Eindhoven - Netherlands

EURATOM Contract No. 030-64-1 TEEN

## LEGAL NOTICE

This document was prepared under the sponsorship of the Commission of the European Atomic Energy Community (Euratom) in pursuance of the joint programme laid down by the Agreement for Cooperation signed on 8 November 1958 between the Government of the United States of America and the European Atomic Energy Community.

It is specified that neither the Euratom Commission, nor the Government of the United States, their contractors or any person acting on their behalf :

Make any warranty or representation, express or implied, with respect to the accuracy, completeness, or usefulness of the information contained in this document, or that the use of any information, apparatus, method, or process disclosed in this document may not infringe privately owned rights; or

Assume any liability with respect to the use of, or for damages resulting from the use of any information, apparatus, method or process disclosed in this document.

This report is on sale at the addresses listed on cover page 4

|                          |          |          |           |           |
|--------------------------|----------|----------|-----------|-----------|
| at the price of FF 19,50 | FB 195,— | DM 15,60 | Lit. 2430 | Fl. 14,30 |
|--------------------------|----------|----------|-----------|-----------|

**When ordering, please quote the EUR number and the title, which are indicated on the cover of each report.**

Printed by Guyot, s.a.  
Brussels, October 1966

This document was reproduced on the basis of the best available copy.

## **EUR 2842.e**

ON THE HYDRAULIC CHARACTERISTICS OF A BOILING WATER CHANNEL WITH NATURAL CIRCULATION  
by C.L. SPIGT (Technological University of Eindhoven)

European Atomic Energy Community - EURATOM  
EURATOM/US Agreement for Cooperation  
EURAEK Report No. 1644 prepared by the Technological University of Eindhoven (Netherlands)  
Euratom Contract No. 030-64-I TEEN  
Brussels, October 1966 - 150 Pages - 71 Figures - FB 195

In this publication the results of an experimental and theoretical study are reported on the hydraulic characteristics of a single coolant channel of simple annular geometry in a boiling water nuclear reactor, with the main emphasis on the stability characteristics of the flow process in such a channel.

The experimental part has been restricted to the operation under conditions of natural circulation. Most attention has been paid to :

## **EUR 2842.e**

ON THE HYDRAULIC CHARACTERISTICS OF A BOILING WATER CHANNEL WITH NATURAL CIRCULATION  
by C.L. SPIGT (Technological University of Eindhoven)

European Atomic Energy Community - EURATOM  
EURATOM/US Agreement for Cooperation  
EURAEK Report No. 1644 prepared by the Technological University of Eindhoven (Netherlands)  
Euratom Contract No. 030-64-I TEEN  
Brussels, October 1966 - 150 Pages - 71 Figures - FB 195

In this publication the results of an experimental and theoretical study are reported on the hydraulic characteristics of a single coolant channel of simple annular geometry in a boiling water nuclear reactor, with the main emphasis on the stability characteristics of the flow process in such a channel.

The experimental part has been restricted to the operation under conditions of natural circulation. Most attention has been paid to :

## **EUR 2842.e**

ON THE HYDRAULIC CHARACTERISTICS OF A BOILING WATER CHANNEL WITH NATURAL CIRCULATION  
by C.L. SPIGT (Technological University of Eindhoven)

European Atomic Energy Community - EURATOM  
EURATOM/US Agreement for Cooperation  
EURAEK Report No. 1644 prepared by the Technological University of Eindhoven (Netherlands)  
Euratom Contract No. 030-64-I TEEN  
Brussels, October 1966 - 150 Pages - 71 Figures - FB 195

In this publication the results of an experimental and theoretical study are reported on the hydraulic characteristics of a single coolant channel of simple annular geometry in a boiling water nuclear reactor, with the main emphasis on the stability characteristics of the flow process in such a channel.

The experimental part has been restricted to the operation under conditions of natural circulation. Most attention has been paid to :

- a. the determination of the liquid flow rate at the inlet and the void and pressure distribution along the height of the coolant channel under steady-state conditions;
  - b. the occurrence and characterization of spontaneous flow instabilities; the analysis of the boiling noise in terms of spectral power density and autocorrelation has been used in determining the onset of those instabilities;
  - c. the determination of the stability characteristics of a steady state by means of frequency response analysis. Autocorrelation, cross-correlation and noise rejection techniques have been used to characterize the severe flow oscillations and to express the stability of the steady state in terms of transfer functions.
- 

- a. the determination of the liquid flow rate at the inlet and the void and pressure distribution along the height of the coolant channel under steady-state conditions;
  - b. the occurrence and characterization of spontaneous flow instabilities; the analysis of the boiling noise in terms of spectral power density and autocorrelation has been used in determining the onset of those instabilities;
  - c. the determination of the stability characteristics of a steady state by means of frequency response analysis. Autocorrelation, cross-correlation and noise rejection techniques have been used to characterize the severe flow oscillations and to express the stability of the steady state in terms of transfer functions.
- 

- a. the determination of the liquid flow rate at the inlet and the void and pressure distribution along the height of the coolant channel under steady-state conditions;
- b. the occurrence and characterization of spontaneous flow instabilities; the analysis of the boiling noise in terms of spectral power density and autocorrelation has been used in determining the onset of those instabilities;
- c. the determination of the stability characteristics of a steady state by means of frequency response analysis. Autocorrelation, cross-correlation and noise rejection techniques have been used to characterize the severe flow oscillations and to express the stability of the steady state in terms of transfer functions.

# EUR 2842.e

EUROPEAN ATOMIC ENERGY COMMUNITY - EURATOM

## ON THE HYDRAULIC CHARACTERISTICS OF A BOILING WATER CHANNEL WITH NATURAL CIRCULATION

by

C.L. SPIGT

(Technological University of Eindhoven)

1966



EURATOM/US Agreement for Cooperation

EURAEK Report No. 1644 prepared by the Technological University of  
Eindhoven - Netherlands

EURATOM Contract No. 030-64-1 TEEN

## SUMMARY

In this publication the results of an experimental and theoretical study are reported on the hydraulic characteristics of a single coolant channel of simple annular geometry in a boiling water nuclear reactor, with the main emphasis on the stability characteristics of the flow process in such a channel.

The experimental part has been restricted to the operation under conditions of natural circulation. Most attention has been paid to :

- a. the determination of the liquid flow rate at the inlet and the void and pressure distribution along the height of the coolant channel under steady-state conditions;
- b. the occurrence and characterization of spontaneous flow instabilities; the analysis of the boiling noise in terms of spectral power density and autocorrelation has been used in determining the onset of those instabilities;
- c. the determination of the stability characteristics of a steady state by means of frequency response analysis. Autocorrelation, cross-correlation and noise rejection techniques have been used to characterize the severe flow oscillations and to express the stability of the steady state in terms of transfer functions.

## Summary

In this publication the results of an experimental and theoretical study are reported on the hydraulic characteristics of a single coolant channel of simple annular geometry in a boiling water nuclear reactor, with the main emphasis on the stability characteristics of the flow process in such a channel.

The experimental part has been restricted to the operation under conditions of natural circulation. Most attention has been paid to:

- a. the determination of the liquid flow rate at the inlet and the void and pressure distribution along the height of the coolant channel under steady-state conditions;
- b. the occurrence and characterization of spontaneous flow instabilities;
- c. the determination of the stability characteristics of a steady state by means of a frequency response analysis.

The range of independent variables was: pressures of 2.03 - 30.7 ata (30-450 lbs/in<sup>2</sup>), channel powers of 10-465 kW, subcooling temperatures of 0-43°C and a hydraulic diameter of 16.16 and 25.03 mm. The range of dependent variables was: inlet velocities of 0-1.4 m/sec, exit qualities of 0-25% and uniform heat fluxes of 0-180 W/cm<sup>2</sup>.

The publication starts with a description of the pressurized and atmospheric boiling water loops, the two test sections and the power supply. After that, a review is given of the measuring, recording and analyzing equipment. Special attention has been paid to the measurement of the void fraction in a two-phase system under steady as well as under transient conditions. The results obtained by the two methods used, e.g. the  $\gamma$ -ray attenuation method and the impedance method, are compared and good agreement is reported.

In the description of the analyzing equipment attention has been paid to the noise-analysis technique. The analysis of the boiling noise in terms of spectral power density and autocorrelation has been used in determining the onset of hydraulic instabilities. Autocorrelation, cross-correlation and noise rejection techniques have been used to characterize the severe flow oscillations and to express the stability of the steady state in terms of transfer functions. In the analysis of the signals use has been made of digital as well as analogue computers.

In the presentation of the results obtained in steady states, the influence of channel power, system pressure, subcooling and hydraulic diameter is shown on the recirculation flow rate, the exit void fraction and longitudinal void and pressure distribution. An analysis was made in terms of the Slip Ratio,  $S$ , and the Two-Phase Friction Multiplier,  $R$ . The void fraction and the two-phase friction loss data have been plotted as a function of the Martinelli and Nelson correlator. Besides, the void fraction data were plotted in the "weighted mean velocity-average volumetric flux density" plane proposed by Zuber and Findlay. From this plot it may be deduced that flat profiles for the velocity or concentration distribution are present under the operating conditions reported.

During operation, it was possible to distinguish between three types of flow oscillations with frequencies of roughly .03, 1 and 15 c.p.s. Systematic research has been carried out as regards the 1 c.p.s. flow oscillations only. After accepting a criterion for de-

fining the onset of the hydraulic oscillations, the influence of system pressure, subcooling and hydraulic diameter on the instability threshold channel power has been systematically examined. It has been found that the effect of increased subcooling upon the onset of severe hydraulic oscillations at low subcooling rates was opposite to that at high subcooling rates. The character of these oscillations has been studied by making recordings during hydraulic oscillations of the relevant physical quantities, such as, for instance, the void fraction along the height, the inlet mass flow, etc.

Results of transfer function measurements from channel power to inlet mass flow and local void fraction are presented. Characteristic for all these transfer functions was the occurrence of a sharp resonance peak when the instability threshold was approached. It is shown that there exists a relationship between the character of the transfer function and the onset of spontaneous flow oscillations. The influence upon the two of the operating conditions is similar.

Burn-out channel powers and heat fluxes are presented for various values of system pressure and subcooling. Nearly all the burn-outs were obtained under unstable flow conditions.

The general equations are derived describing the performance characteristics of a boiling system under steady-state and non-steady state conditions. Special attention has been paid to the formulation of the boundary conditions and the introduction of pressure effects into the equations. The significant differences of the approach as compared with the theoretical models of others are indicated. The dynamic equations were linearized by assuming small disturbances from the steady state. Furthermore, by applying an open-loop analysis, stability criteria were derived for detecting the onset of flow oscillations in natural as well as forced circulation boiling systems. The equations were numerically integrated by means of a digital computer.

Preliminary results of calculations have been reported for the operating and geometry conditions as considered in the experimental program. Fairly good agreement was obtained between theoretically and experimentally obtained quantities of the steady-state performance, the instability threshold power and the character of the hydraulic oscillations.



## Contents

|  |     |
|--|-----|
| Summary  | 1   |
| List of tables and figures                                 | 5   |
| Nomenclature   | 8   |
| 1. Introduction  | 13  |
| 1.1. Aim and scope   | 13  |
| 1.2. Survey of recent work                                 | 16  |
| 2. Description of the apparatus                            | 23  |
| 2.1. Loops and test sections                               | 23  |
| 2.2. Power supply  | 29  |
| 2.3. Measuring equipment                                   | 29  |
| 2.4. Recording equipment                                   | 46  |
| 2.5. Analyzing equipment                                   | 47  |
| 3. Experimental results                                    | 53  |
| 3.1. Introduction  | 53  |
| 3.2. Steady-state quantities                               | 54  |
| 3.2.1. Experimental procedure                              | 54  |
| 3.2.2. Results   | 55  |
| 3.3. Hydraulic oscillations                                | 65  |
| 3.3.1. Signal observations                                 | 65  |
| 3.3.2. The onset of hydraulic oscillations                 | 69  |
| 3.3.3. Characterization of the hydraulic oscillations      | 75  |
| 3.4. Stability measurements                                | 81  |
| 3.4.1. Power modulation experiments                        | 81  |
| 3.4.2. Boiling noise correlation studies                   | 90  |
| 3.5. Influence of the water level                          | 93  |
| 4. Analysis of the experimental results                    | 95  |
| 4.1. The slip between the two phases                       | 95  |
| 4.2. Two-phase pressure losses                             | 102 |
| 4.3. Stability characteristics of a two-phase flow         | 105 |
| 4.4. Burn-out  | 109 |
| 5. Theoretical studies                                     | 113 |
| 5.1. Introduction  | 113 |
| 5.2. Basic equations                                       | 113 |
| 5.3. Simplified equations and boundary conditions          | 118 |
| 5.3.1. Simplified equations                                | 118 |
| 5.3.2. Boundary conditions                                 | 122 |
| 5.4. Studies of Jahnberg and Currin                        | 124 |
| 5.5. Linearization of the equations and solution procedure | 127 |
| 5.6. Stability criteria                                    | 129 |
| 5.7. Results of calculations with the linearized equations | 132 |

6. Conclusions

151

References

153

## List of tables and figures

### Tables

- 2.1. Geometrical data of the test sections.
- 2.2. Location of the sensors.
- 3.1. Physical data.
- 3.2. Conditions at instability threshold and burn-out.
- 3.3. Transfer function for various modulation amplitudes, Test Section II.

### Figures

- 1.1 Feedback paths in a nuclear boiling water reactor.
- 2.1 Pressurized boiling water loop.
- 2.2 Electronic instrumentation.
- 2.3 Flow sheet of the pressurized boiling water loop.
- 2.4 Schematic of the test section with instrumentation.
- 2.5 Capacitive pressure gauge.
- 2.6 Diagram of the scintillation counter.
- 2.7 Scintillation crystal-photomultiplier tube assembly.
- 2.8 Block diagram of the  $\gamma$ -ray attenuation technique.
- 2.9 Preliminary results of the  $\gamma$ -ray void fraction measurements.
- 2.10 Impedance void gauge.
- 2.11 Comparison of  $\gamma$ -ray and impedance void fraction measurements.
- 2.12 Block diagram of the impedance method.
- 2.13 Results of flow calibration tests.
- 2.14 Preliminary results of circulation rate measurements.
- 2.15 Frequency response of the differential pressure gauge.
- 2.16 Block diagram of the Frequency Response Analyzer.
- 2.17 Block diagram of the Noise Correlator.
- 3.1 The circulation rate as a function of channel power for various system pressures, Test Section I.
- 3.2 The circulation rate as a function of system pressure for three channel powers.
- 3.3 The circulation rate as a function of channel power for various subcoolings, Test Section I.
- 3.4 The circulation rate as a function of channel power for various system pressures and subcoolings, Test Section II.
- 3.5 The exit void fraction as a function of channel power for various system pressures, Test Section I.
- 3.6 The exit void fraction as a function of channel power for various subcoolings, Test Section I.
- 3.7 The exit void fraction as a function of channel power for various system pressures and subcoolings, Test Section II.
- 3.8 The longitudinal void fraction distribution for various channel powers, Test Section I.

- 3.9 The longitudinal void fraction distribution for various system pressures, Test Section I.
- 3.10 The longitudinal void fraction distribution for various subcoolings, Test Section I.
- 3.11 The longitudinal void fraction distribution for Test Section I and II.
- 3.12 The apparent longitudinal pressure distribution for various channel powers, Test Section I.
- 3.13 The apparent longitudinal pressure distribution for two system pressures and subcoolings, Test Section I.
- 3.14 Recordings of the signal from the pitot-tube.
- 3.15 Recordings of the signals from the absolute pressure gauge and the pitot-tube at high pressure for Test Section I and II.
- 3.16 High frequency void fluctuations, Test Section I.
- 3.17 Autocorrelations and spectral power densities of the  $\Delta p$  inlet signal.
- 3.18 The influence of system pressure on the onset of hydraulic instabilities, Test Section I and II.
- 3.19 The influence of subcooling on the onset of hydraulic instabilities, Test Section I and II.
- 3.20 Recordings of the signals from the various void gauges and the pitot-tube, Test Section I.
- 3.21 Photograph of hydraulic instabilities.
- 3.22 Recordings of the signals from various physical quantities, Test Section II.
- 3.23 Influence of subcooling on the hydraulic instabilities, Test Section I.
- 3.24 Variations in subcooling-temperature during hydraulic instabilities, Test Section I.
- 3.25 Transfer functions from channel power to inlet mass flow for various channel powers, Test Section I.
- 3.26 Transfer functions from channel power to local void fraction for various channel powers and system pressures, Test Section I.
- 3.27 Transfer functions from channel power to inlet mass flow at various subcoolings, Test Section I.
- 3.28 Transfer functions from channel power to the void fraction at different locations, Test Section I.
- 3.29 Transfer functions from channel power to inlet mass flow for various channel powers, Test Section II.
- 3.30 Results of the analysis of the inherent noise, Test Section II.
- 3.31 Influence of the water level on the steady-state performance, Test Section I.
- 4.1 Void fraction data plotted according to Martinelli-Nelson (M3) for three system pressures, Test Section I.
- 4.2 Void fraction data plotted according to Martinelli-Nelson (M3) for three subcooling temperatures, Test Section II.
- 4.3 Void fraction data plotted according to Zuber and Findlay (Z1) for three system pressures, Test Section I.
- 4.4 Void fraction data plotted according to Zuber and Findlay (Z1) for three subcooling temperatures, Test Section II.
- 4.5 Two-phase friction loss data plotted according to Martinelli-Nelson (M3) for two system pressures, Test Section II.
- 4.6 Ledinegg instability.
- 4.7 Heat fluxes at burn-out and instability threshold as functions of saturation temperature, Test Section I and II.

- 4.8 Heat fluxes at burn-out and instability threshold as functions of subcooling temperature, Test Section I and II.
- 5.1 Ringshaped volume-element.
- 5.2 Steady-state results calculated by a theoretical study based on "first principles" (V4).
- 5.3 Transient results calculated by the study of Jahnberg (J2), Test Section I.
- 5.4 Natural circulation boiler.
- 5.5 Block diagram of natural circulation boiler.
- 5.6 Forced circulation boiler.
- 5.7 Block diagram of forced circulation boiler.
- 5.8 Calculated and measured results of the steady-state characteristics, Test Section I.
- 5.9 Open and closed-loop transfer functions in the intermediate frequency range, Test Section I.
- 5.10 Open-loop transfer functions in the low and high frequency range, Test Section I.
- 5.11 Calculated longitudinal distributions, .0006 c.p.s., Test Section I.
- 5.12 Calculated longitudinal distributions, .121 c.p.s., Test Section I.
- 5.13 Calculated longitudinal distributions, .947 c.p.s., Test Section I.
- 5.14 Calculated longitudinal distributions, 11.82 c.p.s., Test Section I.

## Nomenclature

|                         |  |                   |
|-------------------------|--|-------------------|
| A                       | cross-section, area  | $L^2$             |
| a                       | constant in Eq. (4.13.)  | $Lt^{-1}$         |
| A, B                    | integrals Eqs (2.9.) and (2.10.)                                       |                   |
| b                       | exponent, Eq. (5.31.)  | diml              |
| $b_v, b_d$              | condenser and subcooler constants Eq (5.42.)                           | $L^{-1}t$         |
| $b_q, b_c$              |  | $T^{-1}$          |
| C                       | correction factor in $\gamma$ -ray attenuation method, section 2.3.d   | diml              |
| $C_K$                   | velocity of kinematic waves, Eq. (1.1.)                                | $Lt^{-1}$         |
| $C_o$                   | slope of line, Fig. 4.3  | diml              |
| $C_1$ to $C_4, C_{i,5}$ | coefficients in Eq. (5.35.)  |                   |
| c                       | heat capacity of liquid at constant pressure per unit mass             | $L^2t^{-2}T^{-1}$ |
| D                       | diffusion coefficient  | $L^2t^{-1}$       |
| $D_h$                   | hydraulic diameter   | L                 |
| d                       | constant in Eq. (5.31.)  | diml              |
| $E_1, E_2, E_3$         | functions of time, Eq. (5.29.)   | diml              |
| e                       | latent heat of evaporation at constant volume                          | $L^2t^{-2}$       |
| $e_p$                   | latent heat of evaporation at constant pressure                        | $L^2t^{-2}$       |
| F                       | wall-friction force, per unit cross-sectional area, per unit length    | $ML^{-2}t^{-2}$   |
| $F_1$                   | constant in Eq. (5.41.)  |                   |
| f                       | function, e.g. Eq. (5.10.)   |                   |
|                         | Fanning friction factor  | diml              |
|                         | frequency  | $t^{-1}$          |
| $G_1, G_2$              | open-loop transfer functions, Eq. (5.37.)                              |                   |
| g                       | gravitational acceleration   | $Lt^{-2}$         |
| H                       | transfer function, e.g. Fig. 3.25                                      |                   |
|                         | enthalpy, Table 3.1  | $L^2t^{-2}$       |
| $H_d, H_t$              | distances, Fig. 5.4  | L                 |
| h                       | total energy, Eqs (5.7.) and (5.8.)                                    | $L^2t^{-2}$       |
| I                       | intensity of gamma rays  | $t^{-1}$          |
| j                       | complex variable   | diml              |
| K                       | amplitude ratio, e.g. Fig. 3.25  | diml              |
|                         | constant in Eq. (4.11.)  | diml              |
| k                       | differential pressure coefficient, Eq. (2.7.)                          | diml              |
|                         | pressure loss coefficient, Eq. (5.25.)                                 | diml              |
| $kD_h$                  | distance between shroud and window, Eq. (2.2.)                         | L                 |
| L                       | length of heating element (= 2.4 m)                                    | L                 |
| $L_d$                   | equivalent length of downcomer $(\leftarrow \sum A_c \frac{L_k}{A_k})$ | L                 |
| $L_t$                   | total length of riser, Fig. 5.4  | L                 |
| M                       | mass flow, mass  | $ML^{-3}; M$      |

|                  |  |                 |
|------------------|--|-----------------|
| m                | whole number   | diml            |
| N                | number density of bubbles, function of bubble radius   | $L^{-4}$        |
| n                | number or exponent, Eq. (4.9.)<br>function of time, e.g. Eq. (2.8.)  | diml            |
| P                | momentum flow, Eq. (4.16.)<br>indication of pressure tapping location, e.g. Table 2.2.   | $ML^{-1}t^{-2}$ |
| p                | local pressure   | diml            |
| $p_{abs}$        | system pressure  | $ML^{-1}t^{-2}$ |
| Q                | heat input or heat removal   | $ML^{-1}t^{-2}$ |
| q                | heat flux, heat input per unit of heated surface   | $ML^2t^{-3}$    |
| $q_w$            | heat input per unit cross-sectional area, per unit length  | $Mt^{-3}$       |
| R                | Two-Phase Friction Multiplier, Eq. (4.20.)<br>bubble radius, section 5.2.<br>electrical resistance, Fig. 2.12, of heating element<br>Fig. 3.22 | $ML^{-1}t^{-3}$ |
| Re               | Reynolds number  | diml            |
| r                | radial coordinate  | L               |
|                  | radius   | L               |
| $S, S_a, S_b$    | slip ratio, Eq. (5.23.)  | diml            |
| $S_c$            | temperature correlator, Eq. (5.23.)  | diml            |
| s                | constant in Eq. (5.30.)  | diml            |
| T                | temperature  | T               |
| $T_b$            | liquid temperature at which bubbles detach from<br>the wall  | T               |
| $T_{in}$         | temperature of the liquid at the channel inlet ( $=T_{1,in}$ )   | T               |
| $T_{sat}$        | saturation temperature corresponding with $p_{abs}$  | T               |
| $\Delta T_{sub}$ | subcooling temperature ( $=T_{sat} - T_{in}$ )   | T               |
| t                | time   | t               |
| U                | volume   | $L^3$           |
| u                | heat input by conduction, Eq. (5.5.)   | $Mt^{-3}$       |
| V                | velocity<br>indication of location of void fraction sensors,<br>e.g. Table 2.2.  | $Lt^{-1}$       |
|                  | liquid velocity at channel inlet ( $=V_{1,in}$ )   | diml            |
| $V_r$            | drift velocity ( $=V_s - W_m$ )  | $Lt^{-1}$       |
| W                | volumetric flow per unit cross-sectional area  | $Lt^{-1}$       |
| X                | Lockhart-Martinelli correlator   | diml            |
| $X_{tt}$         | Martinelli-Nelson correlator   | diml            |
| Z                | number of desintegrations per second   | $t^{-1}$        |
| $x, y, z, x_1$   | functions of time, e.g. Eqs (2.5.) and (2.16.)   |                 |
| $x_0$            | amplitude of sine, see section 2.5.  |                 |
| x                | steam quality ( $= M_g / M_t$ )  | diml            |
| z                | coordinate in axial direction  | L               |

#### Greek symbols

|            |  |                 |
|------------|--|-----------------|
| $\alpha$   | void fraction  | diml            |
| $\beta$    | part of heat input removed in condenser, Eq. (5.29.) | diml            |
| $\epsilon$ | conductance, Eq. (2.6.)                              |                 |
| $\eta$     | dynamic viscosity                                    | $ML^{-1}t^{-1}$ |

|   |   |                  |
|---|---|------------------|
| $\kappa$  | heat division parameter of Bowring (in(B11) $\kappa = \epsilon$ ) | diml             |
| $\lambda$   | heat conduction coefficient                                       | $MLt^{-3}T^{-1}$ |
| $\mu$   | absorption coefficient  | $L^{-1}$         |
| $\pi$   | 3.14159   | diml             |
| $\rho$  | density   | $ML^{-3}$        |
| $\sigma$  | part of condenser occupied by steam, Fig. 5.4                     | diml             |
| $\sigma, \sigma_z, \sigma_{x_i}$  | standard deviation, of z, $x_i$ Eq. (2.5.)                        |                  |
| $\tau$  | time displacement   | t                |
|   | shear stress  | $ML^{-1}t^{-2}$  |
| $\Phi, \Phi_{xx}, \Phi_{yy}, \left. \begin{array}{l} \Phi_{nn} \\ \Phi_{xy} \end{array} \right\}$ | spectral power density, of x, y, n                                |                  |
| $\Phi_{nn}$   |   |                  |
| $\Phi_{xy}$   | cross-power spectral density of x and y                           |                  |
| $\varphi$   | phase angle   |                  |
| $\varphi, \varphi_{xx}, \varphi_{yy}, \varphi_{nn}$   | autocorrelation, of x, y, n                                       |                  |
| $\varphi_n$   | normalized autocorrelation, Eq. 3.4                               | diml             |
| $\varphi_{xy}$  | cross-correlation of x and y                                      |                  |
| $\Phi_{1,tt}$   | Two-Phase Friction Multiplier, Eq. 4.21.                          | diml             |
| $\omega$  | angular velocity  | $t^{-1}$         |

### Subscripts

|            |  |
|------------|--|
| a          | acceleration   |
| b.o.       | burn-out   |
| c          | coolant channel  |
| con        | condenser  |
| d          | downcomer  |
| di         | downcomer inlet  |
| do         | downcomer outlet   |
| e          | heating element  |
| e, c       | empty coolant channel  |
| e, l       | empty loop   |
| ex         | exit coolant channel   |
| f          | frictional   |
| f, c       | full channel   |
| h          | hydrostatic  |
| i          | harmonic variation from steady state   |
| in, inlet  | inlet coolant channel  |
| i.t.       | instability threshold  |
| k          | part of downcomer circuit  |
| l          | liquid   |
| m          | mixture  |
| n          | location of sensors  |
| 0          | steady-state value, only used in chapter 5,<br>if necessary to distinguish from non-steady-<br>state value |
| p          | pump   |
| pitot-tube | pitot-tube   |
| s          | vapor or steam   |
|            | shroud   |



|     |                                   |
|-----|-----------------------------------|
| sat | saturated conditions in condenser |
| sub | subcooling                        |
| t   | total                             |
| w   | wall                              |

### Superscripts

|     |  |
|-----|--|
| '   | local value with respect to r, z and t |
| "   | real part of complex variable          |
| ''' | imaginary part of complex variable     |
| —   | weighted mean value                    |
| °   | imposed modulation, see Fig. 5.7       |

### Miscellaneous

|                   |   |
|-------------------|---|
| $\Delta$          | amplitude of sine, e.g. Fig. 3.25<br>increment ( $\Delta z$ , $\Delta r$ , $\Delta U$ )<br>difference between two values, e.g. $\Delta p_{1-2} = p_1 - p_2$<br>deviation from steady state, Eqs 5.32 and 5.33<br>complex quantity |
| $\langle \rangle$ | average value over cross-section  |
| T.P.              | Two Phase   |

### Units

|                   |   |
|-------------------|---|
| temperature       | degree centigrade ( $^{\circ}\text{C}$ )          |
| heat input        | watt (W)  |
| radiation energy  | Electron Volt (eV)                                |
| length            | meter (m) or inches (in)                          |
| source strength   | Curie (C)   |
| voltage           | volt (V)  |
| resistance        | ohm ( $\Omega$ )                                  |
| current           | ampere (A)  |
| mass              | gram (g) or pound (lb)                            |
| time              | second (sec, s)                                   |
| frequency         | cycle or cycle per second (c or c. p. s.)         |
| pressure          | atmosphere absolute (ata)                         |
| pressure capacity | Newton per square meter ( $\text{N}/\text{m}^2$ ) |
| attenuation       | farad (F)   |
| angle             | decibel (dB)                                      |
|                   | degree ( $^{\circ}$ )                             |
| k                 | kilo  |
| c                 | centi   |
| m                 | milli   |
| M                 | mega  |
| $\mu$             | micro   |



## 1. Introduction

### 1.1. Aim and scope

Nuclear reactors in which the fuel rods or plates are cooled by circulating water have shown performance characteristics that make them attractive as possible producers of heat, which can be converted into low-cost electrical power or used for propulsion purposes. Particularly those reactors in which naturally or forcedly circulating coolant boils with or without net steam production, seem to offer such potentialities. A demand for exploiting these characteristics is the ability to predict accurately the heat transfer and fluid flow characteristics in the applied coolant system. This holds even more particularly for those nuclear reactors in which the circulating water is also used as moderator, the density of which has a major effect on its potential to slow down the fission neutrons. In many cases the characteristics of the coolant impose a limit on the power output of a nuclear reactor.

Therefore, in many research establishments an extensive research program is being carried out to obtain basic data on the heat transfer and fluid flow characteristics of naturally and forcedly circulating boiling water systems, especially under conditions prevailing in nuclear reactors. In these studies much attention is paid to the following items.

#### a. The heat transfer characteristics of a boiling liquid.

A great deal of research work in this field is connected with:

- (1) the nucleation characteristics of a heated surface, and
- (2) the sudden breakdown in heat transfer rates occurring under particular conditions in a boiling system.

Under (1) the way in which the heat is transported from the surface to the fluid is being studied. Attention is being paid to the fluctuation in surface temperature during the formation and growth of the bubbles on the surface and the detachment of the bubbles from the surface into the liquid. These studies are carried out in conditions where the mean liquid temperature is equal (saturated), above (superheated) or far below (subcooled) the saturation temperature, and include the effects of surface roughening and additives to the fluid. They are of importance to finding the fundamentals governing the heat transfer laws and to problems in the field of corrosion and the occurrence of severe thermal stresses in the heated surface.

The sudden breakdown in the heat transfer rate as mentioned under (2) results in excess temperatures of the heated surface with possible danger of melting. This phenomenon is known in the literature as "boiling crisis" and the resulting failure of the surface as "burn-out". In order to decrease the safety margin against burn-out in nuclear reactors, many investigations are being carried out to study the flow phenomena associated with burn-out and to set up experimental and theoretical laws for an accurate determination of the conditions in which burn-out will occur. In addition, mechanical and hydraulic methods for increasing the power at which burn-out in a certain operating condition of the reactor would occur, are being studied. The power output of many nuclear reactors is limited by the occurrence of burn-out. These studies are therefore of great importance to the economical development and the safety aspects of the nuclear reactor.

b. The flow characteristics in two-phase systems in steady states.

Subjects of interest are the determination of the amount of steam per unit of volume, the steam mass flow and the pressure variation along a coolant channel for saturated as well as subcooled fluid conditions and with and without heat addition. Furthermore, much work is carried out in the evaluation of the pressure loss across expansions and contractions and in the determination of the velocity and concentration profiles of the steam and water phases along - but particularly also across - a coolant channel. In this respect the transport of the steam phase in radial and axial directions into the water phase by diffusion and convection, and the interaction effects between neighbouring channels, which may be hydraulically coupled, not only at the ends but also along the length of the channel, are major subjects. Finally, the field of the recognition of the various flow regimes (bubbly, churn, slug, annular etc.) and the determination of the conditions under which certain flow regimes may exist, are broad domains of research. All these studies are of importance to the performance calculation of boiling coolant channels, not only to the calculation of the necessary pumping head, the flow distribution at the inlet of a series of parallel channels or the calculation of the steam volume in the nuclear reactor where the coolant is also used as moderator, but also to a detailed analysis of the heat transfer and the performance characteristics in non-steady states, to which they are intimately related.

c. The stability and transient characteristics of a boiling system.

These characteristics are of special importance from an operational point of view. They determine the stability and the controllability, and the knowledge of them is necessary for the development and the evaluation of the safety aspects of an economical nuclear reactor, as well as for an accurate design of the control devices. On the other hand, these studies are related to the onset under particular conditions of spontaneous flow oscillations in naturally as well as in forcedly circulating boiling systems. These oscillations may be of different origin and nature and may have a great influence on the operating limits of a nuclear reactor. They may, for instance, be responsible for large power oscillations owing to neutronic feedback. Furthermore, the heat transfer characteristics may change considerably and an appreciable reduction in the power levels where burn-out occurs may be expected.

It is evident that the results of most of these studies are not only of interest to the nuclear reactor designer, but also to the chemical process- and the steam boiler industry and that they are also applicable to other mixtures than steam and water. The demand for better design-rules in these fields will certainly increase in the future.

In the Laboratory for Heat Transfer and Reactor Engineering of the Mechanical Department of the Technological University of Eindhoven a research program is being carried out covering many aspects of the items listed above (B1-7), (M1), (S1-6) and (V1-3). This program is of a fundamental nature and not directly related to a specific reactor design. A great part of this program is sponsored by the Atomic Energy Commission (A. E. C.) of the U. S. A. and the European Atomic Energy Community (EURATOM). In 1958 the A. E. C. and EURATOM signed an agreement which provides a basis for cooperation in programs for the advance of the peaceful application of atomic energy. This is realized by sharing the scientific and technical information and minimizing the duplication of effort. The work to be described in this publication is part of this Joint A. E. C. - EURATOM research and development program.

Interest has been shown in reactors where the coolant and moderator are formed by boiling water circulating by natural or forced convection and designed for net steam production. In this type of reactor mostly a number of fuel rods, tubes or plates are grouped together, sometimes placed inside a shroud, the whole forming a fuel assembly or fuel channel in which the coolant flows. Many of these channels are present inside a reactor vessel. The work described in this report deals with the performance characteristics and the onset of flow oscillations in such type of coolant channels.

In connection with these reactors, concern has been expressed about different types of coupling effects and flow oscillations. A diagram in which two types of coupling characteristics are indicated is shown in Fig. 1.1. The coupling effect between the steam void volume or the density of the moderator and the reactor power has been mentioned. In Fig. 1.1, this process is indicated by the feedback path outside the broken lines. The reactivity defines the extent, by which a system is supercritical or subcritical, e.g. if, on the average, each neutron produces more or less than one further neutron. If the coupling between steam void-volume and nuclear power turns into regenerative feedback, divergent power oscillations may occur.

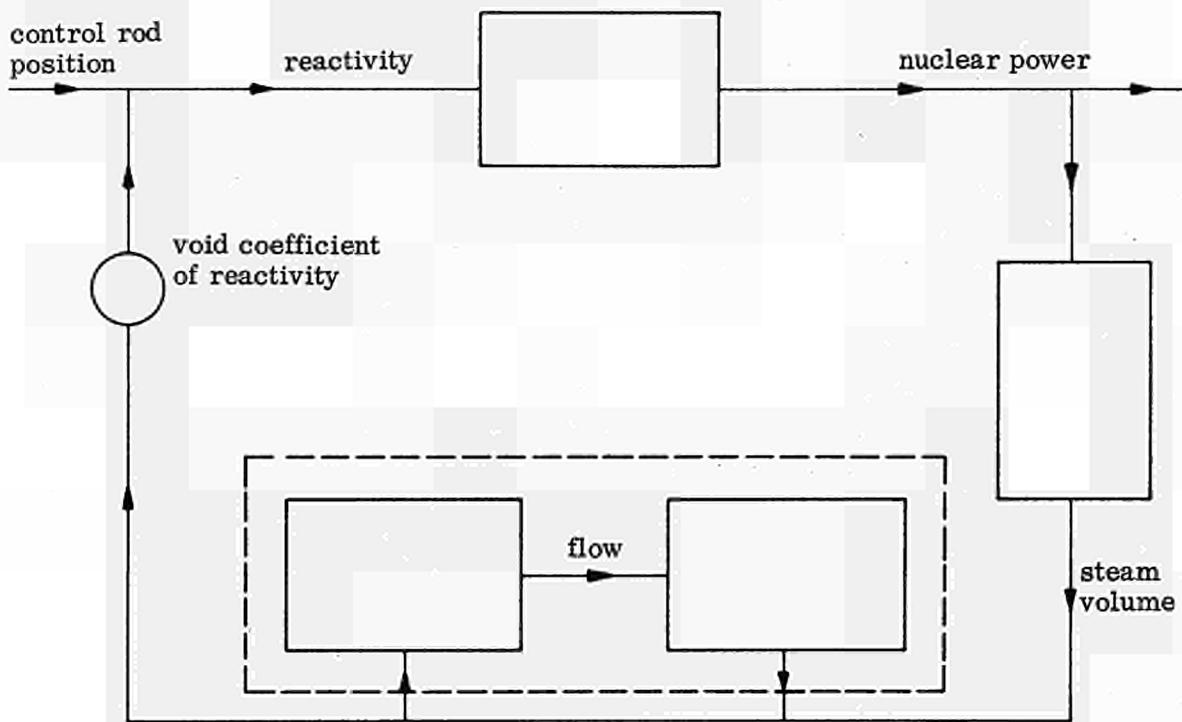


Fig. 1.1 Feedback paths in a nuclear boiling water reactor

A second feedback path is indicated within the broken lines of Fig.1.1. A change in steam-void in a coolant channel causes a change in the pressure drop along the channel and thus on the coolant flow rate in that channel, which, in its turn, causes a change in the steam-void. If, owing to this feedback the system becomes unstable, heavy flow oscillations occur. In this type of flow oscillations the intercoupling of the boiling channel with the other parts of the system plays an important rôle. In the recent literature these flow oscillations are sometimes referred to as pressure drop oscillations and density wave oscillations. In boiling water reactors with forced circulation, incor-

porating a pump which keeps the inlet flow constant and independent of the change in pressure drop along the channel, the coupling effect is not present.

Also, the intercoupling between parallel channels in a boiling water reactor may produce flow oscillations which are related to the second type just mentioned. Both are from a purely hydrodynamic origin.

Besides, other types of hydraulic flow instabilities may occur in a naturally or forcedly circulating coolant channel, for instance, "nucleation instabilities" (these instabilities are caused physically by a building up of a certain superheat followed by a sudden evaporation of the liquid phase with resultant rapid increase in specific volume and in pressure), "flow-pattern instabilities" (these are connected with the variety of possible geometric configurations into which the two phases can arrange themselves), and "acoustical or propagation waves" (connected with the compressibility characteristics mainly of the gas phase in a two-phase mixture).

The hydraulic phenomena occurring in a single coolant channel are mostly studied outside the reactor in a system where the nuclear fuel rod is simulated by an electrically heated tube of the same configuration and dimensions. This publication reports the results of an experimental and theoretical study of the hydraulic characteristics of a single coolant channel of simple geometry in a boiling water reactor, with the main emphasis on the stability characteristics of such a channel. The experimental part is restricted to the operation under conditions of natural convection. In the analysis of the results the relation of natural to forced convection cooling characteristics will be mentioned. Most attention is paid to:

- a. the determination of the liquid flow rate at the inlet and the void and pressure distribution along the height of the coolant channel;
- b. the occurrence and characterization of hydraulic instabilities;
- c. the determination of the stability characteristics of a steady state by means of a frequency response analysis.

This report starts with a short survey of the work in progress elsewhere and related to the present study. After that, it gives a description of the experimental set-up and the measuring, recording and analyzing equipment used in this study. The results of the experimental study are given in chapter 3 and they are analyzed and discussed in chapter 4. In chapter 5 the results are compared with those obtained from a theoretical study on the steady state and dynamic characteristics of a boiling channel.

## 1.2. Survey of recent work

Recently two reports (B8), (N1) have been published describing the experimental and theoretical work performed by many investigators in the field of the dynamic behavior of two-phase flow. Avoiding duplication, only the recent work carried out by four establishments will be reviewed. These are:

- a. the Advanced Technology Laboratories of the General Electric Company (G. E. C.) at Schenectady in the U. S. A. ;
- b. the Heat Transfer Laboratory of the Nuclear Energy Division of the Allgemeine Elektrizitäts Gesellschaft (A. E. G.) at Grosswelzheim in Germany ;
- c. the Space Technology Laboratory (S. T. L.) of the Thompson RamoWooldridge Company at California in the U. S. A. and
- d. the Laboratory of Heat Transfer of the Commissariat à l'Energie Atomique at Grenoble in France.

All four laboratories referred to are carrying out a research program, which is of a fundamental nature and which incorporates experimental as well as theoretical studies. These research programs may be considered as representative of the various approaches to the study of two-phase flow dynamics. The work of the other institutes and investigators will be discussed or referred to in other sections.

G. E. C.

In increasing the specific reactor power, the problem of hydraulic instability seems to become very acute. General Electric have recently revived their interest in the dynamics of boiling water reactors. In the Atomic Power Equipment Department in San José two-phase flow stability work was carried out in the Fuel Cycle Development Program (L1) in collaboration with the A. E. C. A new program on instability and frequency response measurements has been started as a private project of the Company. No results have been published. In the Knolls Atomic Power Laboratory operated by G. E. C., A. B. Jones has written a digital computer program (J1) for calculating the stability of a boiling system using a linearized approach. This work will be discussed in chapter 5.

In the Advanced Technology Laboratory at Schenectady, Zuber and Staub are engaged in a fundamental research program connected with flow and heat transfer phenomena occurring in boiling water channels (B9), (Z1). The overall purpose of the program is two-fold. First, the purpose is to gain an understanding of the various phenomena which lead to thermal-hydraulic oscillations in forced convection two-phase flow systems with heat addition, and secondly, the purpose is, to obtain equations and criteria which can be used for predicting the inception of these oscillations and instabilities as a function of the input parameters and system characteristics. In the analytical approach it is stated that in all analyses but one (V3), (V4), the set of conservation equations, which describe the transient behavior of two-phase flow systems, is incomplete. The equations have always been formulated in terms of the conservation laws for mass (continuity equation), momentum and energy for the mixture. In a multiphase system, however, the number of continuity equations must be equal to the number  $n$  of the phases. These  $n$  equations can be combined in one continuity equation for the mixture but  $(n-1)$  diffusion equations have to be formulated in order to obtain the required total of  $n$  equations. In all cases but one (V3), (V4), this was never done. Instead of seeking a solution in terms of a diffusion equation, as is done in the Eindhoven work, Zuber formulates a void propagation equation in terms of kinematic waves. This equation reads, in the absence of a change of phase and by neglecting density changes of the steam in time and space, (Z2),

$$\frac{\partial \alpha'}{\partial t} + C_K \frac{\partial \alpha'}{\partial z} = 0, \quad (1.1.)$$

where  $t$  is time,  
 $z$  axial coordinate,  
 $\alpha'$  void fraction,

$$C_K = W'_m + \frac{\partial(\alpha' V'_R)}{\partial \alpha'}$$

$W'_m$  volumetric flow of the mixture per unit of area,  
 $V'_R$  local drift velocity, equal to  $(V'_s - W'_m)$  and  
 $V'_s$  local steam velocity.

Equation (1.1.) shows that changes in the volumetric concentration of the void  $\alpha'$  propagate with the velocity  $C_K$  through the system. In other words, the void fraction  $\alpha'$  is constant in waves, which propagate with velocity  $C_K$ . These waves are sometimes called "continuity waves" because they are generated by the equation of continuity. Lighthill and Whitnam (L2) called them "kinematic waves" in order to distinguish them from "dynamic waves", which depend on the second law of motion. It is pointed out that kinematic waves have only one velocity, whereas dynamic waves have at least two. Furthermore, the value of  $C_K$  depends on the flow regime. In case  $C_K = 0$ , changes of  $\alpha'$  cannot propagate through the system. The system then ceases to operate satisfactorily. The approach, in which kinematic waves are introduced gives therefore a stability criterion predicting the operating limits of some systems. In the research program (B9) that has been started the void propagation equation (1.1.) is being elaborated further for predicting the transient response of the vapor volume fraction in a two-phase system with a change of phase. By neglecting the compressibility of the liquid and of the steam phase, the effects of system pressure oscillations and of subcooling, and the effects of energy storage in the two-phase flow, closed form analytical solutions of the void propagation equation have been obtained, giving the response of the vapor volume fraction to different inputs. Together with the conservation laws for mass, momentum and energy for the mixture, the void propagation equation will describe the dynamic behavior of the system. Final results of this study have not yet been reported. Neither is it yet known with what type of hydraulic instabilities the condition  $C_K = 0$  is connected. Comparison with experimental results of other investigators has not been made. In connection with this study much work has been carried out on the determination of the void fraction  $\alpha'$  in a two-phase flow in a steady state (Z1). This work can be considered very important to the solution of several problems in two-phase flow. Reference (Z1) will be discussed in section 4.1.

At the G.E.C. Laboratory, an experimental program has been set up to test the formulation of the analytical model. It is carried out in an experimental loop with Refrigerant 22 (Freon) as the working fluid. This fluid was selected to meet the requirement of obtaining simultaneously recorded data of the heat transfer coefficient, pressure drop, vapor content and the visual identification of the two-phase flow regimes in a vertical forced convection boiling system over a range of reduced pressures from .1 to .7. The heat input to the loop, which is supplied by an electrically heated test element, can be oscillated in order to perturbate the system. These imposed oscillations cover a range of .01 to 10 c. p. s. and may have a maximum amplitude of about  $\pm 30\%$  of the mean input level. The loop has been designed for minimum feedback in either flow or pressure, resulting from these oscillations in the power. This is achieved by selecting a pump with a steep head-flow characteristic, the use of heavy throttling at the inlet and by incorporating a large volume after the test section. Therefore, there is only a very weak coupling of the boiling channel with the other parts of the system and consequently no flow oscillations are present. Preliminary results of the void response to power modulation (which response is measured by an X-ray beam traversing the mixture) have been reported only in the low frequency range (B9). Comparison has been made with results obtained from the theoretical analysis. The predicted average void fraction, rate of propagation and the wave form of the void variations were found to be in agreement with the experimental data.

#### A. E. G.

The object of the A.E.G. program is to develop and to test an analytical formulation, describing the dynamic behavior of a nuclear boiling water reactor (K1). The mathema-



tical formulation starts with the equations of conservation of mass, momentum and energy for the steam-water mixture. Three regions in a boiling channel are being considered: the subcooled region, the boiling region and the chimney.

In the formulation it is assumed that there is thermodynamic equilibrium between the two phases. This means, that boiling under subcooled conditions is ignored. An analytical solution is obtained by integration of the conservation equations over the length of the three regions mentioned. This could be done by assuming that the pressure variation caused by water acceleration is negligible and that the velocity of the steam phase can be separated into a spatial and a time dependent function. In doing this, properly weighted space integrals of the void fraction are obtained for each region, which are needed for the calculation of the water flow rate and the void reactivity, see Fig. 1.1, determining the kinetics of the nuclear reactors. In calculating the water flow rate, the two-phase friction force has also to be known and must be given as a function of a properly weighted void fraction and of the water velocity at the inlet. This friction force is difficult to estimate from existing data. The equations are linearized assuming small deviations from the steady state. By doing this, the weighting functions for the void fraction become only dependent on the steady-state axial void distribution. This means that the spatial form of the void fraction is not time-dependent. The transportation effects in the three regions are allowed for by introducing time delays. Finally, the Laplace transformation leads to transfer functions which are convenient for a stability analysis.

Results of calculations, using this formulation and assuming a space-independent reactor kinetic transfer function, have been compared with experimentally measured transfer functions in the EBWR (Experimental Boiling Water Reactor, A. N. L., U. S. A.). In these experiments the reactivity was sinusoidally disturbed by oscillating the control rod, see Fig. 1.1. The resulting oscillations in nuclear power, particularly the phase shift and attenuation with respect to the reactivity input, were measured. Very good agreement between the calculated and measured transfer functions of the EBWR have been obtained. But the transfer function of the EBWR was measured in a condition very far below an instability and was almost entirely determined by the neutronic behavior of the reactor and therefore, not very sensitive to the hydrodynamic process. Owing to lack of data from loop experiments with strong hydraulic effects, the formulation of the two-phase flow characteristics in the analytical description has not yet been proved. Therefore, an experimental program has also been started.

The experiments are being carried out with a high pressure electrically heated boiling water loop in which a coolant channel of a nuclear reactor can be simulated. This loop can be operated in conditions of natural circulation as well as forced circulation by means of a pump. The maximum pressure and temperature are 100 atmospheres and  $310^{\circ}\text{C}$ , while the maximum heating power that can be supplied is 420 kW. The coolant channels have a length of about 2.5 m. Single and multirod annular test sections can be installed. The pressure in this boiling water loop is controlled by an air-cooled condenser. The volume void fraction in steady states as well as in transient conditions is measured by a  $\gamma$ -beam traversing the mixture, (see also section 2.3.). The Cesium  $\gamma$ -source has a strength of about 50 Curie. For the measurement of mass flow rates turbine flowmeters are applied. Transfer function measurements can be carried out by oscillating the heating power sinusoidally and measuring the phase shift and attenuation of the dependent variables such as void fraction, with respect to the input signal. An important facility of the circuit is that the water flow rate at the inlet can also be modulated sinusoidally in a frequency range from 0 to 4 c. p. s. by changing the inlet resistance. In this way, the transfer function can be measured from water flow rate at

the inlet to volume void fraction along the height of the channel. In many formulations this transfer function is important in the evaluation of the dynamics of a two-phase flow. Beside the transfer functions, all steady-state input data needed for the calculation of the transfer function by the analytical description are measured. So far, only a few preliminary results have been published.

S. T. L.

In the Space Technology Laboratories, experiments are carried out on an electrically heated mock-up of one of the coolant channels of the SPERT (Special Power Excursion Reactor Tests, Idaho, U.S.A.) nuclear reactor. The SPERT program was initiated in order to test the safety of water moderated reactors in general. Ramp-tests were carried out by gradually withdrawing the control rod in order to add reactivity at a linear rate. Stability was investigated by terminating the ramp addition at a preselected reactivity value and by observing the subsequent reactor behavior. The SPERT-I-A reactor, operating at atmospheric pressure, had been found to oscillate at the power density of about 13 kW per liter. These oscillations had a frequency of about 1 c.p.s., while nuclear power varied from 200 kW to 700 MW starting at an initial power of 400 kW.

In the mock-up experiments, the high thermal conductivity of the fuel plates was simulated. Provisions were made for the measurement of the change in density of the water in the channel by X-ray attenuation technique. The density change may be fed back by means of an electronic reactor kinetics simulator to control the electrical power input to the coolant channel. The reactor is thus simulated by the thermal hydrodynamic behavior of a single coolant channel plus electronic simulation of the neutron kinetics. The reactivity feedback can, of course, be eliminated to permit investigation of the dynamics of the coolant channel alone at various conditions of power input. Provisions are made to oscillate the heating power in order to yield a transfer function for the steam-void content. The work includes investigations of both the static and the dynamic steam-void behavior within the channel for natural as well as for forced circulation. Hydrodynamic instability, where flow and void oscillations with a frequency of about 1 c.p.s. spontaneously occur at a constant power input of 1,000 watts without the necessity of neutronic feedback, was observed in the simulated SPERT-I-A channels during natural circulation tests. Measurements of the transfer functions from heating power to steam-void volume for natural circulation boiling show a sharp resonance peak in the void fraction response as the threshold of spontaneous hydrodynamic oscillations is approached. The frequency of the resonance peak is the same as that of the impending hydrodynamic oscillation. It thus appeared that these hydrodynamic oscillations are caused by unstable linear feedback between flow rate and steam-void volume. This resulted from a comparison of the power-void transfer function measured at natural circulation with that at forced circulation under the same conditions. The flow-void feedback dominates the power-void transfer functions of the natural circulation boiling system. In the test it was demonstrated that hydrodynamic instability depends on the steam bubble nucleation properties of the surfaces of the channel.

The power-void transfer function was combined with the neutron kinetics, which resulted in a behavior similar to that observed in the SPERT-I-A reactor. It was shown that at 500 watts in the laboratory channel, and 500 kW in the reactor, the reactor must be decidedly unstable as a result of reactivity feedback at an oscillation frequency of .95 c.p.s. The threshold of reactivity feedback instability would be expected to occur at a power level somewhat below 500 kW. This result is in agreement with the observed spontaneous power oscillations in the reactor which arose at a power level of about

400 kW and with a frequency of 1 c. p. s. The natural circulation flow and void fraction were quite stable in the laboratory channel at 500 watts, indicating that the reactor power oscillation was not caused by hydrodynamic instability.

In the Space Technology Laboratories, an analytical description has also been made primarily to interpret the transfer function measurements made in the atmospheric loop. In this analytical approach the boiling part of the channel is treated as one section. The approach emphasizes the rôle of the non-boiling region and consequently is not applicable in systems where the relative length of the non-boiling region is negligible. Nor was any assumption made regarding the slip between the water and the steam phase. The model employs the experimental observation that the shape of the axial void distribution does not change during power modulation. While the representation is adequate for the S. T. L. experiments (length coolant channel .625 m, maximum power 1 kW), it is not appropriate for longer test sections and higher power levels. The analytical description leads to an explanation of hydrodynamic oscillations as an unstable linear feedback between steam-void volume and flow rate.

#### Grenoble.

In the research program of Grenoble, an experimental as well as a theoretical study has been carried out on the onset of hydrodynamic instabilities in a boiling channel. In the experiments the instabilities manifest themselves by large regular variations with a very defined period in inlet flow and pressure drop at constant heat input. Use is made of an electrically heated boiling loop, which can be operated in conditions of natural and forced circulation at a pressure of 8 atmospheres. In the forced circulation experiments use is made of a bypass across the channel with a large cross-section area in order to obtain a constant pressure drop condition between the inlet and exit of the test channel. The test elements are of circular form and have an inner diameter of 0.06 m and a total length of about 4.5 m. Besides, experiments have been carried out in a small atmospheric boiling loop with the advantage of easy handling and the possibility of making visual observations.

The two main parameters, which have been varied, are the temperature at the inlet and the imposed pressure drop across the channel. Furthermore, the effect of changing the fluid resistance at the inlet and of the length of the chimney (non-heated part on top of the heated channel) on the onset of instabilities has been looked into. By increasing the heating power and keeping the subcooling and imposed pressure drop constant, oscillations occurred at a certain power level. With increasing subcooling or increasing imposed pressure drop the power at which instabilities started, shifted to higher values. The influence of subcooling was less at higher imposed pressure drop. It has been found, that by increasing the power level beyond the instability power, the flow in the atmospheric boiling loop became stable again. So there is an instability region. The two limits come together at low subcoolings and heating powers. In all the experiments the periods of the oscillations vary from 2 to 15 seconds. When increasing the subcooling, the period also increases. It has also been found that there is a continuous transition between the case of natural circulation and that of low imposed pressure drop. The phenomena are interpreted to be the same. An increase of the inlet resistance or a decrease of the height of the chimney has a favorable influence on stability.

In the theoretical program different approaches have been made in an attempt to describe the observed phenomena by as simple a formulation as possible. The furthest developed formulation is the so-called "single-phase model". This is based on the strik-

ing characteristic of boiling that the change in density of the mixture per unit of volume is very great. This causes high accelerations in the fluid which result in important dynamic effects in non-steady conditions. The hypothesis of the model is that this density effect causes also the flow oscillations. Therefore, in the model, only those effects are introduced, that have a direct relationship with the density change. Thus, a fictitious single-phase fluid is defined whose specific density is a function of the enthalpy. The other physical quantities are taken constant. For the relationship between the specific density and enthalpy a hyperbolic function has been assumed, corresponding with a constant slip between the two phases. The conservation laws for mass, momentum and energy for the fluid are then formulated by neglecting bubble formation in subcooled conditions and by taking the temperature and pressure at the inlet constant. Furthermore, a constant pressure drop across the channel and a constant heat input were assumed. Owing to the assumptions made, the momentum equation can be integrated along the channel with as boundary conditions a constant pressure drop between the inlet and the outlet of the channel. In this integration the two-phase pressure drop has been taken equal to the one-phase pressure drop multiplied by a constant. The equations are made dimensionless, and by assuming small deviations from the steady state an analytical solution is obtained. The mechanism of the oscillations observed is demonstrated. Oscillations are sustained owing to the delays introduced by the density effect between a disturbance and its consequences on the mass, the center of mass and the moment of inertia of the mass of the liquid in the channel. Some results of calculations have been reported (B8).

Although the description is simple, a digital computer is needed in order to obtain numerical results. The influence of the different parameters such as pressure, subcooling and imposed pressure drop, are qualitatively in agreement with experimental results. The theoretical formulation predicts for instance that for low values of subcooling an increase of the subcooling has a destabilizing effect, whereas for high values of subcooling the inverse is true.

In general, it can be said that systematic data on the onset of hydraulic flow oscillations and on the stability of a two-phase flow in dependence of the operating condition are scarce. Furthermore, there is a need for detailed information, theoretical as well as experimental, in order to obtain a better characterization of the various types of oscillations. The work to be reported upon here, may give a contribution to an understanding of the two-phase flow stability characteristics.

## 2. Description of the apparatus

In this section a description is given of the equipment used in the research program concerning the characteristics of a naturally circulating boiling system. It starts with a description of the pressurized and atmospheric boiling water loops, the test sections and the power supply. After that, a review is given of the measuring, recording and analyzing equipment. Special attention is paid to the measurement of the void fraction in a two-phase system. When possible, the accuracy obtained in measuring the various physical quantities is indicated. A photograph of the pressurized boiling water loop is given in Fig. 2.1, while the main part of the electronic instrumentation is shown in Fig. 2.2.

### 2.1. Loops and test sections

#### Pressurized boiling water loop.

Most of the experiments described hereafter have been carried out in a pressurized boiling water loop. This apparatus consists of a cylindrical pressure vessel in which water boils at elevated pressures. In this loop it is possible to study the behavior of a unit-cell of a boiling water reactor. In a reactor this unit-cell generally consists of one or more fuel rods placed side by side vertically in a can, usually called the shroud. In hydraulic tests performed outside the reactor, as under consideration, the fuel rods are simulated by electrically heated elements of the same configuration and dimensions. Together with the shroud they form the test section.

A simplified flow scheme of the loop is given in Fig. 2.3.

The test section is placed in the cylindrical part of the pressure vessel. The loop is filled with demineralized water up to a certain level. The channel formed by the heating element and the shroud is called the riser; the one formed by the shroud and the pressure vessel, the downcomer. Since the shroud is open at both ends, the two channels are in direct connection with each other. When the element is heated, the water in the riser starts to boil and vapor is formed. Owing to the resulting density difference between the fluid in the riser and in the downcomer the steam-water mixture in the riser flows upwards by natural convection. At the water surface the steam and water are separated. The water returns to the inlet of the riser through the downcomer. The steam flows to the condenser and the condensed steam is returned to the downcomer.

The pressure vessel is made of stainless steel 316 and withstands a working pressure of 40 atmospheres. The cylindrical part has an inner diameter of .150 m and a length of 3 m. The vessel is provided with the necessary connecting devices for measuring equipment. In order to decrease the heat losses to the exterior the pressure vessel is insulated at the outside with glasswool. During operation the variation in water level, caused by thermal expansion and by the formation of steam is kept within certain limits by means of a water drum connected with the pressure vessel. The water level is observed continuously by means of two water gauges, one positioned at the top of the cylindrical part of the loop, the other placed at the control panel.

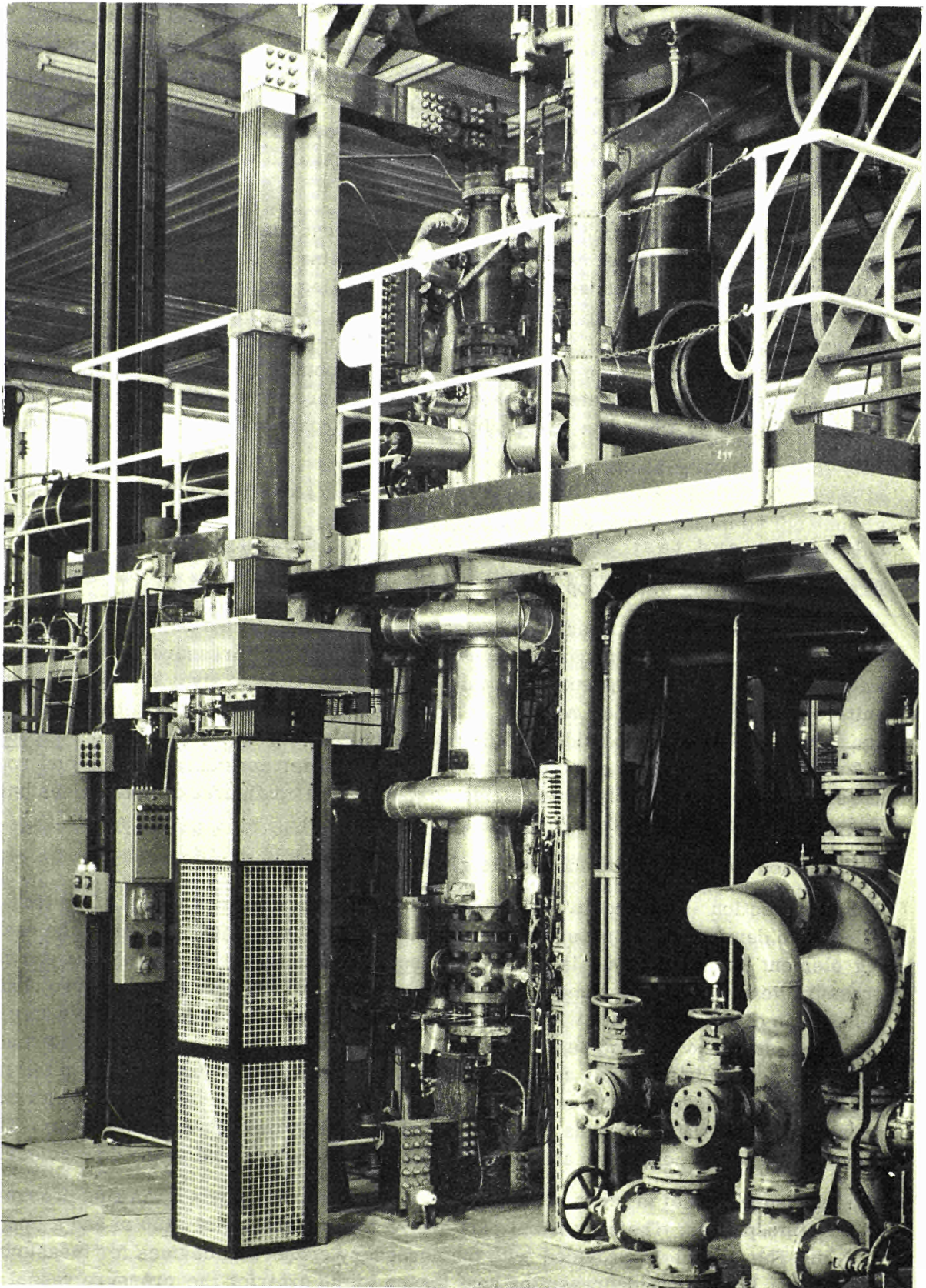
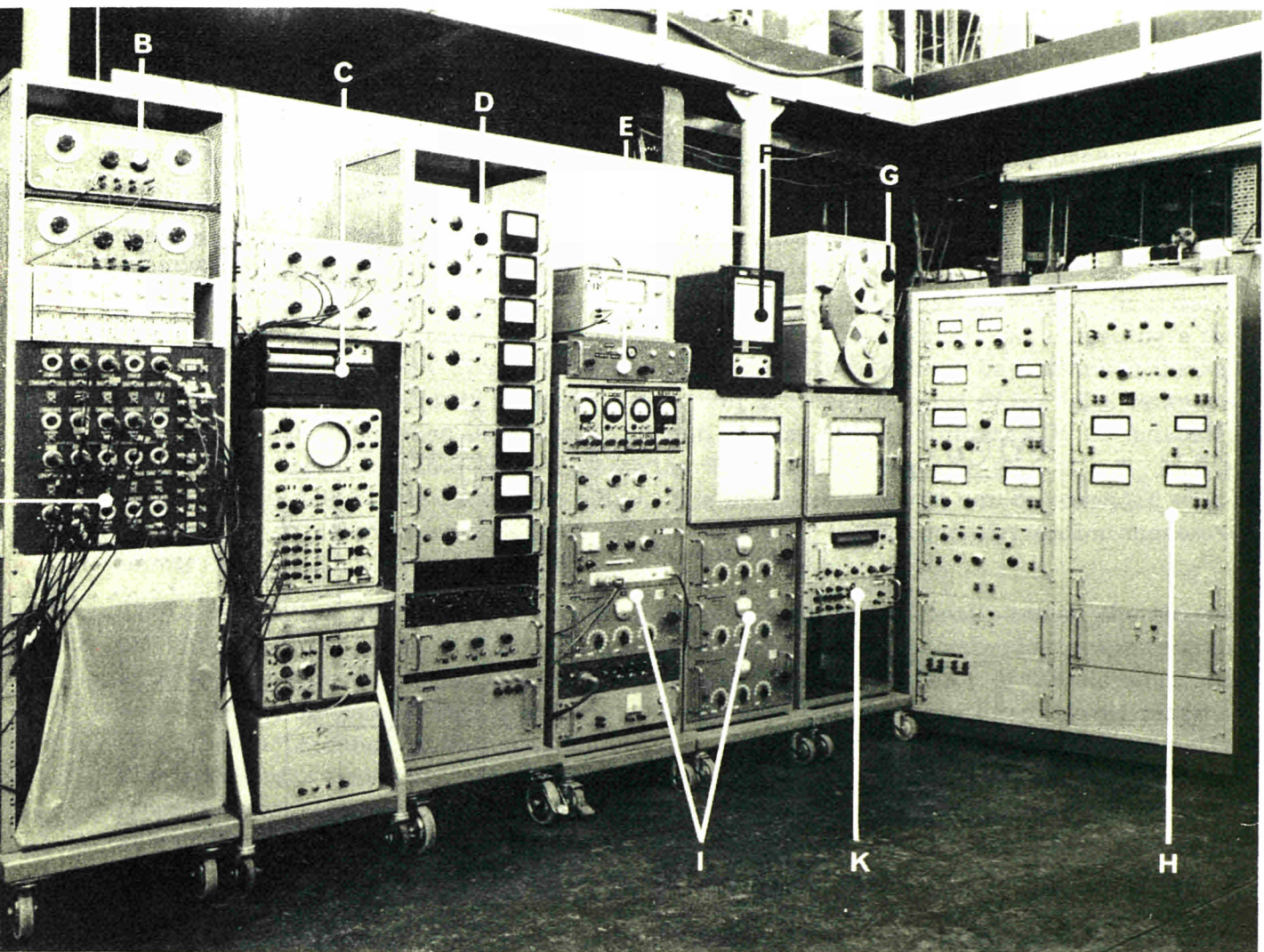


Fig.2.1 Pressurized boiling water loop



- A = matching network
- B = amplifiers and filters
- C = Ultra-Violet recorder
- D = impedance measuring apparatus
- E = burn-out detector
- F = temperature recorders
- G = FM magnetic tape
- H = response analyzer
- I =  $\gamma$ -ray detection apparatus
- K =  $\Delta P$ -equipment

Fig. 2.2 Electronic instrumentation

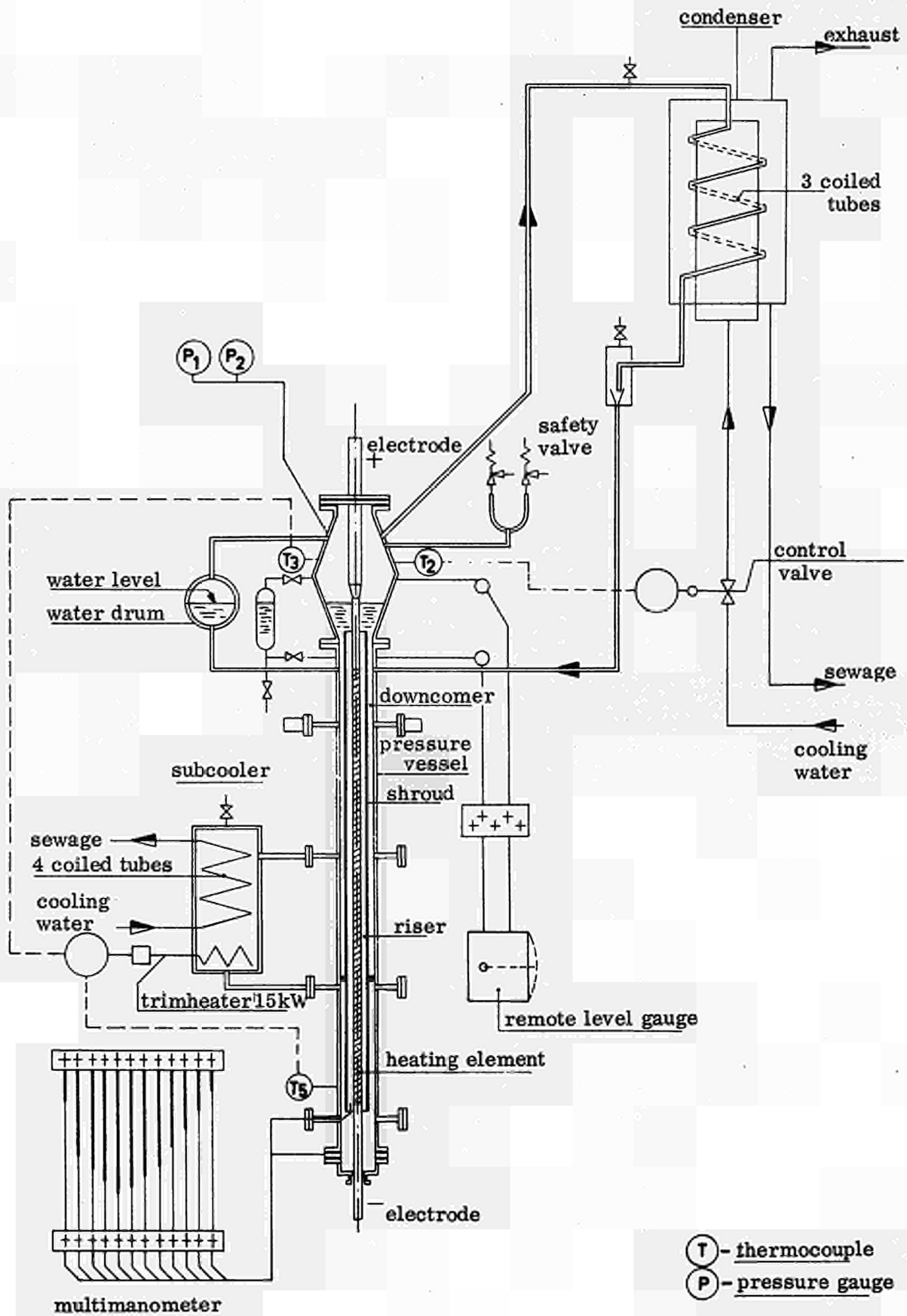


Fig. 2.3 Flow sheet of the pressurized boiling water loop



In the condenser the steam is condensed inside three coiled tubes by sprinkling cold water on the tubes. The coolant flow to the condenser is controlled automatically or manually. The automatic control is achieved by the comparison of the actual steam temperature in the pressure vessel ( $T_2$  in Fig. 2.3) with an adjustable reference value. The control is proportional, integrating and differentiating. The pressure in the system is, therefore, controlled by the condenser.

Before returning to the riser, the water passes through a cooler giving the possibility to subcool the water and to adjust the inlet temperature. (This subcooler, designed for negligible pressure loss, was added to the loop after the initial operation. In order to force the water to flow through the cooler the original downcomer was closed by a teflon seal.) The secondary circuit of the subcooler consists of four helical tubes through which an adjustable quantity of water flows. For a closer control of the inlet temperature a preheater has been installed which can be controlled automatically or manually. Automatic control is achieved by comparing the actual subcooling, e.g.  $T_3 - T_5$  in Fig. 2.3, with an adjustable reference value. The subcooler circuit can be extended with a centrifugal pump and connecting tubes for carrying out forced circulation measurements.

The test section consists of a stainless steel tube placed centrally inside the shroud. On both ends red copper electrodes have been soldered. An asbestos graphite gland with spring pressure at the bottom electrode allows for expansion of the element. The weight of the bottom electrode and the connection to the bus-bars keep the element under tension. A check of the proper behavior of the gland is obtained by measuring the displacement of the bottom electrode with respect to the pressure vessel. The top electrode is connected to a flange which is insulated from the pressure vessel as is the shroud. The bottom electrode is connected to the pressure vessel and both are earthed.

#### The glass loop.

For visual studies a glass loop operating at atmospheric pressure has been erected. It represents the high pressure natural circulation boiling loop described above and consists of a glass vessel with an inner diameter of 150 mm and a length of 2.4 m, an internal glass shroud with an inner diameter of 25 mm and a length of 2 m, and in the center an electrically heated stainless steel tube with an outer diameter of 20 mm and a length of 1.8 m. The loop is adequately equipped for detecting recirculation, steam void, temperature and pressure. It incorporates a subcooler and an adjustable valve for varying the inlet resistance. The power to the heating element is supplied by a 15 kW continuously controllable rectifier fed from the 3-phase 380 V mains.

#### Test sections.

In the pressurized boiling water loop two test sections were employed. The two test sections, denoted as Test Section I and II, differed only with respect to the inner diameter of the shroud, which was 50.0 and 58.8 mm respectively. In all the experiments a heating element of nominally the same dimensions, made of stainless steel 316, was used. The inner and outer diameters of the heating element were constant along the length giving a uniform heat load distribution. The electrical resistance of the heating element and the electrodes together is 5.35 m $\Omega$  and of the stainless steel alone 5.25 m $\Omega$ . The element was internally stiffened by means of ceramic tubes. In these tubes a radioactive source can be placed for void fraction measurements. In three axially different places on the outside of the element, spacers have been fixed to prevent the element from bending. Each spacer consists of three horizontal teflon studs, the outer

diameter and length of which are 5.5 and 7.5 mm for Test Section I, and 6.5 and 11.5 mm for Test Section II respectively. In Table 2.1. the geometrical data of the two test sections are given.

Table 2.1. Geometrical data of the test sections

| Test Section                        | I                       | II                      |
|-------------------------------------|-------------------------|-------------------------|
| <u>Location*</u>                    |                         |                         |
| top-end riser                       | 1.126                   | 1.126                   |
| bottom-end riser                    | -0.021                  | -0.019                  |
| operating water level               | 1.144**                 | 1.144**                 |
| spacers (a)                         | 0.993                   | 0.992                   |
| (b)                                 | 0.572                   | 0.572                   |
| (c)                                 | 0.285                   | 0.285                   |
| <u>Dimensions</u>                   |                         |                         |
| length heating element, m           | 2.400                   | 2.400                   |
| outer diameter heating element, mm  | 33.84                   | 33.78                   |
| inner diameter heating element, mm  | 27.39                   | 27.07                   |
| inner diameter shroud, mm           | 50.00                   | 58.81                   |
| length riser (total), m             | 2.753                   | 2.749                   |
| hydraulic diameter***, mm           | 16.16                   | 25.03                   |
| heated surface, m <sup>2</sup>      | 0.2550                  | 0.2546                  |
| cross-section riser, m <sup>2</sup> | 10.636x10 <sup>-4</sup> | 18.193x10 <sup>-4</sup> |

\* Locations are expressed as parts of the total heated length (equal to 2.400 m) and taken from the bottom-end of the heated length, see Fig. 2.4.

\*\* Water gauge reading 260.

\*\*\* The hydraulic diameter is taken as the difference between the inner diameter of the riser and the outer diameter of the heating element.

The locations indicated are measured from the bottom-end of the heating element and made dimensionless by dividing by the length of the heating element. A schematic drawing of the test section positioned in the pressure vessel is given in Fig. 2.4. In the shroud, impedance gauges are mounted for void fraction measurements in transient conditions. On the outside of the shroud pressure tapings are located for measuring the pressure distribution along the coolant channel. All pressure tubes, which have an inner diameter of 4 mm, are led out of the pressure vessel by means of a specially constructed insulated flange at the bottom of the vessel.

## 2.2. Power supply

The supply of power to the heating element of the pressurized boiling water loop is by means of a power unit consisting of two controlled rectifiers, each fed by a transformer from the 10 kV mains. One of the transformers is equipped with a stepwise and the other with a continuous control.

By means of tapings at the primary side of the first transformer, the output voltage of the rectifier can be set at 10, 13, 16, 19 or 21 V nominally. The output voltage of the other rectifier fed by the continuously controlled transformer, is variable between 15 and 60 V nominally. This is done by a transducer circuit at the primary side of the transformer. The transducer is regulated by a special controller, which can be programmed. The two rectifiers can be used independently or in series. The maximum current and power which can be supplied is 14,000 A, 1,000 kW. The quoted values are somewhat depending on the load on the rectifiers.

The rectifier connections to the copper electrodes of the heating element in the boiling water loop are made of aluminum bus-bars with flexible copper connections (litz) to the electrodes. The end-connections are water-cooled. The negative pole is earthed via a fuse.

In the experiments the rectifiers were mostly connected in series to utilize the whole range of available voltages. The possibility of programming the controller was used in the transfer function measurements, in which a sinusoidal signal was applied at the input of the controller to measure the frequency response characteristics of the boiling system. Frequencies up to 5 c.p.s. have been applied.

## 2.3. Measuring equipment

In the experimental program the following physical quantities have been measured:

- a. heating power,
- b. pressure,
- c. temperature,
- d. void fraction,
- e. mass flow rate.

For the measurement of the quantities in steady-state and transient conditions different techniques have been applied. They will be reviewed in the following. In Fig. 2.4 and Table 2.2. the location of the various sensors is indicated.

### a. Heating power.

The heat generated in the element is measured electrically in steady-state conditions by means of a precision voltage and current meter, and also by means of a light-spot wattmeter. The voltage tapings are placed on the copper electrodes just outside the pressure vessel. The value of the current is obtained from a direct current transducer, positioned around the aluminum bus-bar leading to the heating element. The transducer has a transmission ratio of 3,000. The maximum current on the secondary side is 5 amps. The transducer has been calibrated. For the range of currents used in these experiments the accuracy of the transmission is better than  $\pm .1\%$ . The electrical power read from the light-spot wattmeter (class .2) has been compared with the product of the readings from the volt- and currentmeter in order to check the phase shift and the influence of magnetic fields. Both values of the dissipated power agreed within .5%.

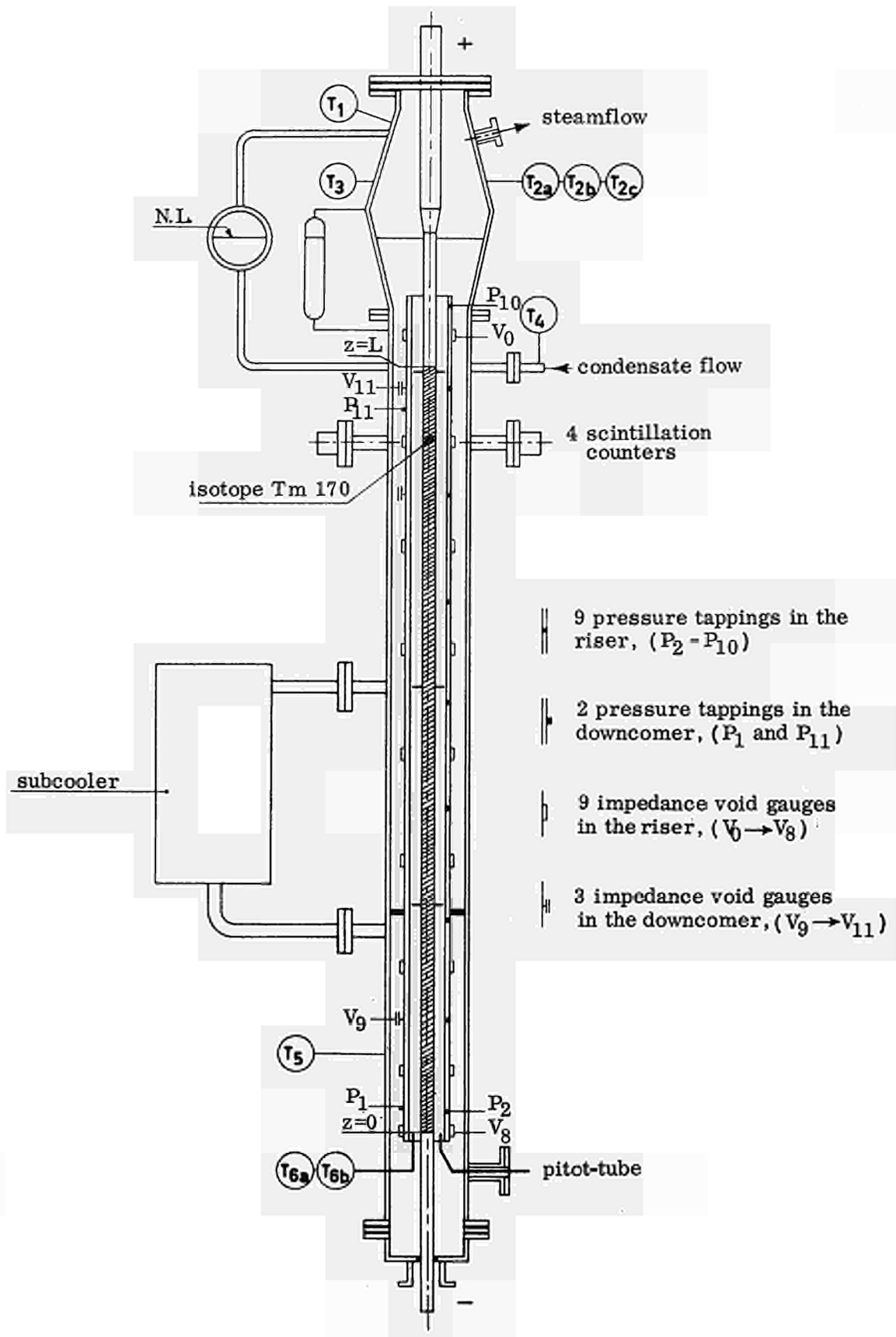


Fig. 2.4 Schematic of the test section with instrumentation

Table 2.2. Location\* of the sensors

| Sensors                  |                 | Test Section    |        | Remarks    |           |
|--------------------------|-----------------|-----------------|--------|------------|-----------|
|                          |                 | I               | II     |            |           |
| <u>Thermocouples</u>     | T <sub>1</sub>  | 1.302           | 1.302  | steamspace |           |
|                          | T <sub>2a</sub> | 1.210           | 1.210  | "          |           |
|                          | T <sub>2b</sub> | 1.210           | 1.210  | "          |           |
|                          | T <sub>2c</sub> | 1.210           | 1.210  | "          |           |
|                          | T <sub>4</sub>  | 1.000           | 1.000  | condensate |           |
|                          | T <sub>6a</sub> | -0.012          | -0.012 | riser      |           |
|                          | T <sub>6b</sub> | -0.012          | -0.012 | "          |           |
| <u>Pressure tappings</u> | P <sub>1</sub>  | 0.096           | 0.059  | downcomer  |           |
|                          | P <sub>2</sub>  | 0.045           | 0.076  | riser      |           |
|                          | P <sub>3</sub>  | 0.132           | 0.128  | "          |           |
|                          | P <sub>4</sub>  | 0.263           | 0.268  | "          |           |
|                          | P <sub>5</sub>  | 0.411           | 0.413  | "          |           |
|                          | P <sub>6</sub>  | 0.552           | 0.550  | "          |           |
|                          | P <sub>7</sub>  | 0.692           | 0.690  | "          |           |
|                          | P <sub>8</sub>  | 0.832           | 0.832  | "          |           |
|                          | P <sub>9</sub>  | 0.972           | 0.975  | "          |           |
|                          | P <sub>10</sub> | 1.076           | 1.072  | "          |           |
|                          | P <sub>11</sub> | 0.971           | 0.974  | downcomer  |           |
|                          | P <sub>12</sub> | -0.009          | -0.009 | pitot-tube |           |
|                          | P <sub>13</sub> |                 |        |            |           |
| <u>Void detectors</u>    | impedance       | V <sub>0</sub>  | 1.043  | 1.043      | riser     |
|                          |                 | V <sub>1</sub>  | 0.903  | 0.903      | "         |
|                          |                 | V <sub>2</sub>  | 0.764  | 0.762      | "         |
|                          |                 | V <sub>3</sub>  | 0.624  | 0.621      | "         |
|                          |                 | V <sub>4</sub>  | 0.485  | 0.480      | "         |
|                          |                 | V <sub>5</sub>  | 0.345  | 0.340      | "         |
|                          |                 | V <sub>6</sub>  | 0.205  | 0.199      | "         |
|                          |                 | V <sub>7</sub>  | 0.066  | 0.058      | "         |
|                          |                 | V <sub>8</sub>  | -0.012 | -0.013     | "         |
|                          |                 | V <sub>9</sub>  | 0.160  | 0.127      | downcomer |
|                          |                 | V <sub>10</sub> | 0.832  | 0.833      | "         |
|                          | V <sub>11</sub> | 0.975           | 0.971  | "          |           |
| $\gamma$ -ray            | V' <sub>1</sub> | 0.903           | 0.903  | riser      |           |

\* Locations are expressed as parts of the total heated length (equal to 2.400 m) and taken from the bottom-end of the heated length, see Fig. 2.4.

One should keep in mind that the measured power is the total power dissipated in the heating element and the electrodes between the voltage tappings. A correction must be made if one wants to know the power dissipated in the stainless steel part of the element only. This correction is about 1.5% of the total power. In the results presented here, no corrections have been made.

For the measurement of the heat generated in the element in non-steady conditions use is made of commercially available Hall generators. These instruments give a signal proportional to the product of voltage and current of the heating element. They have been calibrated in steady-state conditions against the readings of the light-spot wattmeter. The linearity was better than .1% in a range of channel powers from 10 to 400 kW. Also an analysis was made of the sensitivity to phase shift and of the attenuation with increasing frequency. The phase shift and attenuation at 50 c.p.s. was within the accuracy of the analyzing apparatus, see section 2.5. The dynamic characteristics of these instruments are therefore excellent for the frequency range for which they are applied. No corrections are needed. Attention must be given to the fact that these instruments measure the momentary power dissipated in the heating element which is determined by the electrical resistance and thus by the temperature of the heating element. The power reading in transient conditions is therefore dependent on the heat capacity of the element and of the nature of the boiling process at the wall.

#### b. Pressure.

The absolute pressure in the steam space of the pressurized boiling water loop has been measured using two Bourdon pressure gauges, which were calibrated at regular time intervals. The range of these pressure gauges was 0-6 and 0-50 atmospheres respectively. The accuracy of the calibration was about + .1%.

The static pressures along the coolant channels have been measured with a multimanometer. The location of the pressure tappings, which have a diameter of 4 mm is indicated in Fig. 2.4 and is also given in Table 2.2. Nine pressure tappings are located in the riser and two in the downcomer. At the top, the tubes of the multimanometer, each about .9 m long, are connected with each other, see Fig. 2.3. The upper part of the manometer is filled with red-coloured trimethylpentane, which has a density of 690 kg/m<sup>3</sup> and is immiscible with water. The other part and the connecting tubes with the pressure tappings are filled with water. The use of this substance allows the deviations on the manometer to be increased by a factor of about three. Without circulation in the boiler the height of water-columns in the manometer is the same for all tubes. A typical manometer reading, during operation, is indicated in Fig. 2.3.

For the measurement of the absolute pressure in transient conditions a fast pressure gauge has been developed, see Fig. 2:5. The principle of the method is that the change in capacitance due to the displacement of a membrane with regard to a fixed and insulated electrode is detected in a resonance circuit by a capacitance meter, type Van Reysen (Netherlands). The sensitivity and the range of the pressure gauge is mainly determined by the distance between the membrane and the electrode and the slope of the resonance curve. The linearity depends on the part of the resonance curve used and on the dimensions of the facing surfaces. The construction of the pressure gauge was made in such a way that the distance between the electrode and the membrane was adjustable. The distance is normally about 50  $\mu$ . The membrane is made of phosphor-bronze, the housing and electrode of brass. In the development of these gauges difficulties have been encountered owing to induction and temperature effects. The readings are therefore calibrated in steady-state operating conditions against the Bourdon

pressure gauge. The linearity in the applied range is better than 1% while the sensitivity is such that a change of 1 cm water-column in absolute pressure could be detected. The dynamic characteristics of these gauges are mainly determined by the volume of water and the friction losses in the connecting tubes leading to the pressure tapping. In this particular case the connecting tube was about 0.3 m long and the natural frequency of the damped system, estimated from experiments carried out with connecting tubes of different lengths, about 60 c.p.s. No corrections to the measurements are therefore necessary.

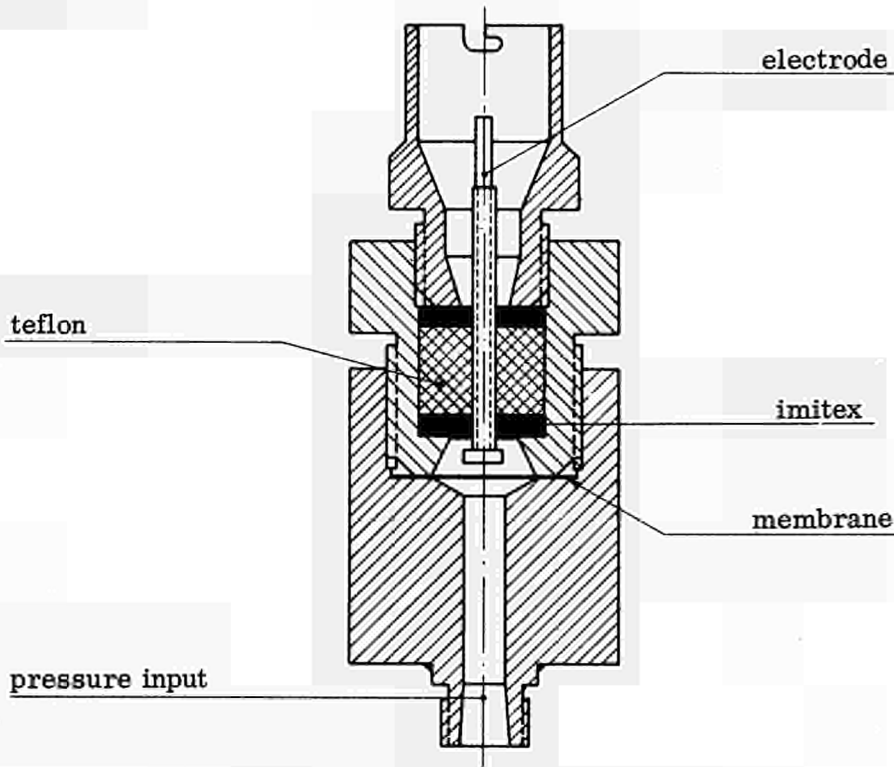


Fig. 2.5 Capacitive pressure gauge

### c. Temperature.

#### Fluid.

For the accurate measurement of the steam and water temperatures and also of differential temperatures for the adjustment of the subcooling, Chromel-Alumel type Soderin (France) thermocouples have been used. In this type of thermocouple there is an Inconel sheath around the wires. The wires and the hot junction are insulated from the sheath by magnesium oxide. The outer diameter of the sheath is 1 mm, except for thermocouple T<sub>1</sub>, see Fig. 2.4, which has an outer diameter of .5 mm. The thermocouples are calibrated at regular time intervals by the Calibration Department of the University, where special calibrating equipment is available. The accuracy of the calibration is  $\pm 8 \mu\text{V}$  which is about  $\pm .2^\circ\text{C}$ . Only those thermocouples have been used which were nearest the I.S.A. standard curve. The special connectors used for connecting the thermocouple wires with the insulated and shielded copper extension leads are placed in a Dewar flask filled with ice. The response characteristics on a step input have been measured. They behave like a first-order system with a time constant of about .4 sec for the 1 mm thermocouples and .06 sec for the .5 mm thermocouple. These response characteristics have been measured by plunging the thermocouples in still water at about  $40^\circ\text{C}$ .

The various thermocouples denoted in Fig. 2.4 are used for the following functions:

condenser control ( $T_{2c}$ ),  
measurement of the saturation temperature ( $T_{2a}$ ),  
measurement of the subcooling ( $T_{2b} - T_{6b}$ ),  
measurement of the inlet temperature ( $T_{6a}$ ),  
control of the preheater in the subcooler circuit ( $T_3 - T_5$ ),  
recording of the steam temperature ( $T_1$ ).

To prevent damage to the preheater, the thermocouples  $T_3$  and  $T_5$  are made to work a little more slowly by increasing the thickness of the sheath. The thermocouples  $T_2$  are shielded for thermal radiation effects from the heating electrode. All measured temperature readings have been corrected for the calibration error.

#### Heating element.

To avoid melting of the heating element at high power ratings, a burn-out detector has been installed as a safety device. This detector works on the principle of a Wheatstone bridge. The upper and lower halves of the heating element act as two arms of this Wheatstone bridge. Therefore, a bronze wire has been fixed inside the heating element at the middle. Any temperature difference between the two parts results in a difference in resistance and will bring the bridge out of balance. This is made visible on a trip-galvanometer. When the needle contacts a preset adjustment, the power on the heating element is switched off. The time between the detection of burn-out and the switching off of the power supply is about 100 msec, of which 80 msec is owing to the main relay and circuit-breaker and 20 msec to the burn-out detector. A special indicator has been developed to indicate which part of the tube has been overheated. Slow variations in the out-of-balance voltage caused for instance by an increase in heating power, are being controlled manually. The occurrence of burn-out is always of a relatively fast nature. The out-of-balance voltage can also be recorded and translated into a temperature variation between the two parts of the heating rod. Owing to the fact that the movement of the needle of the trip-galvanometer has an influence on the voltage at the output, another burn-out detector without a trip-galvanometer has been put in parallel with the original one for recording purposes.

#### d. Void fraction.

One of the important parameters for the evaluation of the performance of a boiling water reactor is the void distribution along the fuel channel. Moreover, for the study of the dynamics of a boiling water reactor it is desired to have a momentary indication of the void fraction at a particular place in a fuel channel. Several techniques can be used for the measurement of the void fraction. In the Laboratory for Heat Transfer and Reactor Engineering of this University three methods are in operation:

1. the  $\gamma$ -ray attenuation method (S5), (H1),
2. the impedance method (S5), (O1),
3. the acoustical method (V2).

In this study the first two methods have been used. The  $\gamma$ -ray attenuation method using the pulse counting technique has been applied for void fraction measurements in steady-state conditions at one fixed location along the channel. The impedance method measuring the conductivity of the two-phase mixture has been used in steady-state as well as in transient conditions at different locations along the channel. It is stressed particularly that both methods measure the void fraction without introducing any disturbance in the two-phase flow.



1. The  $\gamma$ -ray attenuation method.

The  $\gamma$ -ray technique for void fraction measurement has been applied in many laboratories. It is based on the difference in absorption characteristics of  $\gamma$ -rays between water and steam. In the experimental program reported here some special measures have been taken in connection with the construction of the loop and some others to improve the accuracy of the method.

Fig. 2.6. shows a diagram of one of the scintillation counters positioned in the loop. A Thulium-170 source of approximately 300 mCurie and a decay time of 127 days can be

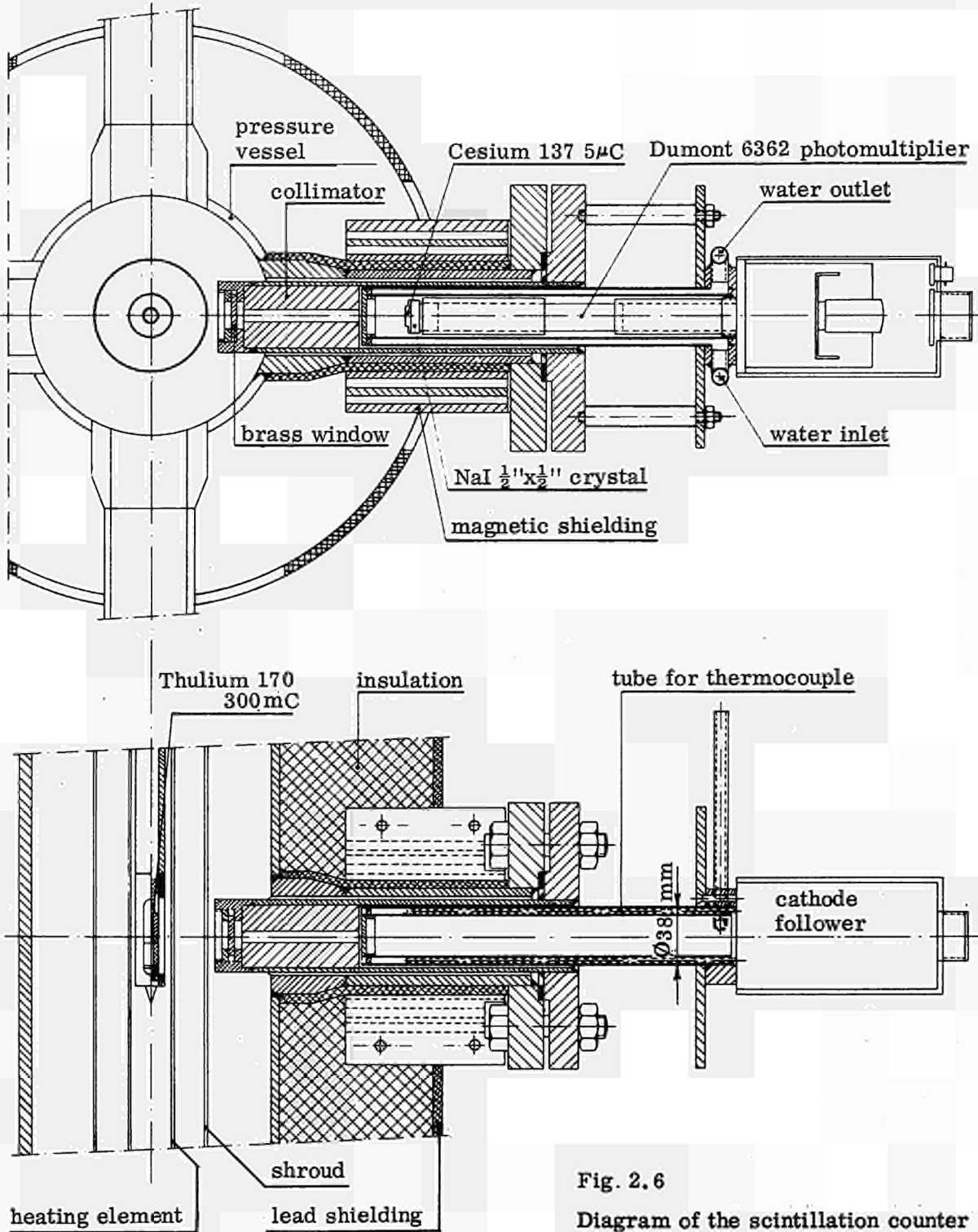


Fig. 2.6  
Diagram of the scintillation counter

positioned inside the heating element. The  $\gamma$ -quanta are going through the two-phase mixture and, after passing a collimator, are detected by four scintillation counters grouped around the riser, each consisting of a NaI(Tl) crystal and a Dumont 6362 photomultiplier. Around the loop, at the position of the Thulium source, a shielding of lead is placed in order to minimize external radiation. A special clipping technique mixes the pulses of the four detectors with a minimum of loss. The pulses are counted by a 10 Mc scaler which is connected to a decimal printer. The housing of the scintillation counters consists of two concentric tubes in which cooling water is circulated, the temperature of which is being recorded. Since the element is heated by direct current there is a strong magnetic field around the loop. As the original mu-metal shielding appeared not to be sufficient, three concentric cast iron rings were placed around the tubes in which the detectors are mounted. A photograph of the scintillation crystal-photomultiplier tube assembly is given in Fig. 2.7. Each photomultiplier is provided with a high voltage unit, see Fig. 2.8. This enables the high voltage of each photomultiplier to be so adjusted that the amplifications of the tubes are the same. It is thus possible to discriminate the Thulium peak (84 keV) in the energy-spectrum in such a way that the best results in the void fraction measurements are obtained. The amplification is automatically controlled by means of a spectrum stabilizer. For the working of the stabilizer a high energy peak in the spectrum is necessary. For this purpose a small Cesium source of 5  $\mu$ Curie is placed in front of the crystal of each photomultiplier. The total amplification of the pulses in the Cesium peak of the photomultiplier and the amplifier is kept constant at an adjusted value by means of a feedback action from the spectrum stabilizer to the high voltage unit, which is indicated on the spectrum stabilizer. In this way changes in amplification caused for instance by temperature effects, magnetic rest-fields and fatigue of the photomultipliers will be corrected automatically.

In all applications of this technique it is assumed that:

- a. the attenuation of the  $\gamma$ -beam is an exponential function of the absorber thickness, which is characterized by a single absorption coefficient;
- b. the ratio of the absorption coefficient and density is independent of temperature;
- c. the absorption in the steam phase is negligible.

The following equation is then used:

$$I_{\alpha} = I_{f,c} \left[ \frac{I_{e,c}}{I_{f,c}} \right]^{\alpha} \quad (2.1.)$$

where  $I$  is the measured intensity and  $\alpha$  the volume void fraction. The indices e, c and f, c refer to an empty and full coolant channel respectively. Equation (2.1.) has been checked in a special set-up in which the  $\gamma$ -beam passed successive layers of air and water. The measured deviation from equation (2.1.) was less than 1%. The intensity with empty and full channel in the pressurized boiling loop is checked every day by measuring in cold conditions the intensities in an empty loop and in a loop completely filled with water respectively. These values have to be corrected for the change in water density with temperature and for the thickness of the water layer between the shroud and the windows in front of the scintillation counters.

Thus:

$$I_{f,c} = I_{e,l} \exp \left[ - \mu_{20} D_h (1+k) \frac{\rho_1(T)}{\rho_1(20^{\circ}\text{C})} \right],$$

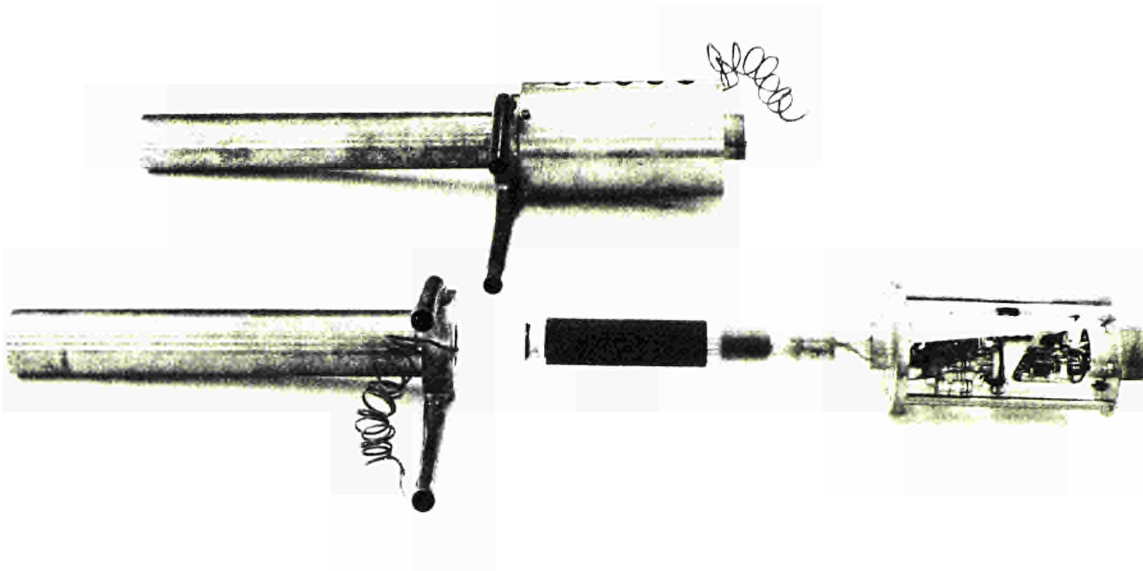


Fig. 2.7 Scintillation crystal-photomultiplier tube assembly

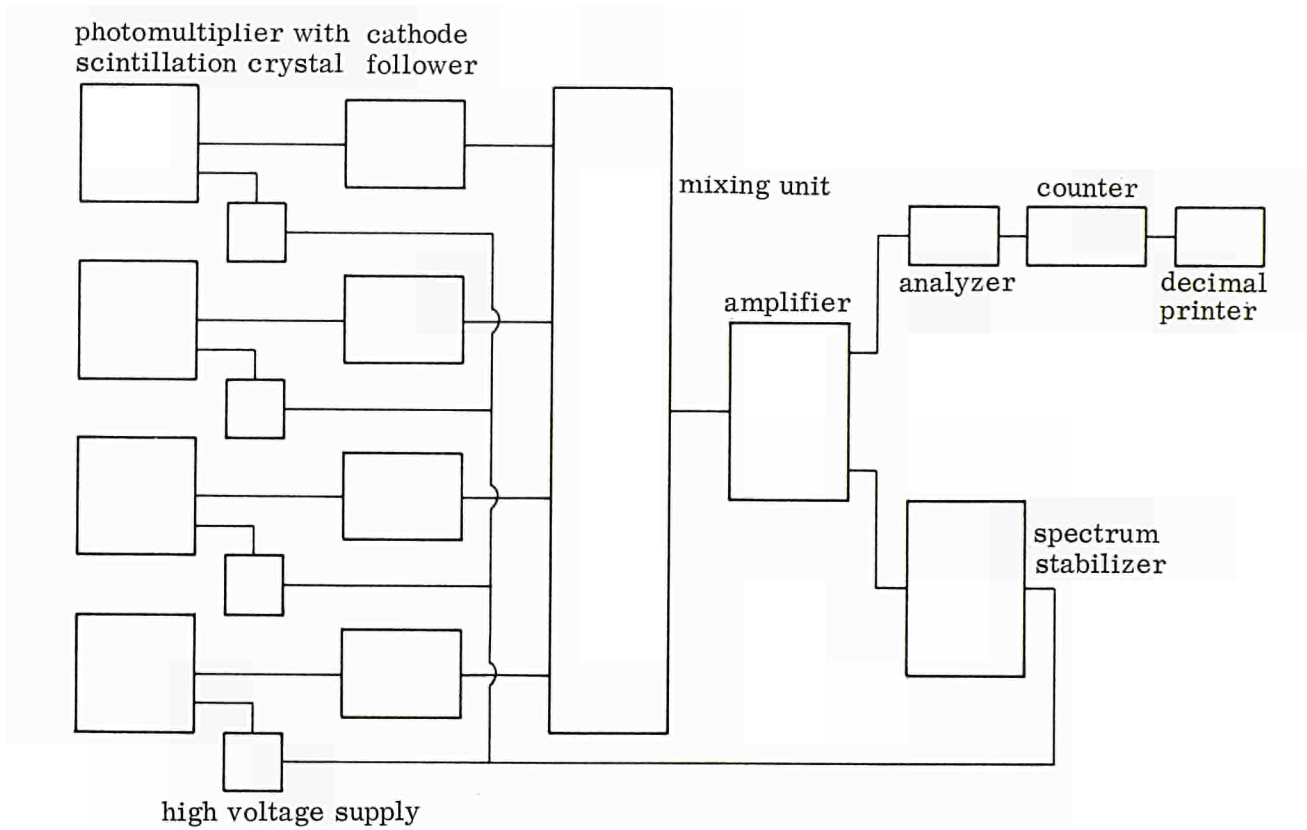


Fig. 2.8 Block diagram of the  $\gamma$ -ray attenuation technique

$$I_{e,c} = I_{e,l} \exp \left[ -\mu_{20} D_h k \frac{\rho_1(T)}{\rho_1(20^\circ\text{C})} \right], \quad (2.3.)$$

where  $I_{e,l}$  is the measured intensity with empty loop,  
 $\mu_{20}$  the absorption coefficient of water at  $20^\circ\text{C}$ ,  
 $D_h$  hydraulic diameter of the test section,  
 $kD_h$  distance between shroud and window,  
 $\rho_1(T)$  density of water at temperature  $T$ ,  
 $\rho_1(20)$  density of water at  $20^\circ\text{C}$ .

The measurement of the temperature effects was made possible by warming up the loop, pressurized at 40 atmospheres with Nitrogen, and by avoiding boiling. The measured values of the empty-to-full ratio of the loop were about 3 to 8% lower than those predicted theoretically by equations (2.2.) and (2.3.) using water densities from the literature. Possibly, this is caused by a temperature influence on the intensity of the  $\gamma$ -rays in empty loop  $I_{e,l}$ . By correcting this quantity by a factor  $C$  which is temperature dependent and of the order of 1.002, the two predicted values of the empty-to-full ratio were closely matched to each other.

The factor  $k$  in equation (2.2.) and (2.3.) has been determined in cold conditions by measuring the intensities with the riser filled with water and an empty downcomer, and the inverse. The influence of the temperature on  $k$  is negligible.

As can be concluded, the determination of the void fraction from  $\gamma$ -ray measurements using the equations (2.1.), (2.2.) and (2.3.) is in fact a determination of a layer thickness. The way in which the void is distributed across the channel must therefore have an effect on the void fraction evaluation. The two extreme phase distributions are those in which the water and the steam phases in the channel are completely separated, and the plane of separation is either cut at right angles by the  $\gamma$ -rays (equation 2.1.) , or is in parallel with them. In the latter case the measured intensity would be

$$I = \alpha I_{e,c} + (1-\alpha) I_{f,c}. \quad (2.4.)$$

The two equations (2.1.) and (2.4.) are equal to each other in case  $\alpha = 0$  and  $\alpha = 1$ . The deviation between the two is greatest when  $\alpha = .5$ . The magnitude of the deviation is dependent on the empty-to-full ratio. It increases with increasing ratio. In the pressurized boiling water loop this ratio, in cold conditions, is about 1.3. Thus the error in using equation (2.1.) for the void fraction measurement may be 3% void. This error decreases with increasing temperature and occurs only when the extreme phase distribution of parallel flow is present.

Another error is introduced by the noise owing to source statistics. The standard deviation of a source with a strength  $Z$  (number of desintegrations per second) during a time  $t$  is  $\sqrt{Zt}$ . Therefore the error in a measurement owing to the statistics of the noise is  $\pm 2\sqrt{It}$ . The number of counts taken in one measurement is about  $10^7$  and the error therefore less than  $\pm .1\%$ . The void fraction is ultimately determined from several intensity measurements, for instance, the  $k$ -factor, the empty-to-full ratio and the measurement at operating conditions. Using the general equation for the stan-

standard deviation  $\sigma_z$  of a function  $z$  of a number of independent statistically varying quantities  $x_i$  with a standard deviation  $\sigma_{x_i}$  :

$$\sigma_z^2 = \sum \left[ \frac{\partial z}{\partial x_i} \cdot \sigma_{x_i} \right]^2, \quad (2.5.)$$

the error in the final result, owing to source statistics could be estimated to be about  $\pm 2\%$  void, concordant with twice the standard deviation.

The dead time of the circuit during which the system is insensitive for  $\gamma$ -quanta has been estimated by measuring the intensities of the four scintillation counters separately and all of them together. The dead time measured in this way is  $3.8 \mu\text{sec}$  at a count rate of 60,000 per second. This value checked perfectly well with measurements made by an oscilloscope.

In all the experiments the determination of the void fraction was based on equations (2.1.), (2.2.), (2.3.). Prior to this, the measured intensities were corrected for the intensity of the Cesium source, the decay time of the Thulium source, the dead time of the circuit and the change in intensity in the empty loop with temperature. Some results of void fraction measurements are given in Fig. 2.9. The heating power in kW is plotted horizontally and the void fraction at the location of the Thulium source vertically. Results of measurements taken at different dates are given for a saturation temperature of 120 and 220°C corresponding to a system pressure of 2.03 and 23.66 ata. As can be concluded the reproducibility is within  $\pm 3\%$  void. Reproducibility was maintained even after dismantling and mounting again the test section.

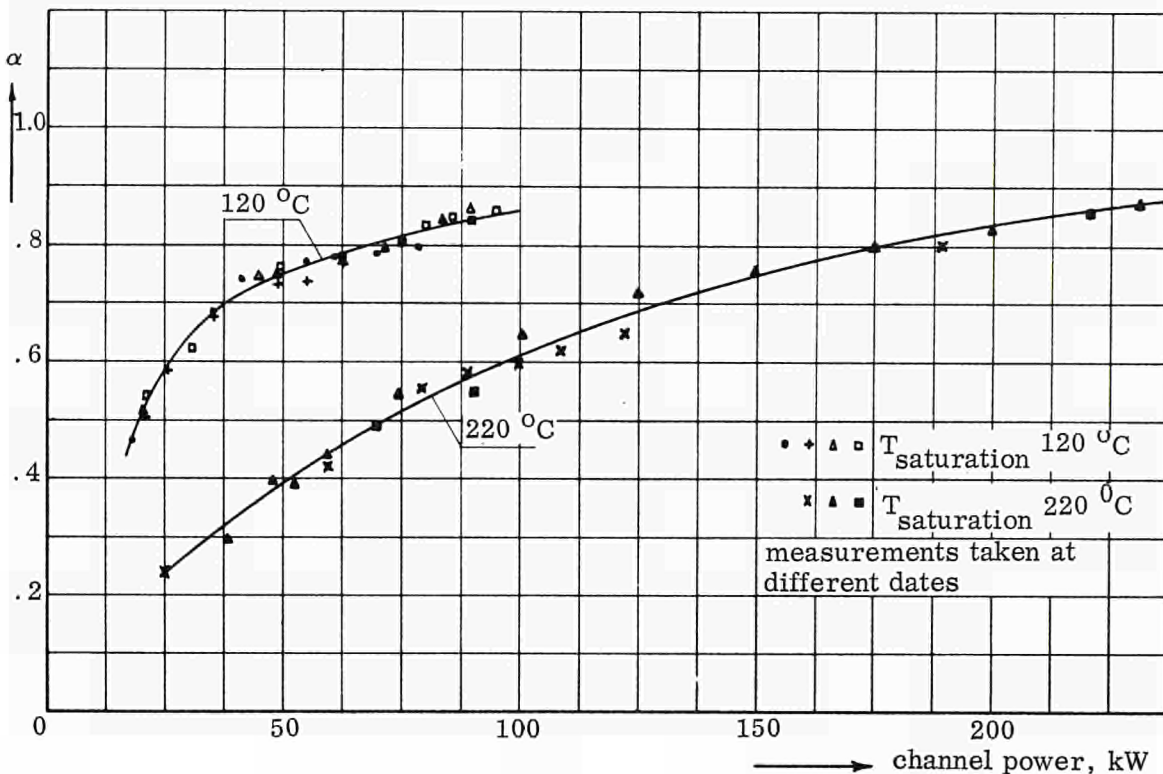


Fig.2.9 Preliminary results of the  $\gamma$ -ray void fraction measurements

## 2. The impedance method.

The technique for measuring the void fraction in a two-phase flow system using the impedance method has been developed for the test section geometry given in section 2.1. The application of this measuring technique is based on the determination of the conductance in a two-phase mixture with respect to that in a one-phase liquid at the same temperature. The heating element is used as the first electrode. In the hull of the shroud four plates are placed at a given axial location, see Fig. 2.10, insulated from the shroud but connected to each other, to act as a second electrode. Nine of these void gauges are located along the coolant channel, see Fig. 2.4. The theoretical basis of this technique was derived by Maxwell (B10), (O1). By assuming an analogy between the electrical conductivity and the dielectric constant of a mixture it follows that

$$\frac{\epsilon - \epsilon_2}{\epsilon + 2\epsilon_2} = \alpha \frac{\epsilon_1 - \epsilon_2}{\epsilon_1 + 2\epsilon_2} \quad (2.6.)$$

where  $\epsilon$  is the conductance of the mixture,  
 $\epsilon_1$  that of the discontinuous phase (steam),  
 $\epsilon_2$  that of the continuous phase (water),  
and  $\alpha$  is the void fraction.

The calibration of the impedance void gauge has been carried out in a perspex loop, filled with water, in which air was blown. The void fraction was taken from the height of the two-phase flow column and was checked by means of static pressure measurements along the height of the loop. Up to void fractions of 40% the difference between the measured values and those predicted by the equation (2.6.) was less than 2% void. Calibrations performed at the Argonne National Laboratory with a similar void gauge up to 90% void were also in good agreement with the theoretically predicted values (M. Petrick, personal communication). In the pressurized boiling water loop a void gauge has been placed at the location of the  $\gamma$ -ray source and the values obtained with both methods could be compared. Some results are given in Fig. 2.11. The difference between the two methods is less than  $\pm 2\%$  void. On the whole the reproducibility of the impedance method is better than that of the  $\gamma$ -ray attenuation method and is less than  $\pm 1\%$  void.

A block diagram of the measuring system is shown in Fig. 2.12. The potentiometer circuit formed by  $R_1$  and  $R_2$  is fed with a 3,000 c.p.s. voltage supplied by an oscillator.  $R_1$  is the resistance of the two-phase mixture and  $R_2$  is a series resistance across which the measuring signal is taken. When  $R_2$  is very small with respect to  $R_1$  (actually about .2% of  $R_1$  at 0% void) the voltage across  $R_2$  is proportional to the conductivity  $1/R_1$  of the fluid. The choice of the 3,000 c.p.s. frequency is a compromise. At high frequencies the capacity of the leads and of the insulation of the gauge has an unfavorable influence on the characteristics of the void gauge. At low frequencies polarization effects become important. A capacitance of 500  $\mu$ F has been connected in series with the void gauge in order to prevent direct currents leaking from the heating element through the water to the measuring system. A separating transformer is incorporated giving the possibility of earthed inputs. After passing a 3,000 c.p.s. band-pass filter the amplitude modulated signal is led to an amplifier and demodulator. The output voltage, after demodulation, is 10 volts dc at 20 mV across  $R_2$ . Beside the direct indication of the output signal on a meter, there are outputs for recording purposes.

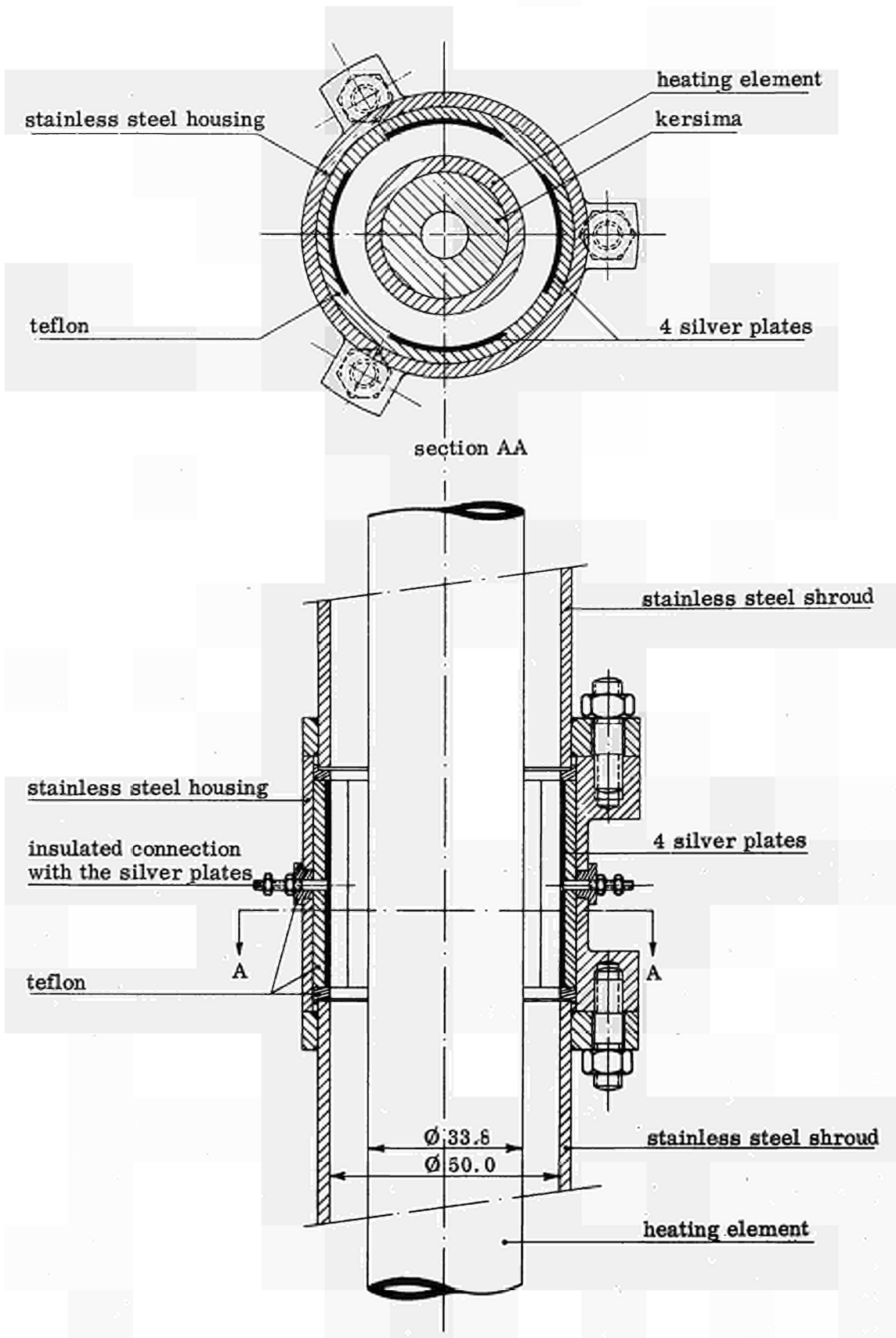


Fig. 2.10 Impedance void gauge

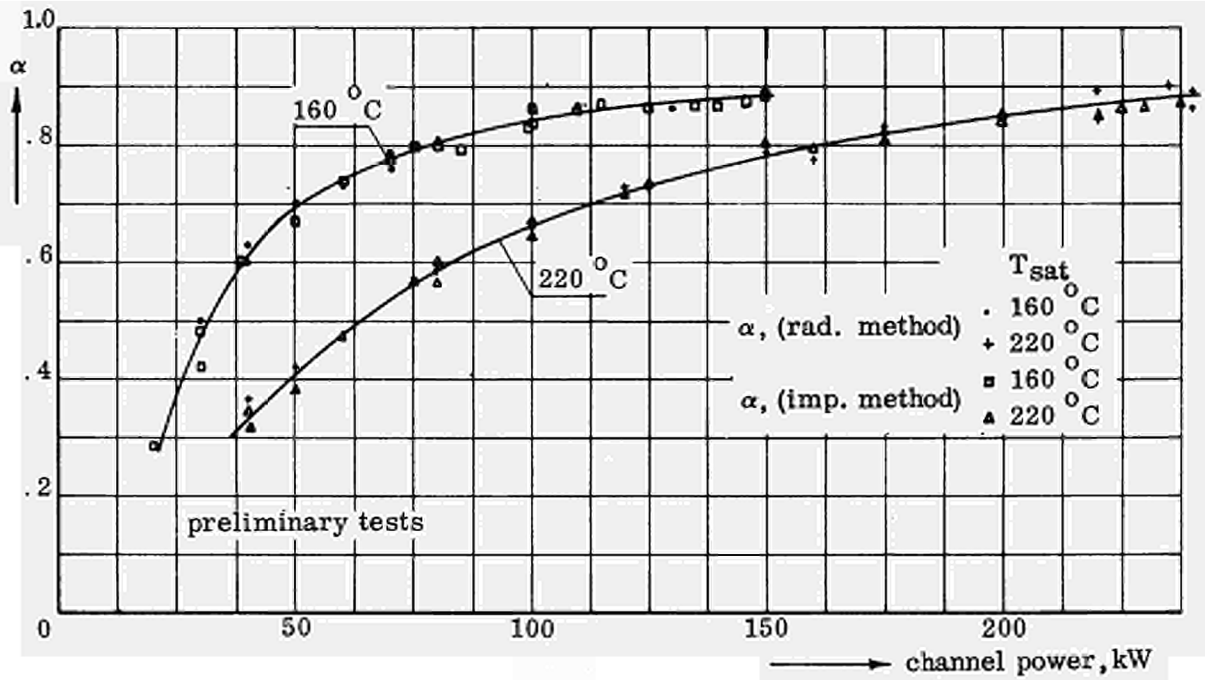


Fig. 2.11 Comparison of  $\gamma$ -ray and impedance void fraction measurements

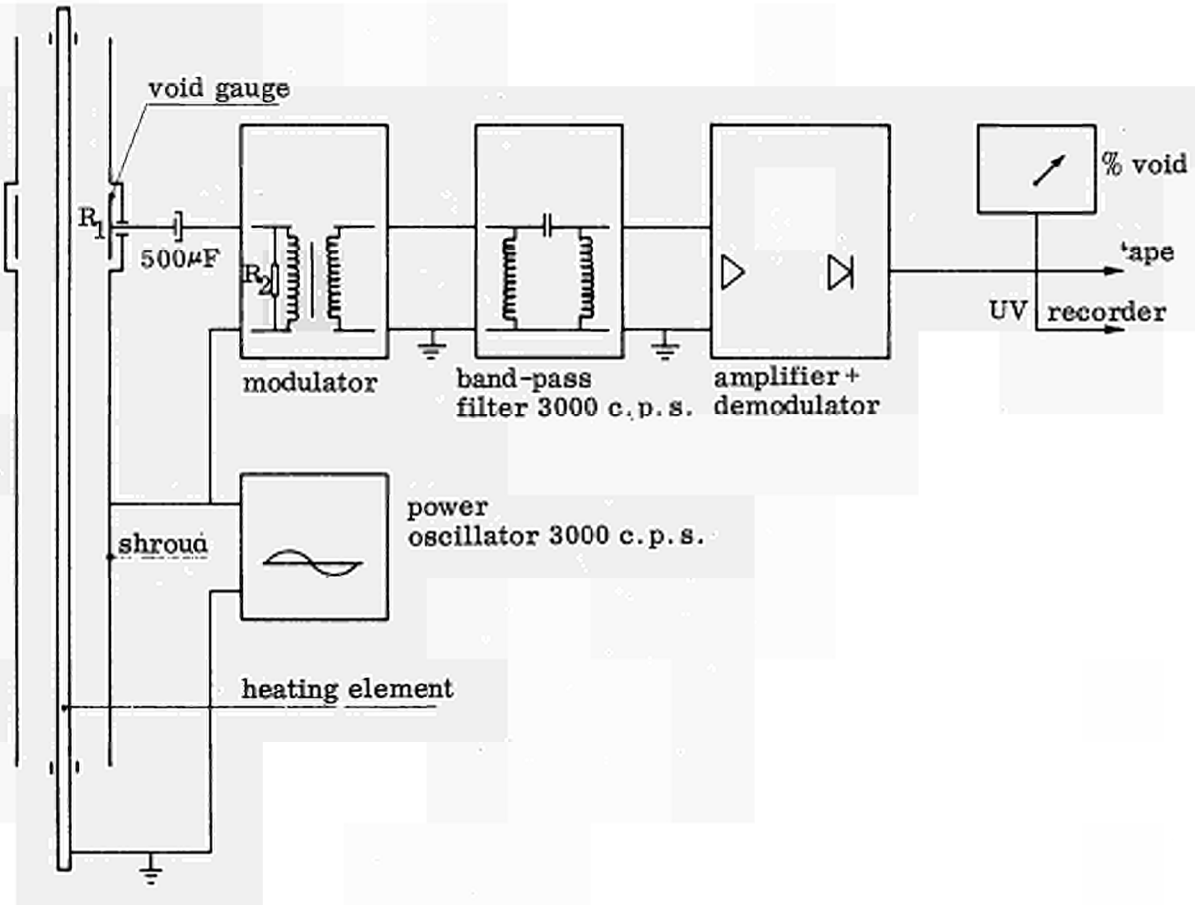


Fig. 2.12 Block diagram of the impedance method



Owing to the fact that the conductance of the water in the pressurized boiling water loop changes with time and temperature, the continuous determination of the 100% water conductance requires the use of a reference gauge, which has the same characteristics as the void gauges. In the beginning, the void gauges 9, 10 and 11, see Fig. 2.4, consisting of parallel plates, and positioned in the downcomer, have been used as reference gauges. In order to increase accuracy, the reading of void gauge 8 positioned in the non-heated part of the coolant channel and with exactly the same dimensions as the other void gauges, was afterwards taken as reference. The adjustable gain of the amplifier is controlled manually on the basis of the reading of this reference gauge. Thus, in actual fact one measures the ratio of the conductance determined by one particular void gauge and that determined by the reference gauge. Differences in temperature of the liquid at the reference gauge and at a particular void gauge as occurring in the experiments had no detectable influence on the measurements. The linearity and stability of the measuring system were excellent. The frequency response characteristics were determined by applying a step input and photographing the rectified output on an oscilloscope. The time necessary to reach the final value was about .7 msec. This means that no corrections were required.

Different configurations of the void gauge have been tested in the perspex loop mentioned. The final construction is shown in Fig. 2.10. To obtain a homogeneously distributed electrical field between the electrodes two measures were taken. First, the surface per unit of height of the four electrode plates together was taken equal to that of the heating element. Secondly, to avoid dispersion of the electrical field, the shroud was placed on the same potential as the electrode plates. The plates are made of silver and embedded in a ceramic ( $Al_2O_3$ ) or teflon ring. The height of the plates was chosen 4.5 cm giving acceptable, not too noisy signals.

#### e. Mass flow rate.

The mass flow rate at the inlet of the coolant channel is established by measuring on a multimanometer the pressure drop across the inlet (pressure tapings 1 and 2 in Fig. 2.4) or the differential pressure from a pitot-tube. The pressure differences  $\Delta p_{1-2}$  and  $\Delta p_{12-13}$  had been calibrated in cold tests in terms of the circulation rate at the inlet of the riser. This calibration was carried out using an especially constructed circuit by which water is pumped through the downcomer and riser and returned to a dump vessel. By measuring the time needed for pumping a known weight of water through the circuit, the water circulation rate could be calculated. Measuring times varied between 270 and 70 sec. The reproducibility of the measuring times in one condition was better than .3%.

Setting

$$\Delta p = k \frac{1}{2} \rho_1 V^2, \quad (2.7.)$$

one can calculate from these tests the factor k as a function of the Reynolds number. In Fig. 2.13 some results are given for Test Section I. Some tests with hot water have been carried out in order to increase the range of Reynolds numbers. Above a Reynolds number of  $3 \times 10^4$ , k is nearly constant and for  $\Delta p_{1-2}$  equal to 1.30 and 1.39 and for  $\Delta p_{12-13}$  equal to 1.45 and 1.30 for Test Section I and II respectively. Under operating conditions the Reynolds numbers are as large as  $4 \times 10^4 - 2.4 \times 10^5$ . A check of the use of equation (2.7.) at these high Reynolds numbers has been obtained by calculating the flow rate from differential pressure measurements made under operating conditions between (a) the pressure tapings 1 and 2, and (b) the tapings 12 and 13 (pitot-tube) and using the appropriate measured values of k. Some results of these calculations are

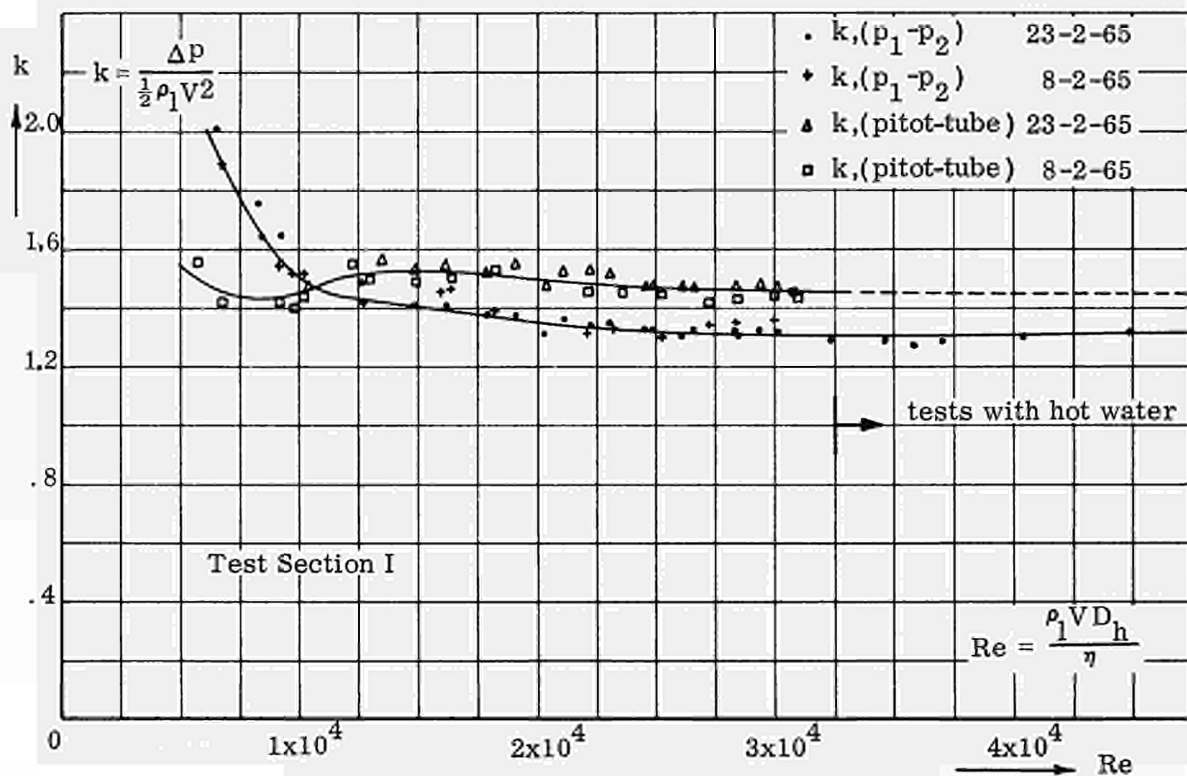


Fig. 2.13 Results of flow calibration tests.

given in Fig. 2.14. The heating power in kW is plotted horizontally, and the circulation rate  $V$  in m/sec related to the cross-section  $A_c$  of the coolant channel is plotted vertically. The values predicted by means of the two methods differed less than  $\pm 3\%$ .

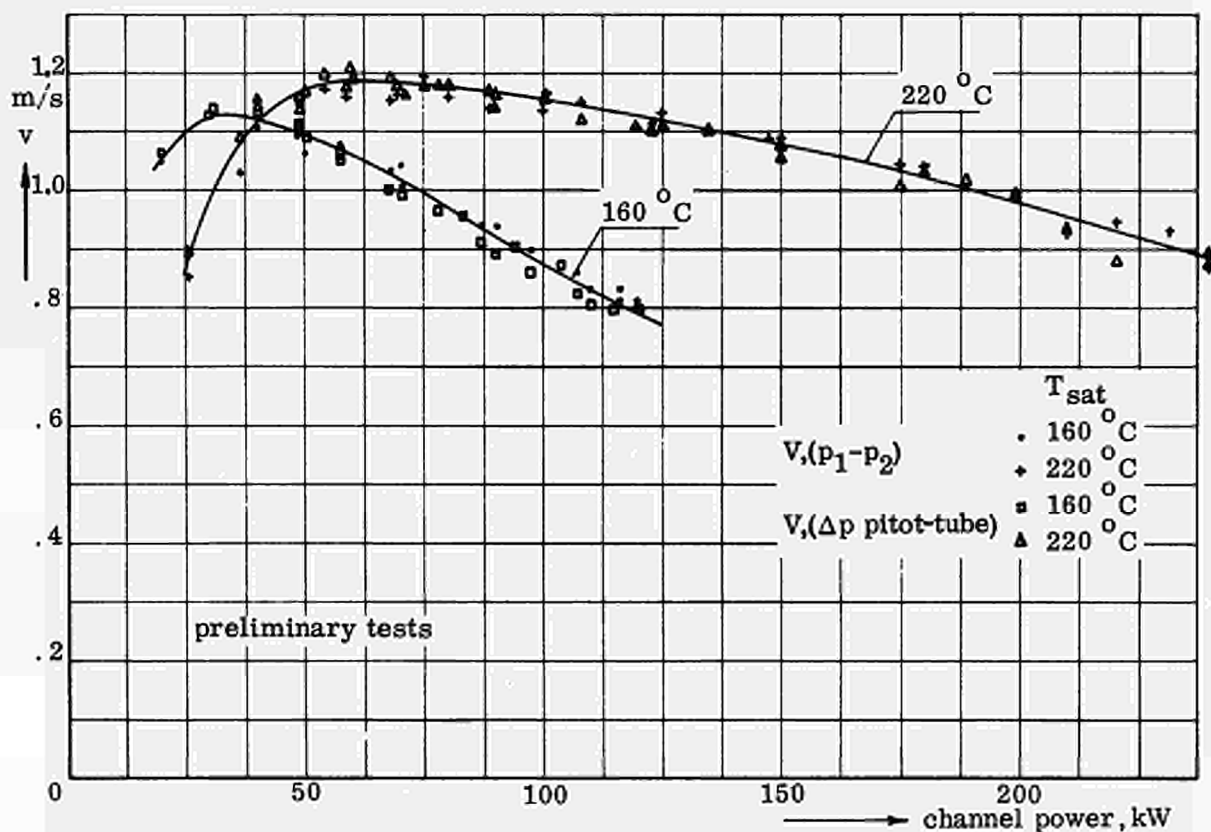


Fig. 2.14 Preliminary results of circulation rate measurements

This means that the flow distribution at the inlet of the riser under operating conditions was about the same as the one in the calibration tests.

During the calibrations the static pressures along the channel (pressure tapings 2 to 10) were measured too. These measurements give an idea of the pressure drop in one phase flow for this particular geometry. The Fanning friction factor  $f$  is equal to  $.00782$  at Reynolds numbers higher than  $3 \cdot 10^4$ . The predicted value for a smooth pipe is  $.00610$  for this Reynolds number. The measured values are about 25% greater than the predicted ones.

For measuring the mass flow rate in transient conditions use is made of commercially available inductive differential pressure gauges, type SEL (England) with a range of  $\pm 25$  and  $\pm 50$  cm water-column. They are connected to the pressure tubes outside the pressure vessels. They were calibrated during steady-state operation against the readings of the multimanometer. The linearity was within 1%. The dynamic characteristics of these pressure gauges together with the connecting tubes and the electronic apparatus consisting of power unit, modulator and demodulator, were measured by recording the output signal on a fast recorder, responding to a step input in the pressure at one side. By taking the natural frequency of the damped system and the logarithmic decrement from the recordings, and by assuming that the behavior of the system can be described by a second-order equation, the dynamic characteristics could be calculated in terms of attenuation and phase shift. The characteristics of the differential pressure gauge connected to the pitot-tube have been plotted in Fig. 2.15. A satisfactory check was obtained by simulating on an analogue computer the corresponding second-order equation and making a recording on a step input. The two recordings were quite similar. All the experimental results have been corrected for phase shift and attenuation.

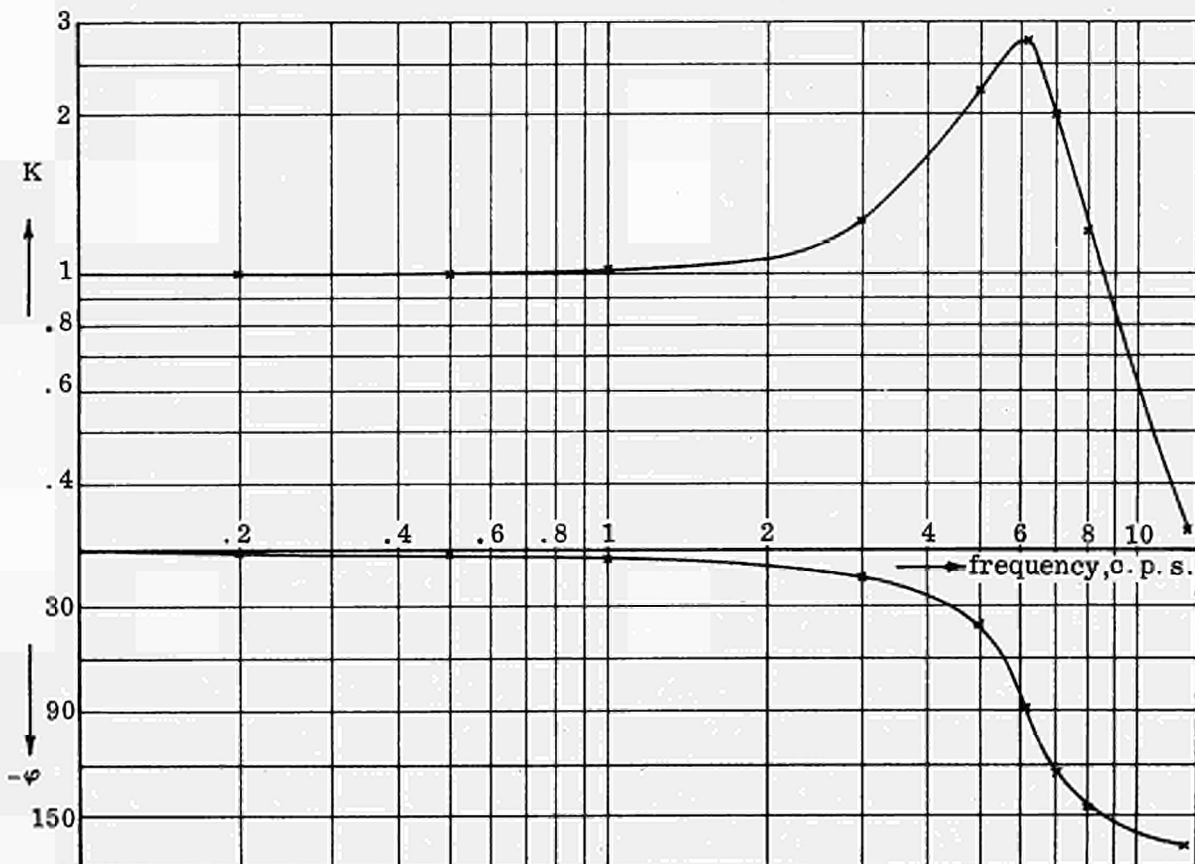


Fig. 2.15 Frequency response of the differential pressure gauge

## 2.4. Recording equipment

### Conventional recorders.

For slow recording purposes use is made of commercially available continuously writing or printing recorders with temperature or mV scales. Most of them have a variable range and the possibility of zero shift and zero suppression. These recorders are calibrated at regular time intervals against a mV-potentiometer with an accuracy of  $\pm .03\%$  of the reading.

### UV-recorder and FM tape recorder.

The signals from the heating power, pressure, temperature, burn-out detector, void fraction and mass flow rate can be recorded at high speeds on a 16-channel Ultra-Violet recorder, type CEC 5-124 (U.S.A.) equipped with photographic paper. For a more detailed analysis the signals can also be recorded on a 14-channel Frequency Modulated magnetic tape system, type Ampex FR 1300 (U.S.A.), that can be operated at 6 different speeds. Before recording, the signals had to be adapted, filtered and amplified. All transmitting lines were checked on their linearity. The attenuation and phase shift introduced by the different elements were measured using the Frequency Response Analyzer. If necessary, all signals were corrected for the dynamic characteristics of the transmitting lines. The signals were recorded together with calibration signals of known frequency and amplitude in order to avoid any confusion on adjustment of the amplification or attenuation of the different elements.

### Datalogger.

In the analyzing program extensive use is made of a datalogger built by Philips Ltd. (Netherlands) on a specification from the Technological University. The datalogger converts analogue signals into a digital code and is especially designed for digitizing signals for performing noise analysis. The datalogger can be used in combination with a magnetic tape system or directly on line with the process.

It consists of:

- a. a 10-channel scanner, which can be expanded to 500 channels without large costs;
- b. an amplifier with an adjustable range setting between 10 and 10,000 mV;
- c. an analogue to digital converter;
- d. a paper tape puncher.

The scanner is equipped with dry-reed relays with gold contacts. These types of relays allow of signals from thermocouples to be converted as well. Any number of scanning points between 1 and 10, forming one cycle, can be selected. By means of a patch panel the sequence of the input signals can be programmed arbitrarily. The sampling rate is controlled by a crystal oscillator in combination with frequency dividers. The time interval between two scanning points is therefore constant between very narrow limits and is exactly known. The sampling time, too, can be adjusted separately. These characteristics are very important when one wants to perform a noise analysis of a signal on a digital computer. The amplifier has an input impedance of 1,000 M $\Omega$ , while the cut-off frequency is adjustable. The output voltage is  $\pm 10$  volts. Owing to the fact that only positive voltages can be converted, a voltage of 5 volts is added to the output signal from the amplifier. The analogue to digital converter has a rate of 1,000 conversions per second. After conversion it gives a command to the puncher. This puncher is a Westrex teletype paper puncher with a speed of 110 characters per second. It is placed on a separate console in order to avoid vibrations. The applied code is the

1 2 4 8 code for the IBM 1620 computer. The punched information consists of the number of the channel (two digits), the signal (three digits) and an end-of-line mark (one digit). The latter can be put after each signal or after each cycle. The channel number and the end-of-line mark can be skipped. Instead of the puncher, a printer or a magnetic tape can be used as recording apparatus. With the teletype puncher a scanning rate of 25 points per second can be reached if only the signal is punched. The datalogger can be operated manually or automatically. The number of cycles scanned is indicated on a counter. The measuring value of the signal can be observed continuously on a panel. The accuracy is checked at regular time intervals by applying a known voltage to the datalogger. No corrections are needed.

## 2.5. Analyzing equipment

### Analogue computer.

An analogue computer was used for studying the mathematical description of the behavior of a boiling water system. The analogue computer is a PACE R-231 equipped with 80 amplifiers, 7 multipliers, 5 function generators, 4 comparators, an automatic print-out device, an XY plotter and a multichannel recorder, type Sanborn (U. S. A.).

### Digital computer.

An extensive use was made of digital computers in analyzing the experimental results and in performing studies on the behavior in steady-state and transient conditions of a boiling water system. Among other things a digital computer program (A1) was written calculating the transfer function from two noisy but correlated signals by computing autocorrelations and cross-correlations, and spectral power density and cross-power spectral density curves.

### Frequency response analyzer.

In the experimental program transfer functions were measured from heating power to the dependent variables as mass flow rate, void fraction etc. This means that the power was modulated with a sine and the amplitude ratio and phase shift were measured of a physical quantity with respect to the oscillating input power. In this type of measurement difficulties may arise owing to the presence of noise on the output signal induced by the boiling process and by magnetic or electrical fields, mostly with far greater amplitudes than the response to the input signal. To reject the induced noise, a Fourier analysis of the output signal is made by means of a special purpose analogue computer called the Transient Frequency Response Analyzer made by Boonshaft Inc. (U. S. A.). A block diagram of this apparatus is given in Fig. 2.16. The oscillator produces a voltage  $x(t) = x_0 \sin \omega t$  of which the amplitude  $x_0$  and the frequency  $f$  can be adjusted in the range of 0-50 V r.m.s. and 0.001 to 1,000 c.p.s. respectively, and which excites the system under test. In addition, the oscillator produces two reference signals  $\sin \omega t$  and  $\cos \omega t$ . The response of the system will be of the form:

$$y(t) = x_0 |H(j\omega)| \sin \{ \omega t + \varphi(\omega) \} + n(t) . \quad (2.8)$$

The term  $n(t)$  represents all noise components and harmonics excited in the system. The amplitude ratio  $|H|$  and phase angle  $\varphi$  can be determined by multiplying the res-

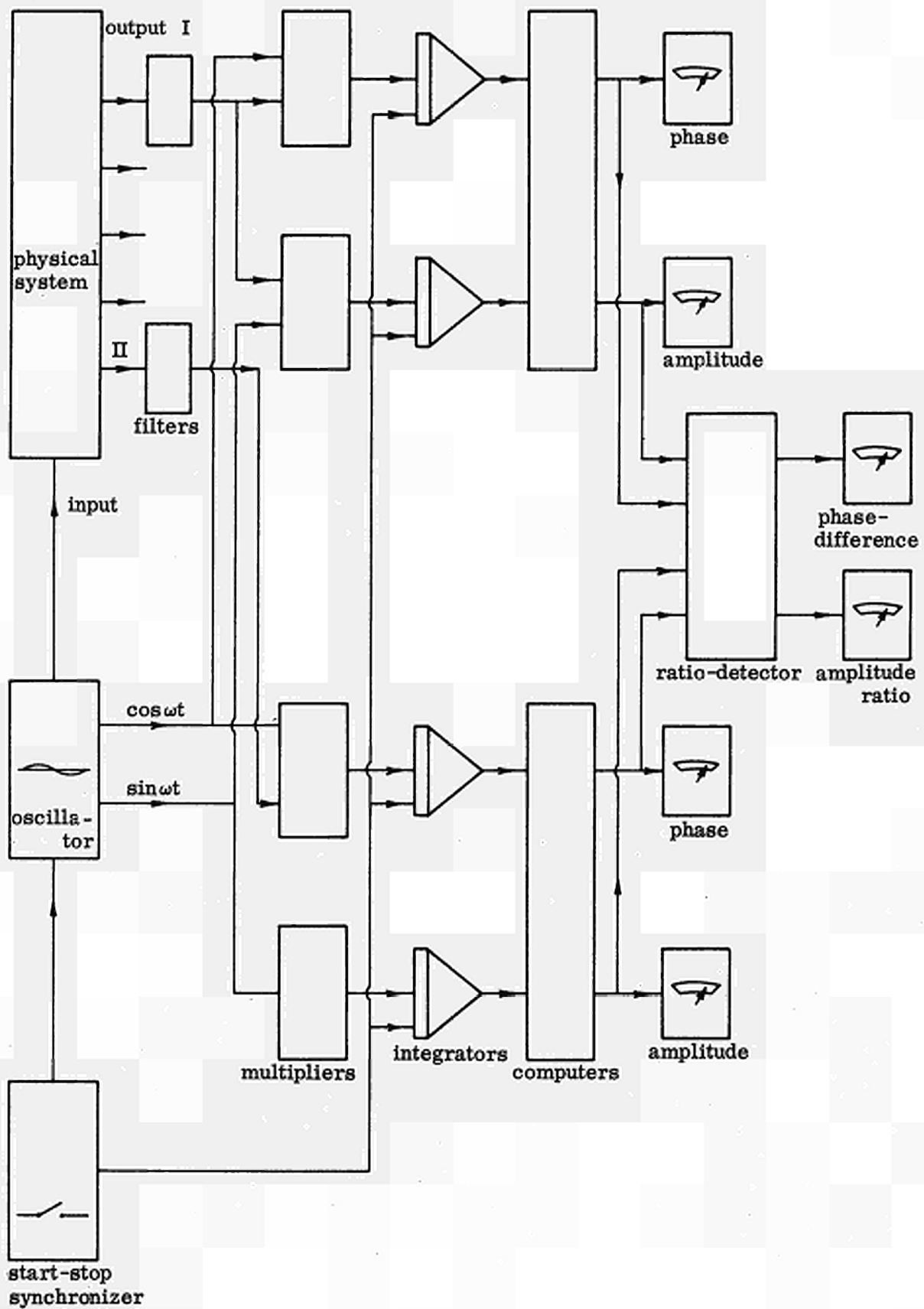


Fig. 2.16 Block diagram of the Frequency Response Analyzer

ponse signal with  $\sin \omega t$  and  $\cos \omega t$  respectively, and by integrating the product over a time  $T$ , which is a whole number  $m$  of periods. Thus

$$A = \frac{1}{T} \int_0^T y(t) \sin \omega t dt , \quad (2.9.)$$

$$B = \frac{1}{T} \int_0^T y(t) \cos \omega t dt , \quad (2.10.)$$

with

$$T = m \frac{2\pi}{\omega}$$

or

$$A = \frac{x_0}{2} |H| \cos \varphi + \frac{1}{T} \int_0^T n(t) \sin \omega t dt , \quad (2.11.)$$

$$B = \frac{x_0}{2} |H| \sin \varphi + \frac{1}{T} \int_0^T n(t) \cos \omega t dt . \quad (2.12.)$$

If the noise component  $n(t)$  contains harmonics of the input signal only, the integrals in the last two equations become zero, independent of the number  $m$  used in the equations. If other frequency components are present, the integrals will approach zero for  $m \rightarrow \infty$ .

For large integration times it then follows that:

$$H = \frac{2}{x_0} \sqrt{A^2 + B^2} , \quad (2.13.)$$

$$\varphi = \text{arctg} \frac{B}{A} . \quad (2.14.)$$

In the block diagram the multipliers and integrators are indicated. The output signal from the system passes a band-pass filter before going to the multiplier. The band-pass filters remove from the signal d.c., low, and high frequency noise. With this apparatus it is possible to carry out frequency response measurements between any two points in a system. The point-to-point frequency response measurement is desirable when the response must be measured between two points I and II, see Fig. 2.16, if the

system cannot be excited in either point. By means of a channel selector any combination can be chosen. In all the experiments to be reported the point-to-point method has been applied. The computers calculate the phase and amplitude ratio according to equations (2.13.) and (2.14.) with respect to the reference signal. The in-phase and out-of-phase components, equations (2.11.) and (2.12.), can also be read. In the ratio detector the amplitude ratio and phase shift between the signals I and II is calculated. The integration time T can be adjusted between 0 and 1,000 seconds by means of the synchronizer, which starts and stops the integration. It is also possible to use this apparatus in combination with a magnetic tape system to calculate the frequency response between two recorded response signals from the system to a sinusoidal or ramp input. The calculating process is then started by a pulse from the magnetic tape recorder. The accuracy of the calculated phase angle is within  $\pm 2^{\circ}$  and that of the amplitude ratio better than .25 dB. The input impedance is 50 M $\Omega$ .

ISAC noise correlator.

The noise correlator ISAC (Instrument for Statistical Analog Computation), made by NORATOM (Norway), is a special purpose analogue computer and can be used in practical applications of statistical methods to problems in automatic control (T1). It can be characterized as follows:

- a. three electrical signals can be recorded simultaneously on a closed-loop magnetic tape in a frequency range of 0-200 c. p. s. Eight different tape speeds can be selected while also the length of the closed loop tape can be changed;
- b. from the recorded signals, it calculates:
  1. the autocorrelation and the cross-correlation;
  2. the spectral power density and the amplitude density curves;
  3. the first order probability distribution functions;
 all computations are performed at the maximum tape speed;
- c. all calculations are performed automatically and the results presented graphically on an XY-recorder.

In this program only autocorrelations, cross-correlations and spectral power density curves have been computed by this correlator.

The autocorrelation is defined as:

$$\varphi_{xx}(\tau) = \lim_{T \rightarrow \infty} \frac{1}{T} \int_0^T x(t) x(t+\tau) dt, \quad (2.15.)$$

where T is the sampling time, x(t) the signal and x(t+ $\tau$ ) the same signal but a time  $\tau$  shifted with respect to x(t). The autocorrelation measures the degree of correlation within one signal and characterizes the sequence of values in a random function of time. The value of the autocorrelation at  $\tau = 0$  is equal to the total spectral power in the signal, presuming that the mean value of the signal is zero.

The cross-correlation is defined as:

$$\varphi_{xy}(\tau) = \lim_{T \rightarrow \infty} \frac{1}{T} \int_0^T x(t) y(t+\tau) dt \quad (2.16.)$$

The cross-correlation expresses the degree of interrelationship between two random variables.



By a Fourier transformation of equation (2.15.) and (2.16.) the spectral power density and the cross-power spectral density are obtained:

spectral power density:

$$\Phi_{XX}(f) = \lim_{T \rightarrow \infty} \frac{2}{T} \int_0^T \varphi_{XX}(\tau) \exp(-j\omega\tau) d\tau \quad , \quad (2.17.)$$

cross-power spectral density:

$$\Phi_{XY}(f) = \lim_{T \rightarrow \infty} \frac{2}{T} \int_0^T \varphi_{XY}(\tau) \exp(-j\omega\tau) d\tau \quad . \quad (2.18.)$$

The cross-power spectral density is a complex function of the frequency  $f$ .

A block diagram of part of the system is given in Fig. 2.17. It shows the recording, playback, correlator and power spectrum sections of the apparatus. There are two magnetic heads, A and B, either containing three channels interleaved. One head is fixed, the other is movable along a slide by a motor-driven spindle. Each input signal is recorded on two tracks on the tape, one by either head. The three input channels are identical. The input signal is applied to a d.c. amplifier followed by an effective low-pass filter. Pulse-frequency modulation is employed and the modulated signal is recorded on the tape loop as a square-wave current saturating the tape.

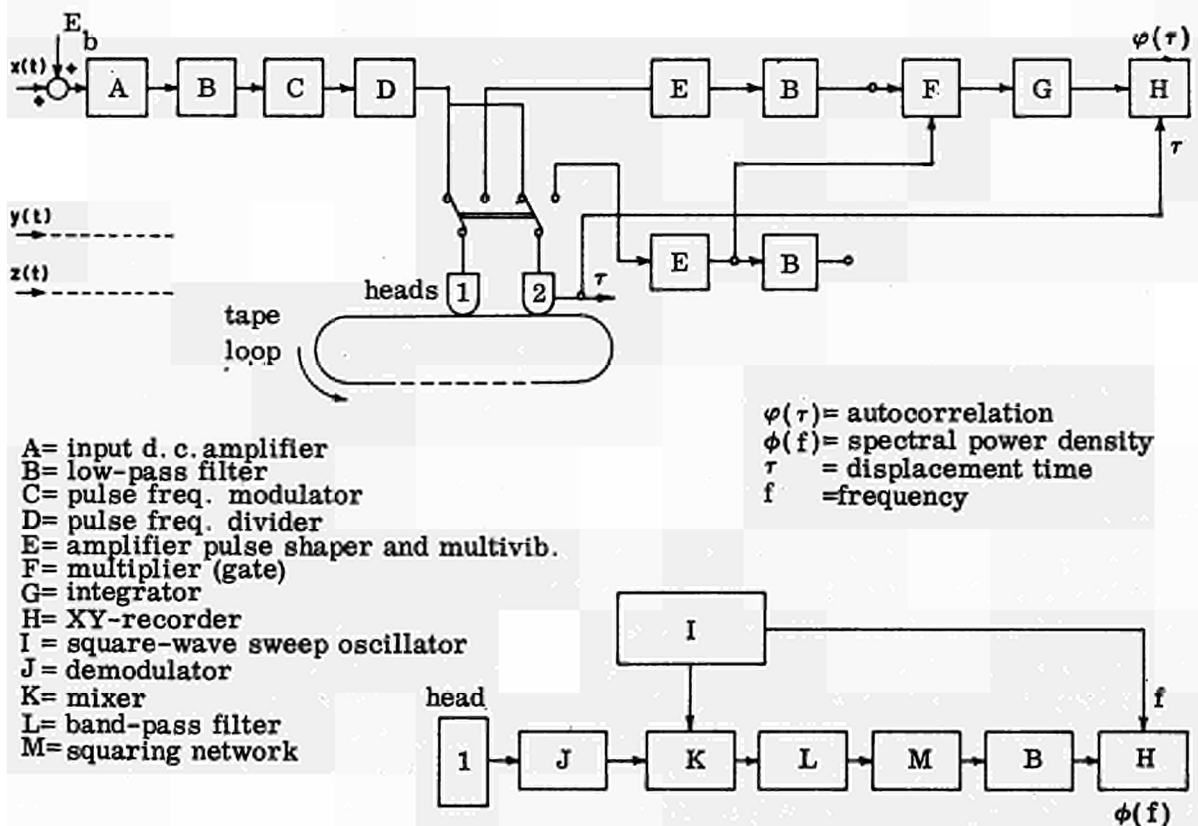


Fig. 2.17 Block diagram of the Noise Correlator.

The correlation functions are obtained by integrating the product of the signals from the heads A and B during one turn of the closed-loop magnetic tape. After integration, the result is automatically plotted on the XY-recorder. The integrator is reset to zero and the movable head is advanced one step and another computing cycle is automatically started. Every step of the movable head represents one value of the displacement time  $\tau$ . The magnitude of each step is chosen at either 1 mm or .25 mm, producing an apparent time displacement of 3.18 msec or .8 msec. The length of the total displacement is 100 mm. The real time displacement equals the product of the apparent time displacement and the playback to recording speed ratio.

The power density curve or the spectral power per unit bandwidth of a signal is not obtained by a Fourier transformation of the autocorrelation, but by passing the signal together with that from an adjustable sweep oscillator through a narrowband-pass filter. By squaring the output of this filter the power content at a certain frequency is obtained.

The power density computations are used for establishing the onset of severe hydraulic oscillations in a boiling channel. In some cases the correlation functions have been used for a characterization of particular phenomena. The ISAC has always been used in combination with the FM tape system mentioned before.

### 3. Experimental results

#### 3.1. Introduction

In the following the results obtained in the experimental program are given. The presentation of the results is split up into three parts. In section 3.2. the characteristics in steady-state conditions of the naturally circulating coolant channel are dealt with. Then, in section 3.3. the onset and characteristics of hydraulic oscillations are described. Next, in section 3.4., the results of the stability measurements using frequency response techniques are reported. Finally, the effect of a change in the water level on the results is discussed in section 3.5.

Before starting a series of measurements, the following routine has to be adhered to:

- a. measuring the intensity of the  $\gamma$ -rays in the empty loop with positioned Thulium source;
- b. filling up the loop with demineralized water;
- c. deaeration of the multimanometer, subcooler, various pressure gauges and, subsequently, readjusting the desired water level;
- d. measuring the intensity of the  $\gamma$ -rays in the filled loop;
- e. warming up the water with low electrical power on the heating element, and checking on the proper elongation of the heating element;
- f. after the water boils and steam is blown off, degassing the loop at about 2 atmospheres; condensed steam and air are taken off directly after the condenser; this procedure is continued until the temperature of the condensate is within a few degrees of the saturation temperature;
- g. approaching a steady-state condition for a preselected saturation temperature (system pressure), subcooling and channel power.

This whole procedure takes about two hours.

For a given geometry, the hydraulic behavior of a natural circulation loop is basically determined by its independent variables:

- a. the total heat input,  $Q$ ;
- b. the system pressure or the corresponding saturation temperature,  $T_{\text{sat}}$ ;
- c. the temperature at the inlet of the coolant channel  $T_{\text{in}}$  or the corresponding subcooling  $\Delta T_{\text{sub}} = T_{\text{sat}} - T_{\text{in}}$ .

The values of the saturation temperatures have been selected at 120, 160, 200, 220 and 234°C for Test Section I and at 120, 200 and 234°C for Test Section II. In Table 3.1. the main physical data of steam and water at these saturation temperatures are given. The influence of subcooling on the hydraulic behavior has been traced systematically at 200°C saturation temperature for both test sections. The channel power is a variable, which is either increased in steps of 5 or 10 kW, or modulated sinusoidally, after which measurements are taken. In all experimental series, the water level at the start was 4.5 cm above the exit of the coolant channel. During operation, the water level read off the water level gauge placed at the top of the cylindrical part of the loop differed at most 3 cm from the initial value, depending on the prevailing conditions. It has been checked continuously if, owing to poor separation of the steam and water phases, steam was present in the downcomer (steam carry-under). This would result in

Table 3.1. Physical data.

| $T_{sat}$<br>°C | p<br>ata | p<br>$\frac{N}{m^2}$<br>( $\times 10^5$ ) | $\rho_1$<br>$\frac{kg}{m^3}$ | $\rho_s$<br>$\frac{kg}{m^3}$ | $\eta_1$<br>$\frac{Nsec}{m^2}$<br>( $\times 10^{-6}$ ) | $\eta_s$<br>$\frac{Nsec}{m^2}$<br>( $\times 10^{-6}$ ) | $H_1$<br>$\frac{J}{kg}$<br>( $\times 10^3$ ) | $H_s$<br>$\frac{J}{kg}$<br>( $\times 10^3$ ) | $e_p$<br>$\frac{J}{kg}$<br>( $\times 10^3$ ) | c<br>$\frac{J}{kg^\circ C}$<br>( $\times 10^3$ ) | $\left[\frac{\partial p}{\partial T}\right]_{sat}$<br>$\frac{N}{m^2 \circ C}$<br>( $\times 10^5$ ) |
|-----------------|----------|---|------------------------------|------------------------------|--|--|--|--|--|--|--|
| 120             | 2.03     | 1.985                                     | 943.1                        | 1.122                        | 234  | 13.40  | 503.5  | 2704.2                                       | 2200.7                                       | 4.244  | .0630  |
| 160             | 6.30     | 6.180                                     | 907.4                        | 3.260                        | 172  | 15.22  | 675.2  | 2756.5                                       | 2081.3                                       | 4.334  | .1575  |
| 200             | 15.86    | 15.551                                    | 864.7                        | 7.857                        | 135  | 17.00  | 851.8  | 2793.7                                       | 1941.9                                       | 4.490  | .3256  |
| 220             | 23.66    | 23.201                                    | 840.3                        | 11.61                        | 125  | 17.94  | 943.0  | 2803.4                                       | 1860.4                                       | 4.612  | .4441  |
| 234             | 30.68    | 30.089                                    | 821.8                        | 15.04                        | 118  | 18.63  | 1008.4                                       | 2805.5                                       | 1797.1                                       | 4.724  | .5425  |

lower circulation rates and higher exit void fractions, and might possibly precipitate the onset of unstable operation conditions. Observing the signals from the impedance void gauges 9, 10 and 11, see Fig. 2.4, might indicate that steam carry-under was not present.

### 3.2. Steady-state quantities

#### 3.2.1. Experimental procedure.

By controlling the condenser and the subcooler in such a way that the heat removal from the loop is precisely compensated by the electrical power input, steady-state conditions were obtained. When the recordings of the saturation temperature  $T_2$  and the subcooling ( $T_3 - T_5$ ) were indicative of a stable system, the following measurements were made:

- measurement of the  $\gamma$ -ray intensity;
- conductivity measurements with the impedance void gauges 0-7, see Fig. 2.4, using void gauge 8 as reference (see section 2.3.);
- measurement of the pressure drop across the inlet of the channel and the differential pressure from the pitot-tube ( $\Delta p_{1-2}$  and  $\Delta p_{12-13}$  respectively);
- measurement of the static pressures along the channel ( $p_2$  to  $p_{11}$  in Fig. 2.4);
- fluid temperatures and subcooling measurements;
- measurement of the heating power, current and voltage;
- measurement of the absolute system pressure and water level.

From measurements (a) and (b), the volume void fraction was calculated with the aid of equations (2.1.) and (2.6.). It should be stressed that these void fractions represent values averaged as regards the cross-section as well as through time. They are the mean values of a very noisy signal. From the readings mentioned under (c) the circulation rate, expressed in meters per second, was calculated using equation (2.7.) and the experimentally determined k-factor. The measured static pressures (see sub d) were transformed into Newtons per square meter and, finally, the fluid temperatures and measured subcoolings (see sub e) were corrected for instrumental and calibration errors. No corrections were applied to the heating power and pressure. After the readings had been taken, the heating power was increased by steps of 5 to 10kW, and, when the process was found stable again, a new set of measurements at the same pressure and subcooling was carried out. This procedure was continued until flow oscillations

started or a burn-out condition occurred. After that, a different pressure or subcooling was adjusted and a new series made. A number of measurements was repeated as a check on the reproducibility.

### 3.2.2. Results.

A prerequisite to an understanding of the dynamic behavior of a two-phase flow is an understanding of the characteristics of a boiling water channel in steady-state conditions. The performance of a natural circulation boiling channel must satisfy the equation:

$$\sum(\Delta p) = 0 \quad . \quad (3.1.)$$

This equation states that the summation of the pressure drop around the closed loop, consisting of riser and downcomer, must be zero for steady-state flow conditions. In a differential element of length with a constant flow area, the overall pressure drop may be written as the sum of the frictional, acceleration and hydrostatic pressure drops of the mixture.

$$\Delta p = \Delta p_f + \Delta p_a + \Delta p_h \quad . \quad (3.2.)$$

A steady-state condition of the flow in the boiling channel is brought about by an equilibrium of the three terms of equation (3.2.) integrated over the riser and the downcomer to the effect that equation (3.1.) is satisfied. In evaluating the three terms in equation (3.2.), the earlier mentioned volume void fraction  $\alpha$ , defined as:

$$\alpha = \lim_{\Delta z \rightarrow 0} \frac{\text{steam volume in } A_c \Delta z}{\text{volume of } A_c \Delta z} \quad , \quad (3.3.)$$

plays an important rôle. ( $A_c$  = cross-sectional area )

In steady-state conditions, extensive experimental series of measurements have been carried out to determine the natural circulation rate and the longitudinal void and pressure distribution as functions of the channel power, the saturation temperature (system pressure), the subcooling rate and of the hydraulic diameter. By measuring the longitudinal void and pressure distribution, more detailed information on the two-phase flow characteristics is obtained. Results of these measurements are given in Figs 3.1 to 3.13. In the following, these results will be discussed.

#### Recirculation rate.

In Fig. 3.1 results are given of the measured water circulation rate as function of the channel power at various saturation temperatures for Test Section I. As is shown, there is a maximum in the circulation rate versus channel power curve. At low power the driving head ( $\Delta p_h$  in equation 3.2.) increases as a result of the increase in void. This produces the rising part of the curve. At high channel power the two-phase friction and acceleration-pressure drops ( $\Delta p_f$  and  $\Delta p_a$  in equation 3.2.) become progressively more important (the two-phase friction-pressure drop increases roughly with  $(1-\alpha)^{-2}$ ) resulting in a decrease in the circulation rate with increasing channel power. At the maximum, an incremental increase in channel power causes the frictional and acceleration losses to increase by the same amount as the driving head. At high system pressures the maximum in the circulation rate shifts to higher power levels, whi-

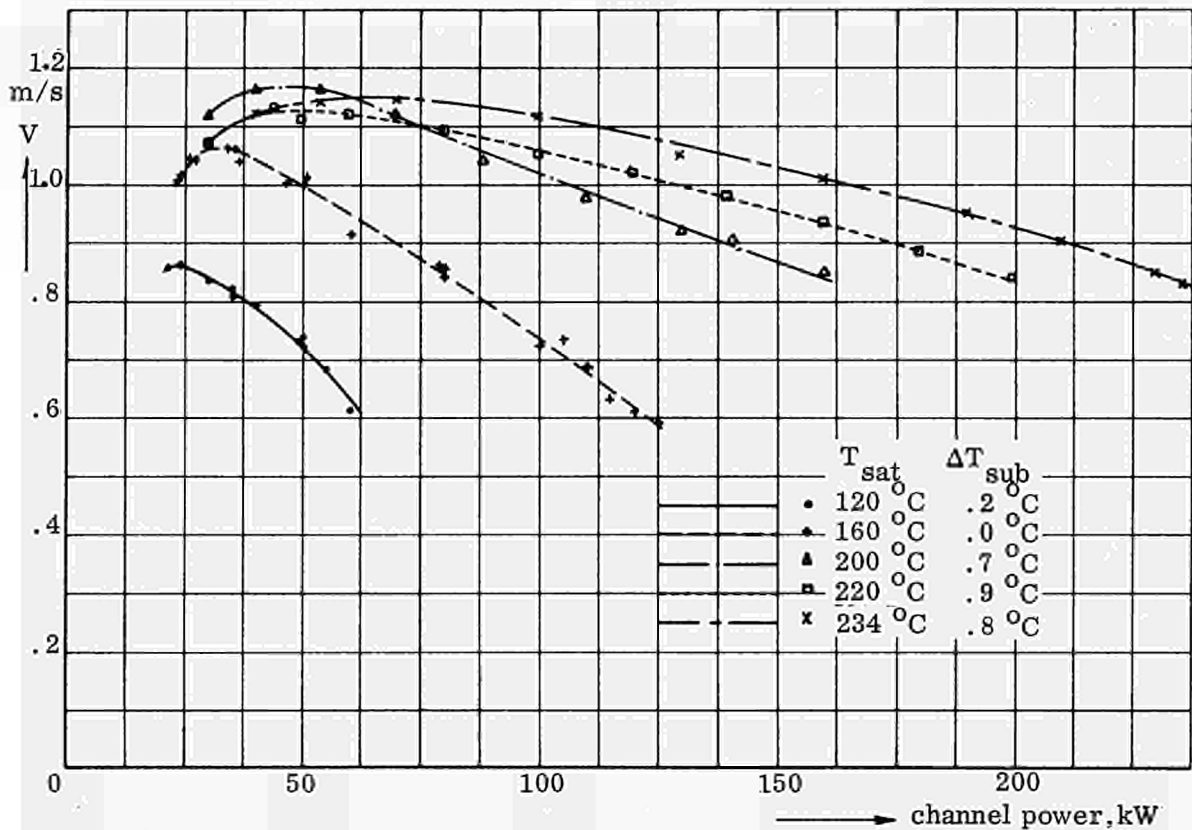


Fig. 3.1 The circulation rate as a function of channel power for various system pressures, Test Section I.

le the maximum becomes flatter and the slope of the recirculation rate versus channel power curve less steep.

As can be concluded from Fig. 3.1, there is a maximum in the circulation rate in dependence of system pressure at low channel powers too. Results of earlier experiments, in which the system pressure was varied systematically at constant channel power, demonstrated this phenomenon more clearly, as appears from Fig. 3.2. At high saturation temperatures, i. e. high system pressures, the driving head decreases with increasing temperature owing to the decreasing void fraction. This results in a decreasing circulation rate. At low saturation temperatures, the subcooled region, defined as the region where the average bulk liquid temperature is below the local saturation temperature, increases with decreasing temperature, since the influence of the pressure difference between top and bottom of the coolant channel due to the hydrostatic head, becomes more significant. The driving head and hence the circulation rate will, therefore, decrease with decreasing pressure. This is confirmed by the results of recirculation calculations (S2). At high channel power this effect is likely to disappear.

The influence of subcooling on the circulation rate for Test Section I is shown in Fig. 3.3. With increasing subcooling, the circulation rate decreases while the maximum circulation rate shifts to higher power levels. This is a direct result of the increase in the length of the subcooled region and the decrease in void fraction in the channel with subcooling. At high channel powers, the circulation rate becomes very insensitive to changes in the inlet-water temperature. The power dissipated in the sub-cooler is then but a small fraction of the total channel power supplied. At very high

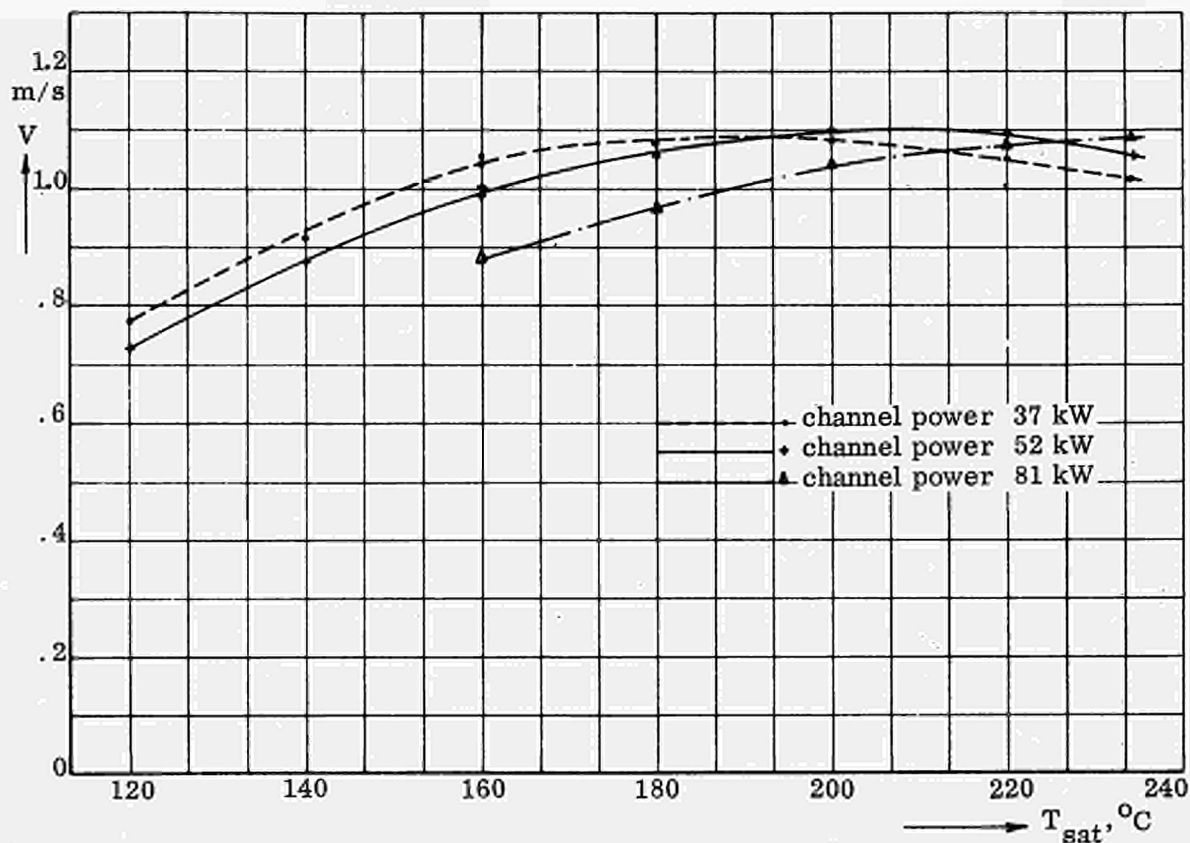


Fig. 3.2 The circulation rate as a function of system pressure for three channel powers.

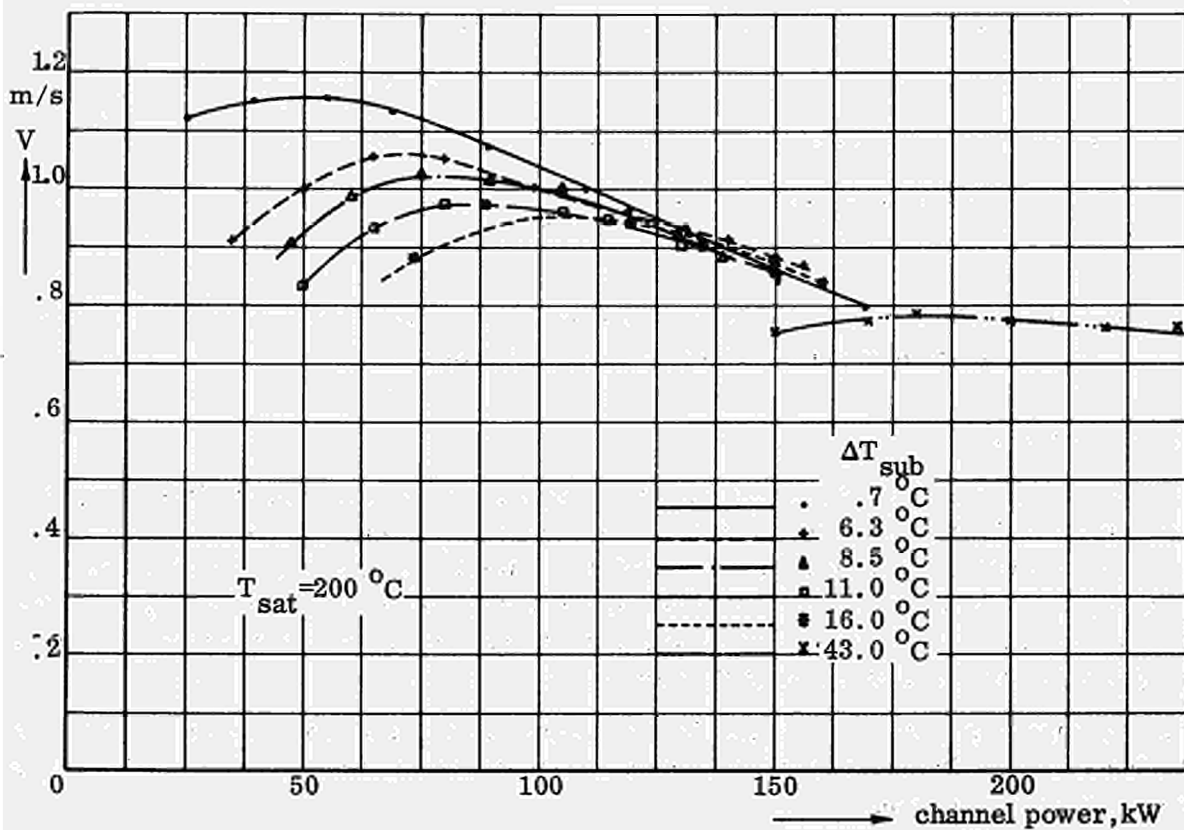


Fig. 3.3 The circulation rate as a function of channel power for various subcoolings, Test Section I.

subcooling rates, on the other hand, the influence of channel power on the circulation rate becomes quite small.

The influence of the operating conditions on the circulation rate for Test Section II, with a hydraulic diameter of 25.03 mm as compared to 16.16 mm for Test Section I, is shown in Fig. 3.4. The most noteworthy effect of increasing the hydraulic diameter is the increase in circulation rate at a fixed operating condition. For instance, the maximum circulation rate at 120°C is increased from .86 m/sec (Test Section I) to 1.1 m/sec (Test Section II) and at 234°C from 1.15 m/sec to 1.38 m/sec. An analysis of this effect can only be obtained by studying the equations describing the performance of a boiling channel.

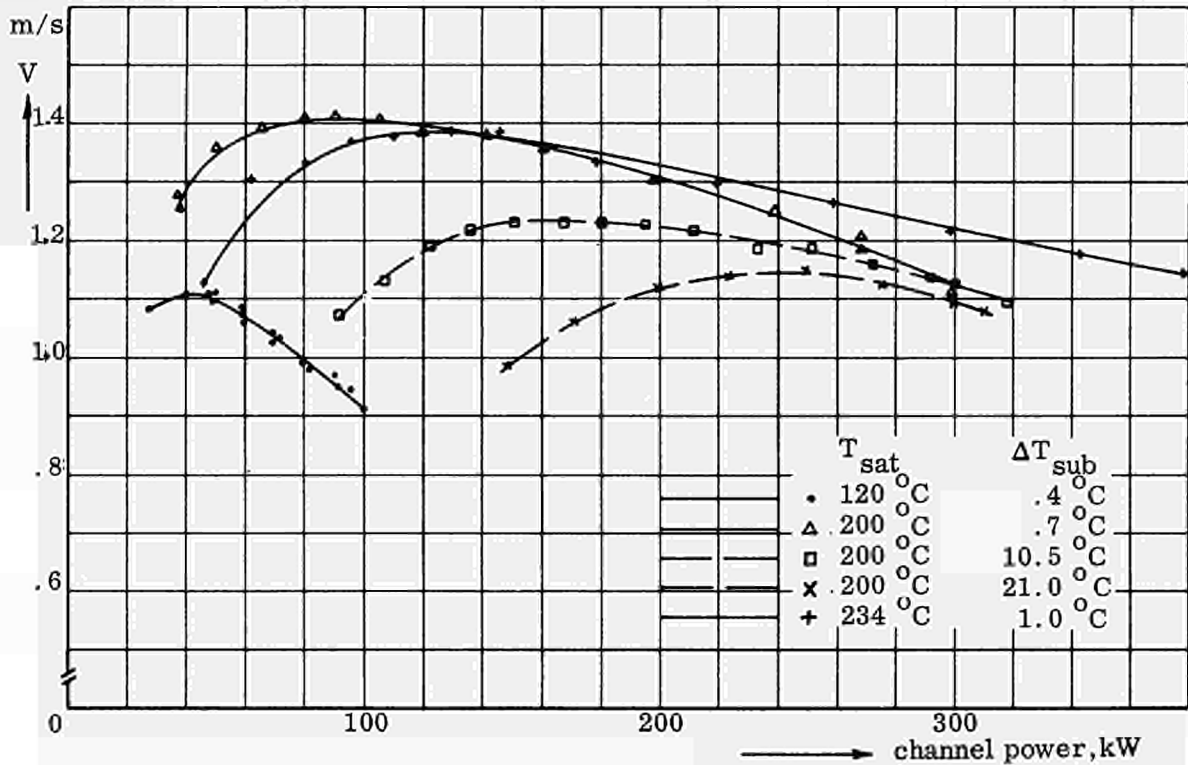


Fig. 3.4 The circulation rate as a function of channel power for various system pressures and subcoolings, Test Section II.

#### Void fraction.

In Figs 3.5 to 3.7, the influence of the operating conditions and of the hydraulic diameter on the void fraction near the exit of the heated part of the coolant channel, i. e. at the position where the Thulium source and the impedance gauge 1 are situated (see Fig. 2.4) is given. It can be shown that in first approximation,  $\alpha/1-\alpha$  is proportional to the channel power, which explains the decreasing slope of the void fraction vs power curves with increasing channel power.

An increase in pressure results in a decrease in void fraction, which is largely due to the increase in density per unit volume of steam. This effect is most significant in the low pressure range.

The effect of subcooling at constant pressure is to decrease the void fraction. Again, the effect of subcooling becomes smaller at high channel power. The decrease in



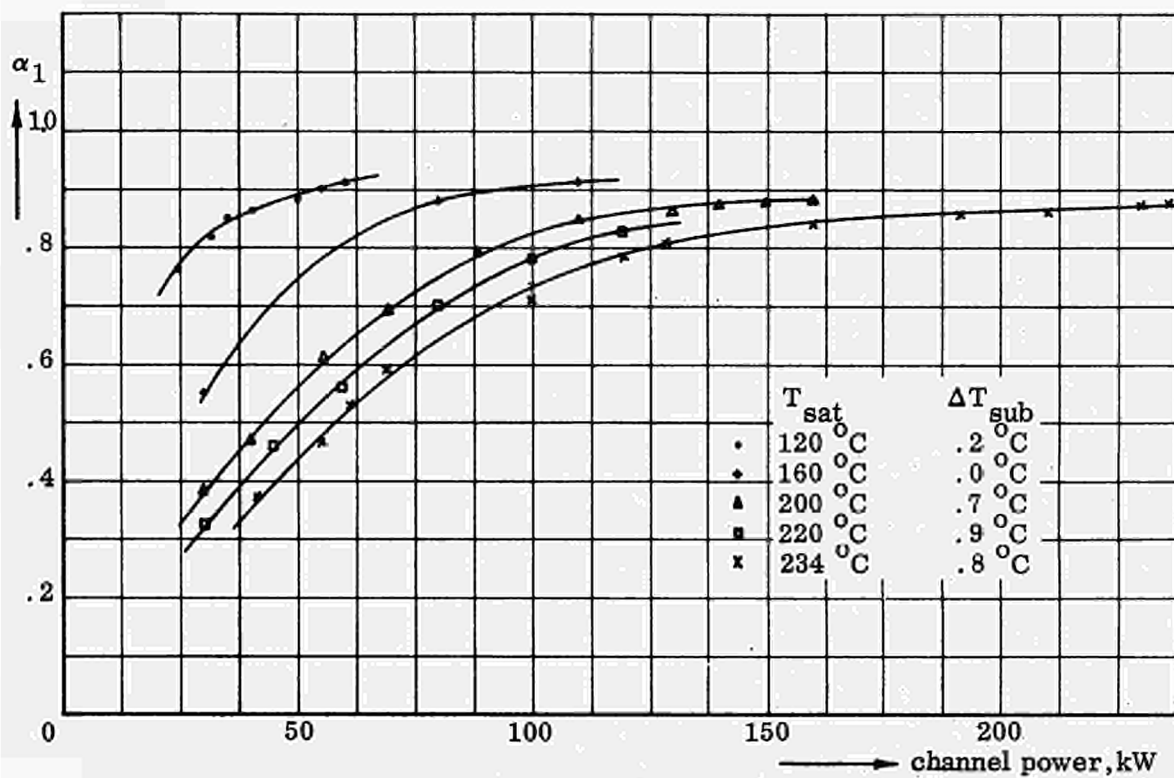


Fig. 3.5 The exit void fraction as a function of channel power for various system pressures, Test Section I.

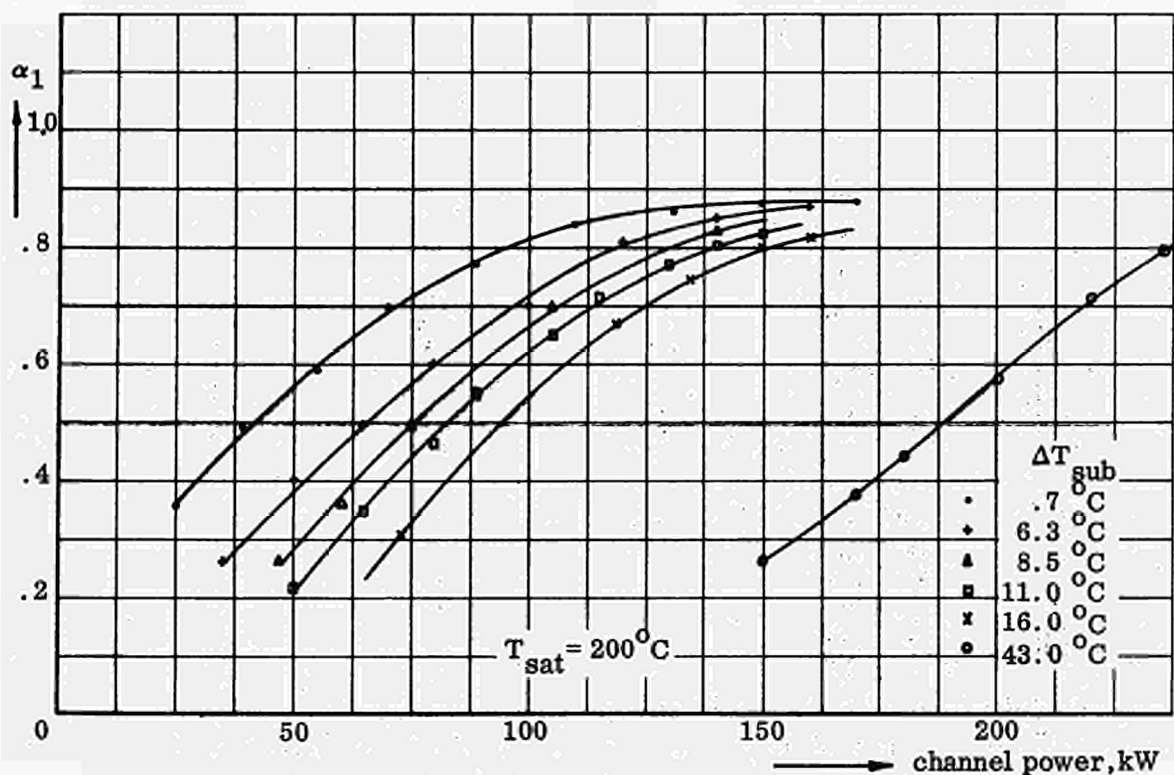


Fig. 3.6 The exit void fraction as a function of channel power for various subcoolings, Test Section I.

void fraction is a direct result of the increase of the subcooled region. The suggestion made by some authors that the influence of subcooling may be found by a horizontal shift of the curves in the void fraction-channel power plane to an amount equal to the heat removed in the subcooler is only true as a rough approximation for low subcoolings in the case of the presented results. An accurate evaluation of the effect of subcooling can be obtained only by properly using the basic equations.

An increase in hydraulic diameter at a given power input, results in a decrease in void fraction, see Fig. 3.7, that is mainly due to the large difference in inlet mass flows for the two test sections.

In considering the Figs 3.5 to 3.7 and also the figures to be presented yet, it must be kept in mind that a change in one of the independent variables results in a change in void fraction and circulation rate as well. However, a change in the circulation rate, in its turn, is effecting the void fraction. A variation in void fraction with a change in one of the independent variables as given in the figures, is, therefore, influenced by the accompanying change in circulation rate.

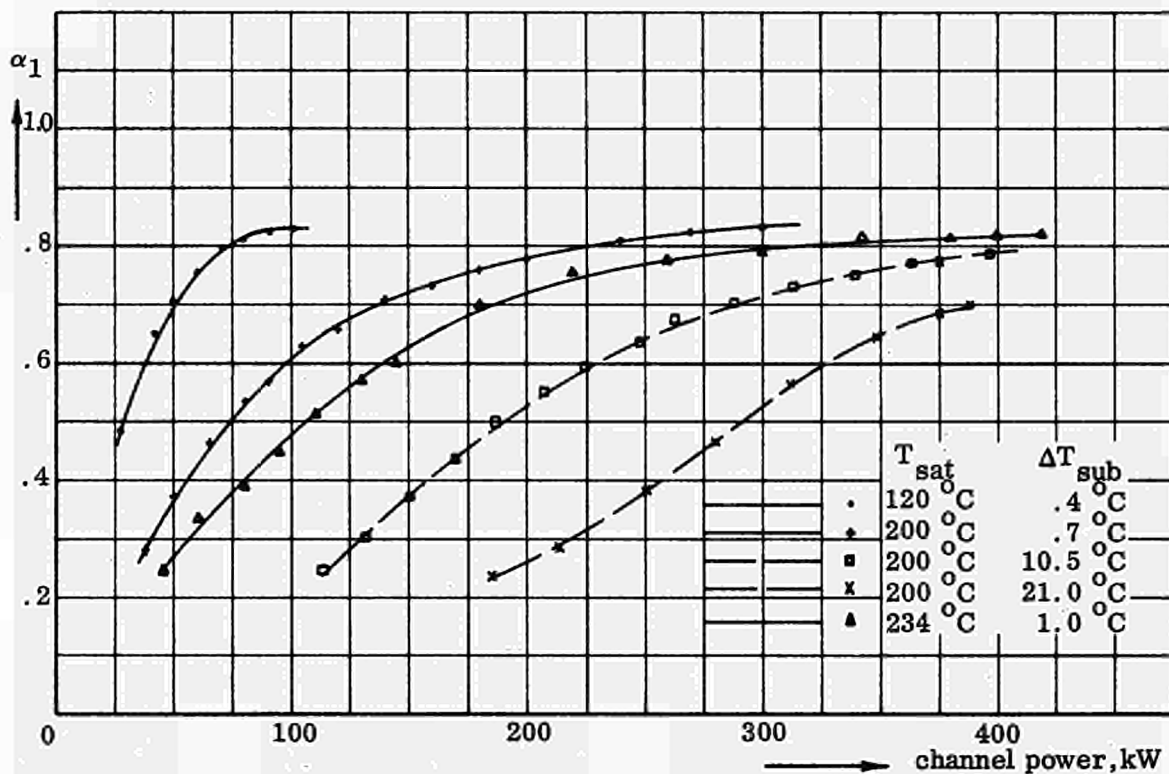


Fig. 3.7 The exit void fraction as a function of channel power for various system pressures and subcoolings, Test Section II.

#### Longitudinal distributions.

At all the operating conditions indicated by the measuring points in Figs 3.1 to 3.7, the longitudinal distribution of the void fraction and the static pressure have been measured too. It is hardly feasible to report all the data of these measurements here. Therefore, only a few results will be presented, showing the influence of the operating conditions and geometry. The bulk of the data will be reported in tabular form elsewhere.

Measured longitudinal void distributions for various operating conditions are shown in Figs 3.8 to 3.11. On the horizontal axis the location of the various void gauges is indicated. In every curve is indicated at what location saturated conditions

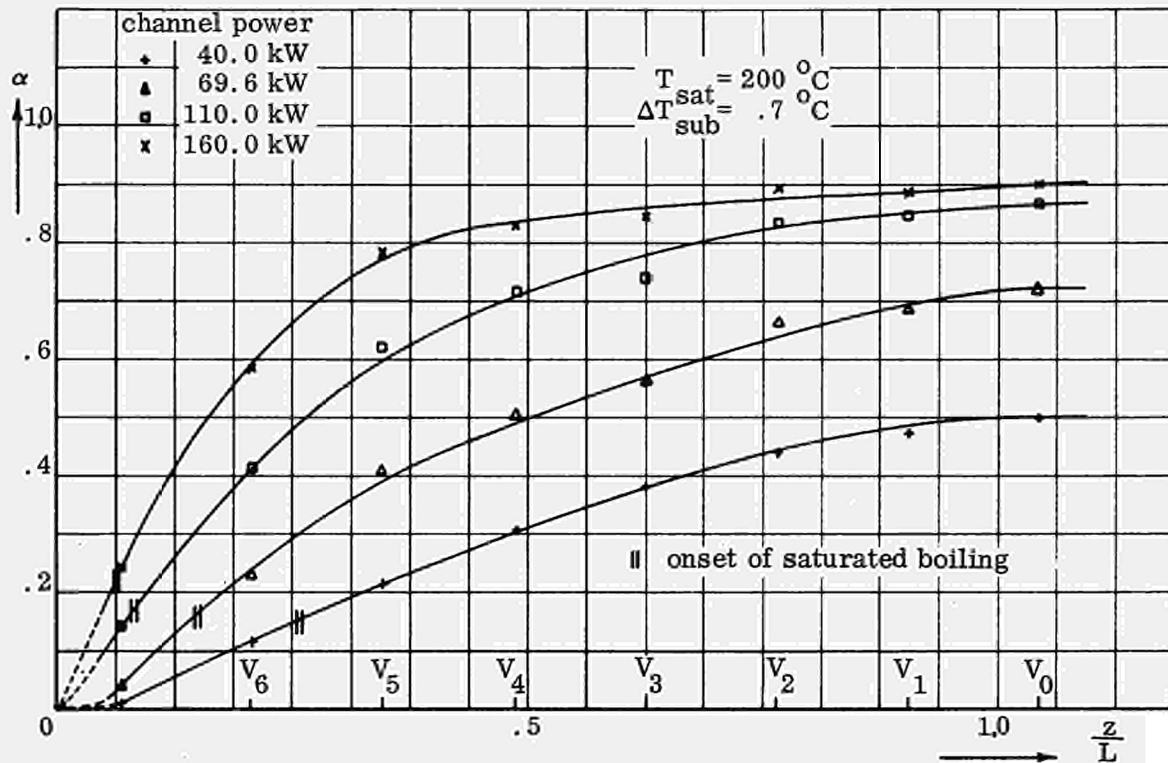


Fig. 3.8 The longitudinal void fraction distribution for various channel powers, Test Section I.

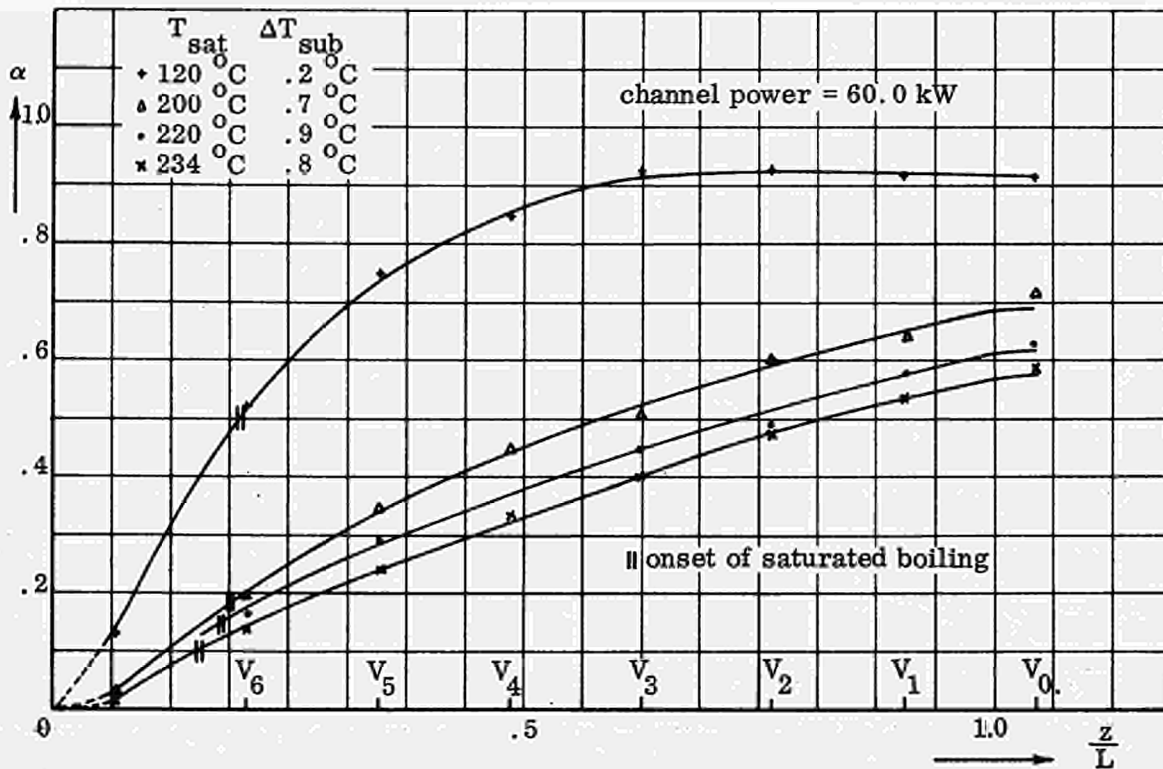


Fig. 3.9 The longitudinal void fraction distribution for various system pressures, Test Section I.

for the bulk fluid are reached, i.e. where the bulk water temperature equals the local saturation temperature. These positions were calculated from a heat balance, taking into account hydrostatic effects (the effect that the saturation temperature changes a-

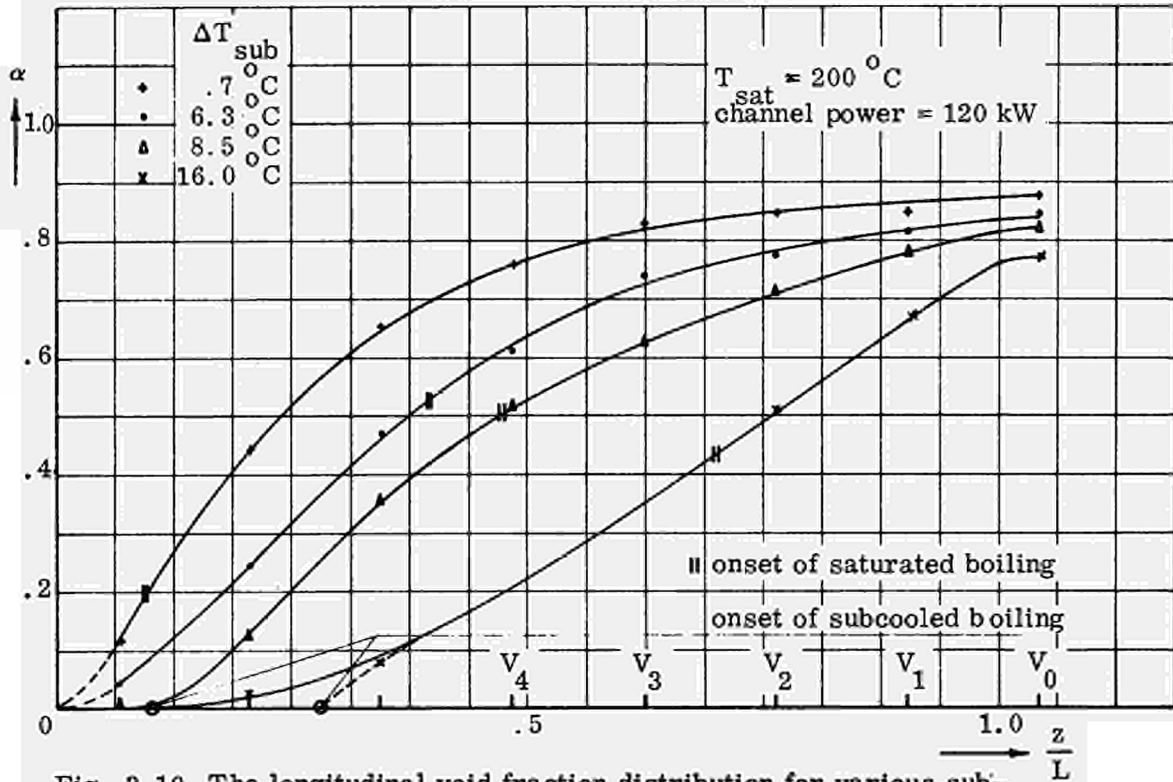


Fig. 3.10 The longitudinal void fraction distribution for various sub-coolings, Test Section I.

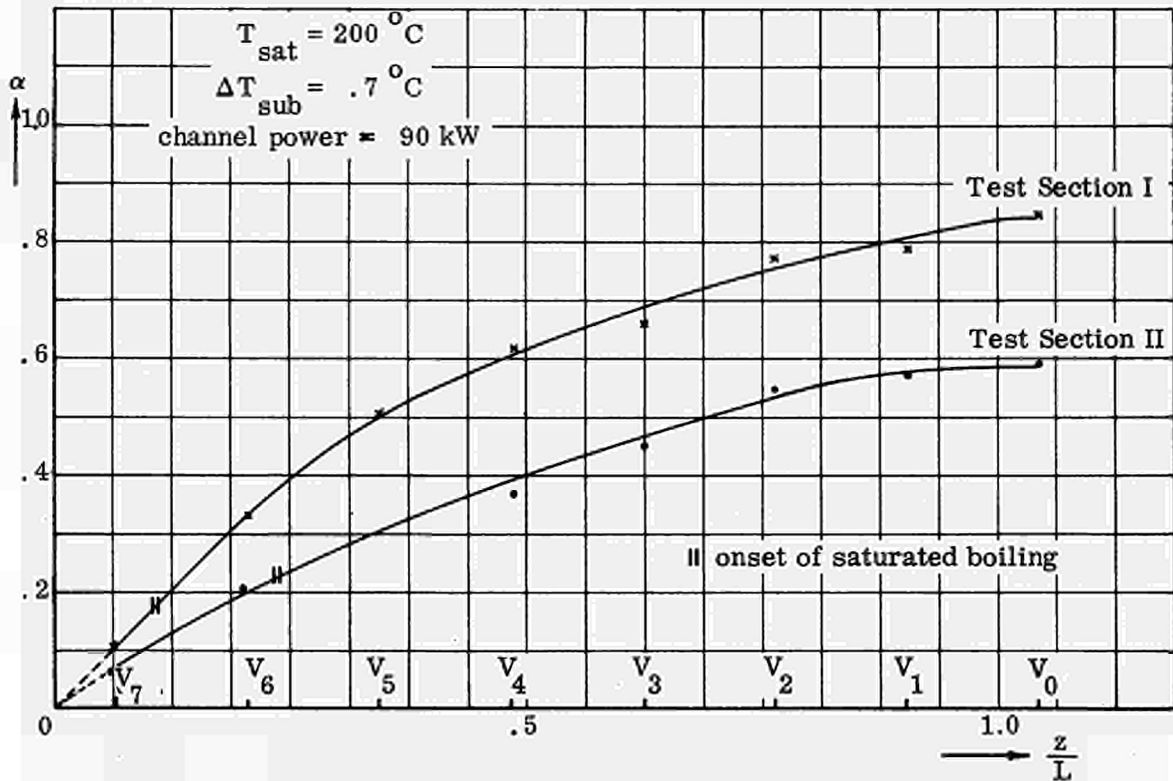


Fig. 3.11 The longitudinal void fraction distribution for Test Section I and II.

long the channel), and the formation of steam in subcooled conditions, see chapter 4. All the curves have been extrapolated, (indicated by broken lines, in Figs 3.8 to 3.11) to the position where, according to Bowring (B11), subcooled boiling starts and the bubbles formed at the surface of the heated wall detach from the wall into the fluid.

In the bulk boiling region, the curves show the same behavior as the curves for the exit void fraction: the slope decreases with increasing distance. At the position where saturated boiling starts, an appreciable amount of steam is present already, in some cases even more than 50% void. This indicates that subcooled boiling has to be taken into account in performance calculations of boiling channels. As is shown in Figs 3.8 to 3.11, boiling starts directly at the inlet of the test section, except at high subcooling rates. The influence of the channel power, system pressure, subcooling and hydraulic diameter on the longitudinal void distribution and on the onset of saturated boiling is obvious. Any increase in channel power and inlet temperature and any decrease in saturation temperature and hydraulic diameter will cause an increase in local void fraction.

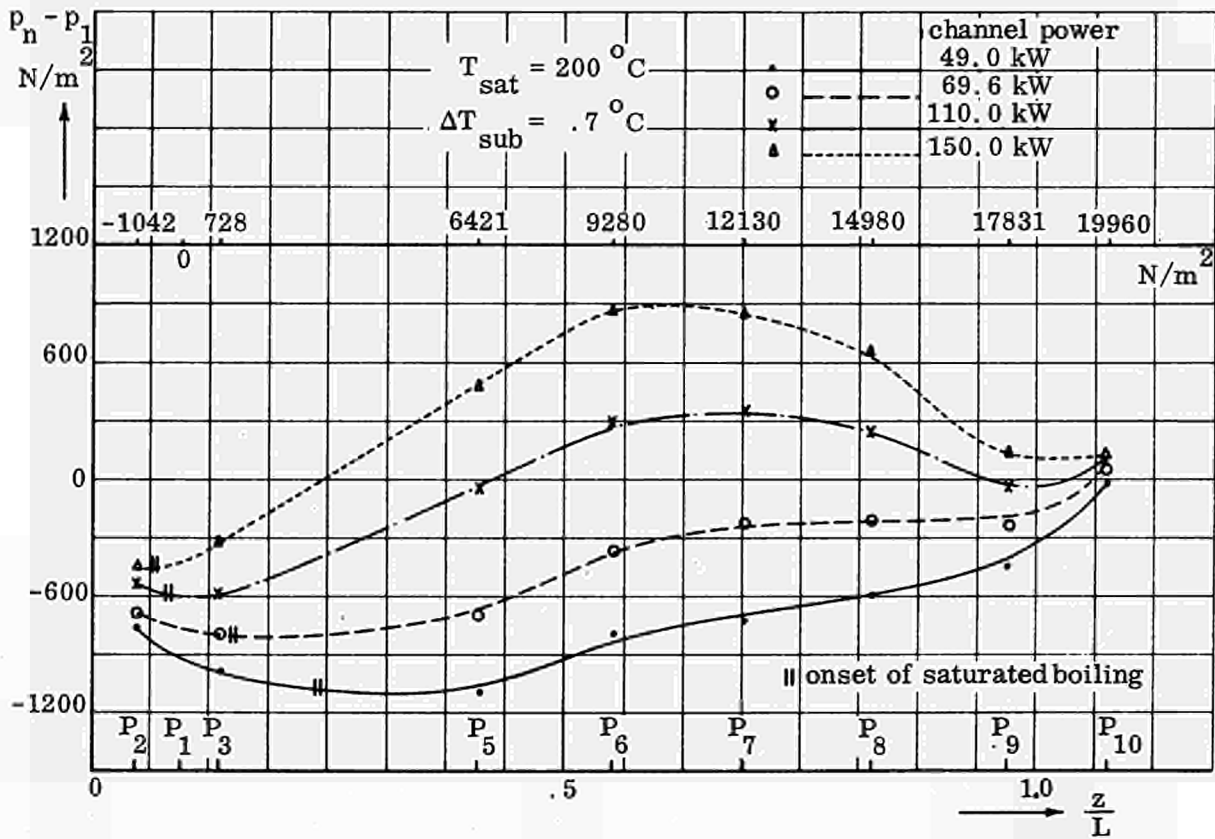


Fig. 3.12 The apparent longitudinal pressure distribution for various channel powers, Test Section I.

Examples of longitudinal pressure distributions are shown in Figs 3.12 and 3.13. On the horizontal axis the location of the various pressure tappings is indicated. The difference between the static pressure along the riser and the pressure measured at the pressure tapping 1 at the bottom of the downcomer is plotted vertically. These pressure differences were read from the multimanometer and transformed into Newtons per square meter. The locations where saturated boiling starts, are indicated. It should be mentioned that the manometer compares the sum of the static pressure in the boiling channel and the pressure head of the water-column in the connecting tube for the different locations.

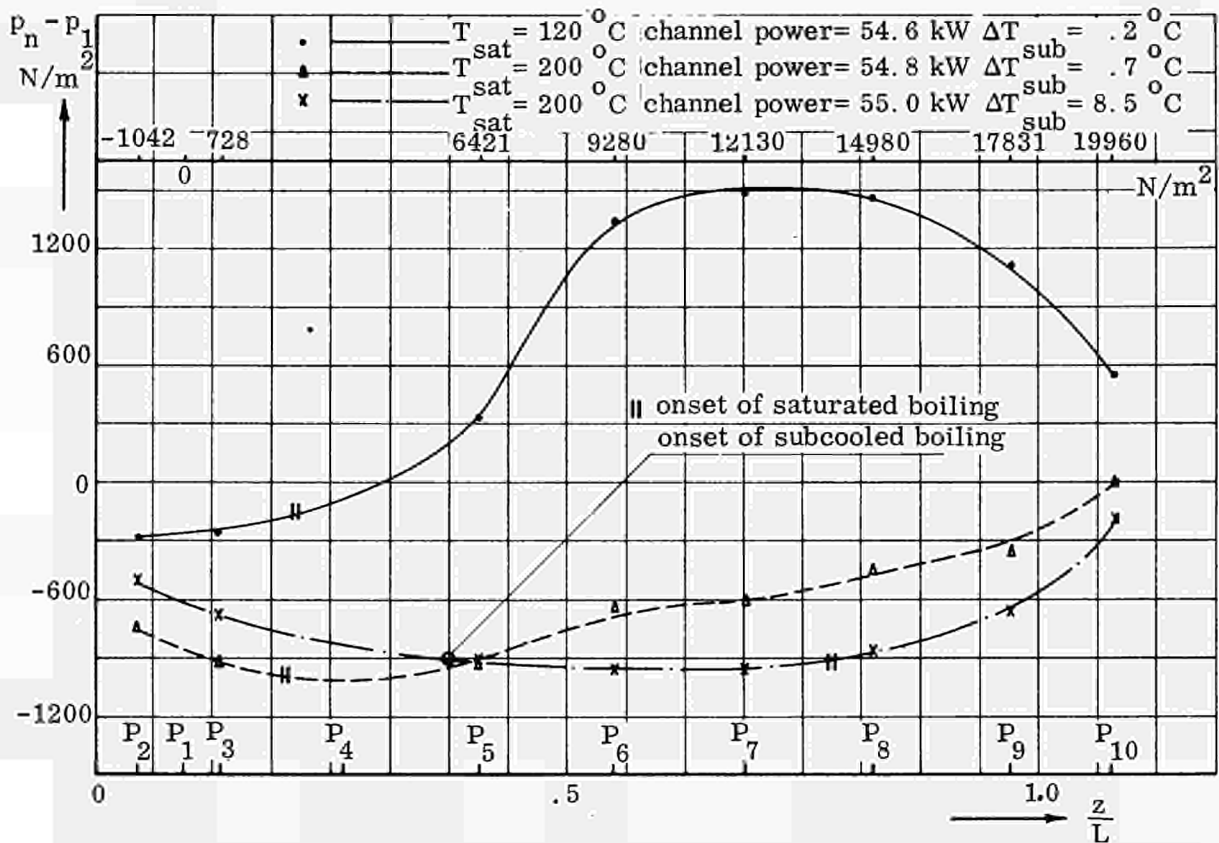


Fig. 3.13 The apparent longitudinal pressure distribution for two system pressures and subcoolings, Test Section I.

Looking at the curve of 49 kW channel power in Fig. 3.12, the decreasing static pressure difference with the increasing distance from the bottom of the channel indicates that the larger part of the pressure losses is formed by the friction and acceleration contributions and that only a small amount of steam is present. Just where the location of the start of saturated boiling is passed, the static pressure difference is increasing again owing to the buoyancy effect of the excess steam formation. At higher channel powers this effect is more pronounced as appears from Fig. 3.12. The highest pressure tapping, indicated by  $P_{10}$ , is located near the outlet of the riser. Beyond that location, the two-phase fluid is subject to expansion resulting in a pressure increase or decrease depending upon the prevailing conditions. By adding to  $p_{10}$  the difference of pressure across the expansion and the pressure losses in the downcomer, the value of the pressure at the location  $P_1$  is obtained again. At very high channel powers, the void fraction and hence the hydrostatic head at the upper part of the boiling channel does not change very much. The friction losses continue to increase owing to the increasing steam mass flow. This results again in a decrease in difference of pressure ( $p_n - p_1$ ) as the distance from the bottom increases.

In Fig. 3.13, the influence of the system pressure and subcooling at an approximately constant channel power is shown. At low pressures and no subcooling, the steam formation and the void fraction start to increase very sharply which results in an increase in difference of pressure directly at the beginning of the heating element. At a subcooling of 8.5°C, there is already an appreciable region where no steam is formed. In both figures the values of the pressure for 200°C are indicated, which must be added to the measured pressure differences in order to obtain the actual values of the static pressure with respect to  $p_1$ . The indicated figures were calculated from the height of the water-column in the connecting tubes.

In this section, results were given of measurements characterizing the steady-state performance of a naturally circulating boiling channel. An attempt was made to plot the presented results in terms of non-dimensional quantities for the heat load, subcooling, pressure and for the dependent quantities. Although the non-dimensional parameters derived by Van der Walle (V4) are similar to those derived by Silver (S7) and Haywood (H2), the use of these parameters in plotting the experimental results was not successful. The divergence of the different curves was even increased. Therefore, the results have been given so far in the form of raw data.

### 3.3. Hydraulic oscillations

#### 3.3.1. Signal observations.

Spontaneous oscillations in naturally circulating boiling water loops have been observed by several investigators, (B12), (F1) and (L1). In carrying out the steady-state measurements presented before, also different types of flow oscillations appeared, although the independent quantities as channel power and condenser and subcooler heat removal were constant. Beside severe oscillations in water level, pressure and flow rate caused by a poor steam-water separation, which were overcome by removing the separator, it was possible to distinguish three types of oscillations having a frequency of roughly .03, 1.0 and 15.0 c.p.s. They will presently be described in the following. A systematic research has been carried out as regards the oscillations of intermediate frequency only.

##### a. Low frequency oscillations.

Slow oscillations of a period of about 20-40 sec have been observed under particular operating conditions in the subcooling temperature  $T_{2b} - T_{6b}$  (Fig. 2.4), which was recorded continuously. By making recordings of the saturation temperature and the inlet temperature separately, it appeared that the oscillation in subcooling could be attributed mainly to saturation temperature oscillations. Observing the signals from other physical quantities revealed that the flow characteristics changed so slowly that quasi steady-state flow conditions prevailed in the boiling water loop. The fluctuations in pressure, saturation temperature, subcooling and mass flow rate were roughly in phase. It was found possible to influence period and amplitude of the oscillations by changing the adjustment of the PID controller of the condenser. It has, however, been checked that similar oscillations were also present without controller, and it was evident that these should not be ascribed to the automatic control system.

In Test Section I, these oscillations were only observed at a pressure in excess of 15 atmospheres. At 200°C for instance, they started at about 200 kW (well beyond the maximum in the circulation rate vs channel power curve) and the amplitude in subcooling temperature was about .2°C. At 234°C, the slow oscillations started at 240 kW with the same amplitude.

In Test Section II, the slow flow oscillations have been observed at all of the three selected saturation temperatures and they had a more severe character. For instance, at 200°C, they started at a power level of 240 kW with a period of 35 seconds and an amplitude of .7°C in subcooling. A systematic influence of subcooling appeared evident. Going from .7 to 20°C subcooling, the power level at which oscillations started increased from 240 to 340 kW whilst the oscillation period was shortened from .35 to 18 seconds. At higher pressures, the fluctuations started at higher power levels while the amplitude of the subcooling fluctuations increased to about 1.2°C.

Increasing the power level sometimes caused the oscillations to stop and in other cases to mix themselves with the 1 c.p.s. oscillations, by which the latter appeared modulated in character.

These slow oscillations might be similar to the pressure drop oscillations measured by Stenning (S8) in a forced circulation system, and which were ascribed to a decreasing pressure drop across the test section with increasing mass flow. The pressure drop characteristics of a coolant channel will be discussed in chapter 4.

b. Oscillations of intermediate frequency.

By increasing the channel power at constant saturation temperature and subcooling, severe hydraulic oscillations with a period of about 1 second have been observed in the mass flow rate. In Fig. 3.14, recordings are reproduced of the signal from the differential pressure gauge connected to the pitot-tube. These recordings have been made in preliminary tests with a test section similar to Test Section I. Three series of recordings for different system pressures are shown. In each series the channel power is increasing from the top to the bottom of the figure. For each single series, the sensitivity of the differential pressure gauge is constant, so that the recordings can directly be compared with each other. The output voltage of the pressure gauge has been translated into Newtons per square meter, using the manometer readings of the pitot-tube.

By increasing the channel power, the average differential pressure decreases, which is in agreement with the character of the circulation rate vs channel power curve as given in Fig. 3.1. By increasing the power from 87 to 90 kW at 120°C saturation temperature, the onset of spontaneous flow oscillations can be observed. The frequency of these oscillations is about 1 c.p.s. while the amplitude is roughly 5 times larger than the average value at low power level. Furthermore, it can be concluded from Fig. 3.14 that at this low system pressure flow reversal is present. At 200°C saturation temperature the oscillations start at a higher power level, while they develop more gradually once the power is increased. Furthermore, the amplitude is smaller and the flow rate periodically drops to zero, but does not reverse. At even higher pressure (234°C saturation temperature), the flow maintains a positive value.

Not only was it possible to observe the flow oscillations in the signal from the pitot-tube, but also in signals from other physical quantities, such as system pressure, void fraction, temperature, etc. These oscillations will be the subject of a more detailed discussion in the following sections.

In some cases these flow oscillations were superimposed on the low frequency oscillations, and thus revealed a modulated type of signal with bursts of oscillations. By further increasing the channel power, this modulated character was made to disappear and only the intermediate frequency oscillations remained. All runs were continued until the signal from the burn-out detector switched off the power supply to the heating element.

By carrying out the experimental series with Test Section I at 220°C saturation temperature, a further phenomenon was observed. During the approach to burn-out and while the flow quantities oscillated with a frequency of about 1 c.p.s., the oscillations in the absolute pressure and saturation temperature changed from 1 c.p.s. to about .5 c.p.s. This occurred at a channel power of 230 kW. At 234°C saturation temperature, the absolute pressure and saturation temperature started to oscillate at 230 kW with a frequency of about .5 c.p.s., whereas the signal from the pitot-tube showed no oscillation. By increasing the channel power to 240 kW, bursts of oscillations with a frequency of about 1 c.p.s. were observed in the pitot-tube signal.



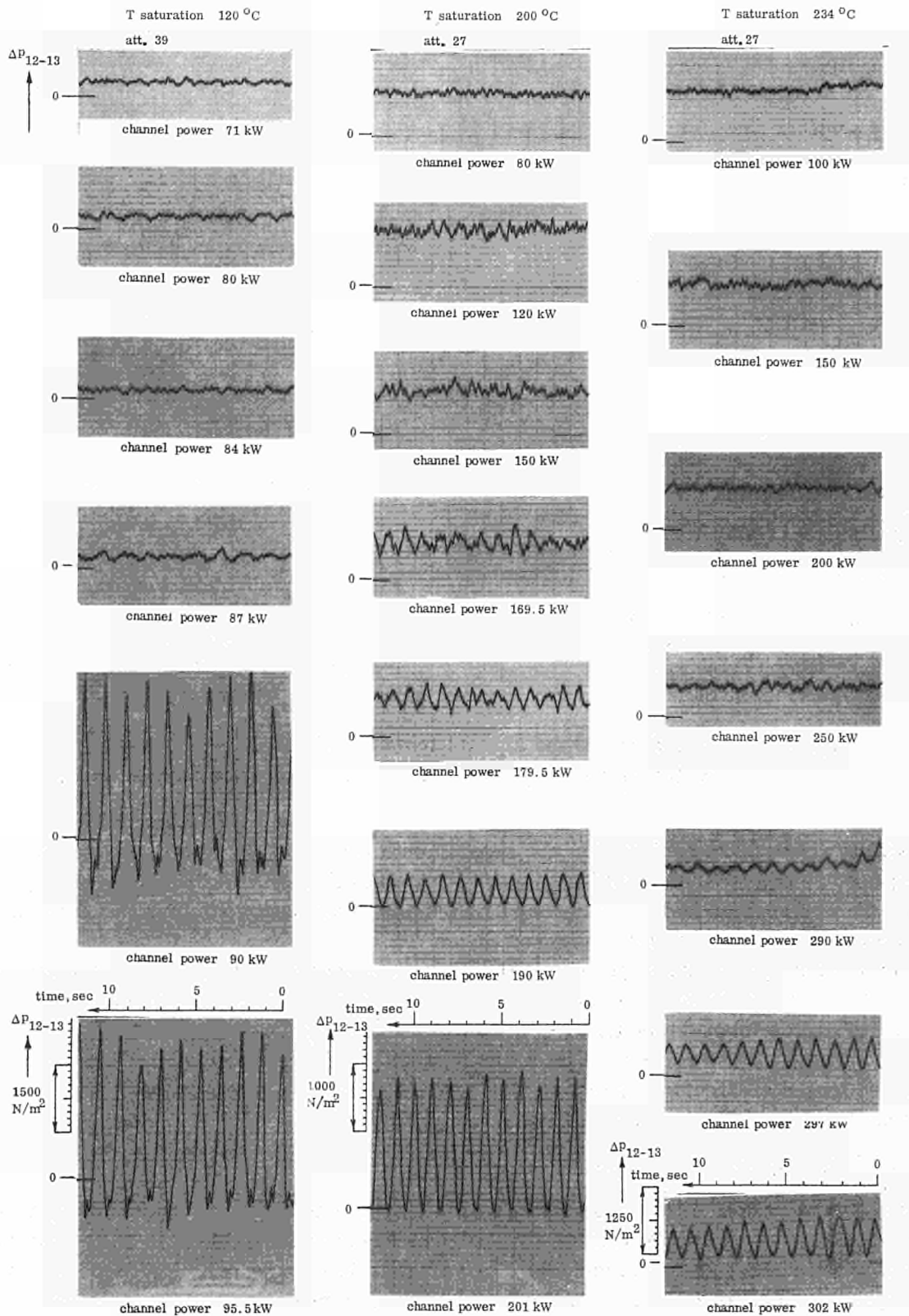


Fig. 3.14 Recordings of the signal from the pitot-tube

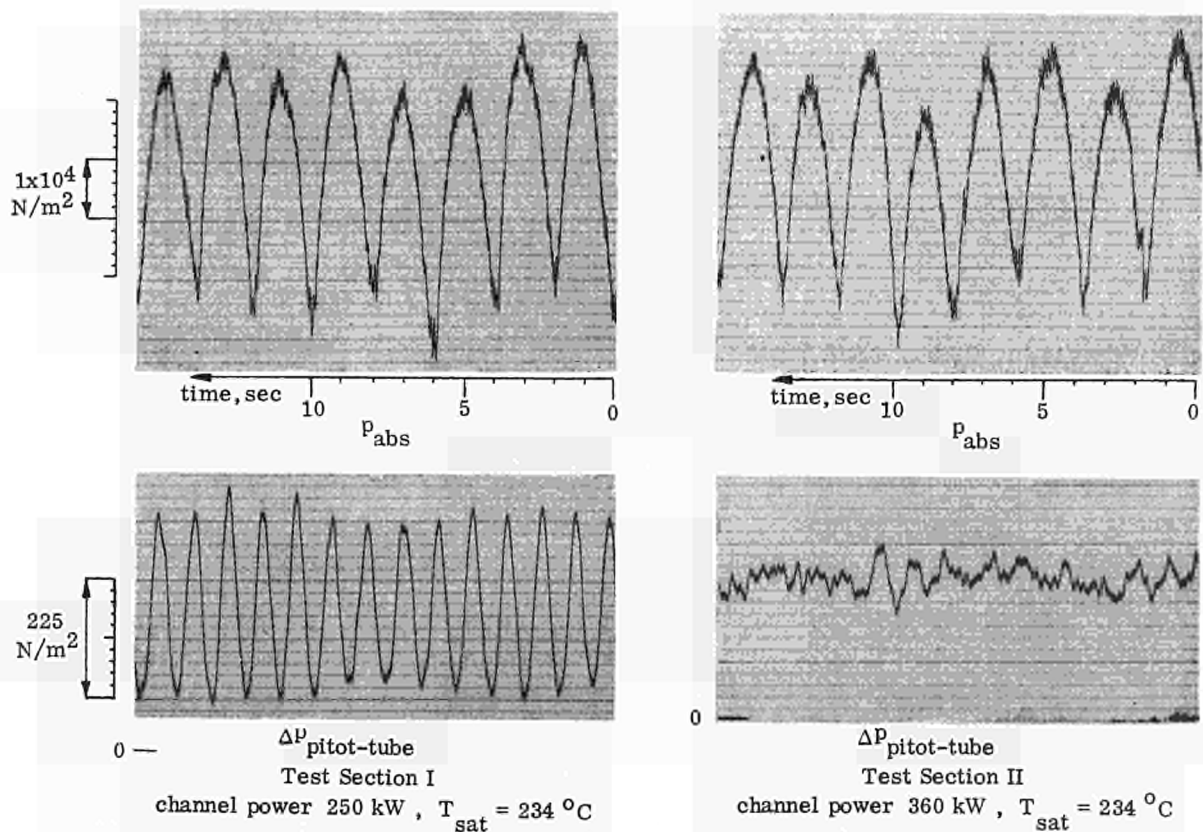


Fig. 3.15 Recordings of the signals from the absolute pressure gauge and the pitot-tube at high pressure for Test Section I and II.

A similar effect was exhibited in the experiments with Test Section II. At a saturation temperature of  $234^{\circ}\text{C}$  and 270 kW channel power, regular oscillations in absolute pressure were observed with a frequency of .5 c.p.s. Until burn-out, the signal from the pitot-tube showed no oscillations.

Some recordings of the signal from the pitot-tube and absolute pressure are given in Fig. 3.15. They show the existence of .5 c.p.s. oscillations in absolute pressure, while the pitot-tube shows no oscillations or oscillations with a frequency of 1 c.p.s. The phenomena were reproducible. It has been checked that these oscillations were not induced by the electronic apparatus. No logical explanation of the cause of these oscillations has as yet been brought forward.

### c. High frequency oscillations.

In observing and analyzing the steam-void fluctuations in the coolant channel, it was noted that fairly regular oscillations of a high frequency were present in the output signal of the various impedance gauges. The variation in output signal corresponded to void changes as large as 20% void. In Fig. 3.16 the autocorrelation and the spectral power density (equations (2.15.) and (2.17.)) are given on an arbitrary linear scale of the signal from the impedance void gauge 5, located in the bottom part of the riser. Both were computed by the ISAC noise correlator. From these curves it can be concluded that, apart from random noise, fairly regular variations are present in the steam-void in the range of 14 to 18 c.p.s.

In (G1) Griffith correlated the void fraction data reported by this University (S1) which were obtained from experiments with a test section having a geometry similar to Test Section I. He used an expression for slug flow density, which applies to low inlet velocities, low qualities and low heat fluxes. In a personal communication, Griffith stated that the slugs he assumed to be present in the Eindhoven loop should follow each other with a frequency roughly between 15 and 20 c.p.s., concordant with the observed frequency in the steam-void. On the other hand, it will be shown in chapter 5 by a theoretical study that instabilities in flow may develop with frequencies of about 12 c.p.s. Therefore, more research is needed to define the characteristics of the observed high-frequency oscillations in steam-void.

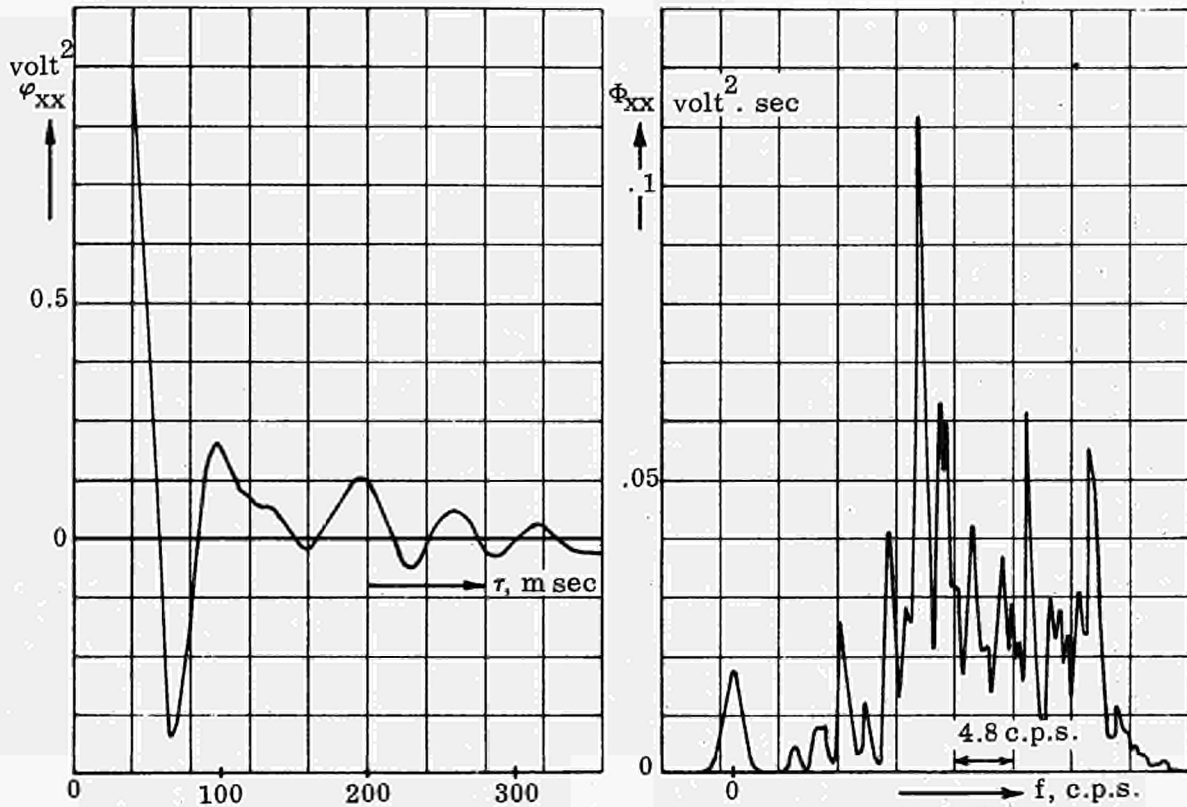


Fig. 3.16 High frequency void fluctuations, Test Section I.

### 3.3.2. The onset of hydraulic oscillations.

Systematic research has been carried out into the onset of severe hydraulic oscillations in the intermediate frequency range, which can be expected to occur and have been observed in the fuel channels of a boiling water reactor. In literature, this type of instability is usually referred to as hydrodynamic instability. There is a great need for systematic data on the occurrence and character of such hydrodynamic instabilities, but little systematic experimental information has been reported so far. Furthermore, the onset of flow instabilities is often only roughly indicated and is not uniformly defined.

In an attempt to obtain a systematic analysis of the onset of hydraulic oscillations in dependence of the operating conditions and geometry, recordings have been made on a

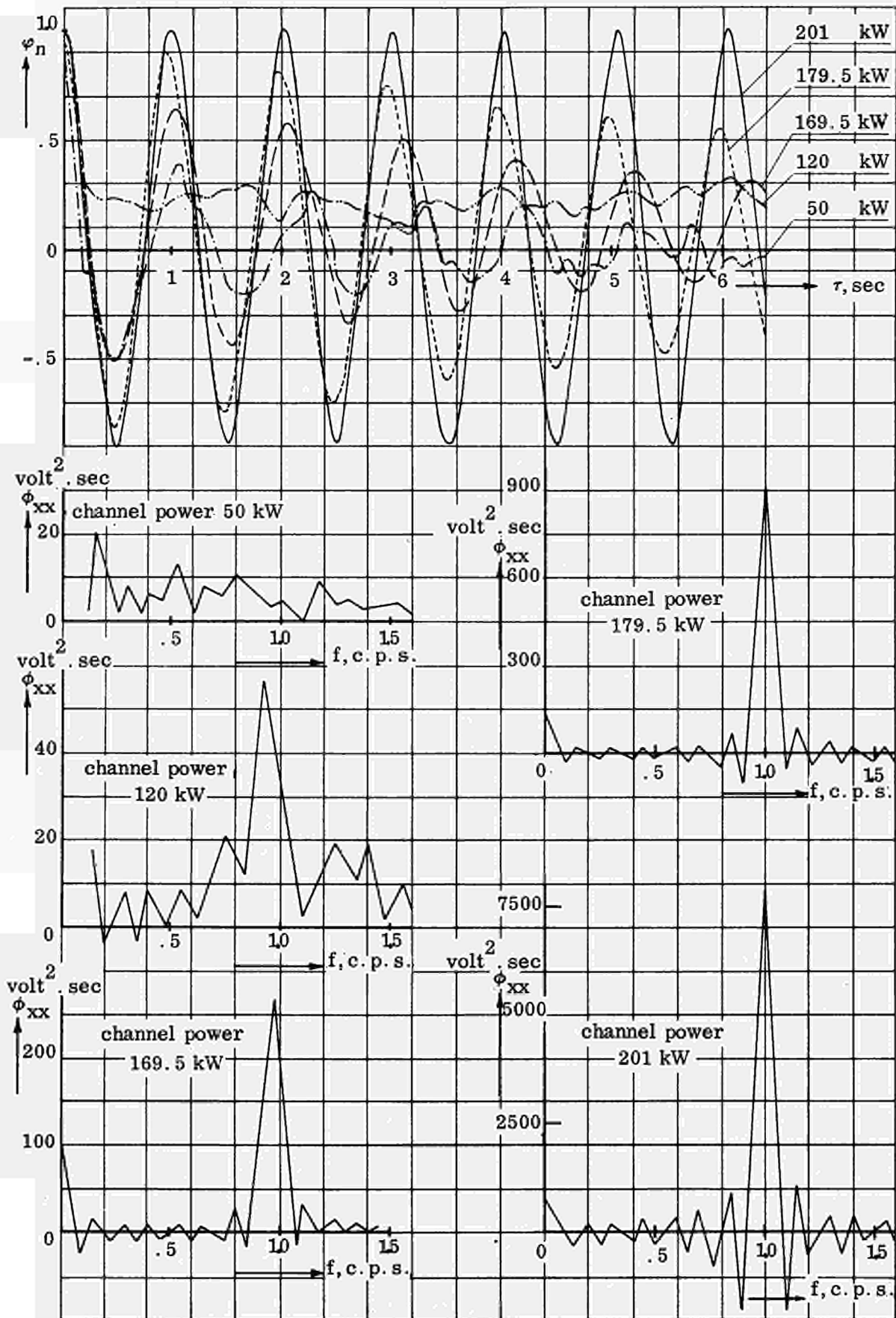


Fig. 3.17 Autocorrelations and spectral power densities of the  $\Delta p$  inlet signal.

FM-magnetic tape of the fluctuating part of the signal from the differential pressure gauge connected to the pressure tapings 1 and 2 (Fig. 2.4), indicating the variations in pressure loss and thus mass flow rate at the inlet of the coolant channel. From these recordings, the autocorrelation and spectral density curves (equations 2.15. and 2.17.) have been computed with the special purpose analogue computer ISAC or with a digital computer using the earlier mentioned computer program (A1). For the latter possibility, the recorded signals were converted into digital data and stored on a paper tape. In the digital computer program, the power density was computed from the autocorrelation by a Fourier transformation.

In Fig. 3.17, an example is given of computed autocorrelations and spectral power densities for a constant system pressure and subcooling temperature, but varying channel power. The conditions correspond to those of Fig. 3.14 at 200°C saturation temperature. The plotted normalized autocorrelations are defined as:

$$\varphi_n(\tau) = \frac{\varphi(\tau)}{\varphi(\tau=0)} \quad (3.4.)$$

The normalized autocorrelation function of a random noise signal will start at unity and decay to zero monotonically. The autocorrelation of a periodic function will be periodic. The autocorrelation curve at 50 kW channel power shows that almost only random noise is present in the signal. When the channel power is increased, fairly regular oscillations appear in the noise. At 201 kW, only regular oscillations are present with a frequency of 1 c.p.s. The same behavior is demonstrated by the power density curves. At low channel power, the power of the signal is distributed over a certain frequency range. At higher channel powers, the power of the signal becomes ultimately concentrated into a single discrete frequency. In the autocorrelation curves and in the spectral power density curves a slight increase of the frequency of the oscillations with channel power can be observed.

The area under the peak in the power density curves at the resonance frequency has been measured. By extracting the square root of the measured value, the root mean square value of the fluctuating part in the relevant narrow frequency band is obtained. By using the calibrations performed, this value can be translated into fluctuations of the differential pressure across the inlet expressed in Newtons per square meter. These values are plotted as a function of channel power for the various saturation temperatures and subcoolings in Figs 3.18 and 3.19 respectively.

The onset of severe hydraulic oscillations is clearly demonstrated in Figs 3.18 and 3.19. For comparison, the steady-state value of the differential pressure across the inlet at the maximum in the relevant circulation rate vs channel power curve (Figs 3.1, 3.3 and 3.4) is also given. Wherever the signal revealed a modulated character (bursts of oscillations), it is indicated. The channel power was increased step by step until the burn-out detector switched off the power.

The influence of system pressure on the onset of hydraulic oscillations is given in Fig. 3.18. As is shown, the fluctuations in the pressure drop across the inlet at a saturation temperature of 120°C are as large as 6 times the value ever obtained in steady-state conditions. At this temperature it is not difficult to determine the channel power at which hydraulic instabilities start. At a channel power of 65 kW, the fluctuations in pressure drop increase sharply. The system pressure has a stabilizing effect in that sense that, at higher pressures, severe oscillations start at higher channel power. Moreover, at higher system pressures, the onset is not sharply defined. There

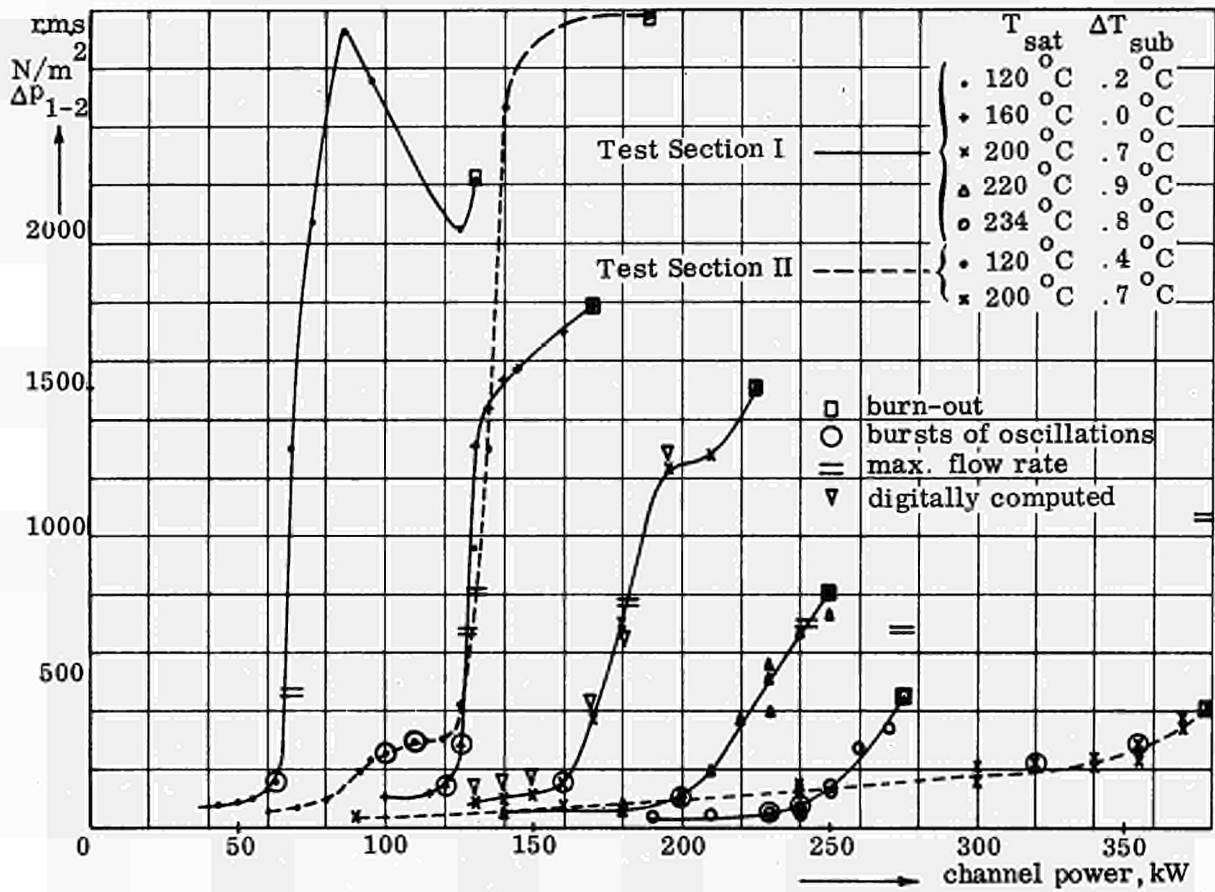


Fig. 3.18 The influence of system pressure on the onset of hydraulic instabilities, Test Section I and II.

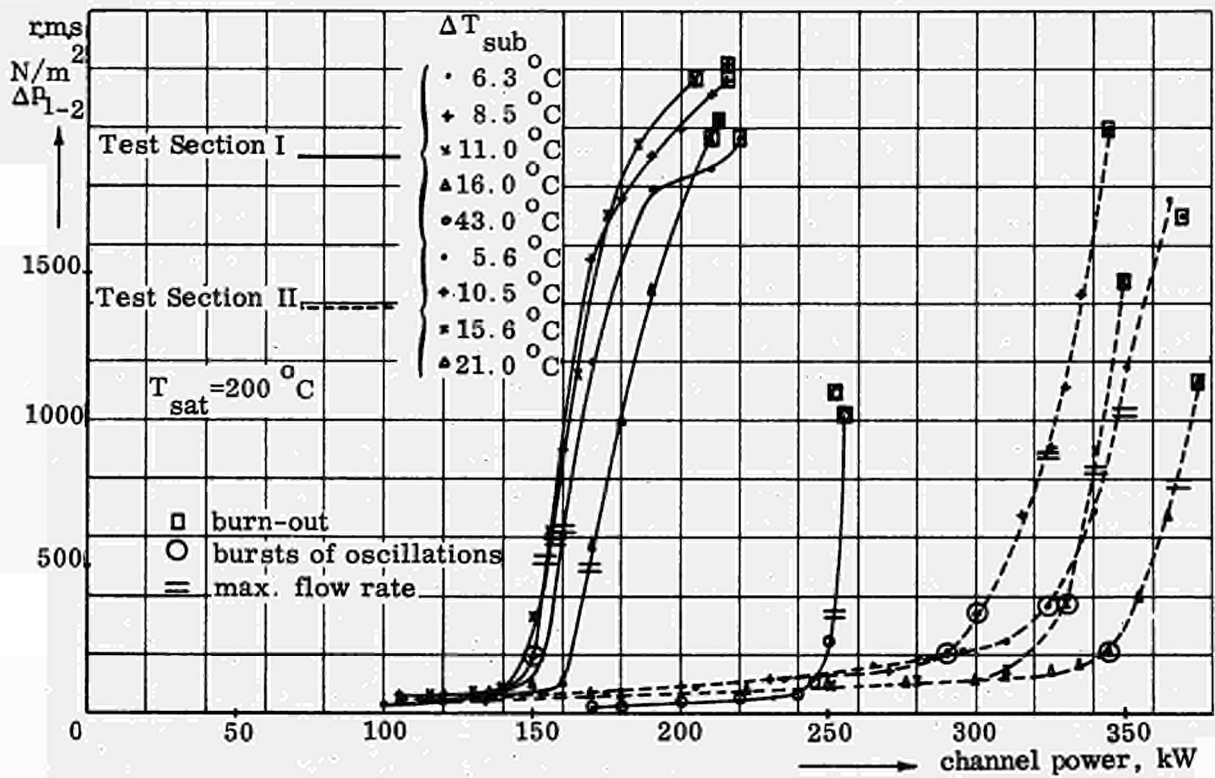


Fig. 3.19 The influence of subcooling on the onset of hydraulic instabilities, Test Section I and II.

is hardly any abrupt change from stable into unstable operation as a result of a single incremental power change, but a steadily growing lack of stability is observed over a range of power inputs. The designer of nuclear reactors must decide what fluctuations should be tolerated and up to how far in the region of flow oscillations, operation is permissible.

At low subcoolings, the effect of increased subcooling upon the onset of severe hydraulic oscillations is opposed to that at high subcoolings, as is shown in Fig. 3.19. At low subcoolings, an increase in subcooling precipitates the onset of large flow oscillations. At high subcoolings an increase in subcooling postpones the onset of large flow oscillations. For instance, at 43°C subcooling for Test Section I, severe hydraulic oscillations occur at about 250 kW channel power, compared with these oscillations starting at about 160 kW for .7°C subcooling (in either case at 200°C saturation temperature). On the contrary, at a subcooling of 11.0°C the oscillations start at about 145 kW channel power. This remarkable effect of subcooling has been reported by Styrikovich (S9) also, but any systematic data were lacking. It can only be explained by analyzing the equations governing this phenomenon. As a first approximation, it can be stated that the observed hydraulic oscillations occur only at a high value of the void fraction at the exit of the channel. Any increase in pressure and subcooling, or both, therefore, have a stabilizing effect. The destabilizing effect of subcooling is possibly caused by the increase in subcooled region, which will result in longer transport times and phase lags in the circuit. This destabilizing effect is predominant at low subcoolings.

The increase in hydraulic diameter has a stabilizing effect. The occurrence of severe hydraulic oscillations in Test Section II at a particular operating condition of pressure and subcooling has been shifted to higher channel powers compared with Test Section I. With Test Section II, the inverse effect of increased subcooling at low and high subcoolings is even more clearly demonstrated, see Fig. 3.19.

In Table 3.2., the channel powers are given at which the flow fluctuations start to increase sharply. These channel powers were obtained by extrapolating linearly the slowly and sharply increasing parts of the relevant curve and by taking the intersection of the two lines as the point of onset of instability. Other definitions of the onset of instability are certainly conceivable. For instance, by assuming that, roughly speaking the noise would increase almost linearly with the channel power, the instability threshold could be defined as the channel power at which the amplitude of the regular oscillations deviate by more than a specific percentage from the linearly increasing noise. It has been checked, by inspection of the recordings, that the assumed point of instability agreed with the channel power where regular oscillations showed up in the recordings. In the table, the frequency of the oscillations at various channel powers and the channel powers where a burn-out condition was detected, are also given. The frequencies were obtained from the autocorrelation curves.

As may be concluded from this table, the frequency of the oscillations decreases monotonically with increased subcooling. Also the frequency tends to increase with increasing channel power, especially under conditions where there is a large difference in saturation temperature and water temperature at the inlet of the channel, i. e. at the lowest system pressure and in the series with subcooling. This seems to suggest that the frequency of the oscillations and the length of the subcooled region are somehow linked up.

The range of channel powers in which oscillatory operating is possible until burn-out occurs, is narrowed with increased pressure. With Test Section II burn-out occurred at a saturation temperature of 234°C before fluctuations in the flow started.

Table 3.2. Conditions at instability threshold and burn-out

| Test Section I         |                              |         |               |                  |                  |                |       |              |                       | Test Section II        |                              |         |               |                  |                  |                |       |              |                       |
|------------------------|------------------------------|---------|---------------|------------------|------------------|----------------|-------|--------------|-----------------------|------------------------|------------------------------|---------|---------------|------------------|------------------|----------------|-------|--------------|-----------------------|
| $T_{o\text{sat}}$<br>C | $\Delta T_{\text{sub}}$<br>C | Q<br>kW | f<br>c. p. s. | $Q_{i.t.}$<br>kW | $Q_{b.o.}$<br>kW | $V^*$<br>m/sec | $x^*$ | re-<br>marks | loca-<br>tion<br>b.o. | $T_{o\text{sat}}$<br>C | $\Delta T_{\text{sub}}$<br>C | Q<br>kW | f<br>c. p. s. | $Q_{i.t.}$<br>kW | $Q_{b.o.}$<br>kW | $V^*$<br>m/sec | $x^*$ | re-<br>marks | loca-<br>tion<br>b.o. |
| 120                    | .2                           | 67      | .62           | 65               | 130              | .55            | .047  | U            | T                     | 120                    | .4                           | 125     | .72           | 125              | 187              | .82            | .040  | U            | T                     |
|                        |                              | 130     | .83           |                  |                  |                |       |              |                       |                        |                              | 180     | .80           |                  |                  |                |       |              |                       |
| 160                    | .0                           | 135     | 1.00          | 125              | 170              | .59            | .087  | U            |                       | 200                    | .7                           | 320     | 1.14          | 345              | 380              | .99            | .104  | D            | T                     |
|                        |                              | 170     | 1.00          |                  |                  |                |       |              |                       |                        |                              | 355     | 1.12          |                  |                  |                |       |              |                       |
| 200                    | .7                           | 160     | .93           | 162              | 225              | .85            | .102  | U            | T                     | 200                    | .7                           | 370     | 1.12          | 330              | 370              | 1.10           | .086  | U            | T                     |
|                        |                              | 180     | .95           |                  |                  |                |       |              |                       |                        |                              | 324     | 1.00          |                  |                  |                |       |              |                       |
|                        | 6.3                          | 160     | .77           | 151              | 220              | .90            | .081  | U            | T                     |                        | 5.6                          | 340     | .94           | 350              | 370              | 1.07           | .062  | U            | B                     |
|                        |                              | 220     | .85           |                  |                  |                |       |              |                       |                        |                              | 340     | .94           |                  |                  |                |       |              |                       |
|                        | 8.5                          | 150     | .70           | 148              | 215              | .87            | .076  | U            | T                     |                        | 10.5                         | 350     | .92           | 308              | 345              | 1.12           | .065  | U            | T                     |
|                        |                              | 215     | .82           |                  |                  |                |       |              |                       |                        |                              | 370     | .87           |                  |                  |                |       |              |                       |
|                        | 11.0                         | 150     | .60           | 145              | 205              | .87            | .069  | U            | T                     |                        | 10.5                         | 300     | .75           | 308              | 345              | 1.12           | .065  | U            | T                     |
|                        |                              | 195     | .70           |                  |                  |                |       |              |                       |                        |                              | 315     | .75           |                  |                  |                |       |              |                       |
|                        | 16.0                         | 205     | .70           | 159              | 213              | .84            | .070  | U            | B ?                   |                        | 15.6                         | 325     | .77           | 326              | 350              | 1.07           | .062  | U            | B                     |
|                        |                              | 170     | .51           |                  |                  |                |       |              |                       |                        |                              | 335     | .74           |                  |                  |                |       |              |                       |
|                        | 43.0                         | 210     | .63           | 248              | 255              | .71            | .078  | U            | B ?                   |                        | 21.0                         | 345     | .73           | 345              | 375              | 1.03           | .060  | U            | B                     |
|                        |                              | 213     | .65           |                  |                  |                |       |              |                       |                        |                              | 350     | .63           |                  |                  |                |       |              |                       |
| 220                    | .9                           | 240     | .31           | 204              | 250              | .83            | .140  | U            | T                     |                        | 21.0                         | 355     | .55           | 345              | 375              | 1.03           | .060  | U            | B                     |
|                        |                              | 252     | .31           |                  |                  |                |       |              |                       |                        |                              | 365     | .55           |                  |                  |                |       |              |                       |
| 234                    | .8                           | 210     | .98           | 204              | 250              | .83            | .140  | U            | T                     | 234                    | 1.0                          | 375     | .56           | 430              | 460              | 1.09           | .144  | S            | T                     |
|                        |                              | 250     | .93           |                  |                  |                |       |              |                       |                        |                              | 430     | 1.09          |                  |                  |                |       |              |                       |
|                        |                              | 250     | .93           | 250              | 275              | .80            | .199  | U            | T                     |                        | 6.0                          | 460     | 1.08          | 465              | 465              | 1.08           | .140  | M            | T                     |
|                        |                              | 260     | .85           |                  |                  |                |       |              |                       |                        |                              | 460     | 1.08          |                  |                  |                |       |              |                       |
|                        |                              | 275     | .87           | 250              | 275              | .80            | .199  | U            | T                     |                        | 11.0                         | 465     | .78           | 465              | 465              | 1.09           | .129  | D            | T                     |
|                        |                              | 275     | .87           |                  |                  |                |       |              |                       |                        |                              | 465     | .78           |                  |                  |                |       |              |                       |

\* Values of V and x at instability threshold channel power,  $Q_{i.t.}$   
 U=Unstable conditions, periodic flow oscillations at b.o.,  
 S=Stable conditions, no flow oscillations at b.o.,  
 T=Top half of heating element, M=Bursts of oscillations at b.o.,  
 B=Bottom half of heating element, D=Divergent oscillations at b.o.



### 3.3.3. Characterization of the hydraulic oscillations.

To obtain more detailed information on the character of the hydraulic oscillations in the intermediate frequency range, some additional recordings have been made and some further experiments have been carried out.

In Figs 3.20 and 3.22, recordings are given from various physical quantities measured during unstable flow conditions in the coolant channel. As a rule, the inlet flow oscillations are measured primarily in experiments on hydrodynamic instability. The void fraction oscillations, are of importance as well, since these oscillations produce oscillations in the nuclear power of a reactor. The behavior of the steam-void in the boiling channel of Test Section I is shown in Fig. 3.20 at a saturation temperature of  $200^{\circ}\text{C}$  and a channel power of 160 kW. Recordings of the signal from the various impedance gauges for three different subcoolings, but at constant channel power and system pressure are given together with a recording from the differential pressure gauge connected to the pitot-tube. For each void signal, the zero value is indicated. The scale for the void indicated for void gauge 1 is roughly linear. The same scale holds good for all void signals. Though the mass flow at the inlet (i. e. the differential pressure from the pitot-tube) at a subcooling of  $.5^{\circ}\text{C}$  exhibits oscillations of a modulated character, the void is oscillating only in the lower part of the channel; only the lowest void detector gives evidence of any void oscillations. As mentioned before, the stability of the system will deteriorate as subcooling is increased. The modulation of the mass flow disappears at a subcooling of  $3^{\circ}\text{C}$  and the void shows oscillations with a longer period over a substantial part of the boiling channel. The void oscillations are now maximal at void gauge 6, and hence not at the bottom of the channel. This location corresponds approximately with that where saturated boiling, as calculated from a heat balance, starts. By further increasing the subcooling to  $9.5^{\circ}\text{C}$ , the maximum in void oscillations shifts to the location of void gauge 5. The void near the exit of the channel is now likewise oscillating with a small amplitude. A study of similar recordings made at a saturation temperature of  $120^{\circ}\text{C}$  demonstrated that the fluctuations in steam-void at the exit of the channel remained small, even in the case where flow reversal occurred.

When one compares the signals under the last operating condition, a phase shift of roughly  $180^{\circ}$  can be observed between the oscillations in void at the bottom and the top. Furthermore, there is a difference of phase of  $180^{\circ}$  between the oscillations in mass flow and the steam-void at the bottom. These results have been confirmed by theoretical calculations, see chapter 5.

The latter effect has also been observed visually in the atmospheric boiling water loop, in which also spontaneous flow oscillations occurred. Some photographs made of these oscillations are shown in Fig. 3.21. When steam forms at the bottom of the channel, the signal from the differential pressure gauge across the inlet has a low value, indicating a low mass flow. After their formation, the bubbles agglomerate into large bubbles and sometimes slugs are formed. They flow to the exit of the channel, which is subsequently replenished with water at a high mass flow rate. During the agglomeration a flow reversal was observed. The whole phenomenon had an explosive character.

In Fig. 3.22, recordings are shown from other sensors for Test Section II at a saturation temperature of  $120^{\circ}\text{C}$  and a channel power of 135 kW. The signals of the differential pressure from the pitot-tube and the pressure tapplings 1 and 2 are roughly in phase, indicating that the pressure losses owing to acceleration of the mass of water moving between the pressure tapplings 1 and 2 are small. The oscillations in absolute system pressure, measured at the bottom of the downcomer, are very small and correspond to variations in saturation temperature of  $.4^{\circ}\text{C}$ . This means that the variations

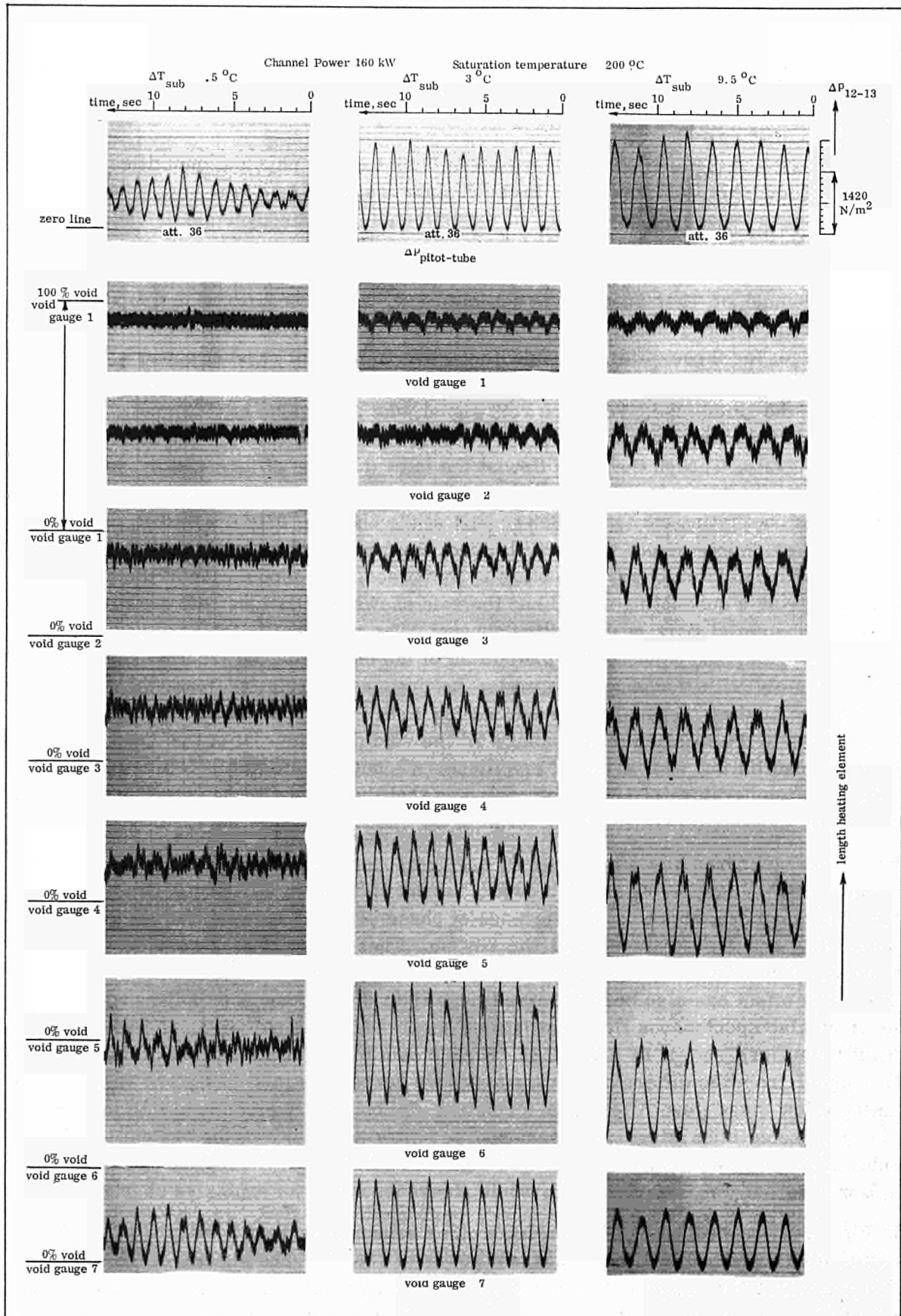
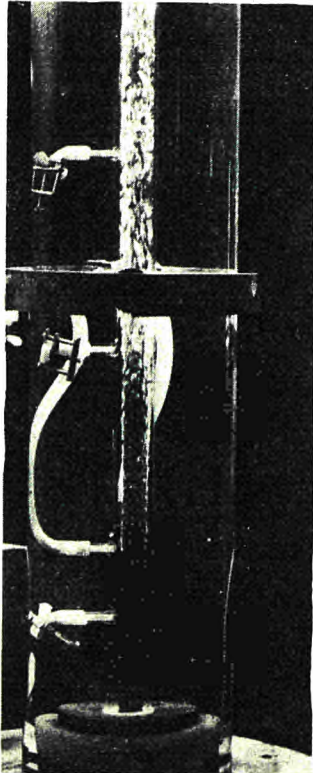
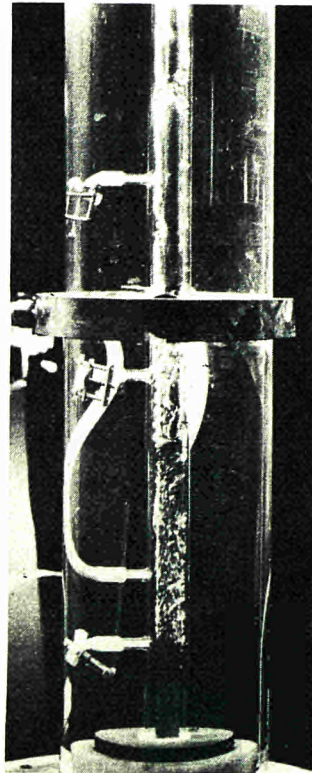


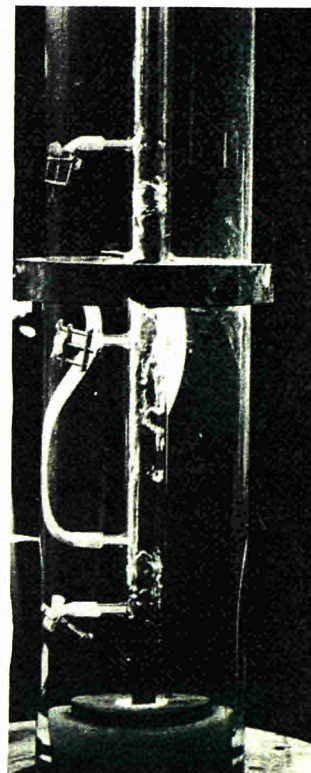
Fig. 3.20 Recordings of the signals from the various void gauges and the pitot-tube, Test Section I.



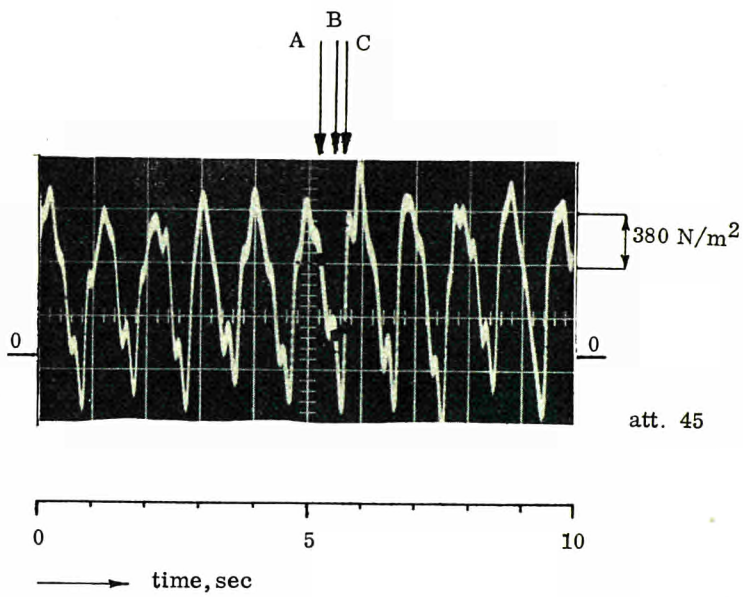
A



B



C



A bubbles rising

B loop being filled with bubbles

C agglomeration of bubbles

att. 45

Fig. 3.21 Photograph of hydraulic instabilities.

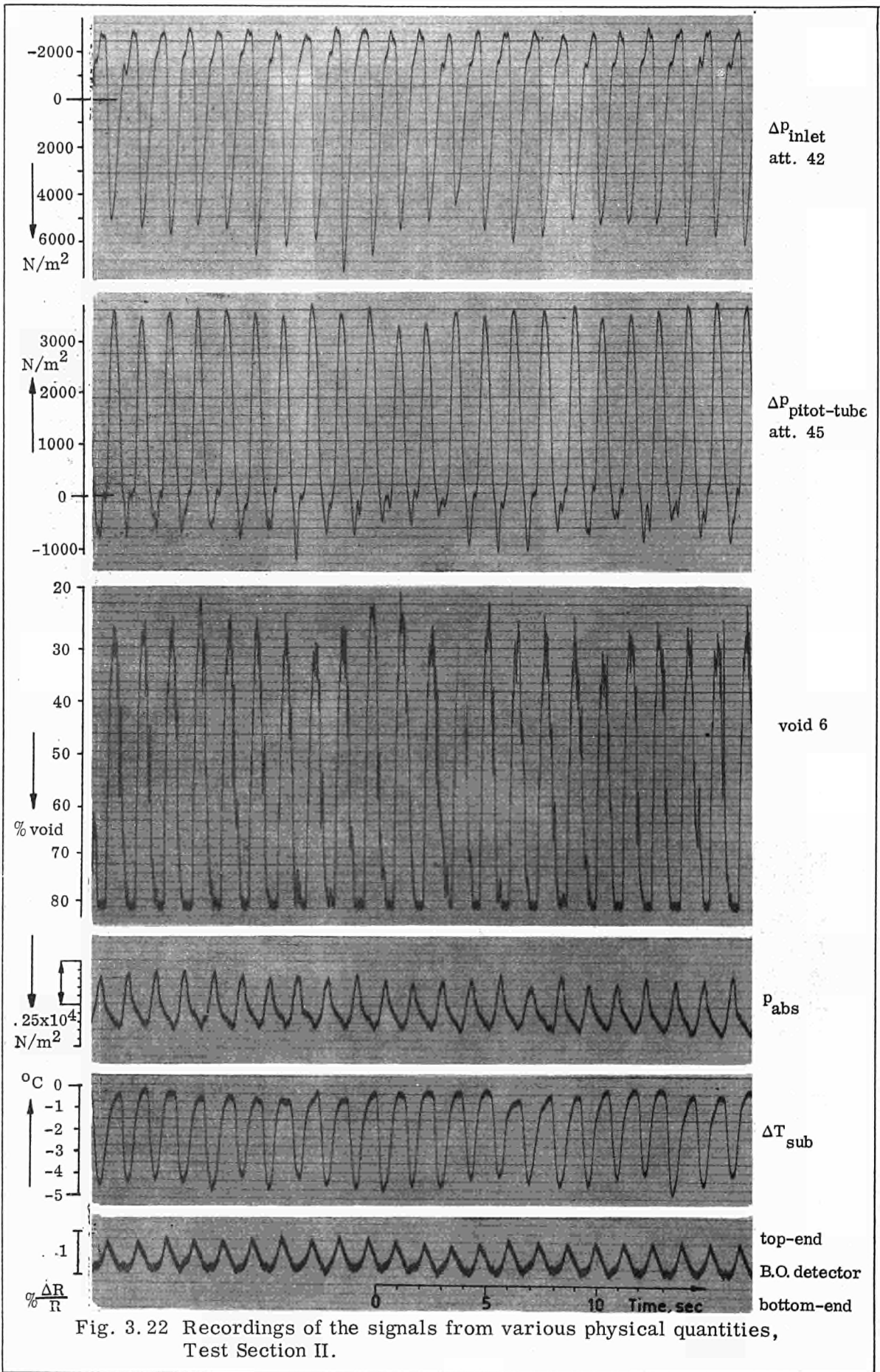


Fig. 3.22 Recordings of the signals from various physical quantities, Test Section II.

in subcooling shown are mainly variations in the inlet temperature of the channel in contrast to the low-frequency oscillations, see section 3.3.1. The signal from the burn-out detector oscillates also, which indicates alternate overheating of the top and bottom halves of the heating element as the flow varied. Although the recordings have been made simultaneously, one has to take care of the dynamic characteristics of the sensors, particularly of the thermocouples and heating element in comparing the recordings with each other.

In order to provide a check and additional information on the opposed effect of decreasing the inlet temperature at low and high subcooling rates, recordings have been made of the signal from the differential pressure of the pitot-tube at three system pressures for various subcooling rates. These are shown in Fig. 3.23 (Test Section I).

At a saturation temperature of  $120^{\circ}\text{C}$  (system pressure 2.03 ata) increased subcooling has a stabilizing effect on the flow oscillations. There is a steady decrease in the amplitude of the flow oscillations with increased subcooling. At a saturation temperature of  $200^{\circ}\text{C}$  the opposite effect is shown. An increase in subcooling from  $.5^{\circ}\text{C}$  to  $6.5^{\circ}\text{C}$  has a destabilizing effect. The amplitude of the oscillations has increased. Any further increased subcooling has a stabilizing effect and ultimately the signal from the differential pressure of the pitot-tube no longer shows any regular oscillations. At a saturation temperature of  $234^{\circ}\text{C}$ , the effect of subcooling is even more clear. An increase in subcooling from 1 to  $10^{\circ}\text{C}$  has a large destabilizing effect on the flow stability. At a subcooling of  $17.5^{\circ}\text{C}$  the flow becomes stable again. It can be concluded from these experiments that, at low system pressure, the subcooling has only a stabilizing effect. At high system pressure, the destabilizing effect becomes predominant.

It is pointed out that in these experiments the subcooling is defined as the difference between the saturation temperature above the water surface and the inlet temperature of the riser. In fact, the subcooling is larger, owing to the higher saturation temperature at the inlet of the channel, which results from the hydrostatic head. This effect is larger at lower pressures, because the fact that at lower pressures the saturation temperature changes more as a function of local pressure than at higher system pressures. For instance at  $120^{\circ}\text{C}$  saturation temperature  $3.5^{\circ}\text{C}$  must be added to the subcooling mentioned in the various figures to arrive at the local value. At 200 and  $234^{\circ}\text{C}$  saturation temperature, this is only  $.6$  and  $.4^{\circ}\text{C}$ . This effect may overshadow the destabilizing influence at the lowest system pressure.

A comparison was made between the onset of flow instability obtained from the root mean square values of the pressure loss across the inlet and those from other physical quantities, such as the differential pressure from the pitot-tube and the void fraction. The curves with exception of those from the absolute pressure and the inlet subcooling showed the same behavior and resulted in the same channel power at which instabilities started within  $\pm 2\%$  of the determined value.

The different behavior of the absolute pressure has already been mentioned, see section 3.3.1. Also the recordings from the inlet subcooling demonstrated another behavior. This is shown in Fig. 3.24, in which the fluctuations in subcooling are plotted as functions of the channel power for different saturation temperatures for Test Section I. As is shown at  $120^{\circ}\text{C}$  saturation temperature, large oscillations in subcooling are present at the very start of the flow oscillations. Even some superheat is building up. At  $160^{\circ}\text{C}$ , these oscillations in subcooling start about 10 kW later than the onset of the flow oscillations, and at  $200^{\circ}\text{C}$  about 20 kW later. At the highest saturation temperatures, no oscillations in inlet temperature were observed. The conclusion is that the inlet temperature starts oscillating only once the flow oscillations are fully developed and have obtained an appreciable amplitude. Fig. 3.24 has been made from recordings

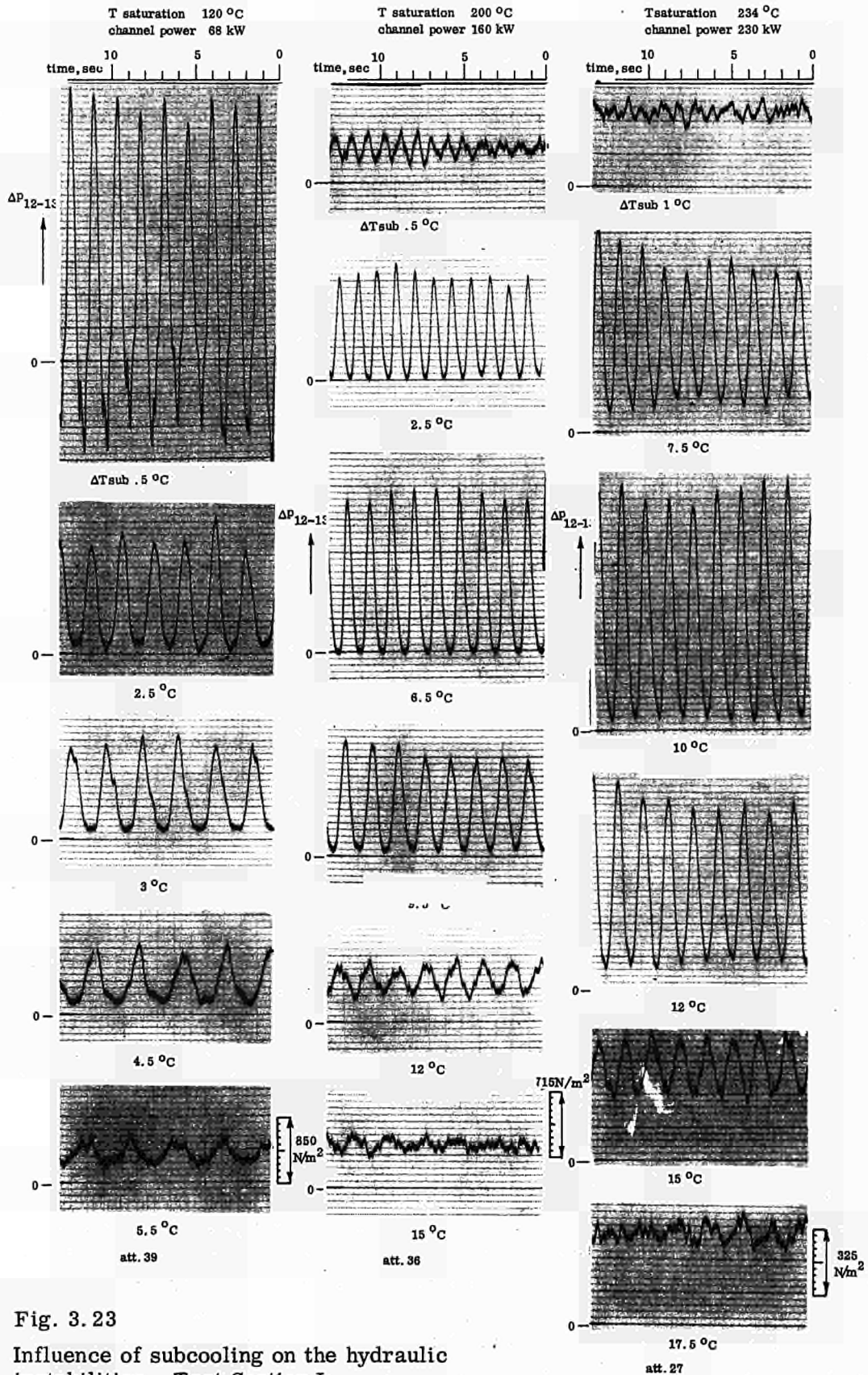


Fig. 3.23  
 Influence of subcooling on the hydraulic instabilities, Test Section I.

on a mV compensation recorder. Owing to the frequency response characteristics of the thermocouple at the inlet and of the recorder, actually the fluctuations might be somewhat larger.

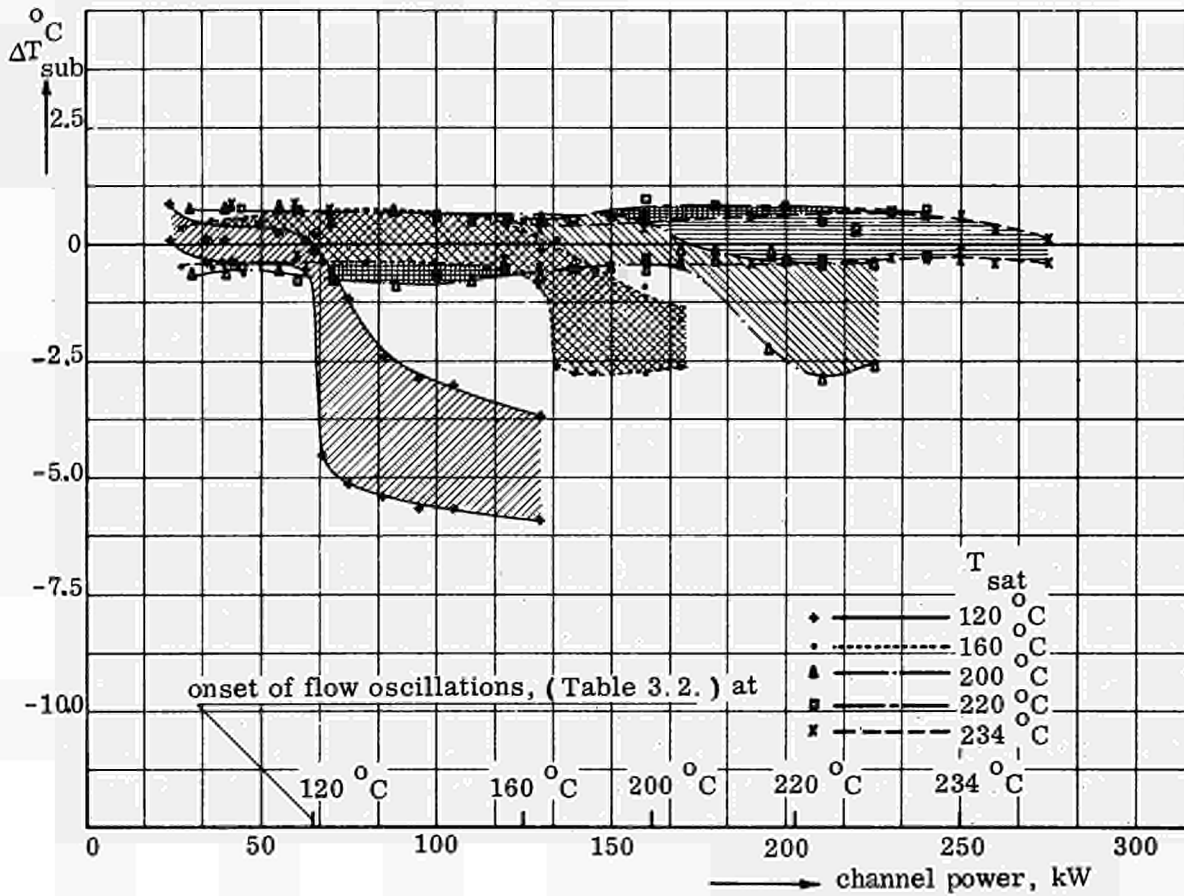


Fig. 3.24 Variations in subcooling-temperature during hydraulic instabilities, Test Section I.

### 3.4. Stability measurements

#### 3.4.1. Power-modulation experiments.

In the following, the stability characteristics of the steady state will be dealt with. A steady state is called stable if, after a small disturbance, the system will ultimately return to the original steady-state condition. The concept of small disturbance is used here, as it will always be possible to destroy completely a steady-state condition as long as the applied disturbance is large enough. Small disturbances can be generated by the inherent noise, variations in load etc.

It is not enough to know if the steady state is stable or not. Also the response characteristics, such as these are manifested by the resulting amplitudes and frequencies, are important to the designer. In order to obtain information on the stability and response characteristics of a steady-state condition of the boiling system, frequency response measurements were carried out in the region of .01 to 2 c.p.s. In these measurements, the heating power to the boiling loop was oscillated with a sine of small amplitude and varying frequency and the resulting time-dependent variation in the physical

quantities was observed. By using the Frequency Response Analyzer mentioned in section 2.5., the amplitude and phase relationship between input and output was calculated, with integration times  $T$  (see equation (2.10.)) of 100 and 1000 seconds depending on the modulation frequency. In the following, this relationship will be called the transfer function. In chapter 4, it will be shown that transfer functions and the occurrence of severe hydraulic oscillations are closely related subjects.

The assumption of small perturbations in a stability analysis means in many cases that the system is linear, which simplifies its analysis and makes the transfer function far more readily applicable. For instance, it can then be easily combined properly with the transfer functions of other parts of the system (e.g. of the reactor kinetics and the turbine or generator load) and the stability of the whole system can thus be analyzed. Also, from the measured transfer functions the response to any disturbance can be calculated within the linear range. Therefore, the experiments have been started by oscillating the heating power with different amplitudes and observing the variation in the response in order to see whether the output amplitude is proportional to the input amplitude and whether the phase shift is independent of the input amplitude. Results of these measurements, carried out at a saturation temperature of 200°C and an average channel power of 275 kW, are given in Table 3.3.

The frequency has been chosen as .5, .8 and 1.0 c.p.s. and at each frequency the amplitude was varied between 10 and 30 kW. The transfer function given is the one from channel power to the differential pressure from the pitot-tube. The measured value of the amplitude of the responding signal per kW channel power oscillation was made dimensionless by dividing it by the corresponding value at zero frequency obtained from steady-state measurements. In the following this ratio will be called the amplitude ratio  $K$ . The variation in measured phase angle lies within the accuracy of the Frequency Response Analyzer. At the frequencies of .5 and .8 c.p.s., the linearity in amplitude

Table 3.3. Transfer function for various modulation amplitudes,

$$\text{Test Section II, } H = \frac{\Delta(p_{12} - p_{13})}{\Delta Q} .$$

| $T_{\text{sat}}$<br>°C | $f$<br>c.p.s. | $Q$<br>kW | $\Delta Q$<br>kW | $K = \frac{ H(f) }{ H(f=0) }$ | $\varphi$<br>° |
|------------------------|---------------|-----------|------------------|-------------------------------|----------------|
| 200                    | .5            | 275       | 10               | 1.34                          | 160            |
|                        |               |           | 20               | 1.35                          | 162            |
|                        |               |           | 30               | 1.36                          | 164            |
| 200                    | .8            | 275       | 10               | 2.53                          | 171            |
|                        |               |           | 20               | 2.49                          | 171            |
|                        |               |           | 25               | 2.56                          | 168            |
|                        |               |           | 30               | 2.56                          | 168            |
| 200                    | 1.0           | 275       | 10               | 4.41                          | 202            |
|                        |               |           | 15               | 4.50                          | 200            |
|                        |               |           | 20               | 4.83                          | 193            |
|                        |               |           | 25               | 4.82                          | 201            |
|                        |               |           | 30               | 4.73                          | 205            |



ratio is within  $\pm 2\%$ . At 1.0 c.p.s. the increase in amplitude ratio is 10% with an increase in the amplitude of the perturbing oscillation from 10 to 30 kW. The actual value of the amplitude ratio at this frequency is about 5, which demonstrates that large amplitudes in inlet mass flow are present. The increase in amplitude ratio is therefore not surprising. Therefore, as a good approximation, an analysis can be made by assuming the system to be linear.

In a system with natural circulation, power modulation gives rise to a response in inlet mass flow as well as in steam-void, in contrast to a forced circulation system with a pump with steep head-flow characteristics. In Figs 3.25 to 3.29, results are given of transfer function measurements carried out under various operating conditions with Test Sections I and II. In these experiments the power oscillation amplitude was about 10% of the mean power level. In the upper part of the diagrams, the amplitude ratio has been plotted and defined before, as function of the frequency of the oscillation in channel power. In the lower parts of the diagrams, the phase shift of the responding signal with respect to the oscillation in channel power has been plotted. It is pointed out that there exists an attenuation and phase shift under dynamic conditions between the electrical power delivered to the test section and the power taken up by the coolant. The experimental data presented are those measured directly. They do partly include this attenuation and phase shift.

Fig. 3.25 shows the transfer function from channel power to the differential pressure from the pitot-tube, i.e. the inlet mass flow rate, for Test Section I, for three channel powers at a saturation temperature of 200°C. From the amplification characteristics it can be concluded that a resonance peak is present which increases in magnitude with channel power, while also the peak shifts to a higher frequency. Comparison of these results in this frequency region with those presented by St. Pierre (S12) and Zivi (Z3) for a forcedly circulating boiling system, which are showing no resonance peak, leads to the conclusion that these resonance peaks are characteristic for a naturally circulating system. In contrast to a forcedly circulating system, in such a system, the inlet mass flow and the steam-void are strongly intercoupled. The resonance peak, therefore, is caused by this intercoupling effect. The amplitude ratios together with the behavior of the phase shifts show that the system is only weakly damped. By increasing the channel power, the damping forces become relatively smaller and the system becomes less stable. At the highest channel power of 145 kW, which was only about 20 kW lower than the channel power where spontaneous severe hydraulic oscillations start, a sharp falling off in the phase shift is observed, indicating that the system approaches an unstable condition.

Similar results are presented in Fig. 3.26. In this diagram the transfer function from channel power to the void fraction measured at location 5, see Fig. 2.4, has been plotted for the same test section and channel powers as in Fig. 3.25. They show the same behavior, although the amplitude ratios are less. In the lower frequency range a second resonance peak is observed at a frequency of 0.04 c.p.s. This frequency corresponds with the period of the observed low frequency oscillations described in section 3.3.1. At a modulation frequency of .04 c.p.s. large oscillations in absolute pressure have been observed with an amplitude of about .1 atmospheres. This might indicate that the second resonance peak could be attributed to intercoupling of the flow process in the boiling channel with that in the condenser, which can be expected to be more important at the lower frequencies. The resonance peak in the lower frequency range could be influenced by the adjustment of the automatic controller of the coolant flow to the condenser. The observed phase lead in the lower frequency range is also thought to be attributable to these pressure variations.

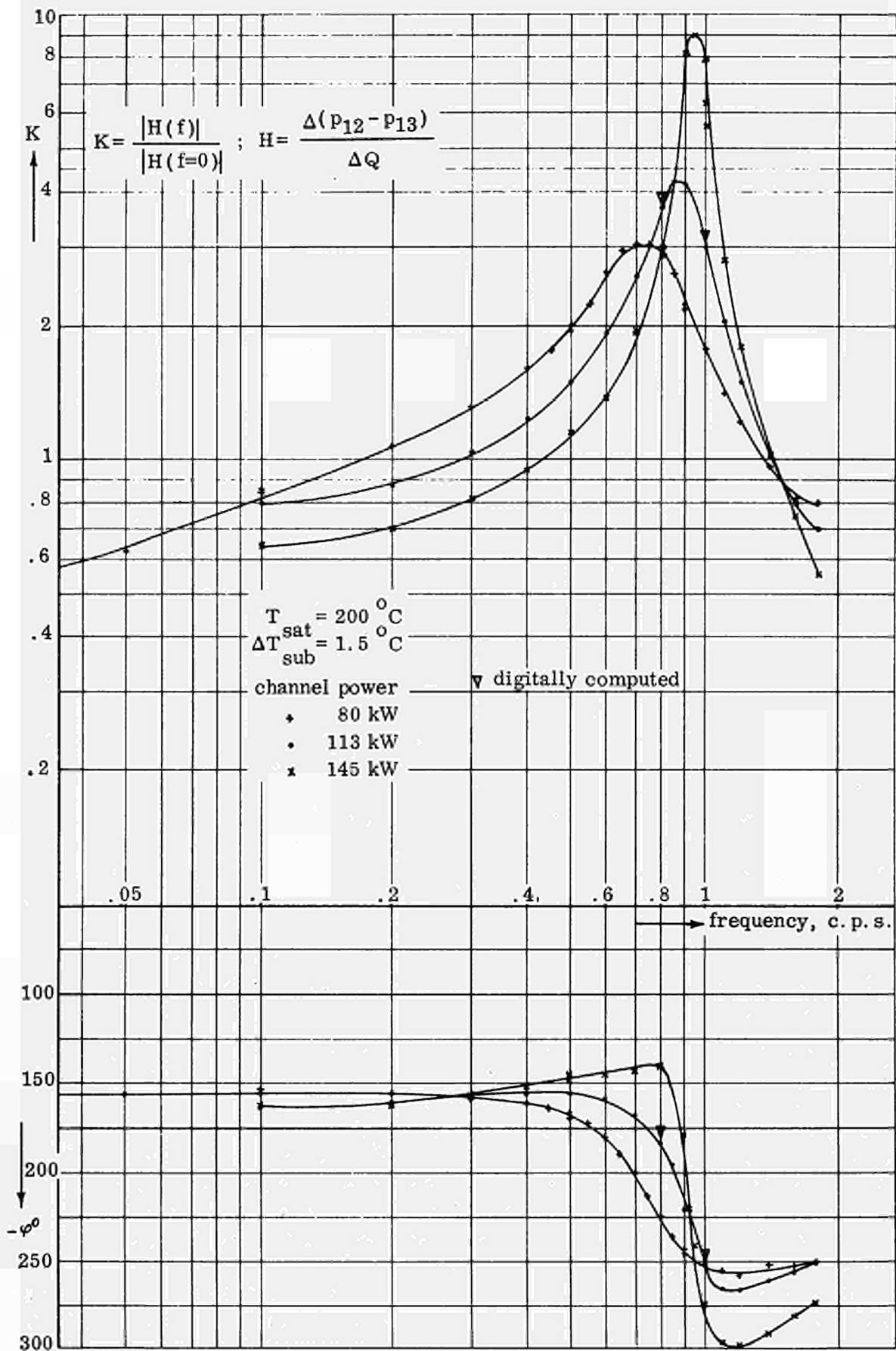


Fig. 3.25 Transfer functions from channel power to inlet mass flow for various channel powers, Test Section I.

In Fig. 3.26, some measuring points are indicated at a saturation temperature of 234°C and a channel power of 113 kW. After comparing these measuring points with those obtained at a saturation temperature of 200°C, it becomes clear that, in the range of .1 - 1.5 c. p. s. any increase in system pressure is to promote the stability of a two-phase system.

In Fig. 3.27, the influence of subcooling on the stability of a steady state is shown. Results of transfer functions are given for Test Section I at a saturation temperature of 200°C and a channel power of 113 kW. The transfer function from channel power to the differential pressure from the pitot-tube has been plotted for three values of subcooling. Comparing the curves of 1.5°C and 10.8°C subcooling at the corresponding resonance frequency shows that the amplitude ratio at 10.8°C subcooling is greater than at 1.5°C subcooling at about the same phase shift. This indicates that increased subcooling in the lower subcooling range does indeed impair the stability of the steady state. At high subcooling rates, the opposite is true. Increasing subcooling from 10.8°C to 32.0°C results in lowering the resonance peak, whilst also the phase shift is reduced. This indicates that at high subcooling rates, any further increase in subcooling has a stabilizing effect. The opposite effects of increasing subcooling in the low and high subcooling ranges are similar to the effects of subcooling observed in the experiments carried out to establish the onset of hydraulic oscillations. The small phase shift in the low frequency range measured at the highest subcooling rate indicated that the prevailing operation condition was situated before the maximum in the circulation rate versus channel power curve; an increase in channel power results in an increase in mass flow rate. (see Fig. 3.3). All other operating conditions are on the descending part of the circulation rate versus channel power curves. The phase shift for these conditions must therefore approach -180° for a frequency approaching zero.

It should be noted that in the transfer function at a subcooling of 10.8°C, a second resonance peak can be observed at a frequency of 1.2 c. p. s. This is shown in the amplitude ratio as well as in the phase shift. This second resonance peak was observed at the end of the experimental program and no time was left to verify whether also the other curves were to reveal a similar effect as well. It might be that this second peak, preceded by a dip, is related to a similar behavior observed in the forced circulation measurement made by St. Pierre (S12). There the appearance of a dip in the frequency response characteristics was attributed to a transport effect associated with the downstream propagation of the void perturbation. It would be interesting to carry-out additional transfer function measurements from channel power to steam-void and recirculation rate in the higher frequency range.

In Fig. 3.28, results are plotted of the transfer function from channel power to the void fraction measured at different locations for Test Section I at a saturation temperature of 200°C and a channel power of 113 kW. This diagram clearly shows that the magnitude of the power-induced oscillations in local void fractions is greater upstream. This corresponds with the observations made in the signals from the steam-void, and recorded for a characterization of the hydraulic oscillations. It is noted that these transfer function measurements have been carried out at low subcooling rates. At higher subcooling, different characteristics may be expected. Also in the curves presented, a phase lead and a small resonance peak in the lower frequency range is being observed.

In Fig. 3.29, finally, results of transfer function measurements carried out with Test Section II have been plotted. The transfer functions from channel power to the differential pressure from the pitot-tube are given at a saturation temperature of 200°C for various channel powers. In these curves the same behavior as in Fig. 3.25 is shown.

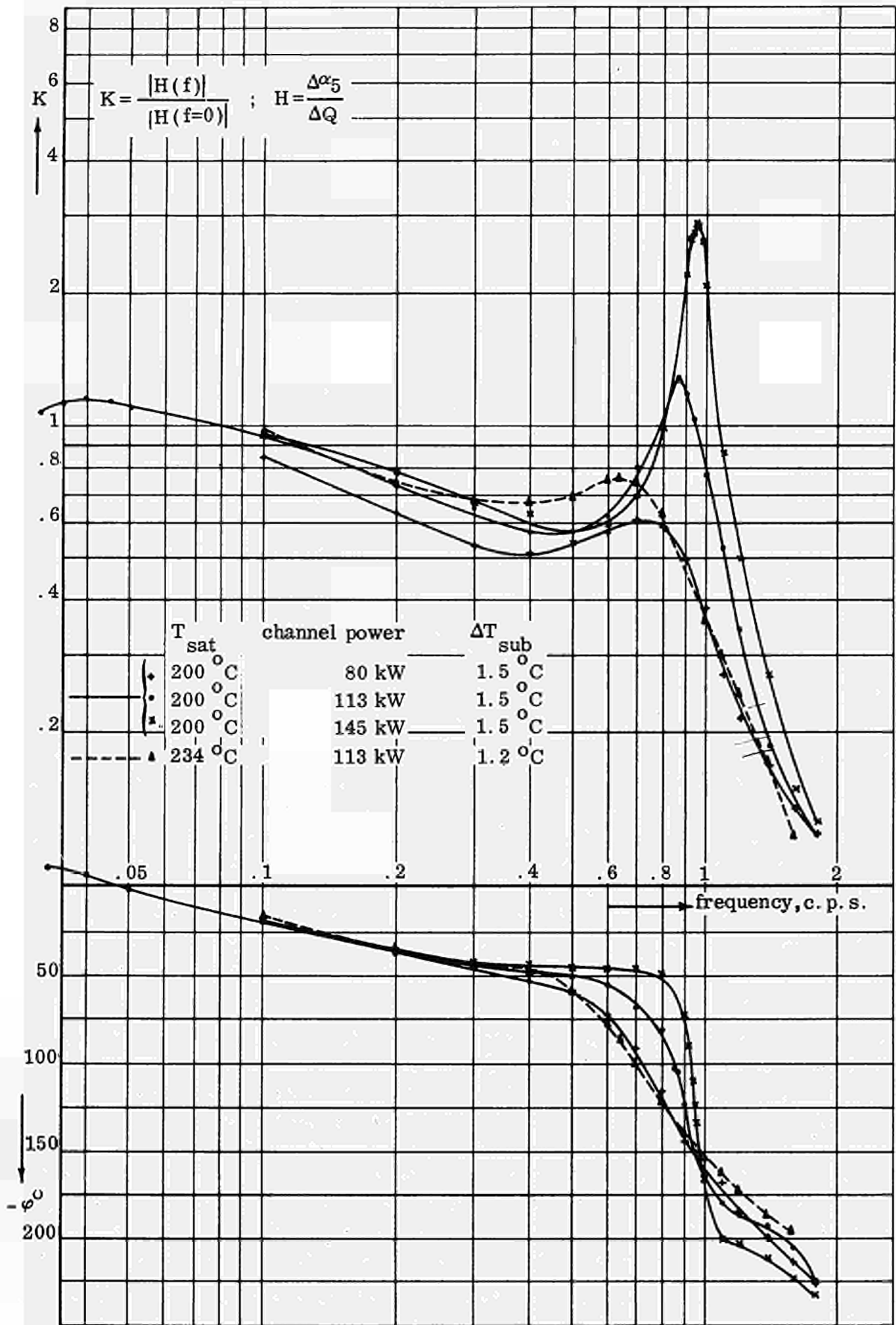


Fig. 3.26 Transfer functions from channel power to local void fraction for various channel powers and system pressures, Test Section I.

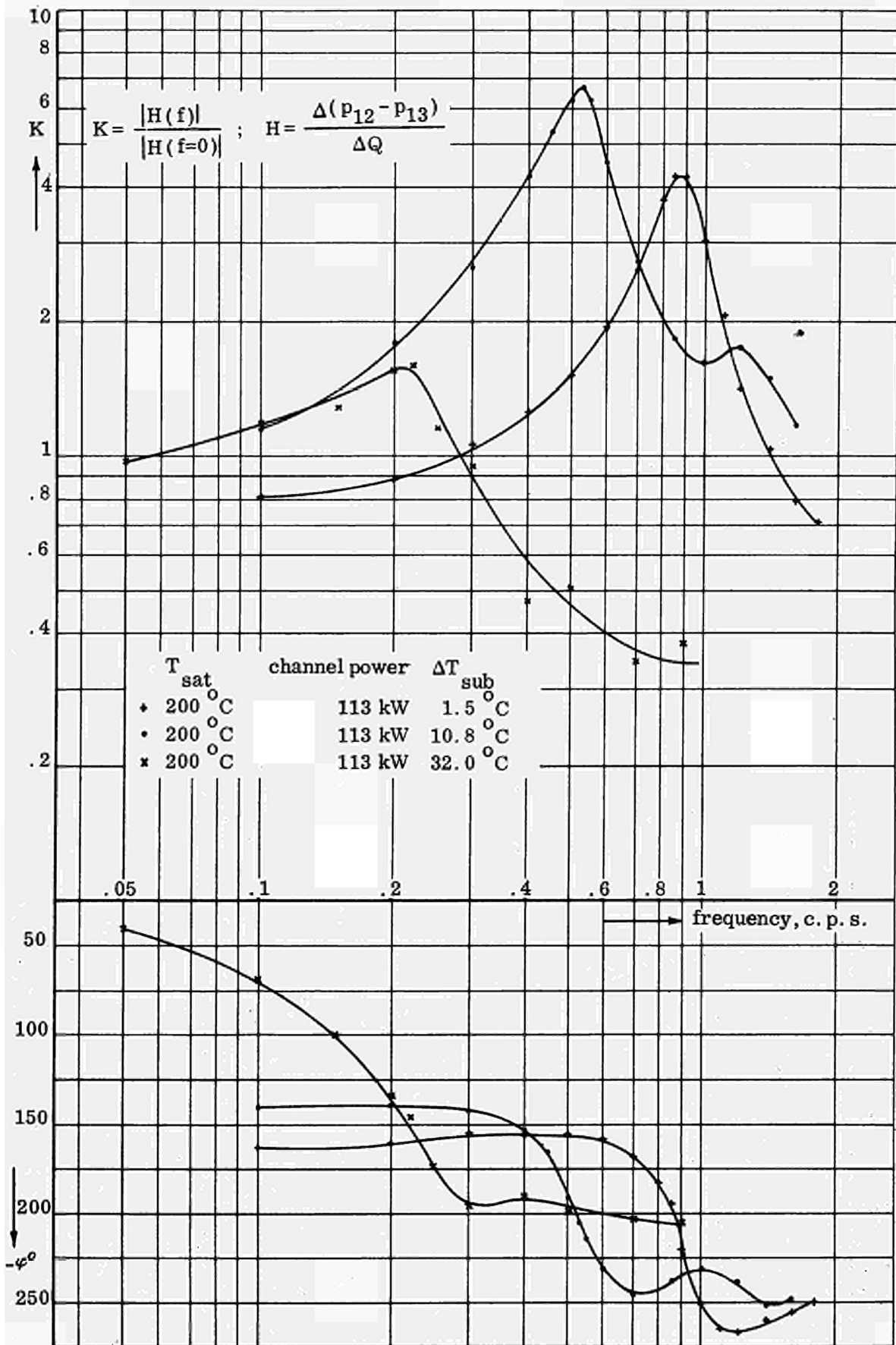


Fig. 3.27 Transfer functions from channel power to inlet mass flow at various subcoolings, Test Section I.

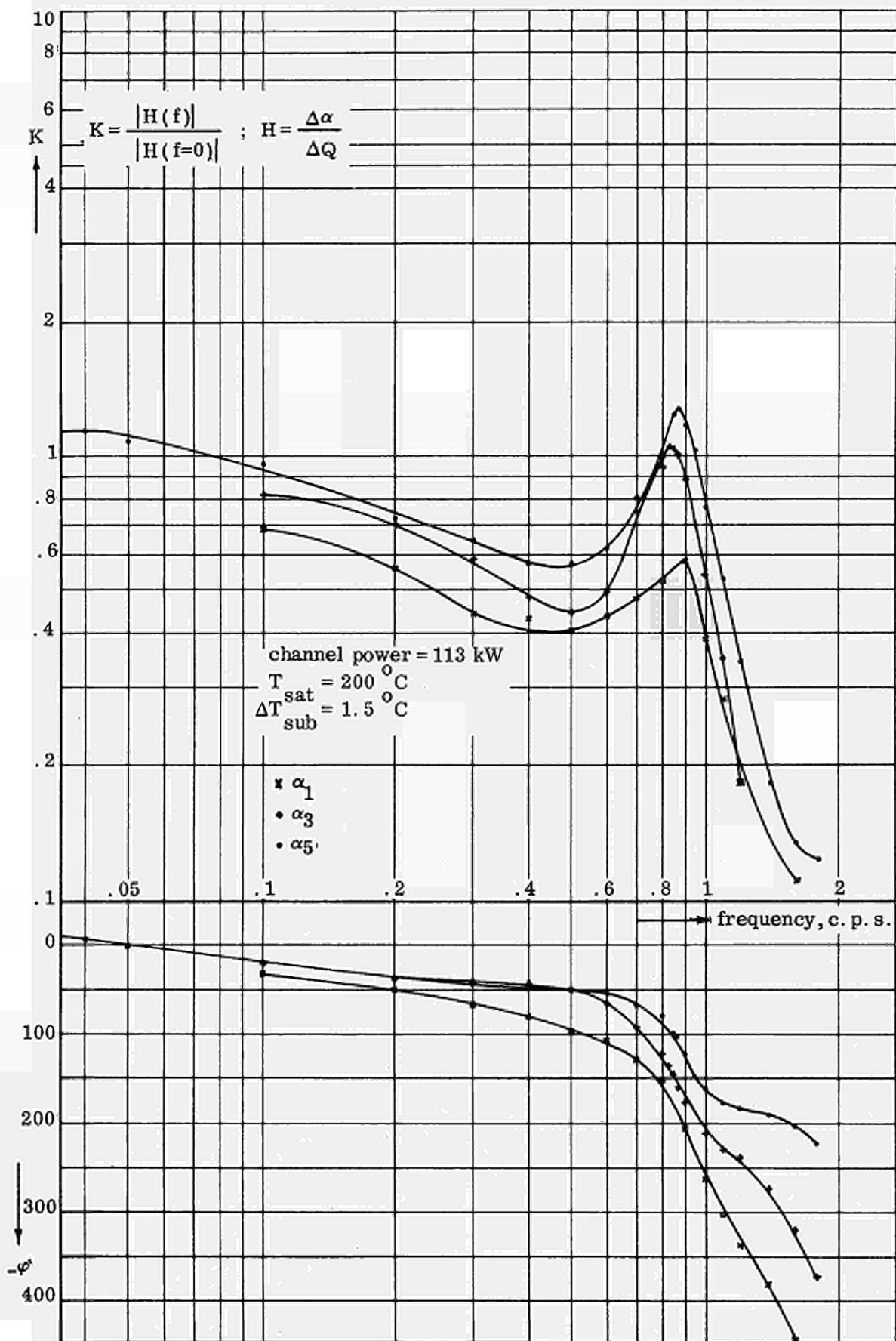


Fig. 3.28 Transfer functions from channel power to the void fraction at different locations, Test Section I.

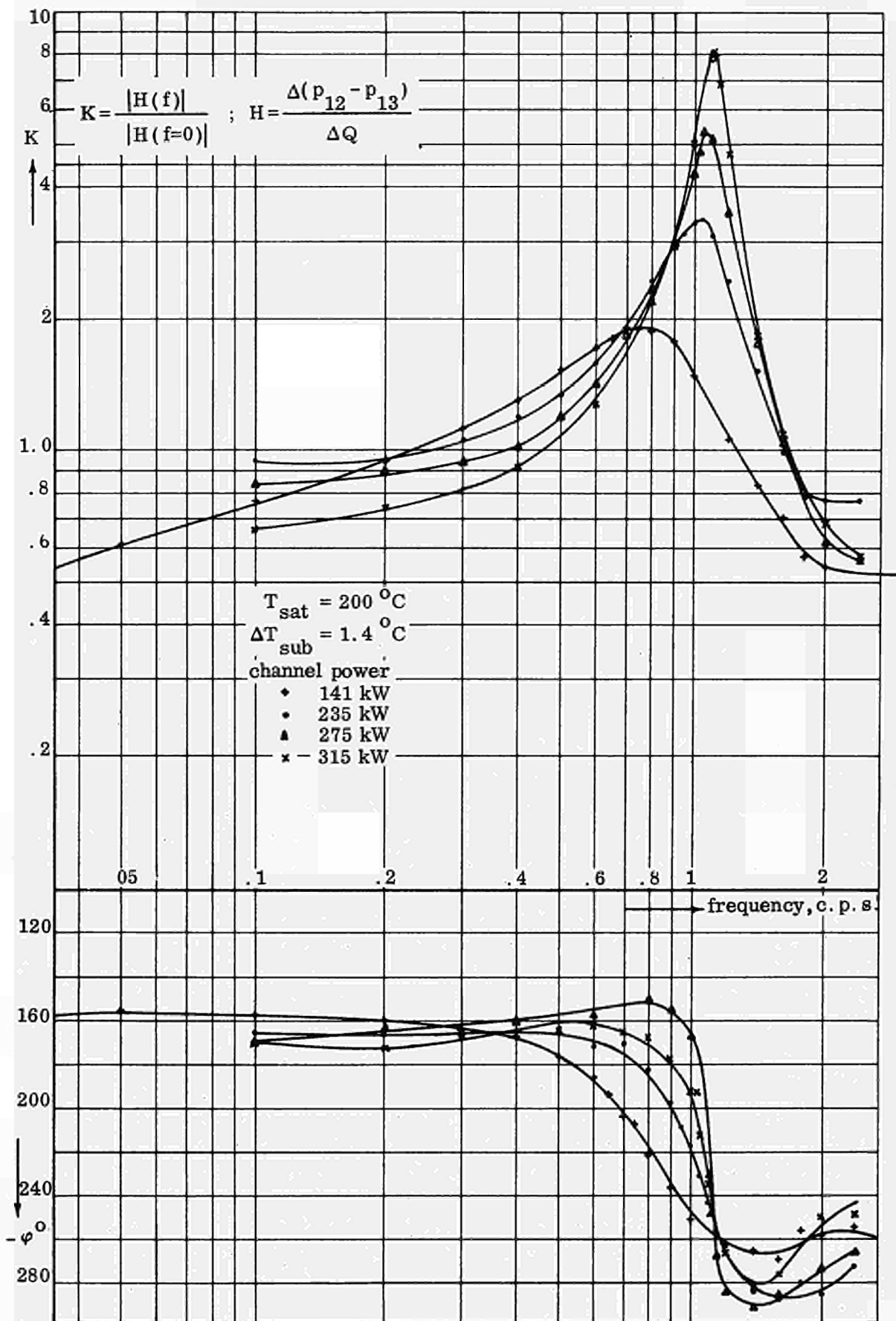


Fig. 3.29 Transfer functions from channel power to inlet mass flow for various channel powers, Test Section II.

An increase in steady-state channel power results in a higher resonance peak and resonance frequency. Comparing the curves measured at 141 kW channel power with the one measured with Test Section I at a fractionally higher channel power of 145 kW leads to the conclusion that an increase in hydraulic diameter will improve the stability of a two-phase flow.

The intercoupling effects between the inlet mass flow and the steam-void have already been mentioned. Owing to the finite volume of the condenser, oscillations in absolute pressure have been observed in the power modulation experiments. These oscillations also influence the steam-void and the inlet mass flow and, therefore, influence the measured transfer functions. Although little work has been done in measuring the transfer function from channel power to system pressure, some indication of the magnitude of the pressure oscillation will be given.

At a saturation temperature of 200°C, a channel power of 113 kW and with nominally no subcooling, a pressure oscillation of 4000 Newtons per square meter amplitude has been observed at a frequency of .1 c.p.s. and an amplitude in channel power of 10 kW. The phase lag of the pressure oscillations with respect to the channel power was about 80°. At a frequency of .8 c.p.s., the amplitude of the pressure oscillation was already decreased to 220 Newtons per square meter and at 1.8 c.p.s., the oscillations were even less than 80 Newtons per square meter. This indicates that the pressure oscillations may produce a detectable influence in the lower frequency range only.

In this section, some results were presented of frequency response measurements carried out on a naturally circulating boiling system. In chapter 4, some comments will be given on the interrelationship between the observed hydraulic instabilities, the measured transfer functions and the steady-state performance characteristics.

#### 3.4.2. Boiling noise correlation studies.

In the foregoing use has been made of the concepts of autocorrelation and spectral power density for establishing the presence of regular hydraulic flow oscillations, resonance frequencies and the onset of hydraulic oscillations in the intermediate frequency range. In applying these concepts, the assumption is always made that the process is stationary, i.e. that the statistical properties are independent of the time. Furthermore, the two quantities have been obtained from a single recording of finite length. The autocorrelation and spectral power density thus estimated are random quantities. The errors introduced by using these quantities have been dealt with by many authors (B13). They depend mainly on the recording length, the time displacement and the bandwidth chosen in the analysis of the signals. In the experimental program, attention has been paid to this and several checks have been made on the reproducibility and accuracy of the results.

As mentioned before, two methods have been employed for estimating the average power per unit bandwidth, to wit the direct analogue computation with the ISAC noise correlator, and the indirect method via the autocorrelation and Fourier transformation, by using a digital computer program (A1). The digital technique generally offers greater flexibility than the analogue method, and produces more information. However, when a specific type of analysis is to be performed repeatedly, it may be more economical or efficient to use a continuous or analogue data processing method.

When the ISAC noise correlator was used, the recording length was taken to be 80 seconds for evaluating the characteristics in the intermediate frequency range of 0.1 to 4 c.p.s. and to be 15 seconds for the high frequency range at about 15 c.p.s. The ratio



of the playback-to-recording speed was 1:16 and 1:1 respectively for the two cases mentioned. In either case the 100 time steps adjustment was selected. (see section 2.5.). A check has revealed that the recording length had no appreciable influence on the results.

In the digital computations, the recording length was likewise 80 seconds. In most cases the signals have been digitized in 1000 samples taken at .08 second intervals. The autocorrelation was computed for 100 values of the time displacement  $\tau$  between 0 and 8 seconds. This was also the integration interval for calculating the spectral power density, which was computed in steps of .05 c. p. s. from 0 to 4 c. p. s. In the choice of the different lengths and time intervals the folding effects and the required resolution have been taken into account (A1). For several cases, the onset of hydraulic oscillations has been determined by the direct as well as by the indirect method. For one case, the results are given in Fig. 3.18. The discrepancy between the calculated points is small. The same threshold for instability is being obtained.

The transfer functions presented in the Figs 3.25 to 3.29 have been obtained, as explained before, by performing a Fourier analysis of the signal resulting in a rejection of the noise and harmonics from the direct response to the perturbing sinusoidal signal. The transfer function can also be computed on a digital computer from recorded signals, using cross-correlation techniques. The digital computer program mentioned before has been extended for making such an analysis. Let  $H(j\omega)$  represent the transfer function of the system between two variables  $x(t)$  and  $y(t)$  and let  $x(t)$  be the perturbing sinusoidal signal of the system and  $y(t)$  the system response signal which is also influenced by extraneous system noise  $n(t)$ . If  $x$  and  $n$  are statistically uncorrelated, then the transfer function can be determined from the power spectrum from the input  $\Phi_{xx}(\omega)$  and the input-output cross spectrum  $\Phi_{xy}(j\omega)$  by, (A1),

$$H(j\omega) = \frac{\Phi_{xy}(j\omega)}{\Phi_{xx}(\omega)} . \quad (3.5.)$$

The power spectrum of the output  $\Phi_{yy}(\omega)$  is given by:

$$\Phi_{yy}(\omega) = \Phi_{xx} |H(j\omega)|^2 + \Phi_{nn}(\omega) . \quad (3.6.)$$

If  $\Phi_{nn}(\omega)$  is very small compared with  $\Phi_{yy}(\omega)$ , then the modulus of the transfer function can be determined from the input-output spectra:

$$|H(j\omega)| = \left( \frac{\Phi_{yy}}{\Phi_{xx}} \right)^{\frac{1}{2}} \quad (3.7.)$$

The power-spectra density technique (equation 3.7.) cannot provide phase-response measurements, and as long as  $\Phi_{nn}(\omega)$  is not small compared with  $\Phi_{yy}(\omega)$ , equation (3.7.) will not give the true gain response. Thus, cross-spectral density techniques should be used whenever extraneous noise is excessive or whenever phase-response information is required. During the frequency response measurements presented in section 3.4.1., all signals have been recorded on a FM magnetic tape. By the computer program, the transfer functions have been calculated between channel power and the dependent variables. In Fig. 3.25 some results are plotted in the graphs obtained by the analogue method. The transfer function from channel power to inlet mass flow rate

computed on a digital computer is being compared with the one computed by analogue techniques. The two methods must, of course, have the same errors when applied to measurements having the same recorded length. It is interesting to notice that the agreement between the two methods is excellent.

The same computer program can be used for calculating the frequency response characteristics between two noisy but correlated signals, which are being generated within the system, without excitation. Owing to the weakness of the signals and lack of adequate signal information in the time or frequency range of interest, this technique may, however, be subject to serious statistical errors. Some results of using this technique are presented in Fig. 3.30b. The modulus of the transfer function of the signal between the pitot-tube and the impedance void gauge located at position no. 4 is given as a function of the frequency on an arbitrary scale. The transfer function has been calculated by means of equation (3.5.) and equation (3.7.) as well. In the region where much signal information can be expected, e.g. in the range of .8 to 1.2 c.p.s. (see also Fig. 3.29) the two methods give practically identical results. In this region, the noise component  $\Phi_{nn}(\omega)$  is small compared with  $\Phi_{yy}(\omega)$ . Outside this region, there is more dispersion in the computed results and rough tendencies can only be detected. In this case, the recording length was 100 seconds. The two signals have been digitized into 2000 samples with a time interval of .05 second. The maximum time displacement was chosen as 15 seconds in steps of .05 second. More development and evaluation work is

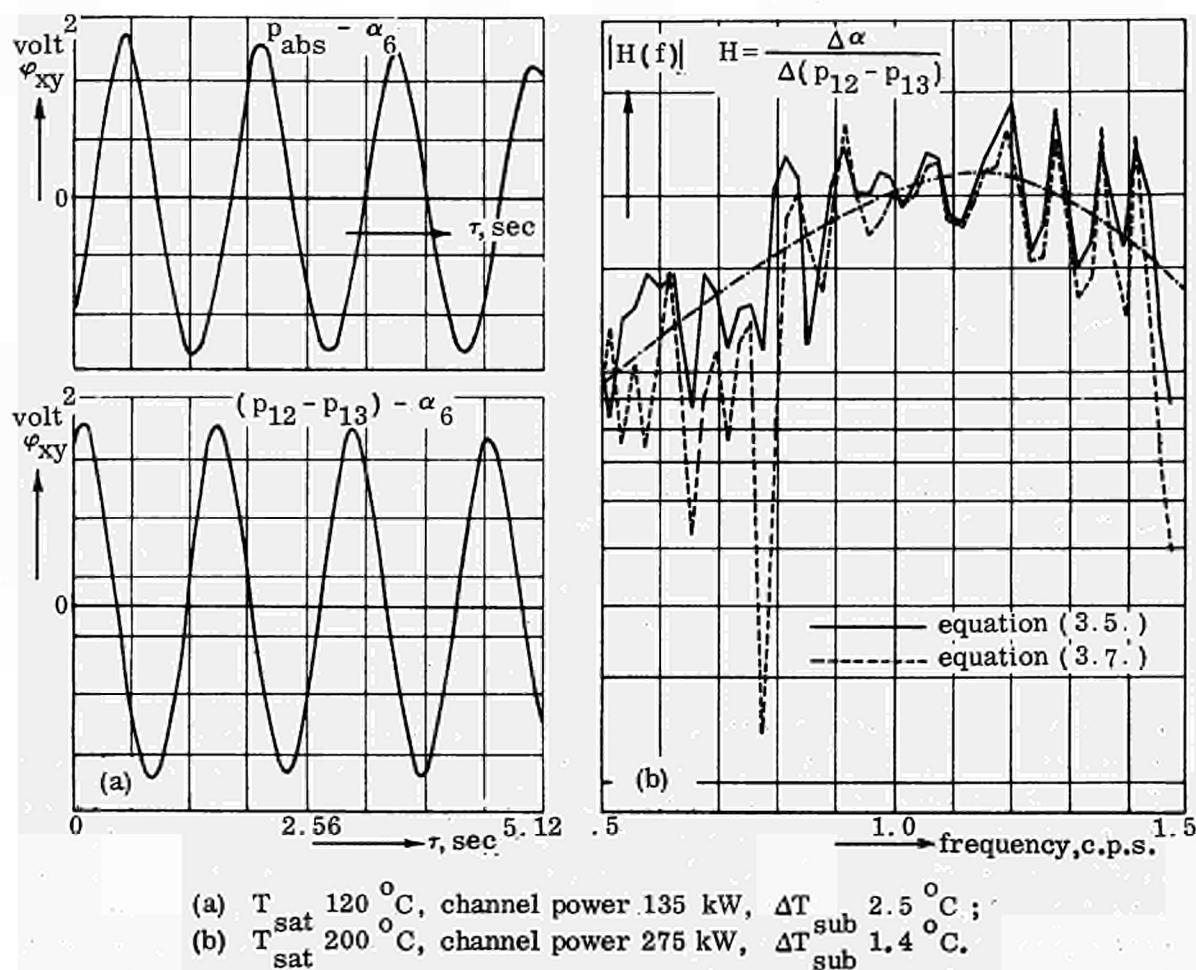


Fig. 3.30 Results of the analysis of the inherent noise, Test Section II.

needed to determine whether a change in the chosen lengths and time intervals will improve the accuracy of the results. Naturally, external excitation by random, periodic or step functions will result in far more reliable results. It is, however, the merit of noise analysis techniques that they allow complicated mechanical devices for external excitation to be avoided. This is, for instance, the case when one likes to measure the transfer function from inlet mass flow to local void fraction.

As was already mentioned in the introduction, the transfer function between the void volume and inlet mass flow plays an important rôle in some stability analyses (K1), (Z3). In Fig. 3.30b, it is shown that there is a flat resonance peak at the position where the transfer function from channel power to inlet mass flow likewise exhibits a resonance peak. The strong interaction between void volume and inlet mass flow rate in a naturally circulating system contributes greatly to the resonance peak shown in Fig. 3.29.

A last application of using cross-correlation techniques in the experimental program is shown in Fig. 3.30a. Cross-correlations have been plotted of the signals from the absolute pressure, the inlet mass flow rate and the void fraction at location 6.

The signals have been recorded during unstable operation, during which large flow oscillations were present. The diagram shows that the signals from the various quantities are strongly correlated. From these cross-correlations, the phase shift between the signals can be obtained directly by measuring the time displacement until the first peak occurs. Keeping in mind that the electrical signal of the impedance void gauge and that of the capacitive pressure gauge are increasing with decreasing void fraction and absolute pressure, the phase difference between the absolute pressure and the void fraction at location 6 as estimated from Fig. 3.30a is  $140^\circ$  and that between the inlet mass flow rate and void fraction at location 6 is equal to about  $155^\circ$ . These values are roughly in agreement with those shown in the Figs 3.20 and 3.22.

In the foregoing, the application and the usefulness of noise analysis in obtaining information on the dynamic behavior of a two-phase system have been demonstrated. The cross-correlation technique has been found to be a powerful technique for eliminating the effects of external noise. The technique using a harmonically oscillating input yields accurate results, but the required measuring time is long. Some improvement may be gained by application of a multi-frequency method in which the input signal is built up from a number of sines. The application of the analysis of the inherent noise to the dynamic analysis asks for further development and evaluation work.

### 3.5. Influence of the water level

As already mentioned in the introduction to this chapter, small variations in water level were present during operation. The water level varied because of thermal expansion of the water and the formation of steam. Therefore, it has been checked whether any changes in water level have some effect upon the measured characteristics.

In Fig. 3.31, the influence of a change in water level upon the static pressure along the coolant channel is given. Horizontally the water level has been plotted as a fraction of the heated length. The location of the exit of the coolant channel has been indicated. Vertically, the pressure difference has been plotted between the static pressure at a particular location and at location 1 at the bottom-end of the downcomer. As can be concluded, a change in water level has no influence, as long as the water level is above the exit of the channel. By lowering the water level to below the channel exit, an appreciable change in the characteristics appears. A decrease in pressure loss across the inlet, corresponding to a decrease in inlet mass flow rate, is being observed. It might

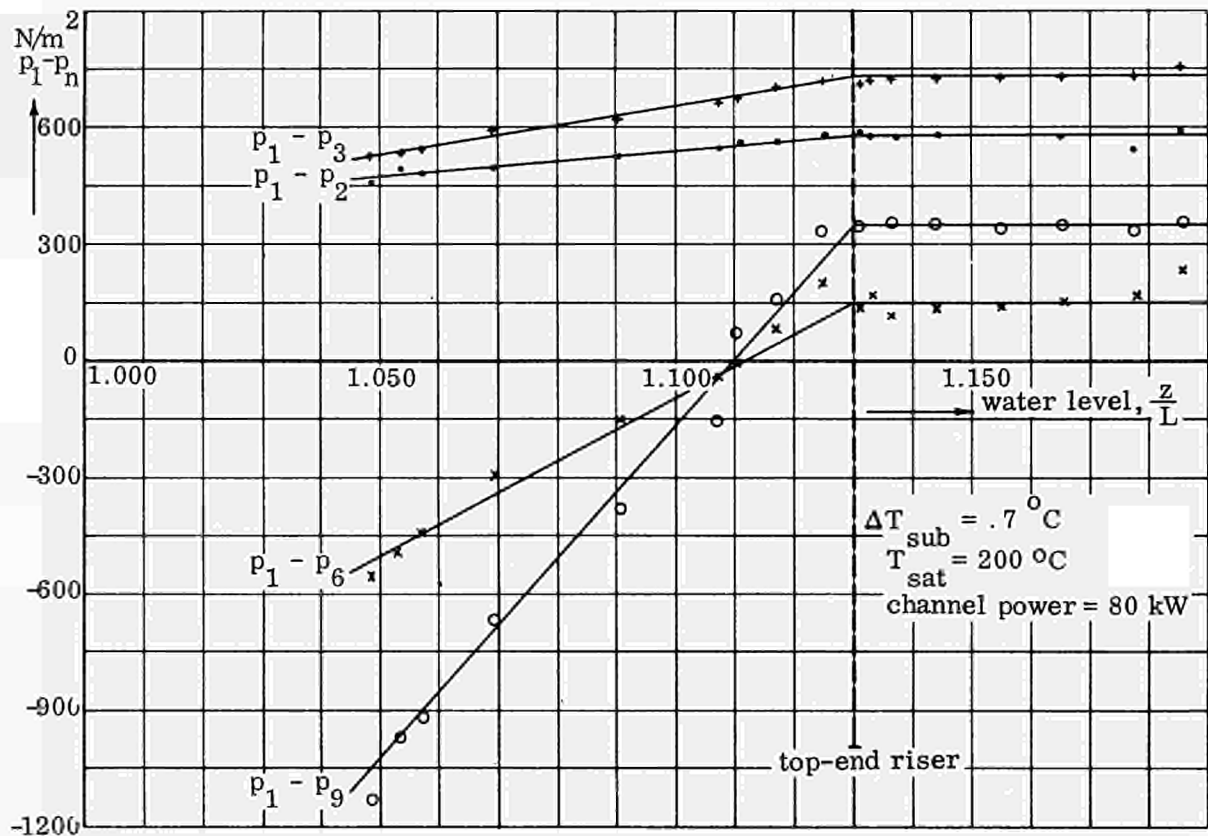


Fig. 3.31 Influence of the water level on the steady-state performance. Test Section I

appear at first sight that the water level could have some effect upon the subcooled length owing to the fact that the water level determines the local pressure and thus the local saturation temperature. From results of these experiments, which are in agreement with those published by Asyee (A2), it is found, that this effect is insignificant. The influence of water level is so small that it may be disregarded, once the exit of the channel is covered. This means also that correction for water level on the performance characteristics, which is commonly applied, is not justified and gives too high values of the subcooled length. It should be noted that the water levels are apparent water levels measured by the water level gauge.

At a saturation temperature of  $200^\circ C$ , also the influence of the water level on the stability characteristics has been measured. Transfer function measurements from channel power to differential pressure from the pitot-tube have been carried out with Test Section II at two water levels,  $z/L = 1.144$  and  $1.130$ . The channel power in these experiments was 275 kW, and the amplitude of the modulation 20 kW. The frequency was varied between .8 and 1.2 c.p.s. The difference in measured phase angle between the two conditions was within the accuracy of the analyzing apparatus, i. e. within  $\pm 3^\circ$ . The difference in modulus of the transfer functions was larger. At a frequency of 1.0 c.p.s., i. e. just at the top of the resonance peak, the difference between the two transfer functions was about 10%. At the higher and lower frequencies tested, the difference was smaller, i. e. at .8 c.p.s. about 5% and at 1.2 c.p.s. about 1%.

Generally, it can be said, that the minor changes in water level as occurring during the operation of the loop had no appreciable influence on the presented data on the steady-state and dynamic characteristics of the naturally circulating boiling channel.

## 4. Analysis of the experimental results

### 4.1. The slip between the two phases

The ability to predict the steam-volume fraction in a two-phase system as a function of the design and operating parameters is very important for a complete performance and stability evaluation of the system. This is especially true for a nuclear reactor where the steam-volume fraction influences the nuclear and thermal heat fluxes (The heat flux is defined as the heating power per unit area of the heated surface). Because of the complexity of the problem, the prediction of the steam-volume fraction  $\alpha$  is almost completely empirical. The existing theoretical and empirical formulations correlate either the actual steam-volume fraction or a quantity involving the velocity of the phases, e.g. the phase-velocity difference  $V_S - V_L$  or the phase-velocity ratio  $V_S/V_L$ , usually called the Slip Ratio  $S$ . They are derived from experiments carried out in air-water or steam-water systems with and without heat addition. The Slip Ratio,  $S$ , for instance is derived from a mass balance perpendicular to the flowing fluid. Commonly it is said that the mass flow of steam  $M_S$  and of water  $M_L$  are equal to:

$$M_S = \alpha \rho_S V_S A_C ; \quad (4.1.)$$

$$M_L = (1-\alpha) \rho_L V_L A_C ; \quad (4.2.)$$

The quantities in these equations represent mean values over the cross-section of the channel. Summation of (4.1.) and (4.2.) yields the total mass flow  $M_t$ , which is constant along the coolant channel under stationary conditions. The ratio of the mass flow of steam to the total mass flow is generally called the steam quality,  $x$ . Introducing this quantity into (4.1.) and (4.2.) and dividing one equation by the other, results in the following expression:

$$\frac{\alpha}{1-\alpha} \frac{\rho_S}{\rho_L} S = \frac{x}{1-x} , \quad (4.3.)$$

where:

$$S = \frac{V_S}{V_L} , \quad (4.4.)$$

and  $V_S$  and  $V_L$  are considered as the mean values of the phase velocities over the cross-section. The Slip Ratio,  $S$ , correlates between the steam quality  $x$  and the void fraction  $\alpha$ . The steam quality can be calculated from a heat balance. By using a correlation for  $S$ , the steam-volume fraction for a particular coolant channel can be established.

Because the steam is flowing at a faster rate than the liquid, it is commonly assumed that the slip factor is greater than unity and only approaches the limit of unity in the event when either of the phases ceases to exist. Especially at high pressures, it is customary to use a slip factor of unity in performance calculations. This should be ascribed to a misinterpretation of the foregoing equations. It should be kept in mind that the right-hand side of equations (4.1.) and (4.2.) are integrals over the cross-section, i.e.

$$M_S = \int_{A_C} \alpha \rho_S V_S' dA \quad (4.5.)$$

In equation (4.5.), the prime denotes local values with respect to the radius, (it is assumed that the physical quantities such as  $\rho_s$  and  $\rho_l$  are independent of the radius, i.e. that the temperature and pressure gradients are not too large). The quantities  $V_s$  and  $V_l$  in equations (4.1.) and (4.2.) are, therefore, not the mean values of the velocities of the steam and water phases over the cross-section, but are according to (4.5.) defined as:

$$V_s = \frac{\int_{A_c} \alpha V'_s dA}{\alpha A_c}, \quad \text{and} \quad V_l = \frac{\int_{A_c} (1-\alpha) V'_l dA}{(1-\alpha) A_c}, \quad (4.6.)$$

which are weighted averages of the steam velocity. The Slip Ratio, S, therefore, is actually defined as:

$$S = \frac{\int_{A_c} \alpha V'_s dA}{\int_{A_c} (1-\alpha) V'_l dA} \cdot \frac{1-\alpha}{\alpha}. \quad (4.7.)$$

The two expressions (4.4.) and (4.7.) are equivalent when the steam concentration over the cross-section is constant. From equation (4.7.), it may be concluded that even where the local velocity of the steam phase equals that of the water phase, the slip ratio may have an appreciable value. Furthermore, depending on the concentration and phase-velocity distribution, the slip ratio may also be smaller than unity. It should be stressed that in any slip-correlation based on experiments, in which the steam and water mass or volume flow rates are calculated or measured and combined with measured values of the void fraction, the measured slip ratio is in fact the slip ratio defined in (4.7.). A slip ratio based on average values of the phase velocities is difficult to establish.

At present, the way of correlating the slip factor or void fraction with proper variables is largely a question of personal preference. Consequently, several correlations based upon different physical mechanisms have been proposed for predicting the slip factor and the void fraction.

One of the earliest methods for correlating void fraction data is that of Martinelli and Lockhart (L6). This method for correlating two-phase flow data was found to be very successful. The Martinelli method is characterized by two basic postulates:

- a. In the event of steady two-phase flow involving no radial pressure gradients, the static pressure drop for the liquid phase must equal the static pressure drop for the gaseous phase, regardless of the flow pattern;
- b. the volume occupied by the liquid plus that occupied by the gas at any instant must equal the total volume of the pipe.

It is then assumed that the two-phase flow, of volumetric flow rates  $W_l$  and  $W_s$ , is related to the two extreme cases in which  $W_s$  or  $W_l$  are equal to zero. Martinelli then defines the parameter X by means of the following equation:

$$X^2 = \frac{\left(\frac{dp}{dz}\right), W_l \text{ flowing alone in the channel}}{\left(\frac{dp}{dz}\right), W_s \text{ flowing alone in the channel}} \quad (4.8.)$$

The ratio of the single-phase frictional pressure drop of the liquid to the corresponding value of the steam is calculated with the aid of the Fanning friction equation. Supposing that for both cases turbulent flow can be assumed,  $X^2$  is equal to:

$$X^2 = \left( \frac{M_l}{M_s} \right)^{2-n} \cdot \frac{\rho_s}{\rho_l} \left( \frac{\eta_l}{\eta_s} \right)^n \quad (4.9.)$$

The exponent  $n$  expresses the Reynolds dependence of the Fanning friction factor in the Blasius equation and is obtained by plotting the single-phase pressure drop versus weight flow on log-log paper. The slope of the curve is equal to  $(2-n)$ .

Parameters similar to these were derived by Levy (L4). Recently Turner and Wallis (T2) reported on a theoretical study on the general equations of a two-phase flow adapting single-phase mixing length results. Used in conjunction with a simple "lumped-flow" model of two-phase flow, the description provided a theoretical foundation for the empirical Martinelli correlation.

In general, the Martinelli correlation was developed from extensive studies of two-component, two-phase horizontal flow at atmospheric pressure with no mass transfer between the phases. The application of the correlation to steam-water mixtures with heat addition and the introduction of the effect of system pressure were carried out by Martinelli and Nelson (M3). Instead of (4.9.), they used the parameter  $X_{tt}$  for their correlation:

$$X_{tt} = X^{\frac{2}{2-n}} \quad (4.10.)$$

In the course of the studies reported here, an attempt was made to correlate the measured void-fraction data with the parameter defined by (4.10.). The quantity  $X_{tt}$ , therefore, was calculated for those locations where void-fraction measurements were made. This means in fact, that the mass flow of steam  $M_s$  or the steam quality  $x$  have to be calculated along the coolant channel. These calculations have been carried out on a digital computer, starting from measured data of inlet mass flow, channel power, subcooling, saturation temperature and from geometrical and physical data.

First, the onset of subcooled boiling (i.e. where bubbles are formed on the heated surface and detach from the wall into the fluid for the first time) and that of saturated boiling are calculated. The onset of subcooled boiling is calculated according to the criteria of Bowring (B11). The water temperature at the location where subcooled boiling starts can be calculated from a heat balance in the non-boiling region. The saturation temperature at that location is calculated after determining the local pressure, taking into account the hydrostatic head and frictional losses. By assuming a heat balance for the steam and water phase in the subcooled boiling region, using the heat division parameter  $\alpha$  of Bowring, the water temperature and the mass flow of steam can be calculated. The local saturation temperature in the subcooled boiling region is determined by computing the local pressure from the measured static pressure data in the coolant channel. The location of the onset of saturated boiling is obtained as the level at which the local water temperature equals the local saturation temperature. The mass flow of steam at that location can be calculated from the criteria of Bowring. The magnitude of it at the end of the coolant channel can be derived from a heat balance for the whole channel. The mass flow of steam at any specific location is obtained by assuming a linear relationship between the mass flow of steam and the distance from the onset of

subcooled boiling, and the onset of saturated boiling, respectively. In this way, the flashing of the water (i.e. the formation of steam owing to a decreasing saturation temperature) has been taken into account on a linear base. The local mass flow of water is obtained by subtracting the mass flow of steam from the total mass flow, the latter being a measured quantity.

From the calculated values of the mass flow rates of steam and water and from the physical data, the magnitude of  $X_{tt}$  is obtained. The value of  $n$  (equation (4.10.)) has been determined to be equal to .18 and .15 for Test Section I and II respectively.

Measured void fraction data plotted against the parameter  $\sqrt{X_{tt}}$  are given in Fig. 4.1 and 4.2. Owing to the fact that the Martinelli-Nelson correlation is based on fully developed flow data, only results of void fraction measurements obtained in the saturated boiling region have been plotted. The effect of system pressure is shown in Fig. 4.1.

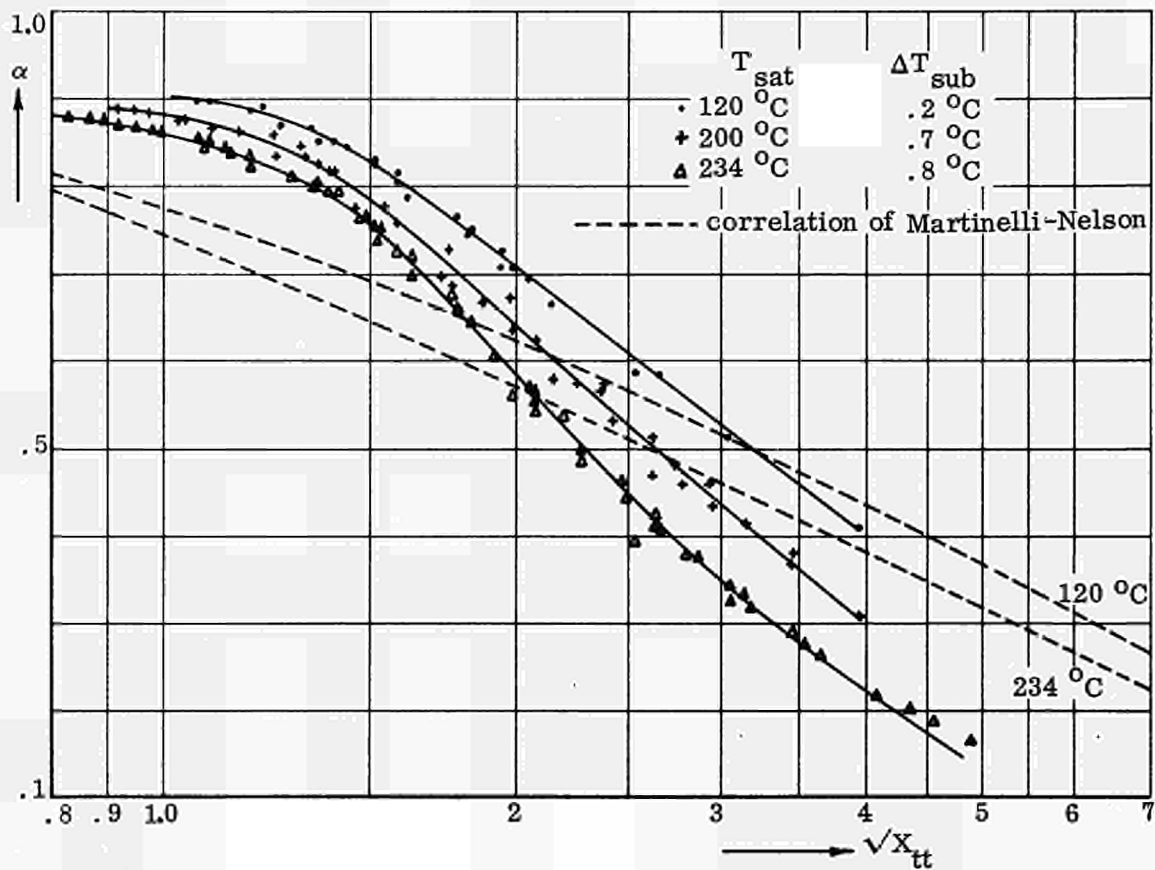


Fig. 4.1 Void fraction data plotted according to Martinelli-Nelson (M3) for three system pressures, Test Section I.

Void fraction data measured at saturation temperatures of 120, 200 and 234°C saturation with Test Section I are given together with the Martinelli-Nelson correlation. Although the data for one saturation temperature can be correlated by  $\sqrt{X_{tt}}$ , the deviation from the Martinelli-Nelson correlation is fairly large. It may be concluded that the Martinelli-Nelson correlation does not cover the void fraction data presented here. It should be pointed out that the pressure effect in the correlation was introduced rather arbitrarily by interpolation between the data obtained at atmospheric pressure and on the assumption that the value of the void fraction equals that of the steam quality at the critical pressure.



In Fig. 4.2 void fraction data, measured at a saturation temperature of 200°C and at three different subcooling rates with Test Section II have been plotted. Also in this case, only data obtained in the saturated boiling region are used. As is shown the effect of subcooling on the correlated data is fairly small for  $\sqrt{X_{tt}}$  larger than 1.5 indicating that the parameter  $X_{tt}$ , (at constant pressure roughly proportional to the inverse square of the steam quality  $x^{-2}$ ) might be a good parameter for correlation. Comparing the Fig. 4.1 with Fig. 4.2 reveals no systematic influence of the hydraulic diameter.

Recently, several studies have been reported on the correlation of void fraction data and calculated slip factors taking into account the phase distributions over the cross-section of the channel.

Bankoff (B14) proposed that the gas phase migrates to the regions with high water velocities where the velocity gradients, and hence the resistance to flow are lowest. Thus, when the phase velocities are averaged over the cross-section, the average magnitude of the gas velocity is greater than that of the liquid, owing to the distribution of the phases alone. Bankoff assumed the velocity of the phases to be equal at any point of a two-phase flow. He then introduced the profiles of the steam velocity as power law functions of the distance from the tube wall and then integrated over the tube cross-sections to obtain the slip-relationship:

$$S = \frac{1-\alpha}{K-\alpha} \quad (4.11.)$$

The value of K is a function of pressure, quality and mass flow rate. For an assumed value of  $K = .89$  good agreement with the Martinelli-Nelson correlation was reported.

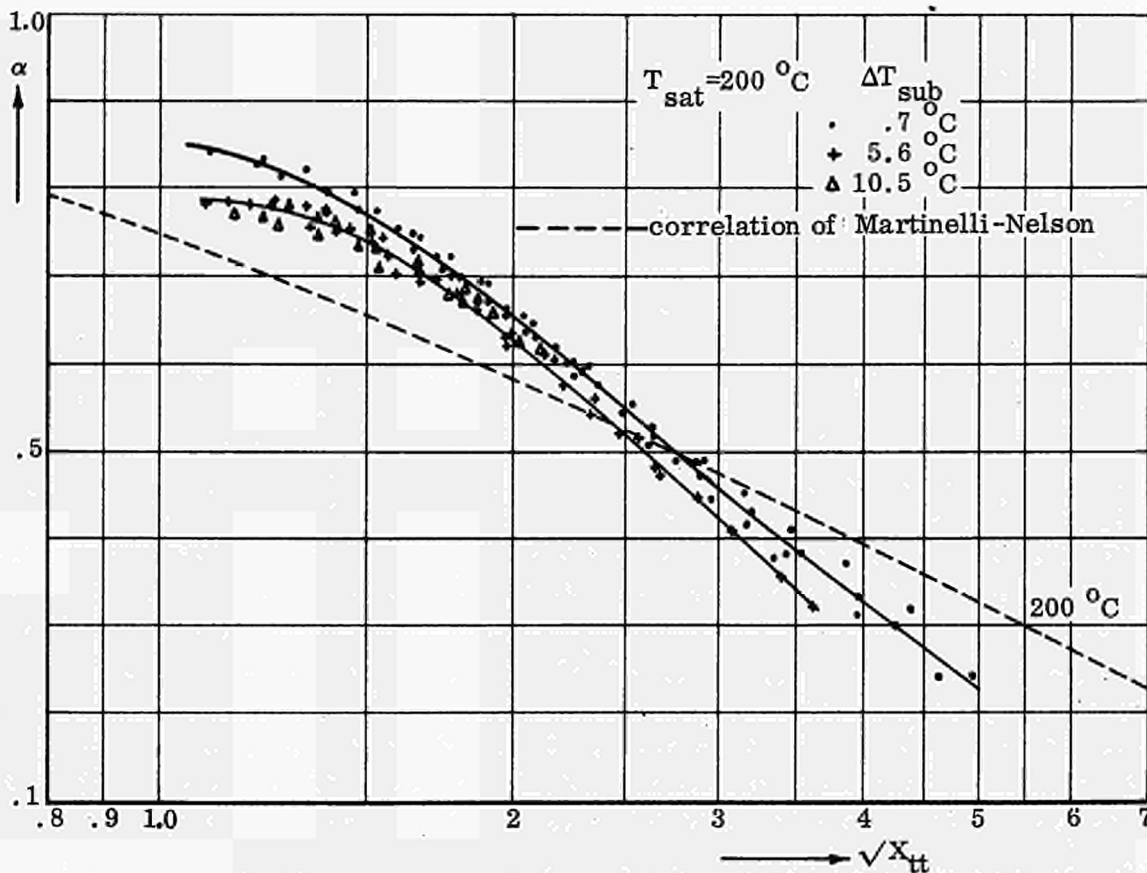


Fig. 4.2 Void fraction data plotted according to Martinelli-Nelson (M3) for three subcooling temperatures, Test Section II.

The distribution effects have also been included in the study from Zuber and Findlay (Z1). Besides, they also considered the local relative velocity between the phases. In their study, the velocities are expressed as vectors. Employing the continuity equations for the two phases and obtaining cross-sectional average values for the physical quantities the following equation was derived:

$$\frac{\langle \alpha' V'_s \rangle}{\langle \alpha' \rangle} = C_o \langle W'_m \rangle + \frac{\langle \alpha' V'_r \rangle}{\langle \alpha' \rangle} \quad (4.12.)$$

The quantities in (4.12.) have already been defined in chapter 1 (see equation 1.1.). The prime denotes again local values with respect to  $r$  and  $z$ , and  $\langle \rangle$  denotes average values over the cross-section. The term on the left-hand side corresponds to the volumetric flow rate of steam per unit cross-sectional area divided by the void fraction. The first term on the right-hand side accounts for the effect of non-uniform flow and concentration profiles. The value of the distribution parameter  $C_o$  is less than unity when the void fraction near the wall is larger than in the center and above unity when the opposite is true. In the latter event, the distribution parameter varies between 1 for flat profiles and 1.5 for peaked profiles. The second term (defined as the weighted average drift velocity) accounts for the effect of the local relative velocity between the two phases. Equation (4.12.) is applicable to any two-phase flow regime and can be used either for predicting the average volumetric concentration or for analyzing and interpreting experimental data. Expressions for the weighted average drift velocities were derived for the slug flow and the churn-turbulent bubbly regime. For fully established flow profiles the value of  $C_o$  in equation (4.12.) is constant. If the weighted average drift velocity does not depend on the concentration, then the quantity  $\langle V'_s \alpha' \rangle / \alpha$  is linearly dependent on the average mixture velocity. It was stated that a changing slope is indicative of changing profiles or developing flow.

The expression (4.12.) was derived for a two-phase flow system in which a change of phase does not occur. Although the void data presented before were obtained during evaporation, the data have been plotted in the weighted mean velocity-average volumetric flux density plane, see Figs 4.3 and 4.4.

In Fig. 4.3 which applies to the same conditions as Fig. 4.1, data obtained in the subcooling region are also included. As is shown, the linear relationship holds good even for an evaporative system and it may be concluded that fully developed flow conditions are present over the larger part of the coolant channel and throughout a wide range of operating conditions. Only at the lower volume flow, a systematic deviation from the straight line is observed. Most of the data points in this region were obtained in lower parts of the boiling region, where the flow profile is probably developing. The slope of the lines is very near to unity which indicates that flat profiles for the velocity or concentration distribution are present. In (Z1) it is noted that, for an established annular flow the data plot is a straight line with a slope equal to about unity. More experimental information is needed to conclude if this also applies to the present experiments.

The intersection with the vertical axis found by extrapolation of the straight line yields the average weighted drift velocity, which decreases with increasing system pressure, being in agreement with the decreasing local slip between the two phases. It turned out that the drift velocities are somewhat higher than those calculated by means of the expressions suggested by Zuber (Z1) for slug flow and for bubbly churn-turbulent flow.

The influence of subcooling on the proposed relationship, shown in Fig. 4.4 is very small. Only in the subcooled region there is some discrepancy between the measured data.

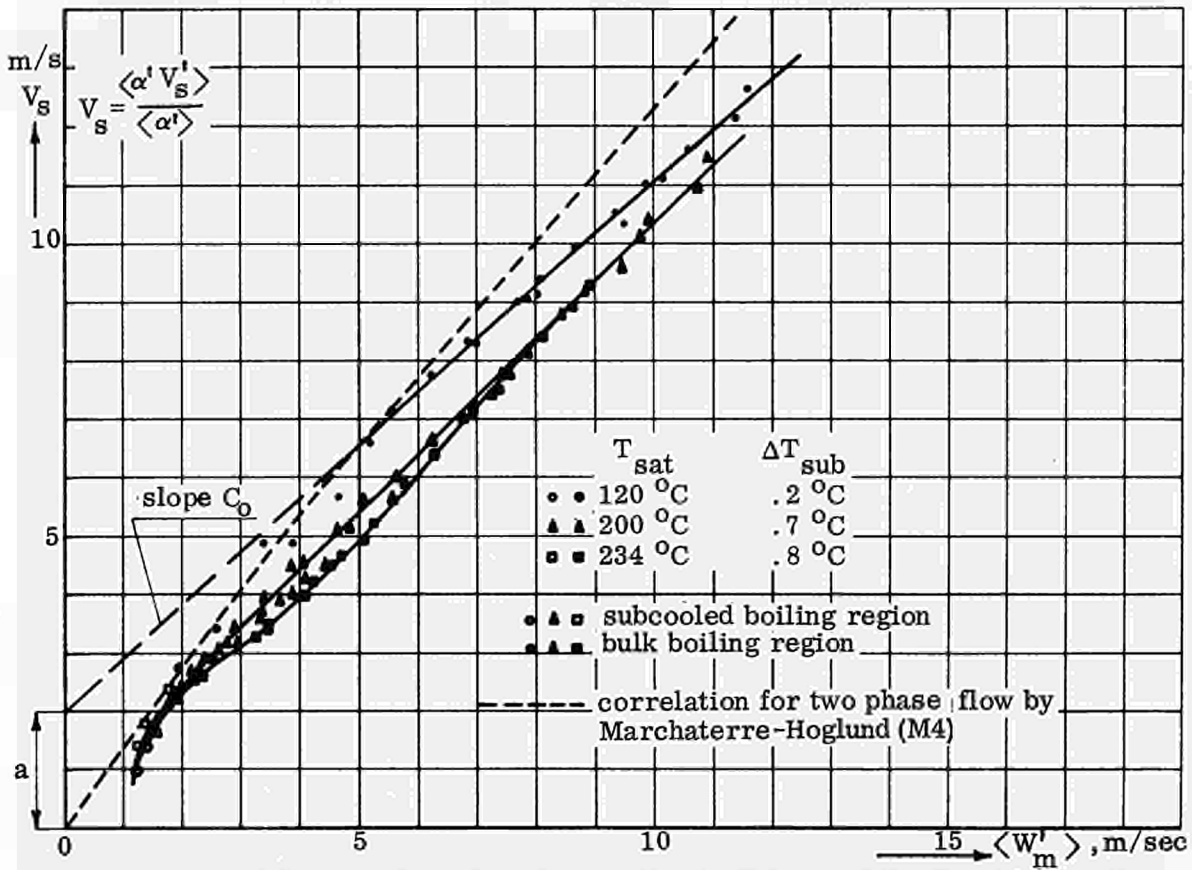


Fig. 4.3 Void fraction data plotted according to Zuber and Findlay (Z1) for three system pressures, Test Section I.

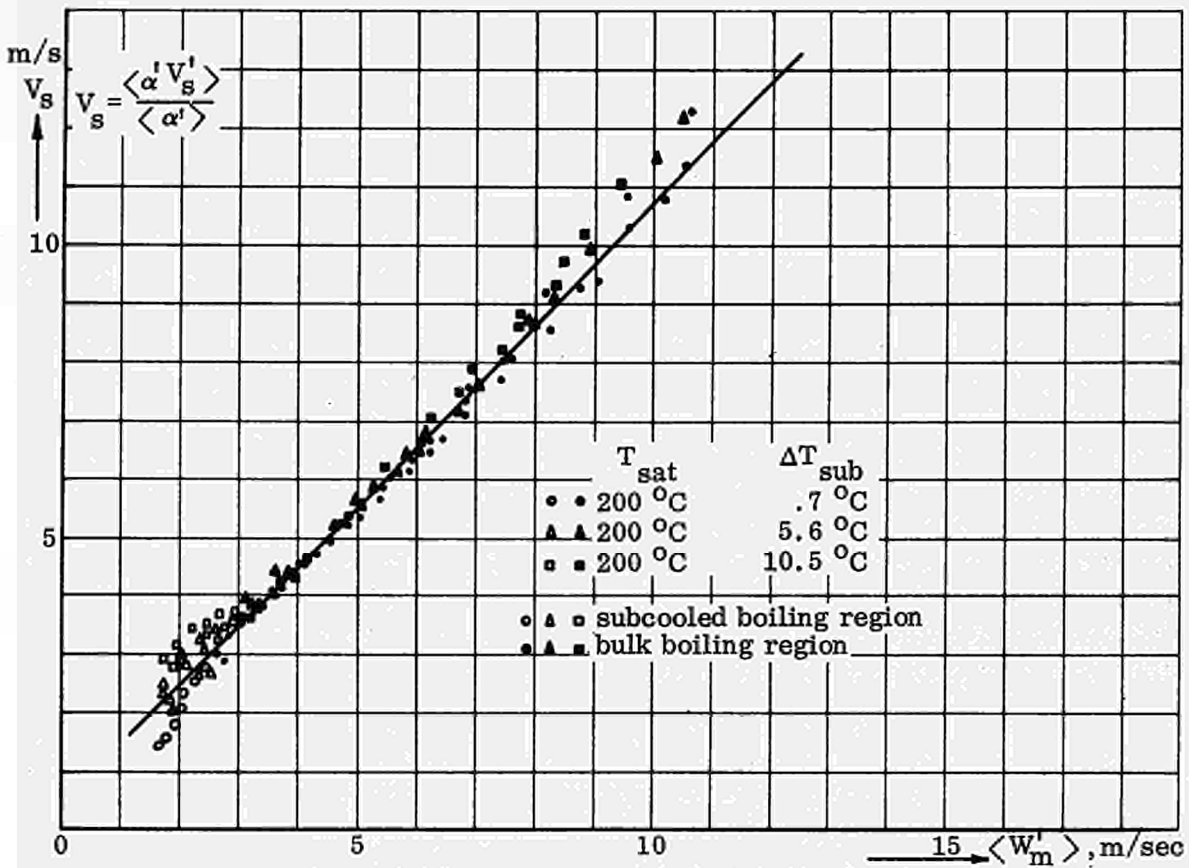


Fig. 4.4 Void fraction data plotted according to Zuber and Findlay (Z1) for three subcooling temperatures, Test Section II.

For comparison, the widely used slip correlation of Marchaterre and Høglund (M4) has been used to calculate data, which are also presented in Fig. 4.3. In their correlation the Slip Ratio,  $S$ , is expressed as a function of the ratio of the volumetric flow of steam and water for different Froude numbers. It turns out, however, that in the region of operation conditions considered here, the Froude number has no effect on the Marchaterre data in the Zuber plot. This would mean that the influence of the Froude number is not significant in the range of operating conditions considered. This was also the case with the system pressure on the Marchaterre data. The Marchaterre-Høglund correlation yields too high values of the weighted average steam velocity and this would result in too low values of the void fraction for a given volumetric flow of the mixture.

In the theoretical analysis to be presented in chapter 5 the Zuber-Findlay correlation has been used (Figs 4.3 and 4.4) which can be expressed in the form of:

$$S = \frac{\frac{a}{V_1} + C_0(1-\alpha)}{1-C_0\alpha}, \quad (4.13.)$$

in which  $S$  and  $V_1$  are defined according to equations (4.7.) and (4.6.) and  $a$  is the steam velocity at zero volumetric mixture flow to be obtained from the intersection of the extrapolated straight line with the vertical axis, see Fig. 4.3. In the applying of this correlation one has to be careful owing to the fact that even minor variations in  $C_0$  have an appreciable influence on the slip ratio and on the calculated void fraction.

Although Bankoff and Zuber have contributed a great deal to the knowledge of the characteristics of a two-phase mixture, more development work is needed, particularly as regards the recognition of flow regimes and the measurement of concentration and velocity distribution over the cross-section. This is a prerequisite to any further analysis of the presented data.

#### 4.2. Two-phase pressure losses

Apart from the void fraction or the slip ratio also a knowledge of the pressure losses in a two-phase mixture is of importance for the evaluation of the performance and stability characteristics of a boiling system. In the experimental program the total pressure drop has been measured between locations of the various pressure tappings, see Fig. 2.4. Although some investigators have looked into the possibility of correlating the total pressure drop with meaningful parameters, which may be convenient for designers, this type of correlation yields only little fresh information from a scientific point of view, because there are too many variables involved. In the elaboration upon the experimental results, the more customary way has been followed of separating, by using the measured void fraction, the total pressure drop into the frictional, acceleration and hydrostatic pressure drop, see equation (3.2.). By considering an elementary volume element  $\Delta U = 2\pi r \Delta r \Delta z$ , see Fig. 5.1 in which  $\Delta z$  is in this case taken as the distance between two locations where the void fraction has been measured, the hydrostatic pressure drop may be written as:

$$\Delta p_h = \frac{\Delta z}{A_c} \int_{A_c} g \left\{ \rho_1 (1-\alpha) + \rho_s \alpha \right\} dA, \quad (4.14.)$$

thus:

$$\Delta p_h = \Delta z g \left\{ \rho_1 (1-\alpha) + \rho_s \alpha \right\}. \quad (4.15.)$$

In equation (4.15.)  $\alpha$  is the average void fraction over the cross-section in a segment  $\Delta z$ , which is obtained by linear interpolation between measured values at the various locations.

The acceleration pressure drop is equal to the difference in rate at which momentum flows into and leaves the volume element. The momentum flow is equal to:

$$P = \frac{1}{A_c} \int \left\{ \rho_1 (1-\alpha)' V_1'^2 + \rho_s \alpha' V_s'^2 \right\} dA, \quad (4.16.)$$

and the acceleration pressure drop is expressed as:

$$\Delta p_a = P_n - P_{n-1}, \quad (4.17.)$$

where  $n$  denotes a location of an impedance void gauge. By defining:

$$\bar{V}_1 = \sqrt{\frac{\int V_1'^2 (1-\alpha') dA}{(1-\alpha) A_c}}, \quad \text{and} \quad \bar{V}_s = \sqrt{\frac{\int V_s'^2 \alpha' dA}{\alpha A_c}}, \quad (4.18.)$$

equation (4.16.) can be written as:

$$P = \rho_1 (1-\alpha) \bar{V}_1^2 + \rho_s \alpha \bar{V}_s^2. \quad (4.19.)$$

From the above mentioned equations it follows that the acceleration pressure drop is dependent upon the concentration and velocity distribution of the two phases over the cross-section. By measuring or calculating these flow distributions, two more slip ratios  $S_a$  and  $S_b$  can be defined, being the ratio between  $\bar{V}_1$  (equation 4.6.) and  $V_1$ , and between  $\bar{V}_s$  and  $V_1$ . For particular flow conditions (e.g. adiabatic dispersed flow), flow distribution measurements are being performed (A4). Also, flow models can be used for calculation of the acceleration pressure drop. For instance, the theoretical flow model reported in (V4) and to be discussed in chapter 5 may yield the theoretical basis for the slip ratio correlations. For flow with distribution laws as suggested by Banhoff (see section 4.1.), the homogeneous flow model, in which it is assumed that  $\bar{V}_s = \bar{V}_1 = V_s = V_1$ , gives too high values and the separated flow model with  $\bar{V}_s = V_s$  and  $\bar{V}_1 = V_1$  too low values of the acceleration pressure drop; differences may reach 25%. In case the local distributions have not been measured and where it is uncertain which type of flow was present under the various operating conditions, the separated flow type model has been assumed to represent the actual conditions.  $V_s$  and  $V_1$  can be calculated with the earlier determined value of the mass flow of steam and of water  $M_s$  and  $M_1$  (equations 4.1. and 4.2.) and the measured void fraction. The acceleration pressure drop can then be evaluated.

By subtracting the calculated acceleration and hydrostatic pressure drop from the total measured pressure drop the friction pressure drop is obtained. It is recognized that the frictional pressure drops thus obtained are incorrect because of the elaboration procedure followed. It should be kept in mind that in deriving two-phase friction losses from pressure measurements along a boiler, accurate results will only be possible when all the distribution effects are known. The computations have been carried out on a digital computer. It is customary to express the two-phase friction pressure drop as

a dimensionless ratio, which is formed by dividing the two-phase friction pressure drop by a liquid-phase pressure drop. The liquid-phase pressure drop is sometimes evaluated at the same total mixture mass flow rate and the ratio is then denoted as R, or at the mass flow rate when the liquid is flowing alone in the channel in which the ratio is denoted as  $\Phi_{1,tt}^2$  e.g. by disregarding the Reynolds dependence of the single-phase Fanning friction factor f:

$$\Delta p_f(T.P.) = R \cdot 4f \frac{\Delta z}{D_h} \cdot \frac{1}{2} \rho_1 V_1^2 \left\{ (1-\alpha) + \frac{\rho_s}{\rho_1} \alpha S \right\}^2, \quad (4.20.)$$

or:

$$\Delta p_f(T.P.) = \Phi_{1,tt}^2 \cdot 4f \frac{\Delta z}{D_h} \cdot \frac{1}{2} \rho_1 V_1^2 (1-\alpha)^2. \quad (4.21.)$$

It can easily be shown that:

$$R = \Phi_{1,tt}^2 (1-x)^2, \quad (4.22.)$$

or:

$$R = \Phi_{1,tt}^2 (1-x)^{2-n}, \quad (4.23.)$$

if the Reynolds dependence is taken into account.

The Martinelli-Nelson (M3) pressure drop correlation for boiling water is the best known and probably the most widely used general correlation available. The correlation is based on data for adiabatic, two component mixture flow in horizontal tubes at atmospheric pressure. On the assumptions already mentioned in section 4.1. Martinelli-Nelson arrived at a correlation between  $\Phi_{1,tt}$  and the non-dimensional correlating parameter  $X_{tt}$  defined in (4.10.). The pressure effect has been incorporated rather arbitrarily, using the data of Davidson (D1) and considering the limits imposed on  $\Phi_{1,tt}$  at the critical pressure. It is considered remarkable that the Martinelli-Nelson correlation has proved to be so successful when it is realized what assumptions had to be made and the fact that so few data were available at the time of its development.

In Fig. 4.5, some data are plotted of the parameter  $\Phi_{1,tt}$  calculated from the experiments with Test Section II at saturation temperatures of 120 and 234°C. As is shown the data are poorly correlated with the parameter  $\sqrt{X_{tt}}$ , and also deviate noticeably from the Martinelli-Nelson curves. It should be kept in mind, however, that this correlation is based on isothermal pressure drop data, whilst moreover the plotted data were obtained under flow conditions with vaporization. Besides, not only were the calculated  $\Phi_{1,tt}$  data determined by the steam quality but also by the mass flow rate, which is an intercoupled quantity in a natural circulation system. Some investigators have reported an apparent flow rate dependency on the two-phase friction losses which is not accounted for by the Martinelli-Nelson correlation.

The bulk of data of the calculation of R and  $\Phi_{1,tt}$  will be reported together with the void fraction data elsewhere. In comparing the data for the two test sections, it was noticed that the values for  $\Phi_{1,tt}$  for Test Section I tended to be lower than those for Test Section II, particularly in the lower range of  $\sqrt{X_{tt}}$  values.

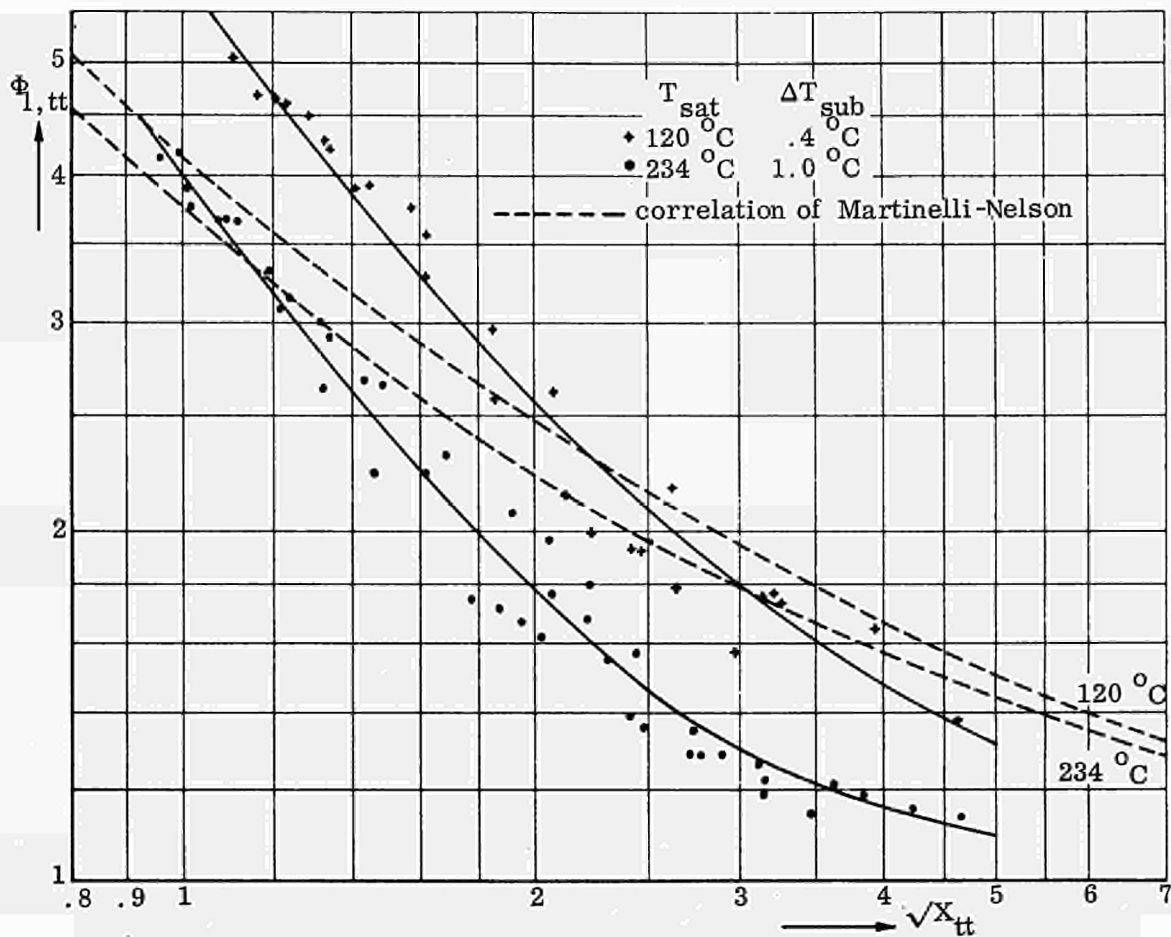


Fig. 4.5 Two-phase friction loss data plotted according to Martinelli-Nelson (M3) for two system pressures, Test Section II.

It is hoped that theoretical studies in which distributional effects are incorporated will provide the theoretical basis that will explain the dependence of the two-phase pressure losses and the void fraction in saturated boiling as well as in subcooled boiling conditions upon the physical quantities determining the flow process. Although some success was obtained in void fraction studies some substantial work has to be undertaken in the field of two-phase friction losses.

#### 4.3. Stability characteristics of a two-phase flow

In section 3.3. a description was given of the different types of flow oscillations observed during the operation of a naturally circulating boiling water loop. Furthermore, results of a systematic research into the onset of severe hydraulic oscillations of about 1 c.p.s. in dependence of the operating conditions and the hydraulic diameter of the boiling channel have been presented. Owing to the fact that, particularly at high system pressures, there is no abrupt change from stable into unstable operation as a result of a single incremental power change, a criterion has been adopted (see section 3.3.2.) for defining the onset of the hydraulic oscillations. In previous publications these oscillations were only qualitatively described, while the onset was only roughly indicated. Summarizing, the following conclusions may be drawn from the experiments, see also Table 3.2.:

- a. the onset of severe hydraulic oscillations is postponed to higher channel powers with increasing pressure; at high system pressures, there is a gradual increase in the amplitude of the flow oscillations with increasing channel power, in contrast with low system pressures, at which the flow oscillations start more spontaneously; the oscillations in steam-void are largest at about the location where saturated boiling starts.
- b. the effect of increased subcooling upon the onset of flow oscillations at low subcooling rates is opposite to that at high subcooling rates; at low subcooling rates, increased subcooling will precipitate and at high subcooling rates this will postpone the onset of severe hydraulic oscillations; this effect is more pronounced at high system pressures and large hydraulic diameters; the frequency of the oscillations will decrease monotonically with increased subcooling.
- c. an increase in hydraulic diameter will postpone the onset of hydraulic oscillations to higher channel powers.

An additional effect was investigated in earlier experiments and reported in (B5). There, experimental results are given for a seven rod bundle test section modelled after a fuel assembly of the Halden Boiling Water Reactor. The experiments consisted of measurements of natural circulation flowrate and measurements of the maximum channel powers obtainable without burn-out. The instability channel-power threshold was investigated as well. Nor could in these experiments any clear threshold of hydrodynamic instability, marked by the rather abrupt appearance of regular oscillations, be detected. In one test, the test section was modified by introducing a constriction at the exit. By this, the two-phase pressure losses near the exit were increased by roughly a factor of seven (B15). The result was that the periodic flow instability threshold was reduced from well over 600 kW to 450 kW channel power. This indicates, that any increase in the pressure drop in the two-phase region will precipitate the onset of hydraulic oscillations. On the other hand it is well known that an increase in the pressure drop in the single-phase section of the system will improve the stability.

By the presented results of the transfer function measurements in section 3.4., it is confirmed that the conclusions mentioned under a, b and c also hold good with respect to the stability characteristics of a steady-state. To the knowledge of the author no experimental results of the stability characteristics of a steady-state condition for a natural circulation system under various conditions of pressure, subcooling and geometry have been reported so far.

In the presented transfer functions from channel power to the differential pressure from the pitot-tube and to the void fraction as a function of the modulation frequency, a resonance peak was revealed in the 1 c.p.s. region, which increased in magnitude and shifted to higher frequencies with increased steady-state channel power. It was shown, after comparison with results reported by St. Pierre (S12) and Zivi (Z3) and after comparison with presented results of a noise analysis (section 3.4.2.), that this resonance peak is characteristic of a naturally circulating system. This resonance peak in the transfer function is caused by strong intercoupling between the steam-void in the channel and the inlet mass flow (see also section 1.2.). In a system with forced circulation this coupling is weaker and it can be removed altogether by applying high inlet throttling or by choosing a pump with steep head-flow characteristics. It is clear, therefore, that in an analysis of hydrodynamic instability not only the region of the two-phase flow, but the entire system including the downcomer and if necessary the pump characteristics must be taken into account. Otherwise the onset of hydraulic oscillations can neither be explained nor predicted.



As was shown earlier, the resonance peak in the transfer functions becomes very pronounced according as the threshold for severe hydraulic oscillations is approached. In Fig. 3.25, for instance, the development of the resonance peak is demonstrated. In the absence of power modulation it was shown in Fig. 3.18 that for the same conditions as for Fig. 3.25 at about 145 kW, both the flow rate and the void fraction are subject to large random fluctuations. When the power level is increased to 165 kW, spontaneous flow oscillations begin to appear. The frequency of the resonance peak at a channel power of 145 kW is .95 c. p. s., which is roughly equivalent to that of the hydraulic oscillations. It can be claimed, that the resonance peak has been transformed into spontaneous flow oscillations owing to the fact that the intercoupling between the steam-void in the channel and the inlet mass flow has become unstable and not to the fact that the flow is responding to a present boiling instability, or flow-pattern instability. This unstable flow-void feedback can be explained as follows. A slight perturbation to a lower flow rate results in an increased vapor volume in the channel. According as the density in the riser is lowered, the driving head around the loop will rise and will accelerate the flow, which results in a lower vapor volume. Rising density will reduce the driving head and decelerate the flow. This oscillatory behavior may be sustained at a regular frequency.

The measured transfer functions have been presented as applicable to linear systems only. In that case, the flow instability would not be limited in amplitude. It will be clear, that according as large flow fluctuations occur, non-linear effects become of importance, which have the effect of limiting the amplitude of the oscillations. From the indicated relationship between transfer functions and hydraulic oscillations it becomes clear that the onset of the hydrodynamic flow oscillations may be explained and calculated by a linear theory, although the limit cycle amplitudes depend upon non-linearities in the system, see also (Z3).

Some investigators (M5), (S8) have made a research into the Ledinegg instability (L3) for explaining the onset of hydraulic oscillations. Ledinegg was amongst the first to point out that an instability can arise in a heated two-phase system having a negative slope in a part of its hydrodynamic characteristics, i. e. in the flow-pressure loss curve. At one time this was regarded as the primary criterion for instability in such systems.

Several curves for the pressure drop in a vertically heated tube versus the liquid flow at the inlet are shown schematically in Fig. 4.6. Curve A represents the pressure drop for pure liquid and curve B represents the pressure drop for pure vapor flow. Region C is the pressure drop at constant channel power in the presence of boiling in the tube. The higher values of the pressure drop in the boiling region are caused by the increased friction and acceleration pressure drop as according the liquid is converted into vapor. It is sometimes stated now, that in that part of the curve where the pressure drop increases with decreasing flow rate and the system is called statically unstable, operation is not possible and an oscillatory behavior occurs.

Upon this pressure drop is superimposed the pressure drop resulting from the external system. Two examples are given in Fig. 4.6, represented by the straight lines D and E. The one indicated by D is that of a constant pressure-drop supply system. This condition is a close approximation of the situation as seen by an individual coolant channel in a parallel arrangement of a large number of channels between two headers. The operation conditions 1 and 2 indicated in Fig. 4.6 might be stable in so far as the static stability is concerned. If the flow rate at point 3 increases or decreases slightly along D, it is seen that the external system is supplying more and less pressure drop

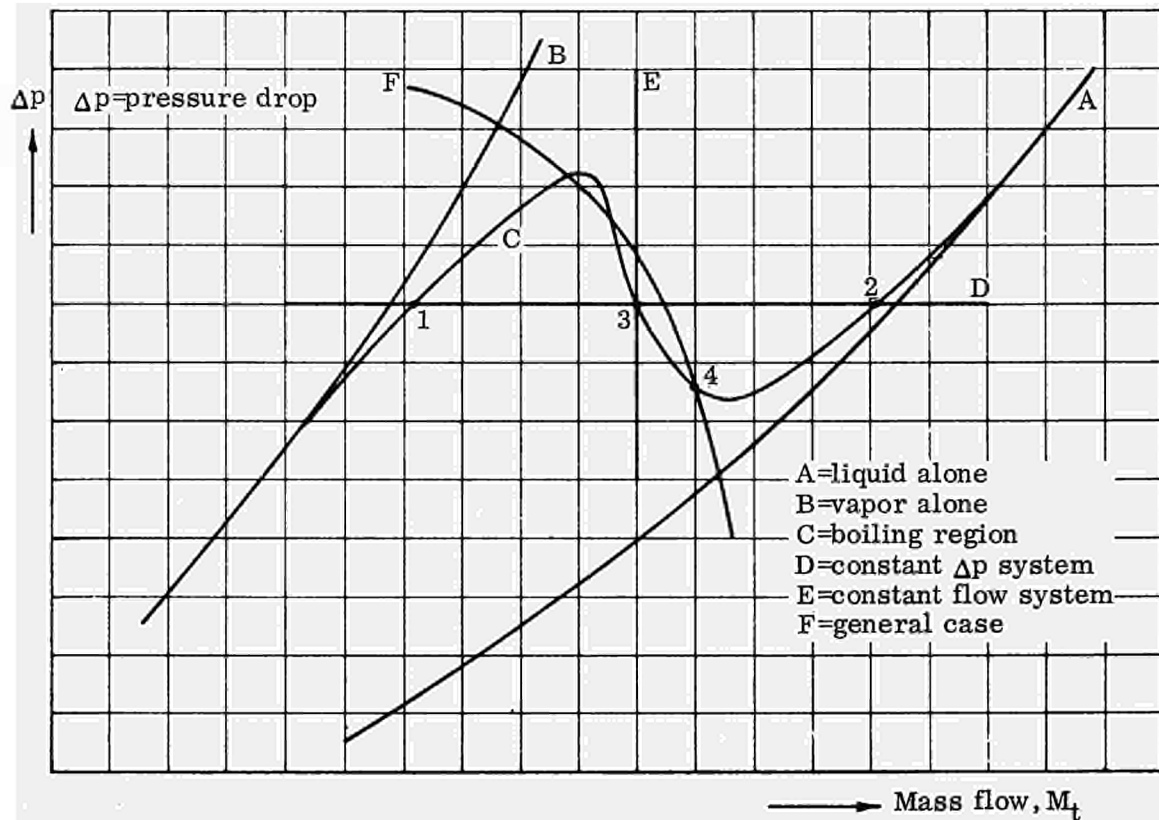


Fig. 4.6 Ledinegg instability.

respectively than is required for maintaining the flow, and the flow rate will respectively increase or decrease until a new operating point is reached (flow excursion). This final condition may be in a region of stable flow, stable flow oscillations or in a burn-out condition. In a constant flow delivery system, such as indicated by E in Fig. 4.6 the system is always stable when steady-state considerations are applied. Such a condition may be encountered physically in a single coolant channel either by using a positive displacement pump which has a steep head-flow characteristic, or by insertion of a throttling valve upstream of the heated section. In the latter case nearly all the flow resistance is from the throttling valve and changes in the resistance of the heated channel produce a negligible effect on the flow rate. In the past (L5) such an arrangement has been used for investigating the behavior of a single boiling channel in all regions of the curve. In reality, of course, no supply system corresponds exactly to either of the extreme cases just described; a possible case is indicated in Fig. 4.7, with a stable and unstable intersection.

Although this analysis is based on forced circulation consideration, in which buoyancy forces and inlet pressure drop may be disregarded, it may as well be applied to a system with natural circulation with a constant driving head equal to the head of the water in the downcomer, or a driving head incorporating the buoyancy forces.

In the recent literature two studies (M5), (S8) have appeared on the occurrence of slow flow oscillations in conditions where the system was statically unstable, i. e. in the decreasing part of pressure drop versus mass flow curve. This oscillatory behavior occurs in the event where the slope of the channel characteristic is less negative than the slope of the curve characterizing the supply, i. e. point 4 in Fig. 4.6. From steady-state considerations, the operational point could be called stable. Dynamically, this operation condition might be unstable, depending on the actual magnitude of either slope. These flow oscillations are called "pressure drop oscillations" and may be similar

to those described in section 3.3.1. Only an analysis of the pressure drop characteristics of the channel, as may be derived from a computation may yield some better insight into these low frequency oscillations.

In (S8) a second type of flow oscillations is mentioned as "density wave oscillations". These oscillations occur at a lower flow rate than where the pressure-drop oscillations were encountered. Sometimes the density wave oscillations appeared as a superimposed transient on the pressure-drop oscillations. These density wave oscillations occurred there, wherever the pressure drop mass flow curve had a positive slope, e.g. in the region of point 1 of the curve C in Fig. 4.6. From the description of these oscillations given by Stenning, it is obvious that these oscillations are very similar to the oscillations of intermediate frequency described in section 3.3.1. Also in the work by Stenning the distinction between either types of oscillations was clearly apparent. However, it is easy to conceive a situation in a system with steep head-flow characteristics of the supply, in which either type of oscillation exhibits nearly the same frequency and in which it would be harder to differentiate between them (M5).

In conclusion it may be said that steady-state considerations make it permissible to operate in a region with a positive as well as a negative slope of the channel pressure drop versus inlet mass flow curve. Flow oscillations result from a dynamic interaction between the void distribution in the channel and the inlet mass flow, which is largely influenced by the boundary conditions imposed on the channel. As a result of the deviations from the steady state, pressure forces arise which influence the stability characteristics. A study of the flow oscillations, therefore, cannot be made from the equations describing the steady state, but must start from equations incorporating dynamic effects. The question whether the boundary conditions are formed by a downcomer or by return piping incorporating a pump does not effect the analysis. For determining the onset of flow oscillations, the equations may be linearized where it concerns small deviations from the steady state. For determining the characteristics of the flow oscillations, non-linear effects must be introduced into the equations.

Any stability criterion for the onset of the flow oscillations described must also be based on considerations incorporating dynamic effects. In such a criterion, the characteristics of the supply system, i.e. of the boundary conditions imposed on the coolant channel, have to be taken into account. In chapter 5, the equations will be given describing the dynamic behavior of a boiling system and a criterion will be derived for predicting the onset of hydraulic flow oscillations.

#### 4.4. Burn-out

All the experimental series for measuring the steady-state characteristics and the onset of hydraulic oscillations have been carried out by increasing the channel power at a constant system pressure and a constant inlet-subcooling. A burn-out detector was used to protect the heater tube against excessive temperature excursions at high channel power. In all series the channel power was increased in small steps until the burn-out trip was reached. It was verified that physical burn-out occurred at fractionally higher channel powers than the trip value both under stable and unstable conditions. The out-of-balance signal from the burn-out detector has been recorded as a check on the temperature rise at burn-out. Burn-out trip under unstable conditions was almost never caused by the fact that the amplitude of the steady oscillations became too large or so divergent that the trip setting was reached. It was nearly always caused by a sudden considerable overheating of the top half of the heater tube. This conclusion was reached because the burn-out detector traces revealed, apart from regular oscillations, a

continuous overheating of the top half. At burn-out the trace went rapidly off scale and a trip was obtained, mostly from the top half of the heating element (S3). All the measured burn-out channel powers have been checked 2 to 3 times, the spread being less than  $\pm 3$  per cent.

The conditions under which burn-out trip was reached are given in Tabel 3.2. The mentioned values of the recirculation rate and the steam quality at the outlet of the channel apply to the operation condition under which flow oscillations started.

The burn-out heat fluxes (e.g. the channel power at which burn-out trip occurred divided by the area of the heated surface) are plotted as functions of the saturation temperature and subcooling temperature in Fig. 4.7 and 4.8 respectively. In these figures also the heat fluxes at the instability threshold have been plotted. As can be concluded from Table 3.2. and Fig. 4.7 the burn-out heat flux increases with saturation temperature and thus system pressure. This is a result similar to that obtained in forced-circulation experiments under stable flow conditions and at low system pressures. It is observed that at higher saturation temperatures the curve of the threshold of instability approaches the burn-out curve. With Test Section II and at a system pressure of 30.7 ata (saturation temperature of  $234^{\circ}\text{C}$ ) burn-out was obtained without the flow passing through the oscillation region.

The curve, representing the burn-out heat flux as a function of subcooling passes through a minimum. The trend of the burn-out heat flux decreasing with increased subcooling for low subcooling rates is the opposite to what is normally observed in burn-out experiments with forced circulation, in which the burn-out heat flux generally decreases

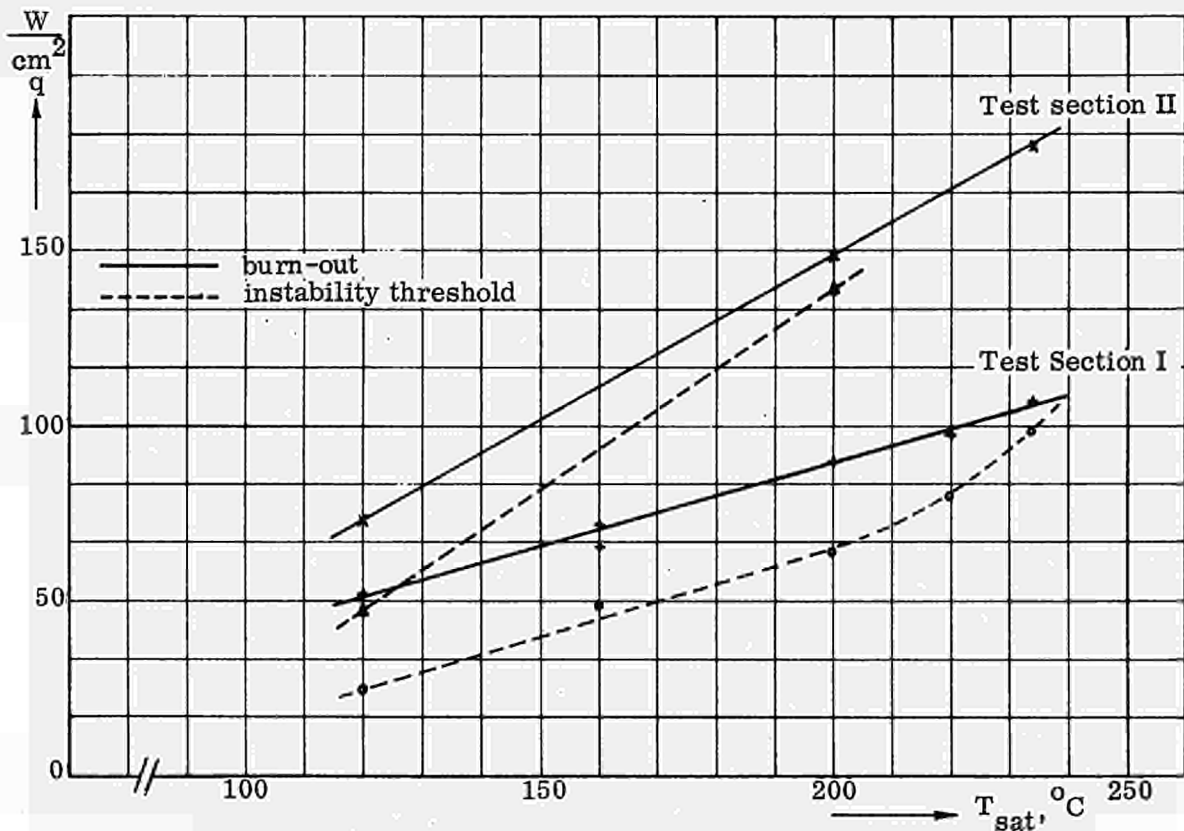


Fig. 4.7 Heat fluxes at burn-out and instability threshold as functions of saturation temperature, Test Section I and II.

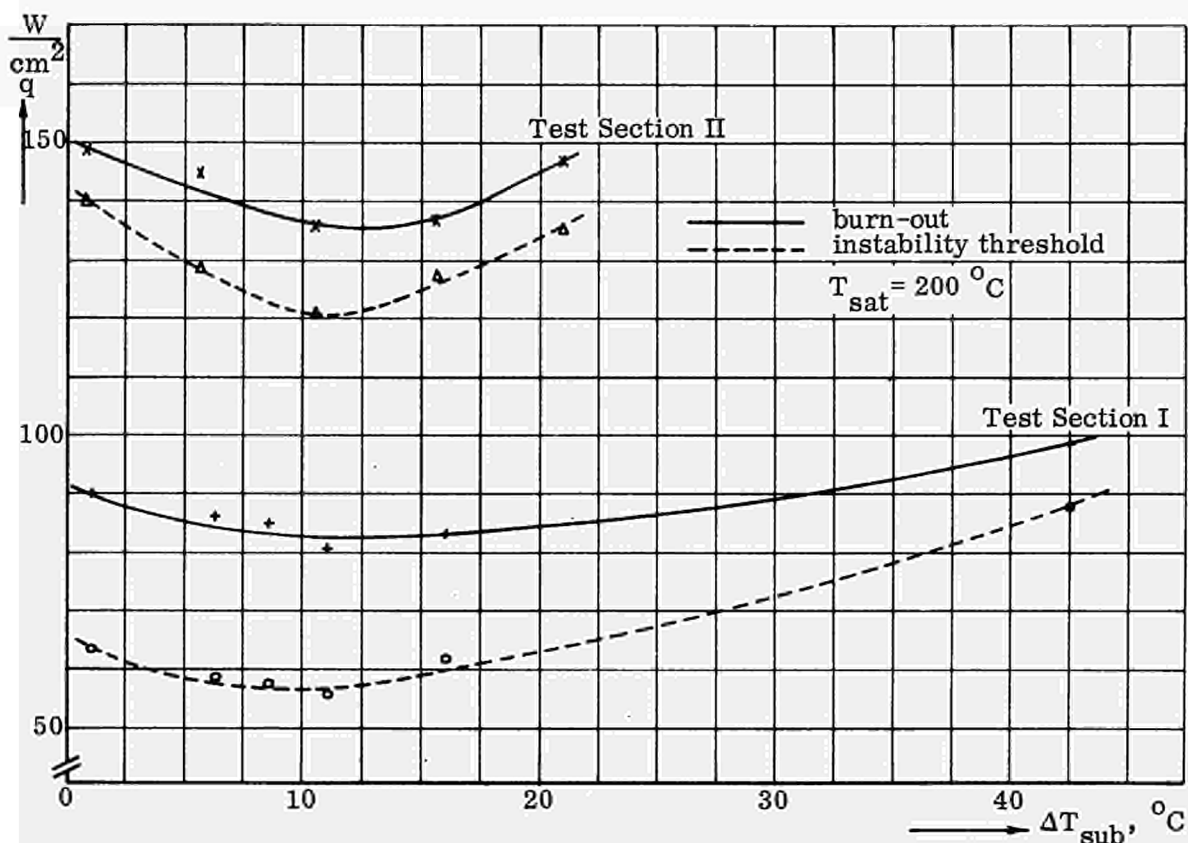


Fig. 4.8 Heat fluxes at burn-out and instability threshold as functions of subcooling temperature, Test Section I and II.

with increasing steam quality at the outlet. One explanation may be that unstable natural convection burn-out for low subcooling rates resembles that with employing a "soft inlet" (i.e. steam quality at the inlet), when at a low flow rate and at low pressure the trend of the burn-out heat flux increasing with increasing quality at the burn-out point has been observed at low quality (M6). At high subcooling temperatures the burn-out heat flux increases again with increased subcooling similar to the behavior of the instability threshold. Then, the flow oscillations become smaller and the subcooled region larger.

It is noted that burn-out occurred at the top half of the heating element, excepted at high subcooling rates, see Table 3.2., where the burn-out detector indicated that the bottom half would be overheated. Similar effects have been measured in earlier experiments with hot patches (B15).

Because burn-out occurred almost only under unstable conditions, the measured values can be expected to be low compared with data obtained under stable conditions with natural or forced circulation conditions. Evidence of this is provided by the measurements reported in (B12), (L1) and (M7).

Levy (L1) reported a departure from the forced circulation burn-out data according as the degree of instability, i.e. the amplitude of the oscillations, increases. He also noted that the unstable flow burn-out heat fluxes increased when the steam quality was lowered. As the oscillations became larger, a slight decrease in burn-out heat flux with steam quality was measured. These observations are similar to those reported here.

Similar results have recently been reported by Becker (B12). He observed, using a closed loop with natural circulation, that by closing the inlet valve by a certain amount, burn-out results were achieved that were identical to those obtained under steady flow conditions using forced convection. Otherwise, the natural circulation loop gave lower burn-out heat fluxes. As already mentioned in section 4.3. any increase in pressure drop in the single-phase part of the system improves its stability.

The remarks given confirm the believe that hydraulic stability plays an important rôle in burn-out. Further research is needed to establish whether the burn-out point and the conditions under which it occurs are governed by a mechanism different from the one present under stable flow conditions. It would be interesting to repeat some of the experiments under the same conditions of pressure, subcooling, mass flow and geometry, but with forced circulation. Besides, it might be of interest to investigate, even under stable flow conditions, the effect of inlet throttling on the burn-out heat flux.

## 5. Theoretical studies

### 5.1. Introduction

Many physical-mathematical formulations have been reported in the literature attempting to describe and to calculate the performance of a two-phase flow system under stationary and transient conditions or to analyze observed particular phenomena such as, for instance, the occurrence of severe hydraulic oscillations.

In (S1), (S2) and (S10), theoretical results are reported of the performance characteristics of a boiling channel under steady-state conditions. Comparisons are made with results yielded by experimental studies. In (S2) the effects of subcooled boiling, the two-phase friction pressure drop, the acceleration pressure drop, the slip ratio, the heat-flux distribution and the incorporation of the variation of saturation temperature along the height of the channel on the performance characteristics have been studied.

Regarding the study of the transient behavior of a two-phase flow and the occurrence of hydraulic oscillations, different approaches have been used in the past. In many studies, the coolant channel is divided into a number of spatial increments for which the general equations, e.g. the conservation laws, the equations of state, etc., are formulated. In some of these studies the number of increments has been assumed to be small, e.g. only two, namely the non-boiling and the boiling region. As a rule, in these studies then time delays are used to simulate the transport time of the fluid through the system. These studies are normally referred to as "lumped parameter studies" (W1), (Q1), (H4) and (Z4) and these should be distinguished from "distributed parameter studies" (C1), (J1), (J2) and (S11), in which the number of increments is large and the increments are mostly evenly distributed along the length of the channel. Another group of studies consists of those in which the occurrence of hydraulic oscillations is considered as an isolated phenomenon and in which an attempt is made to study the possible mechanism or controlling parameters. Examples of this group are the studies of Ledinegg (L3) and Stenning (S8), discussed in section 4.3.

In (B8) and (N1), good reviews have been given of a number of descriptions which appeared in literature prior to 1963. In the introduction, some recent studies were mentioned and discussed. The object of the present study is to investigate the general behavior of a two-phase naturally circulating coolant system and to formulate a description which might serve for calculating the performance characteristics of steam-generating units consisting of channels with large  $L/D_h$  ratios in which the distribution effects are of importance. In the following, the flow equations for a boiler will be derived in a general way. Stability criteria will be defined and preliminary results will be compared with those obtained from the experiments as well with theoretical results derived from (J2) and (C1).

### 5.2. Basic equations

In (V1), (V3) and (V4) results of a theoretical study starting from first principles have been reported. The aim of this study was to provide a basis for a detailed theoretical approach for an understanding of the heat transfer and fluid flow characteristics of a two-phase flow under stationary and transient conditions. So far the study has been restricted to bubbly flow.

The study starts by considering a ringshaped volume element  $\Delta U = 2\pi r \Delta r \Delta z$ , see Fig. 5.1, located at a distance  $z$  from the bottom of a coolant channel of annular and of rotation-symmetrical form. Then the basic equations of motion for the two-phase flow are formulated. These equations are formed by the laws of the conservation of mass, momentum and energy, the equations of state and an equation for the number density distribution of bubbles, describing the bubble transport in axial and radial directions. The number density distribution of bubbles is determined by the process of bubble diffusion, demixing effects near the wall, radial and axial convection of bubbles, interaction effects between adjacent bubbles and growth of the bubbles in the mixture.

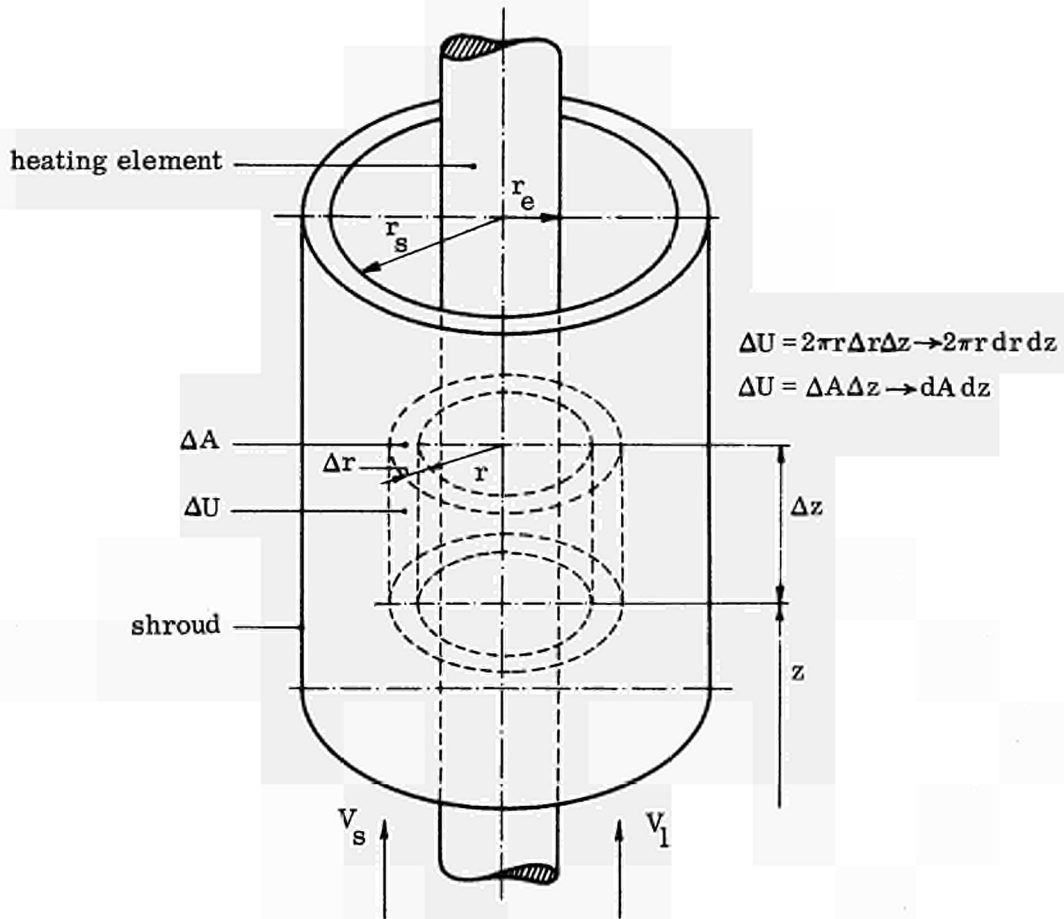


Fig. 5.1 Ringshaped volume-element

In the following the basic equations will be formulated again in a slightly different way. As was done in (V3) and (V4), only the process of bubble diffusion and bubble growth will be considered. The radial component of the liquid and vapor velocities will be ignored. This means that no radial transport of mass, momentum and energy because of convection will take place. Nor will effects of interaction between bubbles be considered.

#### Conservation of mass.

The principle of the conservation of mass, applied to an infinitely small fixed volume element yields a partial differential equation, which is usually called the continuity equation. This equation states that the change in mass with time within the volume element  $\Delta U$ , see Fig. 5.1, is equal to the difference in rate at which mass enters and leaves.



es the volume element. By taking the limit as  $\Delta r$  and  $\Delta z$  approach zero, the conservation law of mass is generally formulated as:

$$\frac{\partial \rho}{\partial t} + \text{div}(\rho \vec{V}) = 0 \quad (5.1.)$$

Keeping in mind that equation (5.1.) has been derived for a unit of volume  $dU = 2\pi r dr dz = dA dz$  and that in a two-phase flow, by definition, a part  $\alpha'$  of this volume is occupied by vapor and a part  $(1-\alpha')$  by liquid, a separation of both terms in equation (5.1.) into contributions from the vapor and liquid and division by  $dz$  yields:

$$\frac{\partial}{\partial t} \left\{ \rho_1 (1-\alpha') + \rho_s \alpha' \right\} dA + \frac{\partial}{\partial z} \left\{ \rho_1 (1-\alpha') V_1' + \rho_s \alpha' V_s' \right\} dA = 0 \quad (5.2.)$$

The single-phase continuity equation is obtained simply by setting  $\alpha' = 0$ . It should be emphasized that the physical quantities denoted with a prime in equation (5.2.) and also in the following equations are considered to be functions of  $r$ ,  $z$  and  $t$ .

Conservation of momentum.

The principle of the conservation of momentum applied to an infinitely small fixed volume element yields a partial differential equation which is usually called the equation of motion. This equation states that the change in momentum with time of the fluid within a volume element is equal to the difference in rate at which momentum flows into and leaves the volume element plus the sum of the surface and body forces acting upon the volume element. By considering only friction, pressure and gravity forces, the general form of the equation of motion reads (B16):

$$\frac{\partial}{\partial t} (\rho \vec{V}) + \text{div}(\rho \vec{V} \vec{V}) + \text{div} \tau + \text{grad} p - \rho \vec{g} = 0 \quad (5.3.)$$

Introducing again the contributions by the liquid and vapor phases in the different terms, similarly as was done with the continuity equation and ignoring convection and pressure gradients in radial direction, the law of the conservation of momentum for a two-phase flow reads:

$$\begin{aligned} & \frac{\partial}{\partial t} \left\{ \rho_1 (1-\alpha') V_1' + \rho_s \alpha' V_s' \right\} dA + \frac{\partial}{\partial z} \left\{ \rho_1 (1-\alpha') V_1'^2 + \right. \\ & \left. + \rho_s \alpha' V_s'^2 \right\} dA - \frac{1}{r} \cdot \frac{\partial}{\partial r} \left( \eta' r \frac{\partial V_1'}{\partial r} \right) dA + \frac{\partial p}{\partial z} dA + g \left\{ \rho_1 (1-\alpha') + \rho_s \alpha' \right\} dA = 0. \end{aligned} \quad (5.4.)$$

Conservation of energy.

The law of the conservation of energy states that the change in energy with time within the volume element is equal to the difference at which energy is flowing into and is leaving the volume element plus the rate at which energy is being produced there and the work done by external forces acting upon the volume element. Expressed in general form and considering only the work done by pressure forces this equation reads:

$$\frac{\partial}{\partial t} (\rho h) + \text{div}(\rho \vec{V} h) + \text{div}(p \vec{V}) + \text{div} \vec{u} = 0 \quad (5.5.)$$

Introducing again the liquid and vapor contributions, similarly as was done with the laws for the conservation of mass and momentum, and keeping in mind the definition of  $\alpha'$  and the fact that all terms in equation (5.5.) have been divided by  $2\pi r dr dz$ , the law of the conservation of energy for a two-phase flow reads:

$$\begin{aligned} \frac{\partial}{\partial t} \left\{ \rho_1 (1-\alpha') h_1' + \rho_s \alpha' h_s' \right\} dA + \frac{\partial}{\partial z} \left\{ \rho_1 (1-\alpha') V_1' h_1' + \rho_s \alpha' V_s' h_s' \right\} dA + \\ + \frac{\partial}{\partial z} \left\{ p (1-\alpha') V_1' + p \alpha' V_s' \right\} dA - \frac{1}{r} \cdot \frac{\partial}{\partial r} \left( \lambda' r \frac{\partial T_1'}{\partial r} \right) dA = 0 . \end{aligned} \quad (5.6.)$$

In deriving this equation it has been assumed that the conduction of heat in axial direction is negligible. In equation (5.6.)  $h_1'$  and  $h_s'$  are the total energy of the liquid and vapor. In practice, the kinetic and potential energy may be disregarded, so that:

$$h_1' = cT_1' + \frac{V_1'^2}{2} + gz \approx cT_1' , \text{ and} \quad (5.7.)$$

$$h_s' = cT_s' + e + \frac{V_s'^2}{2} + gz \approx cT_s' + e , \quad (5.8.)$$

where  $c$  is the specific heat and  $e$  is the heat of evaporation taken at constant volume.

The diffusion equation.

The number density distribution of bubbles  $N'$  which is a function of  $r$ ,  $z$  and  $t$  and the bubble radius  $R$  is an important parameter if one is to describe the two-phase flow process completely. As mentioned earlier, it is assumed that the number density of bubbles  $N'$  changes during transportation in the fluid only owing to radial diffusion of the bubbles. Besides, the radius of the bubbles will change because of the growth of the bubbles and condensation. Considering a fixed volume element and formulating the law of the conservation of the number of bubbles with radius  $R$ , one can express the number density  $N'$  by the relation:

$$\frac{dN'}{dt} + \frac{\partial N' V_s'}{\partial z} - \frac{1}{r} \cdot \frac{\partial \left\{ D' r \frac{\partial N'}{\partial r} \right\}}{\partial r} = 0 , \quad (5.9.)$$

where  $D'$  is the diffusion coefficient.

In (V4) this equation has been further developed. In a prolonged study, the additional effects of radial convection of bubbles and the mutual interaction between adjacent bubbles are being considered.

The equations of state.

The equations of state are expressions for the physical quantities of the fluid in an analytical, tabular or graphical form. As such are given the changes with temperature of

the density of the vapor and liquid phases, of the specific heat, of the heat of evaporation, and of the change in temperature with pressure under saturated conditions:

$$\begin{aligned} \rho_s &= f(T_s) , & e &= f(T_1) , \\ \rho_l &= f(T_1) , & T_s &= f(p) . \\ c &= f(T_1) , & & \end{aligned} \quad (5.10.)$$

Furthermore, expressions have to be derived for the coefficient of viscosity  $\mu'$ , the heat conduction coefficient  $\lambda'$  and the diffusion coefficient  $D'$  for a two-phase mixture as they appear in the equations (5.4.), (5.6.) and (5.9.). In (V4) the increase with respect to a single-phase flow of the viscosity, the heat conduction and the diffusion owing to the two-phase character of the flow and the presence of nucleate boiling is being ascribed to an increased turbulence level caused by the relative motion of the bubbles with respect to the surrounding liquid. The local agitations produced by the various bubbles is averaged and a mean turbulence intensity is ascribed to the fluid that varies with time and position.

The equations (5.2.), (5.4.), (5.6.) and (5.9.) and the equations of state are further developed in (V1), (V3) and (V4). These four equations describe in principle any two-phase bubble flow condition as a function of the independent variables  $x$ ,  $r$ ,  $t$  and  $R$ . Supplementary equations have been derived for the local slip of the bubbles with respect to the surrounding liquid, the temperature in the heating element (energy equation for the heating element) and the boundary conditions, particularly the generation of bubbles. After the introduction of dimensionless parameters it was found that 8 similarity parameters govern the solution of the exact equations. The complete mathematical treatment of the problem is to be published elsewhere.

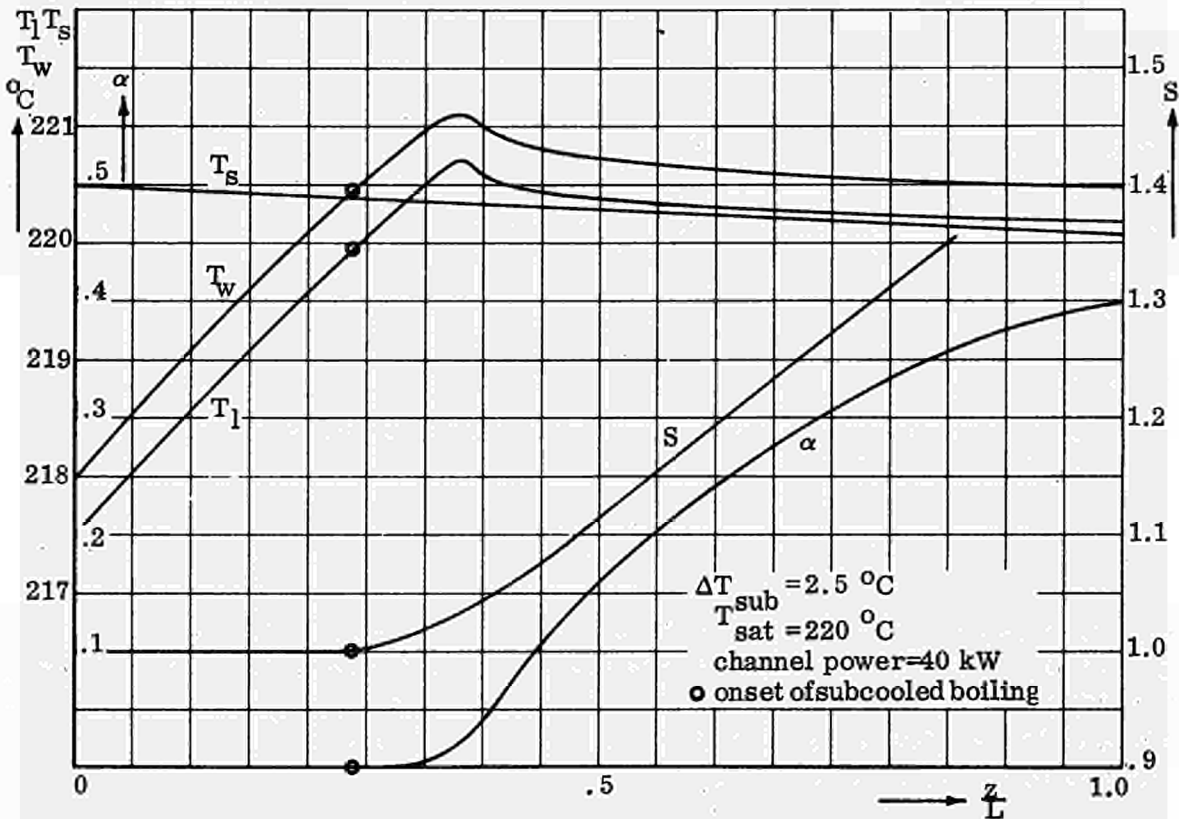


Fig. 5.2 Steady-state results calculated by a theoretical study based on "first principles" (V4).

So far, the equations for the steady state have been elaborated further and programmed for a digital computer. Some preliminary results are reproduced in Fig. 5.2, where the calculated variation in vapor temperature  $T_s$ , average liquid temperature  $T_l$ , the temperature of the heated wall  $T_w$ , the void fraction  $\alpha$  and the Slip Ratio  $S$  have been plotted as functions of the location along the boiling channel for one operational condition and for a geometry very close to Test Section I. The onset of subcooled boiling is indicated. Beside the assumptions mentioned before, it was assumed in these preliminary calculations that the local slip between the bubbles and the surrounding liquid is negligible. Nevertheless, it is demonstrated in Fig. 5.2 that the overall slip is not equal to unity, because of the non-uniform void concentration across the boiling channel, as already discussed in section 4.1.

In the bulk boiling region, the water remains somewhat superheated. There is an overshoot present in the wall and liquid temperature with respect to the saturation temperature. The magnitude of this overshoot depends largely upon the distribution of the nucleation centers on the heating element and data relevant to this must be added to the input data fed into the digital computer. In the calculation of the void fraction, not any constants are involved that have to be correlated with experimental results.

The study is being continued by further analyzing the effects of different quantities on the results.

### 5.3. Simplified equations and boundary conditions

For a performance and design calculation of the characteristics of a two-phase flow system under stationary and transient conditions the equations formulated before are yet too complex to serve as a basis. Therefore, the equations (5.2.), (5.4.), (5.6.) and (5.9.) will be integrated first with respect to  $dA = 2\pi r dr$  between the limits  $r_e$  and  $r_s$ , being the outer radius of the heating element and the inner radius of the shroud respectively. The radial variations of the flow quantities are taken into account by introducing empirical or theoretical correlations. The integration is performed by assuming that the densities of the liquid and steam  $\rho_l$  and  $\rho_s$ , and that the specific heat  $c$  and the heat of evaporation  $e$  are independent of the radius and that the cross-sectional area of the coolant channel  $A_c$  is constant along a small section of the boiler. For performing the integration mean quantities will be introduced.

#### 5.3.1. Simplified equations.

Conservation of mass.

By integrating equation (5.2.) and by introducing the mean quantities  $V_l$  and  $V_s$  defined in (4.6.), the conservation of mass equation reads:

$$\frac{\partial}{\partial t} \left\{ \rho_l (1-\alpha) + \rho_s \alpha \right\} + \frac{\partial}{\partial z} \left\{ \rho_l (1-\alpha) V_l + \rho_s \alpha V_s \right\} = 0 \quad (5.11.)$$

As has already been explained in section 4.1., the ratio of  $V_s$  and  $V_l$  is the well-known Slip Ratio  $S$ , (equation 4.7.). With the Slip Ratio  $S$  not only the local slip defined as the difference between the gas and the liquid phase velocities ( $V'_s - V'_l$ ) is taken into account, but also the distribution of either phase over the cross-section. Introducing  $S$  into equation (5.11.) yields:

$$\frac{\partial}{\partial t} \left\{ \rho_l (1-\alpha) + \rho_s \alpha \right\} + \frac{\partial}{\partial z} \left\{ \rho_l (1-\alpha) V_l + \rho_s \alpha S V_l \right\} = 0 \quad (5.12.)$$

In literature equation (5.12.) is customarily derived on the assumption that a single-valued velocity is associated with either phase at each cross-section of the channel. The ratio of the two velocities is then taken as the slip ratio. But the notion of single-valued velocity does not correspond with the way in which the slip factor S is determined experimentally, see section 4.1.

Conservation of momentum.

The integration of the friction term in equation (5.4.) results into:

$$-\frac{1}{A_c} \int_{A_c} \frac{1}{r} \cdot \frac{\partial}{\partial r} \left( \eta' r \frac{\partial V_1'}{\partial r} \right) dA = -\frac{2\pi}{A_c} \left[ \eta' r \frac{\partial V_1'}{\partial r} \right]_{r_e}^{r_s} = +\frac{2\pi}{A_c} (r_s \tau_{w_{r_s}} + r_e \tau_{w_{r_e}}) = F, \quad (5.13.)$$

where F is the wall-friction force per unit of length and per unit of cross-sectional area; F is usually given as an empirical or theoretical correlation. By integrating equation (5.4.) and introducing the mean quantities  $V_1$ ,  $V_s$ ,  $\bar{V}_1$  and  $\bar{V}_s$  defined in (4.6.) and (4.18.) and substituting the equations (4.7.) and (5.13.) the law of the conservation of momentum reads:

$$\begin{aligned} \frac{\partial}{\partial t} \left\{ \rho_1 (1-\alpha) V_1 + \rho_s \alpha S V_1 \right\} + \frac{\partial}{\partial z} \left\{ \rho_1 (1-\alpha) \bar{V}_1^2 + \rho_s \alpha \bar{V}_s^2 + p \right\} + \\ + g \left\{ \rho_1 (1-\alpha) + \rho_s \alpha \right\} + F = 0 . \end{aligned} \quad (5.14.)$$

In nearly all cases related to performance calculations, the acceleration term in (5.14.) is calculated by putting  $\bar{V}_1$  equal to  $V_1$  and  $\bar{V}_s$  equal to  $V_s$ . As already explained in section (4.2.), for an exact calculation of the acceleration pressure drop one needs to know the local distributions of the two phases and of the velocities. By measuring these distributions one could obtain two more "slip"-correlations  $S_a$  and  $S_b$ , being the ratio of  $\bar{V}_1$  and  $V_1$ , and of  $\bar{V}_s$  and  $V_1$  respectively.

Conservation of energy.

The following mean quantities are defined:

$$T_1 = \frac{\int_{A_c} (1-\alpha') T_1' dA}{(1-\alpha) A_c} ; \quad \bar{T}_1 = \frac{\int_{A_c} (1-\alpha') V_1' T_1' dA}{(1-\alpha) V_1 A_c} . \quad (5.15.)$$

From the earlier made assumption that there is no pressure gradient along the radius of the channel, it follows that there is no variation in saturation temperature over the cross-section. Integration of the heat conduction term yields:

$$\frac{1}{A_c} \int_{A_c} \frac{1}{r} \cdot \frac{\partial}{\partial r} \left( \lambda' r \frac{\partial T_1'}{\partial r} \right) dA = \frac{2\pi}{A_c} \left[ \lambda' r \frac{\partial T_1'}{\partial r} \right]_{r_e}^{r_s} = q_w , \quad (5.16.)$$

$q_w$  is the amount of heat taken per unit length and per unit cross-sectional area which is transported from the heating wall into the fluid. By integrating equation (5.6.) and by substituting equation (5.16.) and the mean quantities  $V_s$  and  $V_l$  defined in (4.6.) the conservation of energy equation reads:

$$\begin{aligned} & \frac{\partial}{\partial t} \left\{ \rho_l (1-\alpha) c T_l + \rho_s \alpha (c T_s + e) \right\} + \\ & + \frac{\partial}{\partial z} \left\{ \rho_l (1-\alpha) V_l \left( c \bar{T}_l + \frac{p}{\rho_l} \right) + \rho_s \alpha V_s \left( c T_s + e + \frac{p}{\rho_s} \right) \right\} - q_w = 0 . \end{aligned} \quad (5.17.)$$

There is no study known to the author in which the difference in  $T_l$  and  $\bar{T}_l$  is recognized and taken into consideration. In all studies reported up till now,  $\bar{T}_l$  is assumed equal to  $T_l$ . The difference between  $T_l$  and  $\bar{T}_l$  may be of importance in cases where large temperature gradients are present. By introducing a temperature correlator  $S_c$ , being the ratio of  $\bar{T}_l$  and  $T_l$ , the flow distribution effects can be taken into account.

Diffusion equation.

Also the diffusion equation has to be integrated with respect to  $2\pi r dr$ . Moreover, this equation has also to be integrated with respect to the bubble radius  $R$  between the limits 0 and  $\infty$ . The integration has been performed in (V4). It would go too far to repeat this here. The result of this integration is that the substantial change with time of the number density of the bubbles averaged over the cross-section and bubble radius is proportional to the product of the number density of the active crevices times the bubble detachment frequency. The boiling process at the heated wall forms the boundary condition for the diffusion equation.

Owing to the complex nature of the diffusion equation and the difficulties involved in using this equation in a performance calculation of a two-phase system in both a steady-state and transient condition, this equation will no longer be used any more. What is needed now is another equation for determining the quantity of steam as a function of time  $t$  and the space coordinate  $z$ . Therefore, the energy equation is split up into two separate equations, one equation governing the warming up of the liquid phase of the flow and a second equation representing the heat supply to the vapor part. The ratio  $\kappa$ , of the heat supplied to the steam phase and the total heat input, is given by a correlation based on experimental and theoretical studies.

The final equations in which the quantities  $S_a$ ,  $S_b$  and  $S_c$  have been introduced are given below together with the equations of state, the correlation functions for the three slip ratios  $S$ ,  $S_a$  and  $S_b$ , for the two-phase frictional force  $F$ , and for the heat division parameter  $\kappa$  and the temperature correlator  $S_c$ .

Describing equations.

I. Conservation laws.

Mass

$$\frac{\partial}{\partial t} \left\{ \rho_l (1-\alpha) + \rho_s \alpha \right\} + \frac{\partial}{\partial z} \left\{ \rho_l (1-\alpha) V_l + \rho_s \alpha S V_l \right\} = 0 . \quad (5.18.)$$

## Momentum

$$\begin{aligned} & \cdot \frac{\partial}{\partial t} \left\{ \rho_1 (1-\alpha) V_1 + \rho_s \alpha S V_1 \right\} + \frac{\partial}{\partial z} \left\{ \rho_1 (1-\alpha) S_a^2 V_1^2 + \rho_s \alpha S_b^2 V_1^2 + p \right\} + \\ & + g \left\{ \rho_1 (1-\alpha) + \rho_s \alpha \right\} + F = 0 . \end{aligned} \quad (5.19.)$$

## Energy

### Liquid

$$\frac{\partial}{\partial t} \left\{ \rho_1 (1-\alpha) c T_1 \right\} + \frac{\partial}{\partial z} \left\{ \rho_1 (1-\alpha) V_1 \left( c S_c T_1 + \frac{p}{\rho_1} \right) \right\} = (1-x) q_w . \quad (5.20.)$$

### Vapor

$$\frac{\partial}{\partial t} \left\{ \rho_s \alpha (c T_s + e) \right\} + \frac{\partial}{\partial z} \left\{ \rho_s \alpha S V_1 \left( c T_s + e + \frac{p}{\rho_s} \right) \right\} = x q_w . \quad (5.21.)$$

As can be concluded, the total energy equation can be obtained by eliminating  $x$  from the two separate equations.

## II. Equations of state.

$$\rho_s = f(T_s) \quad \rho_1 = f(T_1) \quad T_s = f(p) \quad c = f(T_1) \quad e = f(T_1) . \quad (5.22.)$$

## III. Correlation functions.

|                    |                          |         |
|--------------------|--------------------------|---------|
| $S, S_a$ and $S_b$ | slip ratios              |         |
| $S_c$              | temperature correlator   | (5.23.) |
| $F$                | wall-friction force      |         |
| $x$                | heat division parameter. |         |

In these equations, the independent variables are the time  $t$  and the coordinate along the coolant channel  $z$ . The channel power per unit of cross-sectional area and per unit of length must be prescribed. The four main variables in the conservation laws (5.18.) to (5.21.) are  $\alpha$ ,  $V_1$ ,  $T_1$  and  $T_s$ . The quantities  $\rho_s$ ,  $\rho_1$ ,  $p$ ,  $c$  and  $e$  are determined by the equations of state (5.22.). The quantities  $S$ ,  $S_a$ ,  $S_b$ ,  $S_c$ ,  $F$  and  $x$  have to be given by means of the correlation functions (5.23.). The number of unknowns, equal to 15, is in agreement with the number of available equations.

In this section it has been shown, that one has to make use of correlation functions, owing to the integration of the basic equations over the cross-section of the channel. The main aim of the theoretical study started by Van der Walle (V4) is to provide a theoretical basis for these correlation functions. Where it is uncertain which flow distribution is present in the boiling channel, the quantities  $S_a$ ,  $S_b$  and  $S_c$  will be put equal to unity in the further elaboration of the equations (5.18.) to (5.23.).

### 5.3.2. Boundary conditions.

The equations (5.18.) to (5.23.) describe the performance characteristics of a boiling channel under steady state as well as under non-steady state conditions. The equations can be integrated numerically with respect to  $z$  and  $t$ . The equations describing the steady-state characteristics can be derived from (5.18.) to (5.23.) by omitting all time-dependent terms.

The boundary conditions for the boiling channel and thus for the describing equations are formed by the characteristics of the other parts of the loop, e.g. condenser, sub-cooler, etc. In nearly all theoretical studies these imposed boundary conditions are simplified by assuming, for instance, a constant pressure at the exit of the channel and a constant temperature at the inlet of the channel. A more exact formulation of the boundary conditions is obtained by setting up the conservation laws for the different parts. When a schematic flow sheet of the boiling apparatus is considered, see Fig. 2.3 and Fig. 5.4, two main parts can be distinguished:

- a. the part of the loop situated between the exit of the coolant channel and the inlet of the downcomer; this part includes the condenser and consists of a volume of water and a volume of steam;
- b. the part of the loop situated between the inlet of the downcomer and the inlet of the coolant channel; this part includes the subcooler and consists of two volumes of water, with different temperatures, i.e. the hot part and the cold part of the downcomer.

In formulating the boundary conditions, it will be assumed that the water and steam temperature in part a (condenser) and the water temperature in the hot part of part b (downcomer) are equal to each other and that the water temperature in the cold part of the downcomer is equal to the temperature at the inlet of the channel. The mean conditions in the subcooler will be assumed as being equivalent to the arithmetic mean of the conditions prevailing at the cooler inlet and at the cooler outlet. Furthermore, it will be assumed that density variations in the downcomer with time can be neglected.

For the two parts mentioned the conservation laws will be formulated.

#### Conservation of mass.

The law of the conservation of mass, already extensively formulated in section 5.2., but this time applied to the external system between exit and inlet of the coolant channel, and hence including the condenser and the subcooler, reads after application of the assumptions mentioned earlier:

$$\left\{ A_c \rho_l (1-\alpha) V_l + A_c \rho_s \alpha S V_l \right\}_{\text{ex}} - \left\{ A_c \rho_l V_l \right\}_{\text{in}} = \frac{d(U_{\text{con}} \rho_{\text{con}})}{dt} \quad (5.24.)$$

In equation (5.24.) the subscript "ex" denotes the exit and "in" the inlet of the coolant channel and  $U_{\text{con}}$  and  $\rho_{\text{con}}$  the volume and the density in the condenser. The term on the right-hand side of equation (5.24.) has to be split up into a part of the condenser occupied by water  $(1-\sigma)U_{\text{con}} \cdot \rho_{l, \text{con}}$  and a part occupied by steam  $\sigma U_{\text{con}} \cdot \rho_{s, \text{con}}$ . Owing to the change in water level with time under fluctuating conditions  $\sigma$  will vary with time, see Fig. 5.4.

#### Conservation of momentum.

The law of conservation of momentum, applied to the downcomer (part b), is used to



derive an equation for the differential pressure over the coolant channel, see Fig. 5.4:

$$p_{in} - p_{ex} = \rho_{1,con} g H_d + \rho_{1,in} g H_t - \rho_{1,con} g (H_d + H_t - L_t) - A_c \frac{dV_{1,in}}{dt} \sum \rho_{1,k} \frac{L_k}{A_k} +$$

$$- k_{in} \frac{1}{2} \rho_{1,in} V_{1,in}^2 - k_{ex} \frac{1}{2} \rho_{1,ex} V_{1,ex}^2 - \text{friction losses in downcomer.} \quad (5.25.)$$

The first three terms on the right-hand side represent the hydrostatic head in the downcomer. The quantity  $H_d$  varies with time. The fourth term represents the acceleration loss, summed up for the various parts and related to conditions at the inlet. The fifth and the sixth term are the pressure losses across the inlet and the outlet of the coolant channel. The friction losses in the downcomer (last term in equation (5.25.)) will be accounted for in the further elaboration, by raising the value of  $k_{in}$ .

The law of conservation of momentum across the water height above the coolant channel is used to derive an expression for the pressure in the condenser:

$$p_{con} - p_{ex} = -k_{ex} \frac{1}{2} \rho_{1,ex} V_{1,ex}^2 - \rho_{1,con} g (H_d + H_t - L_t) . \quad (5.26.)$$

Conservation of energy.

The law of the conservation of energy will be formulated for either part (a and b) separately. The heat removed in the condenser will be denoted as  $Q_{con}$ , that in the sub-cooler with  $Q_d$ . The law of the conservation of energy for the condenser reads:

$$\left[ A_c \left\{ \rho_1 (1-\alpha) V_1 \left( cT_1 + \frac{p}{\rho_1} \right) + \rho_s \alpha S V_1 \left( cT_s + e + \frac{p}{\rho_s} \right) \right\} \right]_{ex} +$$

$$- \left[ A_d \left\{ \rho_1 V_1 \left( cT_1 + \frac{p}{\rho_1} \right) \right\} \right]_{di} = Q_{con} + \quad (5.27.)$$

$$+ \frac{d}{dt} \left[ \rho_s \sigma U_{con} (cT_s + e) + \rho_1 (1-\sigma) U_{con} cT_1 \right]_{con} .$$

In equation (5.27.) the second term on the left-hand side is the rate at which energy is leaving the condenser into the downcomer (subscript di).  $\sigma U_{con}$  is the part of the condenser volume which is occupied by steam and  $(1-\sigma)U_{con}$  that occupied by water.

The law of the conservation of energy for the downcomer yields:

$$\left[ A_d \rho_1 V_1 \left( cT_1 + \frac{p}{\rho_1} \right) \right]_{di} - \left[ A_c \rho_1 V_1 \left( cT_1 + \frac{p}{\rho_1} \right) \right]_{in} = Q_d + \frac{d}{dt} \sum \left\{ U_d \rho_1 cT_1 \right\}_k . \quad (5.28.)$$

The last term in equation (5.28.) is the change in energy with time within the various parts of the downcomer.

The total amount of heat supplied to the two-phase mixture is equal to  $Q = \int_0^{L_t} A_c q_w dz$  (see equations (5.20.) and (5.21.)). When it is assumed that under steady-state conditions a part  $\beta$  is removed from the two-phase mixture in the condenser, and in the downcomer a part  $(1-\beta)$ , the expressions for  $Q$ ,  $Q_{con}$  and  $Q_d$  under non-steady conditions can be written as:

$$\begin{aligned} Q &= Q_0 \left\{ 1 + E_1(t) \right\}, \\ Q_{con} &= \beta Q_0 \left\{ 1 + E_2(t) \right\}, \\ Q_d &= (1-\beta) Q_0 \left\{ 1 + E_3(t) \right\}, \end{aligned} \quad (5.29.)$$

in which  $Q_0$  is the channel power under steady-state conditions. The three functions  $E_1$ ,  $E_2$  and  $E_3$ , represent the dynamic characteristics of respectively the heating rod (accumulation of heat owing to the heat capacity of the rod and the heat transfer process at the wall; the incorporation of this effect in a distributional way can be done by formulating the energy equation in the heating rod for a small segment and deriving an expression for  $q_w$  (equation 5.21.) and the heat input), the condenser (including the controller) and the subcooler. These functions may also be used to introduce into the described flow process, forcing functions, e.g. perturbations (step, ramp or sine) into the controlling variables, such as channel power, system pressure and inlet subcooling.

The boundary equations (5.24.), (5.25.), (5.27.) and (5.28.) relate the conditions at the exit to those at the inlet of the coolant channel. The equations (5.18.) to (5.21.) calculate, together with the equations of state (5.22.) and the correlation functions (5.23.), the values of  $T_1$ ,  $T_s$ ,  $V_1$  and  $\alpha$  at the exit of the channel. By means of the four boundary equations, (and by using values for  $k_{in}$ ,  $k_{ex}$ , the equations of state, the correlation functions and geometrical and operational data), the values of these quantities at the inlet can be calculated again (e.g.  $T_1$ ,  $T_s$  and  $V_1$ , while  $\alpha=0$ ) as well as the change in water level  $H_d$ . The conditions at the exit of the channel and in the condenser are related by equation (5.26.).

The equations were derived for a naturally circulating system. The incorporation of a pump will generally only effect equation (5.25.).

The derived equations, which are clearly non-linear may be solved by direct numerical integration in the two directions  $z$  and  $t$  by a finite difference technique. Also, when there are assumed to be only small disturbances from the steady-state, the dynamic part of the equations can be linearized and a solution be found in the frequency domain. In the following, calculation results will be reported of two theoretical studies made by Jahnberg (J2) and by Currin (C1), who integrated numerically, after making some further simplifications, the derived equations. After that the linearized approach will be dealt with.

The objective of all these studies is to determine the steady-state characteristics, the onset of hydraulic oscillations and the response of the system to external perturbations.

#### 5.4. Studies of Jahnberg and Currin

In the analysis of Jahnberg (J2) the one-dimensional approach, as derived before (equations (5.18.) and (5.23.)) was followed. This means that there are two independent variables  $z$  and  $t$ . In calculating the dynamic characteristics of a boiling system the following assumptions have been made for solving the equations (5.18.) to (5.23.):

- a. The pressure drop along the channel is small compared with the mean system pressure. This permitted the use of space and time independent values for the specific density for either phase of the fluid and implies no change in boiling temperature along the channel. Also, the specific heat of water and the heat evaporation have been chosen as space and time independent values.
- b. It is assumed that boiling under subcooled conditions does not occur. A small correction is applied to the frictional pressure drop in the non-boiling region, accounting for surface boiling. The onset of saturated boiling is calculated from a heat balance. In the saturated boiling region, the water temperature is assumed to be equal to the saturation temperature corresponding with the system pressure. This means  $x=1$  in equation (5.20.) and (5.21.).
- c. In the energy equation, the internal energy has been put equal to the enthalpy.
- d. The contribution to the pressure drop of the acceleration of the fluid in the non-boiling region of the channel has been disregarded.
- e. The thermal capacity of the heating element has been disregarded, so that no energy equation for the heating element is used.
- f. In the boundary conditions (equations (5.24.) to (5.28.)), the energy equations have been disregarded. It has, therefore, been assumed that, under non-steady conditions there are no variations in water level, and that the system pressure and the inlet temperature are constant. Two sets of boundary conditions for the pressure drop are considered. First, the difference in pressure over the heated channel, including inlet and outlet losses is prescribed (this is a reasonable approximation for a coolant channel in a reactor with many channels). Secondly, a complete natural circulation loop, including riser and downcomer is being considered and the total pressure drop is assumed to equal zero.

The above assumptions imply that the description of the dynamic behavior of a boiling channel made by Jahnberg will probably only be correct at medium pressures.

Experimental correlations have been used for the Slip Ratio,  $S$ , and the two-phase friction force, expressed with the multiplier  $R$ , (equation 4.20.). Both correlations were based on the work reported by Martinelli and Nelson (M3). The following expressions have been used:

Slip ratio:

$$S = (1 + s x^{3/4}) \left( .795 + .410 \frac{\rho_1 A_c}{M_t} \right) \quad , \quad (5.30.)$$

where  $s$  is a pressure dependent parameter. During the transient calculations the velocity dependence of the slip ratio has been disregarded.

The two-phase friction multiplier  $R$  is expressed by:

$$R = 1 + dx^b \quad , \quad (5.31.)$$

where  $d$  and  $b$  are pressure dependent quantities.

Starting from the Jahnberg equations, corrected for the effect mentioned under d, a digital computer program has been written (A3) possessing a greater flexibility as regards the choice of the expressions for  $S$  and  $R$ . In studying the possible solution technique of the set of equations it was found that this system possesses "characteristics" which render the computation procedure in the physical  $z-t$  plane much more straightforward than the finite difference technique as described in the original publication by

Jahnberg. The solution of the system was programmed therefore by using the "method of characteristics" which is a more or less "natural" method for the numerical solution of this system of partial differential equations. The advantages are that the equations become simple and that the correct ratio between the integration steps in  $z$  and  $t$  direction is automatically obtained.

With this computer program, some calculations have been performed for Test Section I at a saturation temperature of  $200^{\circ}\text{C}$  and a subcooling temperature of  $.7^{\circ}\text{C}$ . From the first results it was clear that the correlations for  $S$  and  $R$  as presented in the equations (5.30.) and (5.31.) were not in agreement with the steady-state experimental results. These correlations yielded too low values for the natural circulation rate and too high values for the exit void fraction. Therefore, the constants  $s$  and  $d$  in equations (5.30.) and (5.31.) were chosen in such a way that the recirculation rate and the exit void fraction under steady-state conditions were about the same as they were measured experimentally. Then the response of the system was calculated, following a 2% step input in power (equation 5.29.).

In Fig. 5.3 the velocity of the fluid at the inlet of the channel is plotted as a function of time for three channel powers. As is shown, divergent oscillations occur at channel powers of 75 and 70 kW. At 65 kW channel power, the oscillations have a constant amplitude and a period of 1.5 seconds and the two-phase system has an indifferent stability. At this channel power the system is becoming unstable. Compared with the measured value of 162 kW the predicted value is very low. Nor is the predicted frequency in agreement with the measured one, see Table 3.2.

It is considered remarkable that the calculations, based on Jahnbergs equations should result in such a large discrepancy with the measured results. In (B12) calculations are reported which approached experimentally determined values more closely. As an aid

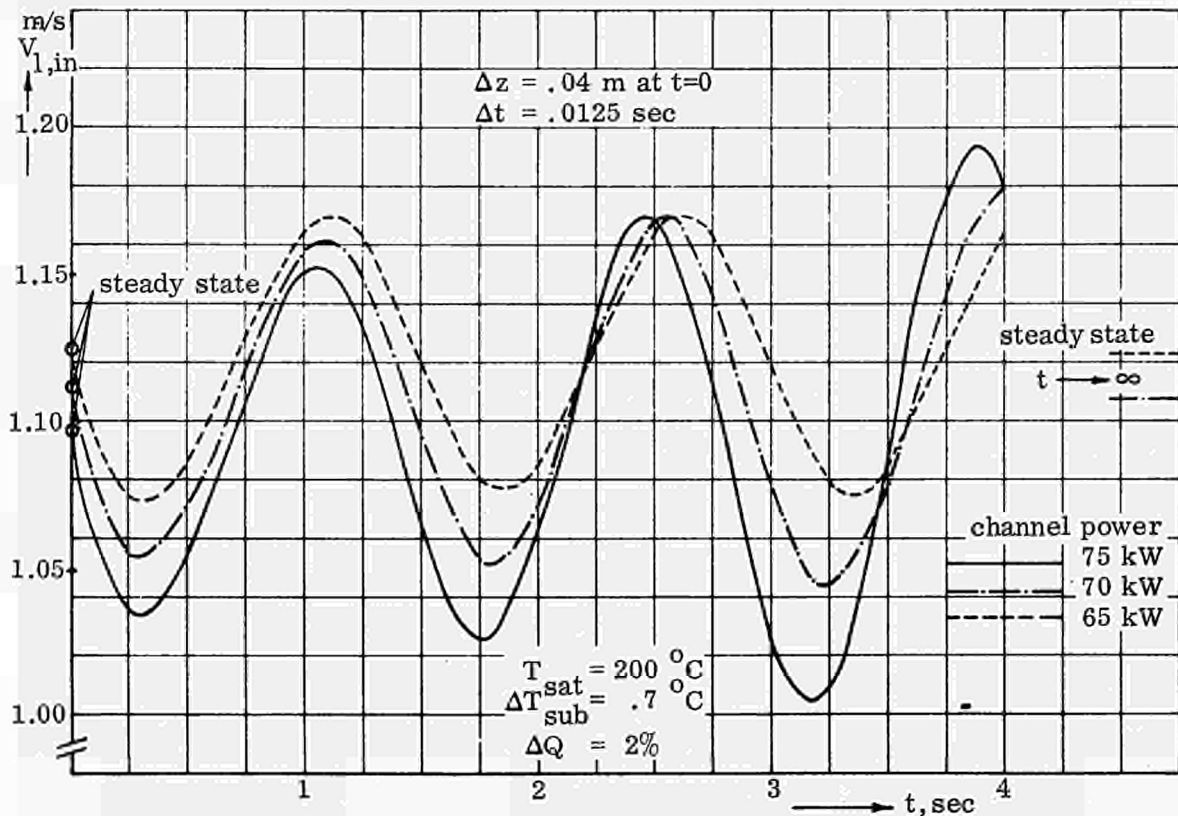


Fig. 5.3 Transient results calculated by the study of Jahnberg (J2), Test Section I.

to those wishing to repeat the calculations, the main input data will be given. Apart from the physical data of water and steam and the geometrical data given in Table 2.1. and 2.2. the following data have been used.

$$\begin{aligned}
 C &= .2 \text{ (equation A10 in (J2))} \\
 4f &= .031 \text{ and } B=0 \text{ (equation A4 in (J2), } 4f = f \text{ in equation A4)} \\
 k_{in} &= 1.4 \text{ (equation (5.25.)), including downcomer friction losses)} \\
 k_{ex} &= 0 \text{ (equation 5.25.)} \\
 s &= 3 \text{ (equation 5.30.)}
 \end{aligned}$$

$$L_d = A_c \sum \frac{L_k}{A_k} = .489 \text{ m (equation 5.25.)}$$

$$d = 110 \quad \text{and } b = 1 \text{ (equation 5.31.)}$$

In the calculations it has been assumed that during a time step of .1 second the channel power has increased to 1.02 times the original steady-state value. In the event when a pure step function in power as input is chosen, a singularity occurs at  $t=0$  in the mathematical formulation, because of the assumption that the density of steam along the boiler is constant.

By introducing the correlations for the Slip Ratio,  $S$ , and Two-Phase Friction Multiplier,  $R$ , which will be used in the linearized approach to be reported yet, an even slightly lower instability threshold channel power was found.

Recently the description of Jahnberg has been improved upon by incorporating some initially disregarded effects (H3). Comparative results have not been reported so far.

A similar study has been reported by Currin (C1). A digital computer program was written (HYDNA code) in order to detect the flow instability in a coolant channel. In this program, the effects of subcooled boiling have been taken into account. The courtesy of the Westinghouse Corporation, U.S.A., made it possible to perform some calculations with this computer program for the geometry and operating conditions of Test Section I.

At a saturation temperature of  $120^{\circ}\text{C}$ , the instability threshold was between 54 and 60 kW channel power. The frequency of the divergent oscillations was .6 c.p.s. At  $160^{\circ}\text{C}$  saturation temperature, constant amplitude oscillations appeared in the output when the channel power was increased from 120 to 140 kW. At saturation temperatures of  $200$  and  $220^{\circ}\text{C}$ , the solution of the equations gave evidence of a stable system until the maximum channel power explored of 210 and 260 kW respectively. By comparing these results with the experimental results given in Table 3.2., the conclusion is reached, that the HYDNA code overrates the instability threshold at the higher system pressure. At low system pressure the calculated results are in fairly good agreement with the experimental ones.

Using the computer program of Jahnberg as well as that of Currin, the inverse effect of increased subcooling at low and high subcooling rates was qualitatively demonstrated.

### 5.5. Linearization of the equations and solution procedure

As has been shown in the analysis of the experimental results, the two-phase flow process may be regarded as a linear process for small disturbances from the steady-state, even at high channel powers. For studying the dynamic behavior of a vertical boiler,

the equations (5.18.) to (5.23.) (conservation laws, equations of state and correlation functions) will be linearized with respect to small deviations from the steady state. This will also be done for the boundary conditions, equations (5.24.) to (5.29.).

Furthermore, only the response will be studied to a sinusoidal modulation in the controlling variables, e.g.  $Q$ ,  $Q_{con}$  and  $Q_d$  (equation 5.29.). In this way, transfer functions may be obtained from these variables to dependent variables, such as mass flow, void fraction, etc.

Similar approaches have been reported by Jones (J1) and Solberg (S11). The equations described in (S11) have been programmed for an analogue computer and the solution is, therefore, somewhat limited by the choice of the number of increments in axial direction. Both approaches are based on assumptions similar to those made by Jahnberg, but they do, for instance, incorporate the effect of subcooled boiling. Because of these assumptions, particularly as regards the boundary conditions and the pressure effects, the influence of any pressure variations with  $z$  and  $t$  upon the conservation laws for mass and energy has been disregarded. Therefore, the momentum equation can be handled separately. Jones takes into account the characteristics of the heating element. He assumes that there is a fixed location of the boiling boundary and computes at that location the variation in void fraction from a heat balance. In the law of the conservation of momentum, he disregards the discontinuous pressure variation because of this sudden change in void fraction. The stability of the system is then examined by using the tools of the feedback control system theory, and more specifically, the Nyquist criterion. In his equation, he uses the correlations of Bankoff and Martinelli-Nelson for the slip and two-phase friction multiplier, which are rather implicitly incorporated into the equations.

The basic equations derived before will now be further elaborated. They include all the effects which have as yet been disregarded by others.

In the following, only the main steps of the elaboration procedure will be given. The complete linearized equations and the solution procedure will be reported elsewhere (V5). In the elaboration procedure, the equations have been made dimensionless by properly using significant parameters. This procedure holds certain advantages, such as, for instance, independency of units, a variation of the quantities between narrower limits and a more readily apparent comparison between various operating conditions and geometries. Next, it is assumed that the variations of all variables with time are insignificant compared with the steady-state magnitudes of these variables. For instance, for the liquid phase velocity is written:

$$V_1 = V_{1,0} + \Delta V_1 \quad , \quad (5.32.)$$

where  $\Delta V_1$  is the small time-dependent part of  $V_1$ , and  $V_{1,0}$  the steady-state value. Furthermore, it is assumed that the variation of  $\Delta V_1$  with time is harmonic, and hence that:

$$\Delta V_1 = V_{1,i} \cdot e^{j\omega t} \quad , \quad (5.33.)$$

with  $V_{1,i}$  being the complex amplitude of the disturbance. This is also done for  $\alpha$ ,  $T_s$ ,  $T_1$ ,  $\rho_s$ ,  $\rho_l$ ,  $p$ ,  $S$ ,  $F$ ,  $\kappa$ ,  $H_d$  and for  $Q$ ,  $Q_{con}$  and  $Q_d$ .

After substituting (5.33.) etc. into the earlier derived equations and then subtracting the steady-state equations, a set of equations describing the deviations from the steady-

state is obtained. In these equations all quadratic terms of the variables are disregarded, so that the remaining equations become linear. It should be noted that by this procedure the equations describing the steady-state performance characteristics are not linearized.

The harmonic variations of the variables are complex quantities and have to be expressed in their real and imaginary constituents, e.g. in a form as:

$$V_{1,i} = V_{1,i}'' + j V_{1,i}''' , \text{ etc.} \quad (5.34.)$$

The ultimate result of this substitution is doubling the number of equations and variables in the unsteady case. By eliminating the variables  $\rho_1$ ,  $\rho_s$  and  $p$  (real and imaginary parts), using the equations of state and the variables  $S$ ,  $F$  and  $\kappa$  (real and imaginary parts), using the correlation functions, two sets of four equations (a "real" set and an "imaginary" set) are obtained from the conservation laws of the coolant channel (5.18.) to (5.21.), which actually constitute a single system of 8 equations with 8 unknowns, to wit:  $V_{1,i}''$ ,  $V_{1,i}'''$ ,  $\alpha_i''$ ,  $\alpha_i'''$ ,  $T_{1,i}''$ ,  $T_{1,i}'''$ ,  $T_{s,i}''$ ,  $T_{s,i}'''$ . These 8 equations are ordinary differential equations. For instance, the real part of the law of the conservation of mass is expressed by:

$$C_1 \frac{dV_{1,i}''}{dz} + C_2 \frac{d\alpha_i''}{dz} + C_3 \frac{dT_{1,i}''}{dz} + C_4 \frac{dT_{s,i}''}{dz} = C_{1,5}'' \quad (5.35.)$$

The coefficients on the left-hand side of the equation are real, and are determined by the solutions of the non-linear equations describing the steady state.

The term on the right-hand side incorporates the time-dependent terms, the variation with  $z$  of the steady-state quantities and the forcing functions, i.e. the channel power and condenser and subcooler heat removal by which the system can be excited.

The system of equations is integrated numerically with respect to  $z$  for a given starting value of the 8 unknowns at the channel inlet. The integration procedure which is performed along the channel and which is carried out using a Runge-Kutta procedure, results in values of the 8 unknowns at the riser exit, and finally, after application of all (linearized) boundary conditions, new values for the mentioned quantities at the channel inlet and the quantity  $H_{d,i}$  are determined. This is indicated schematically in Fig. 5.5.

Generally, the last determined values will not agree with the first estimates. In determining the correct starting values, use is made of the linearity of the system, which allows of applying the principle of superposition for adding up various solutions. This procedure will be reported extensively elsewhere (V5).

The integration of the equations describing the steady state is also performed, using a Runge-Kutta procedure. The determination of the correct value at the inlet is carried out by an iteration procedure using the boundary conditions.

The equations have been programmed for a digital computer. The formulation of the solution procedure as well as the drafting of the digital computer program have been carried out by the Consultant Firm Rescona Ltd. at Amstelveen. The correlation functions for  $S$ ,  $F$ ,  $\kappa$  and for  $k_{ex}$  are introduced in the program in the form of subroutines, which results in a large flexibility.

## 5.6. Stability criteria

So far, only a closed-loop system has been considered, i.e. the riser coupled with the downcomer. From the digital computer program, the closed-loop characteristics can

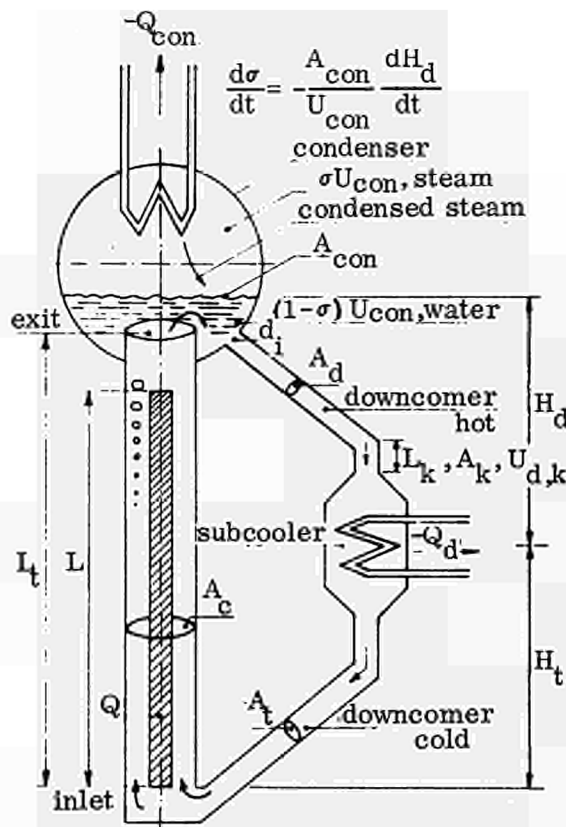


Fig. 5.4 Natural-circulation boiler

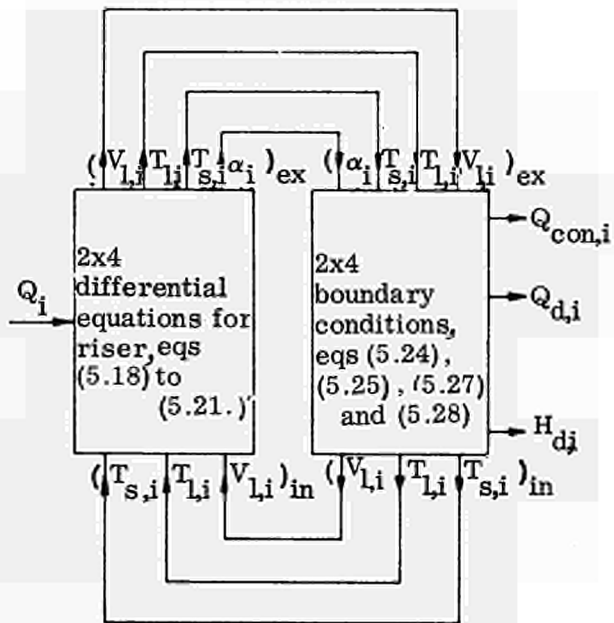


Fig. 5.5 Block diagram of natural-circulation boiler

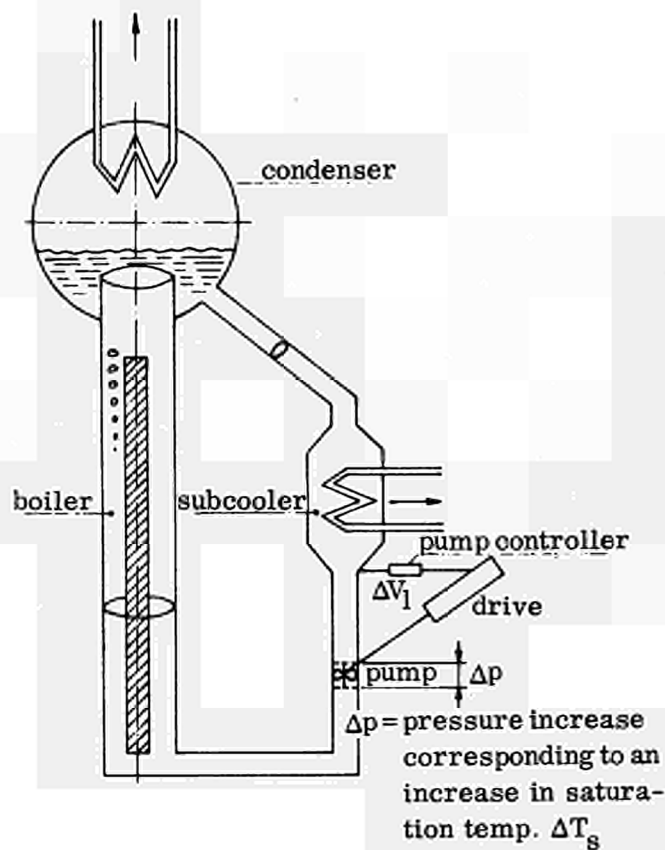


Fig. 5.6 Forced-circulation boiler

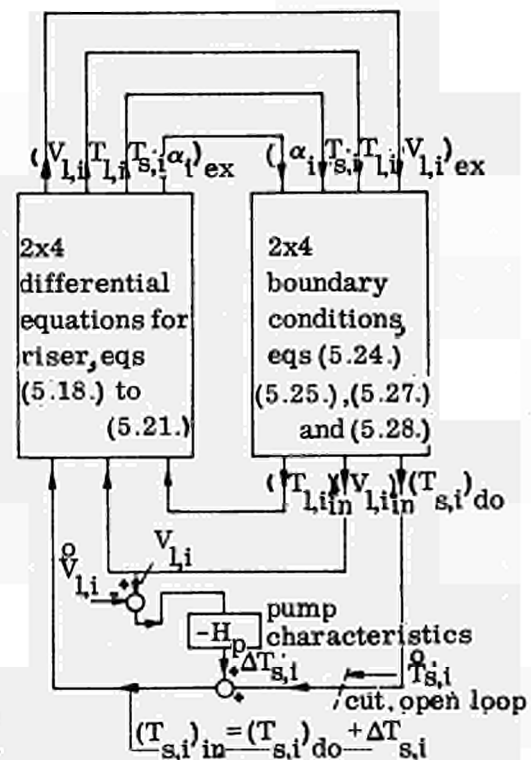


Fig. 5.7 Block diagram of forced-circulation boiler



be calculated, for instance, the transfer functions from the channel power to dependent variables, such as mass flow, void fraction, etc.

In stability analysis, it is often much more convenient to consider an open-loop analysis. System stability can be examined by applying the concepts of control system theory. Any instability condition is then more readily signalized, and the necessary measures for improving the stability can be readily determined. For defining stability criteria the open-loop analysis will be followed. The problem is, however, where the required cut in the closed-loop has to be made. In order to investigate this problem the schematic diagrams of Fig. 5.6 and Fig. 5.7 have been drawn up.

The hydraulic instabilities that are of interest here are those that are typical for a natural circulation system. In a forced circulation boiler with steep head-flow characteristics, no hydraulic instabilities, such as considered here, have been found. This suggests considering a forced circulation boiler, as shown in Fig. 5.6. A pump is present in the downcomer, which pump generates a pressure rise, corresponding with a rise in saturation temperature  $\Delta T_s$ . The pump measures the fluctuations in mass flow  $V_{l,i}$  and translates these variations into a rise in saturation temperature of  $\Delta T_{s,i}$ . Now it is assumed that the system is brought into excitation by controlling the pump with a sinusoidal signal corresponding to a desired fluctuation in mass flow  $\overset{o}{V}_{l,i}$ . The magnitude of  $\Delta T_{s,i}$ , see Fig. 5.7, is dependent upon the difference between  $\overset{o}{V}_{l,i}$  and  $V_{l,i}$ . The dependence may be simply expressed by:

$$\Delta T_{s,i} = -H_p (V_{l,i} - \overset{o}{V}_{l,i}) \quad , \quad (5.36.)$$

where  $H_p$  is a measure of the pump characteristics. The larger  $H_p$  becomes, the higher is the pressure rise upon a certain change in mass flow. Actually,  $H_p$  is a transfer function and thus a complex quantity. The following transfer functions for the open-loop without a pump and with a cut, as indicated by the broken line in Fig. 5.7, are defined as:

$$G_1 = \left\{ \frac{\left( \begin{matrix} T_{s,i} \\ \text{do} \end{matrix} \right)}{\left( \begin{matrix} \overset{o}{T}_{s,i} \\ \text{in} \end{matrix} \right)} \right\}_{H_p = 0} \quad , \quad \text{and} \quad G_2 = \left\{ \frac{V_{l,i}}{\left( \begin{matrix} \overset{o}{T}_{s,i} \\ \text{in} \end{matrix} \right)} \right\}_{H_p = 0} \quad (5.37.)$$

Here  $G_1$  and  $G_2$  determine the change in saturation temperature (pressure) and mass flow rate at the outlet of the downcomer upon a variation in saturation temperature (pressure) at the inlet.

The transfer function for the closed-loop from imposed modulation in mass flow to the saturation temperature at the inlet of the channel can then be written as:

$$\frac{T_{s,i}}{\overset{o}{V}_{l,i}} = \frac{H_p}{1 - G_1 + H_p G_2} \quad , \quad (5.38.)$$

or as:

$$\frac{T_{s,i}}{H_p \overset{o}{V}_{l,i}} = \frac{1}{1 - G_1 + H_p G_2} \quad . \quad (5.39.)$$

An instability condition is obtained when the transfer functions (5.38.) and (5.39.) approach infinity. There are two conditions where this is indeed the case:

- a. For large values of  $H_p$ , the system will always be stable, as long as  $G_2$  does not approach zero. For large values of  $H_p$ , the transfer function (5.38.) approaches the value of  $1/G_2$ . From the definition of  $G_2$ , it may be concluded that  $G_2$  will normally never approach zero, unless resonance conditions appear within the boiling channel.
- b. For sufficiently low values of  $H_p$ , the transfer function (5.39.) approaches the value of  $1/(1-G_1)$ , and an instability condition is obtained when  $G_1$  becomes +1 for some frequency (for small values of  $H_p$  the quantity  $H_p \overset{\circ}{V}_{1,i}$  (in equation (5.39.)) becomes equal to  $\Delta T_{S,i}$ , see Fig. 5.7).

It appears to be advantageous, therefore, to calculate the open-loop transfer functions  $G_1$  and  $G_2$  and see whether the modulus of  $G_1$  approaches a condition of +1, and at the same time whether the phase angle has reached a value of about  $0^\circ$  or  $360^\circ$  for  $H_p=0$ , or whether the modulus of  $G_2$  has become sufficiently small, for large values of  $H_p$ .

In the following, some results will be presented of calculations in which the equations outlined before were used.

### 5.7. Results of calculations with the linearized equations

Before starting any calculation, the input data must be specified. In the following some results of calculations are presented to demonstrate that the approach outlined in the previous sections is applicable. In these first calculations, some input data have been simplified.

In the channel equations for the riser, (5.18.) to (5.23.), the quantities  $S_a$ ,  $S_b$  and  $S_c$  have been put equal to unity. In the equations of state, c and e are assumed to be independent of variations in  $T_1$  with z and t. The variations in  $\rho_s$ ,  $\rho_1$  and  $T_s$  have been taken into account by introducing into the equations values of  $\partial\rho_s/\partial T_s$ ,  $\partial\rho_1/\partial T_1$  and  $(\partial T/\partial p)_{sat}$  obtained from physical tables, see for instance, Table 3.1.

In applying the correlation functions for the Slip Ratio, S, the wall-friction force, F, and the heat division parameter,  $\kappa$ , it is assumed, that under dynamic conditions, the magnitude of these quantities is determined by the steady-state equations from the instantaneous values of the flow variables.

For the slip ratio, equation (4.13.) is used with experimentally determined values of a and  $C_o$ , see Figs 4.3 and 4.4. For the wall-friction force, F, the Fanning equation is used in the single-phase region, with the experimental values of f, see section 2.3. In the two-phase region, use is made of the Two-Phase Friction Multiplier, R, see equation (4.20.), as evaluated by Martinelli and Nelson (M3) and formulated by Jones (J1), (KAPL-2170 and 2208). No correction has been applied for any mass flow effect.

The correlation of  $\kappa$  was based on the criteria of Bowring (B11). The onset of subcooled boiling and the first detachment of bubbles was calculated according to (B11). The onset of saturated boiling was calculated from a heat balance. In the non-boiling region,  $\kappa$  is put equal to zero. In the subcooled boiling region,  $\kappa$  is chosen as:

$$\kappa = \frac{T_1 - T_b}{T_s - T_b} , \quad (5.40.)$$

where  $T_b$  is the liquid temperature at which, according to (B11), bubbles detach from the wall. In the saturated boiling region,  $\kappa$  is assumed to be equal to:

$$\kappa = 1 + F_1 \frac{(T_1 - T_s)}{T_{sat}}. \quad (5.41.)$$

By means of the factor  $F_1$ , any superheating of the liquid in the saturated boiling region can be adjusted. The assumption that in the subcooled region there is no thermodynamic equilibrium and that in the saturated boiling region a complete thermodynamic equilibrium is present, appears to have been made fairly arbitrarily, but this will come about gradually, see Fig. 5.2. The main advantage of this choice for the  $\kappa$  procedure is that only a single set of equations is used for the entire channel.

The procedure for  $\kappa$  in the subcooled region differs from that suggested by Bowring, who assumed  $\kappa$  to be constant in that region. The new procedure eliminates any difficulty in the formal linearization procedure wherever  $\kappa$  should exhibit discontinuities at the locations of the onset of subcooled and saturated boiling. Furthermore, any constant value of  $\kappa$  seems hardly acceptable physically. It has been checked that, in steady-state calculations, either procedure gives about the same result as regards the operating conditions and geometry under discussion.

For the boundary conditions, equations (5.24.) to (5.28.), the following data have been used:

$$\begin{aligned} U_{con} &= .1454 \text{ m}^3 \\ \sum U_d &= .033 \text{ m}^3 \\ H_{d0} &= 1.702 \text{ m} \end{aligned}$$

$$\begin{aligned} A_{con} &= .495 \text{ m}^2, \text{ (see Fig. 5.4)} \\ A_d &= .0096 \text{ m}^2 \\ H_t &= 1.044 \text{ m} \\ \sigma_0 &= .75 \end{aligned}$$

$$\begin{aligned} A_c \sum \frac{L_k}{A_k} &= .489 \text{ m (in Test Section I)} \\ &= .776 \text{ m (in Test Section II), equally divided between the cold and the hot} \\ &\quad \text{parts, see Fig. 5.4.} \end{aligned}$$

$$\begin{aligned} k_{in} &= 1.4 \text{ (Test Section I and II), including downcomer friction losses.} \\ k_{ex} &= 0. \end{aligned}$$

Furthermore, the functions  $E_2(t)$  and  $E_3(t)$ , equation (5.29.), have been put equal to zero.  $E_1(t)$  is a sinusoidal function, i.e. the channel power has been modulated with a sine. In the calculations the number of steps in axial direction was 80 in the steady-state calculations and 40 in the dynamic calculations. For the other input data, reference is made to Tables 2.1. and 2.2.

The results of these calculations will be presented in the following.

#### Steady-state calculations.

The calculated distribution of the void fraction and the liquid and saturation temperature have been plotted in Fig. 5.8. The distribution of the temperatures resembles that calculated with the aid of the theoretical model based on first principles, see Fig. 5.2, and results in this case from the assumed  $\kappa$  procedure. Owing to the choice of the slip correlation and the two-phase friction multiplier it is not surprising that there should be an excellent agreement between the measured and predicted void fraction data and some discrepancy between the values of inlet mass flow rate. The fact that the choice

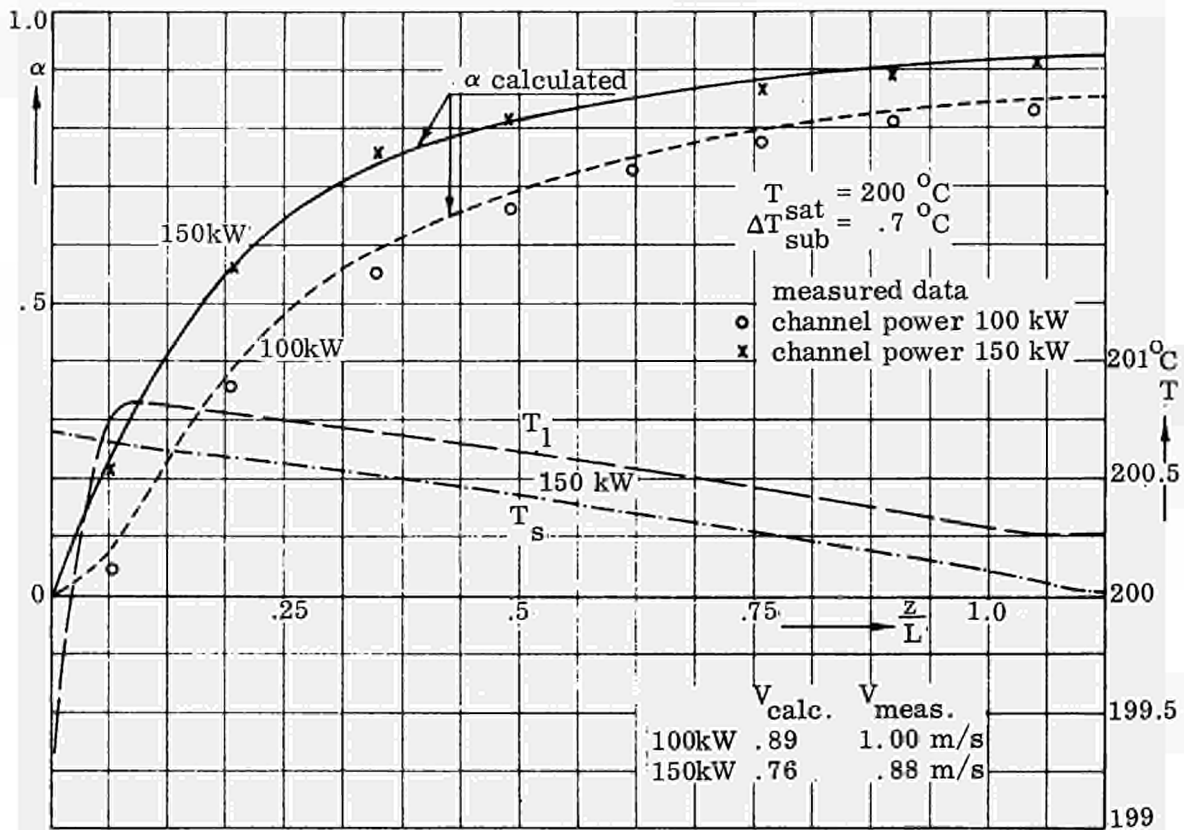


Fig. 5.8 Calculated and measured results of the steady-state characteristics, Test Section I.

of the Two-Phase Friction Multiplier,  $R$ , has practically no influence on the void fraction has already been reported in (S2). The calculated slope of the mass flow rate versus channel power curves corresponds, however, to the measured one.

The results of the mass flow rate can only be brought in better agreement, by a further and more thoroughgoing analysis of the measured pressure loss data.

#### Stability characteristics.

In Fig. 5.9, open and closed-loop characteristics have been plotted for a saturation temperature of  $200^{\circ}\text{C}$  in the intermediate frequency range of .6 to 1.4 c. p. s. for different channel powers. In the plot of the open-loop characteristics,  $G_1$ , it is shown that an unstable condition is passed when progressing from 150 to 151 kW channel power. At 150 kW the modulus of  $G_1$  becomes larger than unity but the phase angle does not approach the value of 0 or  $360^{\circ}$ . At 151 kW the modulus of  $G_1$  is larger than unity and the phase angle becomes zero, which indicates that the system is unstable.

Here it should be pointed out that conditions of  $G_1$  in which the argument is zero, but the modulus is in excess of unity are not unstable in the linearized approximations. However, these conditions are generally termed "conditionally stable" conditions in control theory, as large amplitude fluctuations tend to decrease effectively the modulus with only small changes in the phase because of non-linear saturation effects. In practice, these conditions are therefore only stable for very small oscillations and tend to develop self-sustained finite amplitude oscillations. Furthermore, by calculating the conditions between 150 and 151 kW channel power, a condition will be found where the condition  $G_1 = 1$  is exactly fulfilled.

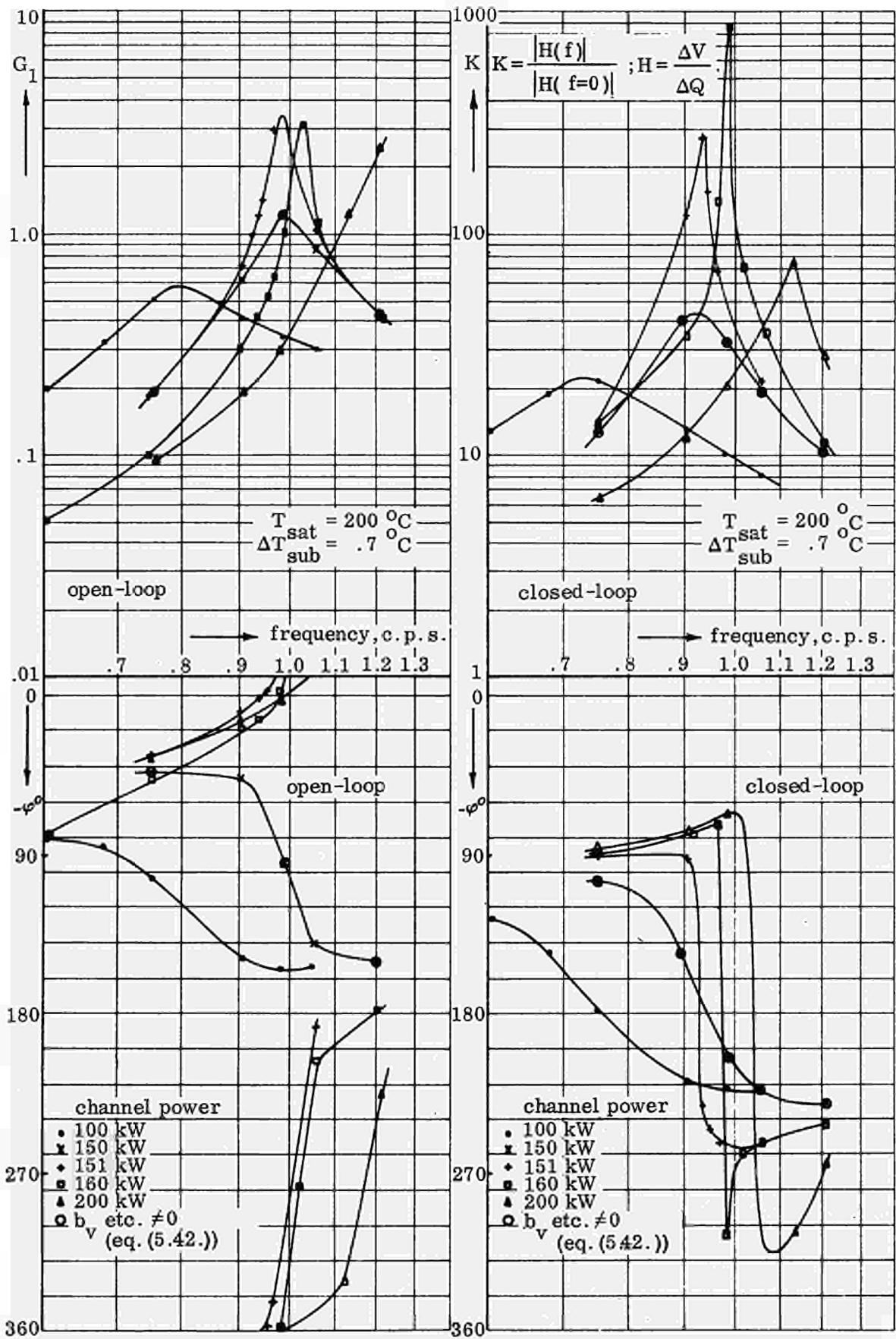


Fig. 5.9 Open and closed-loop transfer functions in the intermediate frequency range, Test Section I.

A comparison between the open and closed-loop results at 150 and 151 kW leads to the conclusion that large amplitudes in inlet mass flow occur. Also in the closed-loop, a condition will be found corresponding to  $G_1 = 1$ , where the amplitude ratio becomes infinite.

These characteristics indicate that  $G_1$  is a good criterion for detecting any instability. The instability threshold is most sharply determined and readily defined by a plot of  $G_1$  and particularly of the argument of  $G_1$ , against the frequency. The closed-loop characteristics are only of limited value in that respect.

The predicted instability threshold of 151 kW at a frequency of .947 c.p.s. is in fairly good agreement with the experimentally determined values of 162 kW and a frequency of .93, see Table 3.2.

As is shown in Fig. 5.9, the system is stable again at a channel power of 200 kW. When the argument is zero, the modulus is less than unity. Some investigators, for instance at Grenoble (F1), have reported an experimentally measured instability region. In the experiments reported here, always a condition of burn-out was reached when the channel power was increased into the fluctuating region. It might be interesting to repeat the calculation for the geometry and operating conditions for the Grenoble loop.

It is fairly difficult to compare the calculated closed-loop results with the experimentally determined transfer functions. In the calculation, the characteristics of the heating element have not yet been taken into account, whereas in the measured transfer functions, the response characteristics of the heating element are incorporated. The heating element will behave roughly as a first-order system, and this results in an attenuation and a phase shift and may account for the discrepancy between the experimentally and theoretically obtained transfer functions.

A further calculation was performed in which the characteristics of the condenser and subcooler have been accounted for.

For  $E_2$ , equation (5.29.), was written:

$$E_2(t) = \left[ b_q T_{s,i} + b_v W_{m,i} \right]_{re} e^{j\omega t} , \quad (5.42a)$$

and for  $E_3$ :

$$E_3(t) = \left[ b_c T_{l,i} + b_d V_{l,i} \right]_{di} e^{j\omega t} . \quad (5.42b)$$

The values of  $b_q$ ,  $b_v$ ,  $b_c$  and  $b_d$  have been chosen as .025, .1075, .0006 and .1454. Calculated points for this condition have been plotted in Fig. 5.9. In the frequency range under consideration, a small change in condenser and subcooler characteristics has no influence upon the results in the intermediate frequency range.

In Fig. 5.10, open-loop characteristics are presented for the low and high frequency ranges. In these frequency regions,  $|G_1|$  likewise approaches or exceeds unity and the phase angle is likely close enough to  $0^\circ$  for oscillations to develop.

As is shown, in the low frequency range the incorporation of the subcooler and condenser constants (equations (5.42. a and b)) greatly influences the results. It may be concluded that low frequency oscillations will develop over a wide range of heating powers. The channel power has a stabilizing influence in this low frequency range. These results are comparable with the observed low frequency oscillations, see section 3.3.1. and correspond with the observations made by Stenning (S8).

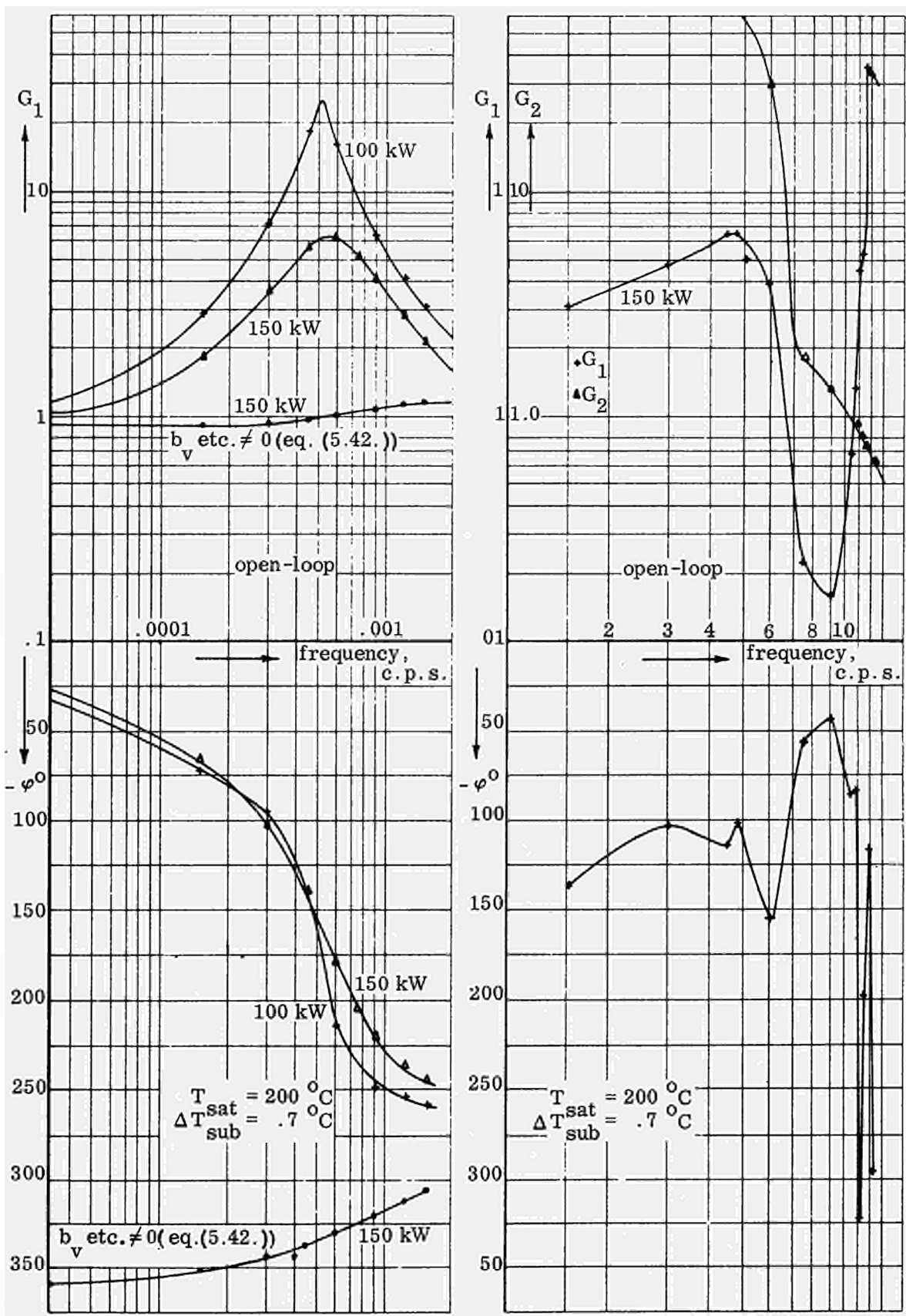


Fig. 5.10 Open-loop transfer functions in the low-and high frequency range, Test Section I.

In the high frequency range, the sudden increase in  $|G_1|$  is accompanied by a sudden drop in  $|G_2|$ . The phase angle of  $G_1$  exhibits very strong variations with frequency. The instability of a forced convection boiler as given by the condition  $G_2 \ll 1$  appears to be only possible at the high frequency range. Further experimental and theoretical research is needed to investigate whether the fluctuation in void fraction found experimentally (see section 3.3.1.) corresponds to the theoretically predicted instability.

#### Longitudinal distribution.

At a saturation temperature of  $200^\circ\text{C}$  and a channel power of  $150\text{ kW}$  (and in one case also at  $151\text{ kW}$ ) the distribution along the channel has been calculated of the variation in the saturation temperature (pressure), in liquid temperature, in the liquid velocity and in the void fraction upon a sinusoidal variation in channel power. This has been done for four frequencies, i. e. at  $.0006\text{ c.p.s.}$  (at the maximum of  $G_1$ ), at  $.121\text{ c.p.s.}$ , at  $.947\text{ c.p.s.}$  (at the instability threshold) and at  $11.82\text{ c.p.s.}$  These distributions are presented in Figs 5.11 to 5.14. In the upper part of the diagrams, the modulus is plotted per  $\text{kW}$  channel power variation and in the lower part the phase shift is plotted with respect to the channel power modulation.

At a frequency of  $.0006\text{ c.p.s.}$ , Fig. 5.11, it is shown that at the inlet of the coolant channel the variations in saturation temperature, liquid temperature and mass flow rate are in phase with each other. Furthermore, the amplitude of the variations in liquid temperature at the inlet is much smaller than that of the saturation temperature. Also the phase shift along the channel is roughly constant, which is indicative of a quasi-steady-state behavior. These results are in agreement with the observations made

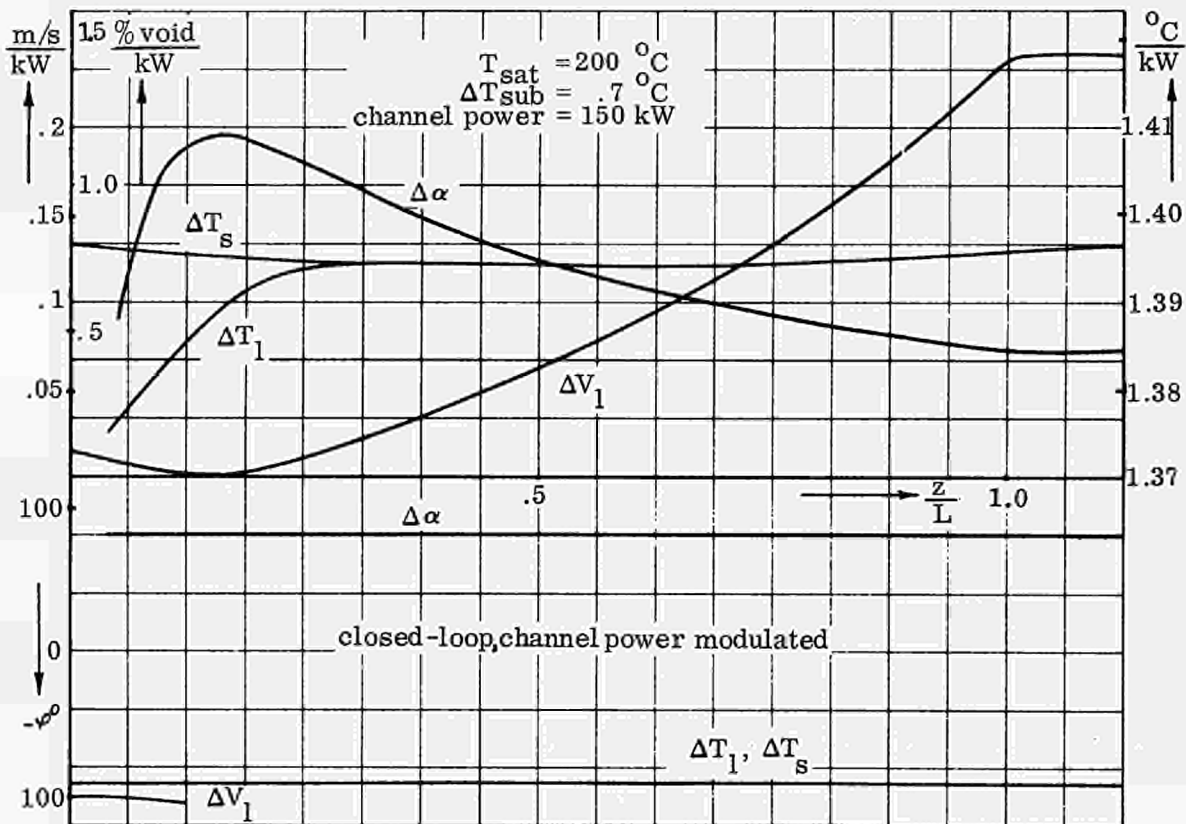


Fig. 5.11 Calculated longitudinal distributions,  $.0006\text{ c.p.s.}$ , Test Section I.



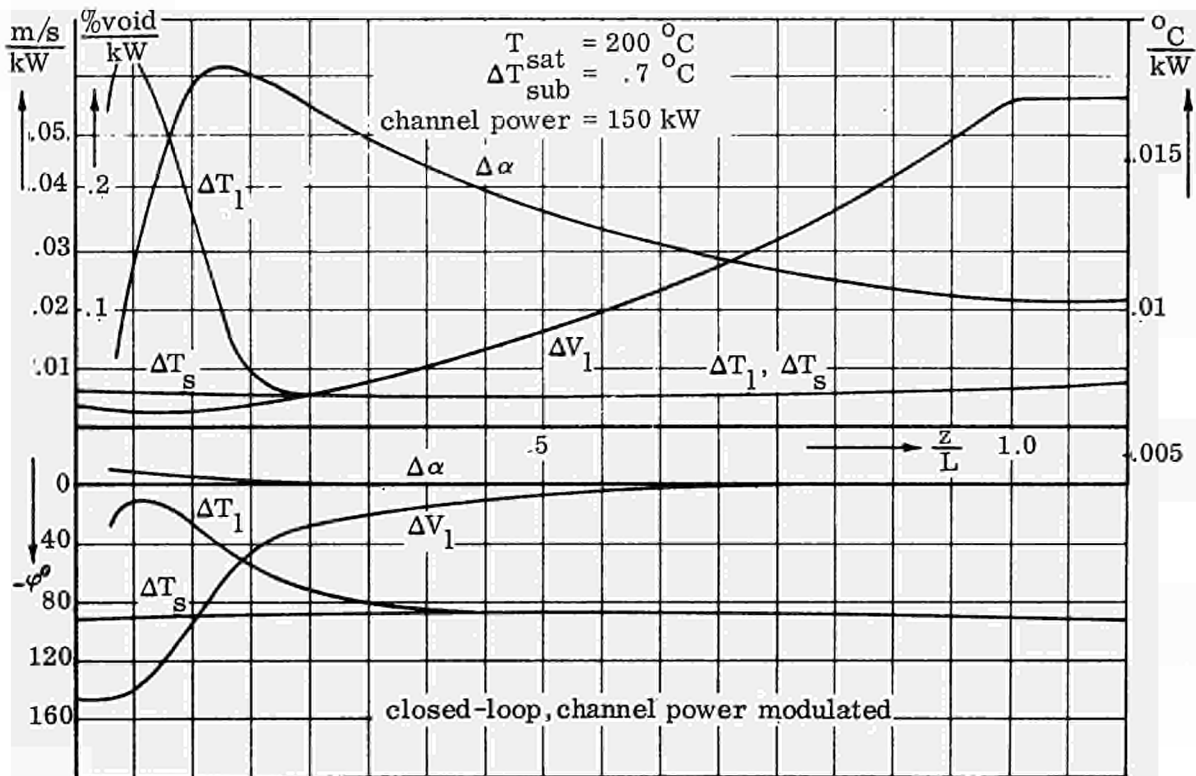


Fig. 5.12 Calculated longitudinal distributions, .121 c.p.s., Test Section I.

during the low frequency oscillations, see section 3.3.1. From Fig. 5.11 it may also be concluded that the variation in void fraction is largest at the bottom part of the channel. The phase lead in void fraction has also been observed in the modulation experiments; this can be attributed to the influence of the condenser characteristics. A further analysis of the influence of the system characteristics on the stability may be of importance to the nuclear as well as the steam boiler industry.

At the frequency of .121 c.p.s., the amplitudes of the four signals are much smaller than at the modulation frequency of .0006 c.p.s. and also much smaller than at the higher frequencies to be presented yet. The tendency can be observed that at the inlet of the channel, the variation in liquid temperature becomes larger than that of the saturation temperature. The variations in void fraction and in inlet mass flow are roughly in phase and  $140^{\circ}$  out of phase respectively with the channel power. This is in agreement with the transfer function measurements, see for instance Figs 3.25 and 3.26.

In Fig. 5.13, the results are shown for a frequency of .947 c.p.s. and at 151 kW channel power, just after the predicted onset of hydraulic instabilities. At 150 kW channel power, just before the predicted onset, the curves are only given for the void fraction and the liquid velocity. As is shown, when the system is unstable (151 kW), there is a difference in phase of about  $180^{\circ}$  between the void fraction at the inlet and exit of the channel and between the void fraction at the inlet and the inlet mass flow rate. Also there is a difference in phase of roughly  $180^{\circ}$  between the void fraction at the inlet and the saturation temperature at the outlet, which almost corresponds to the system pressure. Finally, the void fraction and the liquid temperature at the inlet are about in phase. All these results correspond to the observations made in the recorded signals during hydraulic oscillations, see for instance Fig. 3.20 and Fig. 3.22. Going from stable

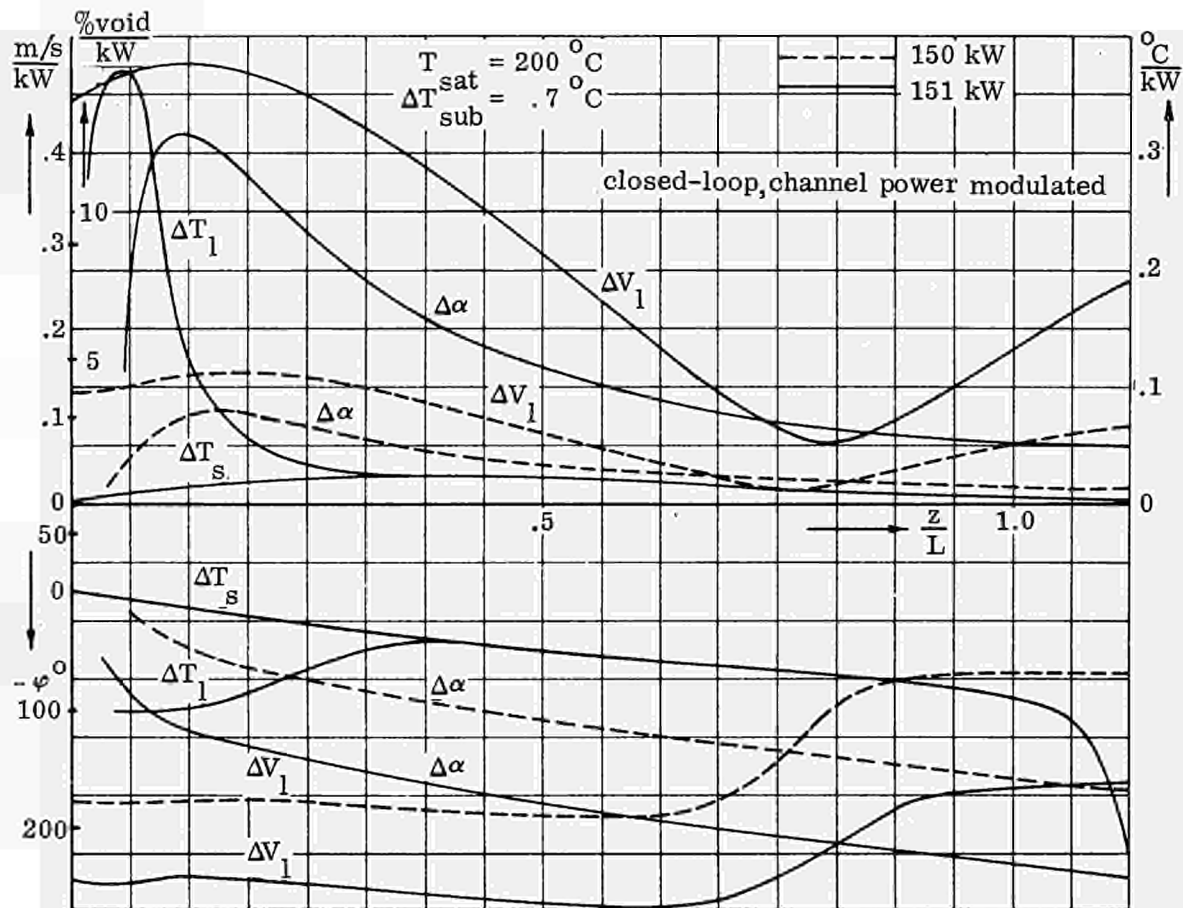


Fig. 5.13 Calculated longitudinal distributions, .947 c.p.s., Test Section I.

into unstable operation, the amplitude of the void fraction and mass flow oscillations increases considerably. The oscillations in void fraction are largest at the bottom of the channel. Furthermore, large oscillations in inlet temperature occur, in contrast to those in the saturation temperatures. This is likewise in agreement with the experimental results presented before, see Fig. 3.22 and section 3.3.3.

The oscillations in liquid velocity at a channel power of 151 kW are largest at the inlet and outlet of the channel and smallest at about .8L from the bottom of the channel. At this minimum, a large variation in phase shift of about 120° occurs. The fluctuations at the inlet and outlet are, therefore, about opposed in phase and resemble more or less a standing wave, i.e. it represents approximately a half-wave length oscillation in the velocity distribution.

The high frequency oscillation, Fig. 5.14, is characterized by near-zero variations of the liquid velocity at the inlet; this shows that this instability is essentially that of the forced convection boiler. In the liquid velocity large variations in phase shift occur wherever the amplitude of the oscillations is small. It may be concluded therefore, that these oscillations have again the character of standing-wave oscillations, but this time with smaller wavelengths than appeared in the 1 c.p.s. instability. The velocity distribution of Fig. 5.14 shows that it is approximately an oscillation with 3/4 wavelength over the channel length. The subsequent sharp peaks in the  $G_1$  distribution of Fig. 5.10 are almost certainly the result of higher-order instability with successively shorter wavelengths.

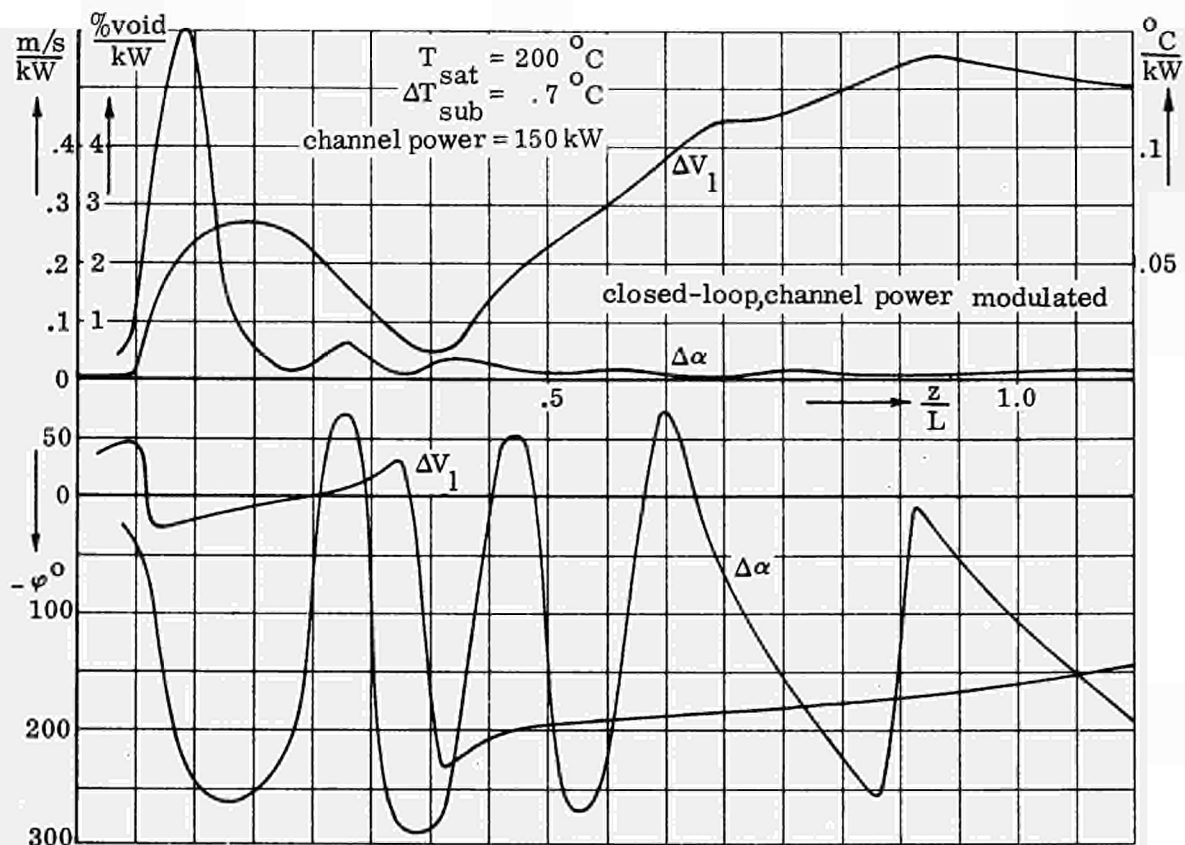


Fig. 5.14 Calculated longitudinal distributions, 11.82 c.p.s., Test Section I.

Some more calculations have been carried out to look into the influence of system pressure, hydraulic diameter and the magnitude of the two-phase friction loss on the onset of the hydraulic instabilities in the intermediate frequency range. A start was also made to detect the influence of subcooling at the inlet. Owing to programming difficulties, possibly resulting from the subroutines, the run with subcooling has not yet been completed successfully.

#### System pressure.

Calculations have been performed at 120°C and 234°C for Test Section I. At a saturation temperature of 120°C and a subcooling of .2°C it was found that at a channel power of 60 kW the system was stable, but at one of 65 kW unstable. The frequency where the phase shift became zero at 65 kW was 1.18 c.p.s. At 234°C saturation temperature and a subcooling of .8°C the instability threshold was detected between 255.5 and 258 kW channel power and the zero phase shift frequency at 258 kW was equal to 1.061 c.p.s.

#### Hydraulic diameter.

A calculation was performed at 200°C for Test Section II. At 200°C saturation temperature and a subcooling of .7°C, the instability threshold was found between 305 and 307.5 kW channel power at a frequency of 1.28 c.p.s. at 307.5 kW.

The results as regards the influence of the pressure and the geometry are in fairly good agreement with the experimentally obtained values of the instability threshold, see Table 3.2. The largest deviation, one of 10%, was obtained in Test Section II.

### Two-phase friction loss.

One calculation was performed in which, at a saturation temperature of 200°C, and a subcooling of .7°C and for Test Section I, the Two-Phase Friction Multiplier, R, was multiplied by a factor of 1.25. The result was, that the theoretically obtained instability threshold decreased from 151 kW to 140 kW channel power. This result is qualitatively in agreement with the experimentally observed shift, see section 4.3.

In this section the equations have been derived describing the performance characteristics under steady and non-steady conditions. Special attention has been paid to the formulation of the boundary conditions and the introduction of the pressure effects. Furthermore, a stability criterion was defined for detecting the onset of flow oscillations in the intermediate frequency range. Preliminary results have been reported for operating and geometry conditions similar to those of the experiments. The steady-state performance characteristics as well as the instability-threshold channel powers predicted theoretically were in good agreement with the measured data. Furthermore, it was shown that the experimentally determined character of the hydraulic instabilities was similar to that predicted theoretically. It would be interesting to extend this description with an energy equation for the heating element. Moreover, further analysis work is necessary regarding the phenomena governing the onset and character of the hydraulic instabilities and concerning the choice of which parameters are of less significance and may hence be safely disregarded. In a further study attention must also be given, particularly in the low frequency range, to the pressure-drop characteristics of a boiling channel and to the influence of condenser and subcooler characteristics on the stability.

## 6. Conclusions

The results of an experimental and theoretical study have been reported on the steady-state and stability characteristics of a naturally circulating boiler. In general it can be said that there is a lack of systematic data on the onset of hydraulic flow oscillations and on the stability characteristics of a two-phase flow in dependence of the operating conditions. Furthermore, there is a need for more detailed information, theoretical as well as experimental, in order to obtain a better characterization of the various types of flow oscillations. The work described gives a contribution towards a better understanding of the two-phase flow stability characteristics.

One of the most important variables determining the heat transfer and fluid flow characteristics of a boiling channel is the void fraction. Therefore, much work has been devoted to the development of a new technique for void fraction measurement, i. e. the impedance void fraction method. As appears from the results, this measuring method is entirely suitable for void measurement under steady-state and transient conditions. The method is simple and inexpensive in comparison with the  $\gamma$ -ray attenuation technique. Similar experiences have been reported in (C2) and (O1). Although the impedance method is particularly suited to void fraction measurements in transient conditions, the  $\gamma$ -ray attenuation technique may be better suited for void distribution measurements.

In the experimental program, use has been made of the characteristics of the noise, expressed in autocorrelations, cross-correlations, spectral power densities and cross-power densities in determining the onset and character of flow oscillations and the stability characteristics of a steady state in terms of transfer functions. The application and the effectivity of noise analysis in obtaining information on the dynamic behavior of a two-phase system has been demonstrated. The cross-correlation technique has been found to be a powerful technique for eliminating the effects of external noise. The technique using a harmonically oscillating input yields accurate results, but the required measuring time is long. Some improvement may be gained by application of a multi-frequency signal method. The application of the analysis of the inherent noise asks for further development and evaluation work.

Results were given of measurements determining the steady-state performance characteristics of the boiling channel with natural circulation. An attempt was made to plot the results in terms of non-dimensional quantities for the heat load, subcooling, pressure and for the dependent quantities. Although this was not successful, it would be interesting to continue the analysis in this way and to include experimental results from other sources, especially from those carried out with other liquids.

An analysis of the experimental results was made in terms of the Slip Ratio,  $S$ , and the Two-Phase Friction Multiplier,  $R$ . It was shown that the slip ratio is a ratio of weighted average phase velocities and therefore dependent on the distribution of the void fraction across the channel. Furthermore, it has been shown that, in deriving two-phase friction losses from pressure measurements along a boiler, accurate results can only be obtained when the influence of the cross-sectional distributions is understood.

The void fraction data were plotted in the "weighted mean velocity-average volumetric flux density" plane, proposed in (Z1). From this plot it may be deduced that flat profiles for the velocity or concentration distributions are present under the operating conditions reported.

Although the work reported in (B14), (T2), (V4) and (Z1) contributed a great deal towards the knowledge of the characteristics of a two-phase mixture, more development is needed, particularly as regards the recognition of flow regimes and the theoretical and experimental prediction of concentration and velocity distributions over the cross-section of the flow channel. This is a prerequisite to any further analysis of the presented steady-state data. The presently available experimental correlations for S and R are not altogether satisfactory in this respect.

During operation, it was possible to distinguish between three types of flow oscillations with frequencies of roughly .03, 1 and 15 c.p.s. By adopting a criterion for defining the onset of the 1 c.p.s. hydraulic oscillations, the influence has been systematically measured of the system pressure, subcooling and hydraulic diameter on the instability threshold channel power. At high system pressures, there was a gradual increase in amplitude of the flow oscillations with increasing channel power, in contrast with low system pressures, at which the flow oscillations tend to start more spontaneously. At low subcooling rates, increased subcooling precipitates, and at high subcooling rates this postpones the onset of severe hydraulic oscillations. This effect is more pronounced at high system pressures and for test sections with large hydraulic diameters. Any increase in hydraulic diameter postpones the onset of hydraulic oscillations to higher channel powers. Recordings of the relevant physical quantities revealed that during hydraulic oscillations the void fraction near the inlet and outlet of the coolant channel were roughly  $180^\circ$  out of phase. The same was true for the void fraction and the mass flow rate at the inlet.

The influence of the operating conditions on the stability of a steady state, when expressed in transfer functions, was similar to that on the instability threshold channel power. It was also found that, as regards the stability characteristics, the influence of increased subcooling at low subcooling rates is opposite to that at high subcooling rates. From the transfer function measurements it could be concluded that the two-phase flow process may be regarded as a linear process for small disturbances from the steady state, even at high channel powers.

Characteristic of all measured transfer functions was the appearance of a sharp resonance peak when the instability threshold was approached. The resonance peak is characteristic of a naturally circulating system and is caused by a strong intercoupling between the steam void and the inlet mass flow. The flow oscillations appear owing to the fact that this intercoupling becomes unstable, and not to the fact that the flow is responding to a present boiling instability or flow-pattern instability. The intercoupling effects are strongly influenced by the boundary conditions. It is, therefore, clear that in an analysis of hydrodynamic instability, not only the region of the two-phase flow, but the entire system, including the downcomer, and, if necessary, the pump characteristics have to be taken into account. Furthermore, any study of the flow oscillations must start from equations incorporating dynamic effects. A stability analysis based on steady-state characteristics as, for instance, proposed in (L3), is only of limited value.

Burn-out channel powers and heat fluxes have been presented for various values of system pressures and subcoolings. Nearly all burn-outs were obtained under unstable flow conditions. The results confirm the belief that hydraulic stability plays an important

rôle in burn-out. It would be interesting to repeat some of the experiments under conditions of forced circulation and with a heating element having a different time constant. Besides, it might be of interest to investigate the effect of inlet throttling on the burn-out heat flux, even under stable flow conditions.

A set of basic equations has been derived describing the performance characteristics in steady-state and transient conditions of a boiling system. These equations have been integrated over the cross-section of the coolant channel. Owing to this integration, it was shown that correlations have to be introduced which account for distributional effects. Special attention has been paid to the formulation of the boundary conditions and the introduction of pressure effects. As was shown in the analysis of the experimental results, the two-phase flow process may be regarded as a linear process for small disturbances from the steady state. Therefore, the derived equations were linearized. By considering an "open"-loop, two stability criteria were defined for detecting the onset of flow oscillations. These criteria are defined by means of the transfer functions for the "open"-loop from an imposed variation in saturation temperature at the inlet to the resulting variation in saturation temperature and mass flow rate at the outlet of the downcomer. It might be concluded that an instability determined by the latter transfer function is related to a forced convection boiler incorporating a pump with steep head-flow characteristics in which resonance conditions may appear within the boiling channel. The first mentioned transfer function is related to a natural circulation boiler.

Preliminary results of the steady-state performance and "open"- and "closed"-loop characteristics have been reported. The steady-state performance characteristics as well as the instability threshold channel powers predicted theoretically were in good agreement with the measured data. Furthermore, it was shown that also in the very low and high frequency region, flow oscillations may develop. The experimentally determined character of the 1 c.p.s. flow oscillations was similar to that predicted theoretically. The 1 c.p.s. flow oscillation resembles more or less a standing wave, i.e. it represents approximately a half wavelength oscillation in the velocity distribution.

It will be necessary to extend the theoretical description with an energy equation for the heating element. Only then will it be possible to compare the theoretically and experimentally obtained closed-loop characteristics in detail. Moreover, further analysis work is necessary regarding the phenomena governing the onset and character of the hydraulic instabilities and concerning the choice of which parameters are of less significance and may hence be safely disregarded. In a further study attention must also be given, particularly in the low frequency range, to the pressure-drop characteristics of a boiling channel and to the influence of the condenser and subcooler characteristics on the stability.

## References

- A.1 Anonymous, Determination of power spectra and transfer functions from digital processing of measuring signals, Report Technological University of Eindhoven, WW016-R77, 1964 (program prepared by Rescona Ltd., Amstelveen).
- A.2 Asyee, J., Proeven over de warmte-afvoer van een splijstofelement uit een kernreactor van het kokend water type, (Experiments on the heat removal from a fuel rod of a boiling water reactor), Thesis Technological University of Delft, 1959.
- A.3 Anonymous, A digital computer program for the calculation of non-steady two-phase flow in a vertical boiler based on a model of Jahnberg, Report Technological University of Eindhoven, WW016-R76, 1964, revised 1965 (program prepared by Rescona Ltd., Amstelveen).
- A.4 Adorni, A., Casagrande, I., Cravarolo, L., Hassid, A., Silvestri, M., Experimental data on two-phase adiabatic flow: liquid film thickness, phase and velocity distribution, pressure drops in vertical gas-liquid flow, Report Centro Informazioni Studi Esperienze, Milan, R-35, 1961.
- B.1 Bogaardt, M., Spigt, C.L., Research program on heat transfer and stability problems in boiling water reactors, 1st. Joint USAEC-Euratom Two-Phase Flow Meeting, Brussels, 1962.
- B.2 Bogaardt, M., Spigt, C.L., Some results of measurements in steady and non-steady state in an annular geometry obtained in the two-phase flow program of the Laboratory for Heat Transfer and Reactor Engineering of the Technological University of Eindhoven, 2nd. Joint USAEC-Euratom Two-Phase Flow Meeting, Germantown, 1964.
- B.3 Bogaardt, M., Spigt, C.L., Dijkman, F.J.M., Madsen, N., Heat transfer and stability in boiling water reactors, Third United Nations International Conference on the Peaceful Uses of Atomic Energy, Geneva, 1964.
- B.4 Bogaardt, M., Spigt, C.L., Dijkman, F.J.M., Verheugen, A.N.J., Comparison of results of analysis of boiling system dynamics by analog and digital methods, Eighth National Power Instrumentation Symposium of the U.S.A., New York, 1965.
- B.5 Bowring, R.W., Spigt, C.L., Seven rod bundle, natural circulation stability and burn-out tests with water at up to 28 atmospheres pressure, Nuclear Science and Engineering, Vol. 22, p. 1-13, 1965.
- B.6 Bogaardt, M., Spigt, C.L., Dijkman, F.J.M., Verheugen, A.N.J., On the heat transfer and fluid flow characteristics in a boiling channel under conditions of natural convection, Symposium of the Institution of Mechanical Engineers on Boiling Heat Transfer in Steam Generating Units and Heat Exchangers, Manchester, 1965.
- B.7 Bogaardt, M., Spigt, C.L., Het burn-out verschijnsel in water-gekoelde kernreactoren (Burn-out in water-cooled nuclear reactors), De Ingenieur, Vol. 77, no. 37, p. O 11-23, 1965.



- B.8 Bouré, J., Instabilités hydrodynamiques limitant la puissance des reacteurs à eau bouillante, Report Centre d'Etudes Nucléaires de Grenoble, T.T. 55, (two parts), 1965.
- B.9 Bywaard, G., Staub, F.W., Zuber, N., A program for two-phase flow investigation, Ninth quarterly report, April-June 1965, Report General Electric, GEAP 4910, 1965.
- B.10 Bakker, P.J., Heertjes, P.M., Porosity determination of fluidised beds, British Chemical Engineering, Vol. 4, p. 524-530, 1959.
- B.11 Bowring, R.W., Physical model, based on bubble detachment, and calculation of steam-voidage in the subcooled region of a heated channel, Report OECD Halden Reactor Project, HPR 10, 1962.
- B.12 Becker, K.M., Jahnberg, S., Haga, I., Hansson, P.T., Mathisen, R.P., Hydrodynamic instability and dynamic burn-out in natural circulation two-phase flow; an experimental and theoretical study, Third United Nations International Conference on the Peaceful Uses of Atomic Energy, Geneva, 1964.
- B.13 Blackman, R.B., Tukey, J.W., The measurement of power spectra, Dover Publications Inc., New York, 1958.
- B.14 Bankoff, S.G., A variable density single-fluid model for two-phase flow with particular reference to steam-water flow, Transactions of the ASME, Journal of Heat Transfer, Vol. 82, p. 265-272, 1960.
- B.15 Bowring, R.W., Spigt, C.L., Results of burn-out and instability experiments on a seven-rod bundle up to 30 atmospheres pressure-second series with inlet subcooling and natural convection, Report Technological University of Eindhoven, WW016-R31, 1963.
- B.16 Bird, R.B., Stewart, W.E., Lightfoot, E.N., Transport phenomena, John Wiley & Sons Inc., New York, 1960.
- C.1 Currin, H.B., Humm, C.M., Rivlin, L., Tong, L.S., HYDNA-digital computer program for hydrodynamic transients in a pressure tube reactor of a closed channel core, Report Westinghouse Electric Corporation, CVNA-77, 1961.
- C.2 Cimorelli, L., Premoli, A., Measurement of void fraction with impedance gauge technique, Energia Nucleare, Vol. 13, no. 1, p. 12-23, 1966.
- D.1 Davidson, W.F., Hardie, P.H., Humphreys, C.G.R., Markson, A.A., Munford, A.R., Ravese, T., Studies of heat transmission through boiler tubing at pressures from 500 to 3300 pounds, Transactions ASME, Journal of Heat Transfer, Vol. 65, p. 553-591, 1943.
- F.1 Fabrega, S., Instabilités hydrodynamiques limitant la puissance des reacteurs à eau bouillante, Report Euratom, EUR 1509f, 1965.
- G.1 Griffith, P., The prediction of low quality boiling void, Transactions of the ASME, Journal of Heat Transfer, Vol. 86, p. 327-333, 1964.
- H.1 Hooker, H.H., Popper, G.F., A gamma-ray attenuation method for void fraction determination in experimental boiling heat transfer test facilities, Report Argonne National Laboratory, ANL 5766, 1958.
- H.2 Haywood, R.W., Research into the fundamentals of boiler circulation theory, Proceedings of the Institution of Mechanical Engineers, Vol. 166, p. 63-66, 1952.

- H. 3 Hansson, P.T., Axelsson, E., A digital model for one-dimensional time-dependent two-phase hydrodynamics, Report Aktiebolaget Atomenergi, Studsvik, RFR-492, 1965.
- H. 4 Hayama, S., A study on the hydrodynamic instability in boiling channels, Bulletin of the JSME, Vol. 6, p. 549-556, 1963.
- J. 1 Jones, A.B., Dight, D.G., Hydrodynamic stability of a boiling channel, Reports Knolls Atomic Power Laboratory, Schenectady, KAPL 2170 (1961), 2208 (1962), 2290 (1963), 3070 (1964).
- J. 2 Jahnberg, S., A one-dimensional model for calculation of non-steady two-phase flow, EAES-Symposium on Two-Phase Flow, Studsvik, October 1963.
- K. 1 Kirchenmayer, A., Dynamics of boiling water reactors, Advanced course on the dynamic behavior of boiling water reactors, Report Institutt for Atomenergi, Kjeller, KR-35, 1962.
- L. 1 Levy, S., Beckjord, E.S., Hydraulic instability in a natural circulation loop with net steam generation at 1000 psia, ASME-AIChE Heat Transfer Conference, Buffalo, paper no. 60-HT-27, 1961.
- L. 2 Lighthill, M.J., Whitham, G.B., On kinematic waves, I. Flood movement in long rivers, Proceedings of the Royal Society, London, Vol. 229 A, p. 281, 1955.
- L. 3 Ledinegg, M., Unstabilität der Strömung bei Natürlichem und Zwangsumlauf (Flow instability in natural and forced circulation), Die Wärme, Vol. 61, p. 891-898, 1938.
- L. 4 Levy, S., Theory of pressure drop and heat transfer for annular steady state two-phase two-component flow in pipes, Proceedings of Second Midwestern Conference on Fluid Mechanics, p. 337, 1952.
- L. 5 Lottes, P.A., Anderson, R.P., Hoglund, B.M., Marchaterre, J.F., Petrick, M., Popper, G.F., Weatherhead, R.J., Boiling water reactor technology status of the art report, Vol. I, Heat transfer and hydraulics, Report Argonne National Laboratory, ANL-6561, 1962.
- L. 6 Lockhart, R.W., Martinelli, R.C., Proposed correlation of data for isothermal two-phase, two-component flow in pipes, Chemical Engineering Progress, Vol. 45, p. 39, 1949.
- M. 1 Madsen, N., Temperature fluctuations at a heated surface supporting pool boiling of water, Symposium of the Institution of Mechanical Engineers on Boiling Heat Transfer in Steam Generating Units and Heat Exchangers, Manchester, 1965.
- M. 2 Martinelli, R.C., Boelter, L.M.K., Taylor, T.H.M., Thomsen, E.G., Morrin, E.H., Isothermal pressure drop for two-phase two-component flow in a horizontal pipe, Transactions of the ASME, Journal of Heat Transfer, Vol. 66, p. 139-151, 1944.
- M. 3 Martinelli, R.C., Nelson, D.B., Prediction of pressure drop during forced circulation boiling of water, Transactions of the ASME, Journal of Heat Transfer, Vol. 70, p. 695-702, 1948.
- M. 4 Marchaterre, J.F., Hoglund, B.M., Correlation for two-phase flow, Nucleonics, Vol. 20, no. 8, p. 142, 1962.
- M. 5 Maulbetsch, J.S., Griffith, P., A study of system-induced instabilities in forced-convection flows with subcooled boiling, Report Massachusetts Institute of Technology, TR 5382-35, 1965.

- M.6 Macbeth, R.V., An appraisal of forced convection burn-out data, Symposium of the Institution of Mechanical Engineers on Boiling Heat Transfer in Steam Generating Units and Heat Exchangers, Manchester, 1965.
- M.7 Micropołski, Z.L., Shitsman, M.Ye., Pikus, V.Yu., Investigation of the effect of the frequency and amplitude of flow pulsations on critical heat fluxes, *Inzhenerno Fizicheskij Zhurnal*, Vol. 7, no. 6., p. 13-15, (WAPD Translation - 7).
- N.1 Neal, L.G., Zivi, S.M., Hydrodynamic stability of natural circulation boiling systems, Report TRW Space Technology Laboratories, Redondo Beach, STL 372-14, 1965.
- O.1 Ørbeck, I., Impedance void meter, Report Institutt for Atomenergi, Kjeller, KR-32, 1962.
- Q.1 Quandt, E.R., Analysis and measurement of flow oscillations, Chemical Engineering Progress Symposium, Series 57, no. 32, p. 111-126, 1961.
- S.1 Spigt, C.L., Simon-Thomas, J.P., Bogaardt, M., Introductory laboratory studies of boiling water stability, Symposium of the Institution of Mechanical Engineers on Two-Phase Fluid Flow, London, 1962.
- S.2 Spigt, C.L., Dijkman, F.J.M., Callen, J.D., Bogaardt, M., Theoretical and experimental results on steady-state boiling in an annular geometry, EAES-Symposium on Two-Phase Flow, Studsvik, 1963.
- S.3 Spigt, C.L., Dijkman, F.J.M., Bogaardt, M., The onset of hydraulic instabilities in an annular channel, EAES-Symposium on Two-Phase Flow, Studsvik, 1963.
- S.4 Spigt, C.L., Bogaardt, M., Some burn-out and instability experiments on a 7-rod cluster, EAES-Symposium on Two-Phase Flow, Studsvik, 1963.
- S.5 Spigt, C.L., Wamsteker, A.J.J., Van Vlaardingen, H.F., The application of the impedance method for transient void fraction measurement and comparison with the  $\gamma$ -ray attenuation technique, EAES-Symposium on In-Core Instrumentation, Oslo, 1964.
- S.6 Spigt, C.L., Dijkman, F.J.M., Bogaardt, M., Les phénomènes accompagnant le début de l'instabilité de l'écoulement dans les canaux verticaux bouillants, VIII ièmes Journées de l'Hydraulique de Société Hydrotechnique de France, Lille, 1964.
- S.7 Silver, R.S., A thermodynamic theory of circulation in water-tube boilers, Proceedings of the Institution of Mechanical Engineers, Vol. 153, p. 261-271, 1945.
- S.8 Stenning, A.H., Veziroglu, T.N., Flow oscillation modes in forced convection boiling, Proceedings of the 1965 Heat Transfer and Fluid Mechanics Institute, Stanford University, 1965.
- S.9 Styrikovich, M.A., Hydrodynamics and heat transfer during boiling in high pressure boilers, Academy of Science SSSR, Moscow, 1957, AEC translation, Tr-4490, 1961.
- S.10 Solberg, K.O., Bakstad, P., Rasmussen, J., VOIFLO-I, A steady state FORTRAN code for hydraulics of a boiling loop, Report Institutt for Atomenergi, Kjeller, KR-85, 1965.
- S.11 Solberg, K.O., The Kjeller model for the dynamics of coolant channels in boiling water reactors, Report Institutt for Atomenergi, Kjeller, KR-51, 1963.
- S.12 St. Pierre, C.C., Frequency response analysis of steam voids to sinusoidal power modulation in a thin-walled boiling water channel, Report Argonne National Laboratory, ANL 7041, 1965.

- T.1 Thie, J., Reactor Noise, An AEC monograph, Rowman and Rittlefield Inc., New York, 1963.
- T.2 Turner, J.M., Wallis, G.B., Two-phase flow and boiling heat transfer; the separate-cylinders model of two-phase flow, Report Thayer School of Engineering, New Hampshire, NYO-3114-6, 1965.
- V.1 Van der Walle, F., Lamein, H.J., Spigt, C.L., Bogaardt, M., A new model of two-phase flow in vertical boilers, EAES-Symposium on Two-Phase Flow, Studsvik, 1963.
- V.2 Van der Walle, F., Verheugen, A.N.J., Haagh, V.J.M., Bogaardt, M., A study of the application of acoustical methods for determining void fraction in boiling water systems, Symposium on Two-Phase Flow, Exeter, 1965.
- V.3 Van der Walle, F., Spigt, C.L., Lamein, H.J., Bogaardt, M., A theoretical study on two-phase flow characteristics, Symposium on Two-Phase Flow, Exeter, 1965.
- V.4 Van der Walle, F., Lamein, H.J., On the hydrodynamic aspects of two-phase flows in vertical boilers, Report Technological University of Eindhoven, WW016-R50, October 1963. (Prepared by Rescona Ltd. under contract with the Technological University).
- V.5 Van der Walle, F., Lamein, H.J., A digital computer program for the non-linear steady state and quasi linear dynamic calculation of boiling hydraulic loops, Report Consultant Firm Rescona Ltd., R-64-10, 1966.
- W.1 Wallis, G., Heasley, J., Oscillations in two-phase flow systems, Transactions of the ASME, Journal of Heat Transfer, Vol. 83, p. 363-369, 1961.
- Z.1 Zuber, N., Findlay, J.A., Average volumetric concentration in two-phase flow systems, Transactions of the ASME, Journal of Heat Transfer, Vol. 87, p. 453-468, 1965.
- Z.2 Zuber, N., On the problem of hydrodynamic diffusion in two-phase flow media, All-Union Conference of Heat and Mass Transfer, Minsk, 1964.
- Z.3 Zivi, S.M., Wright, R.W., Yeh, G.C.K., Kinetic studies of heterogeneous water reactors, Annual report 1962 TRW Space Technology Laboratories, Redondo Beach, STL 6212, 1963.
- Z.4 Zivi, S.M., Wright, R.W., Kinetic studies of heterogeneous water reactors, Annual report 1960 TRW Space Technology Laboratories, Redondo Beach, RWD-RL-190, 1961.

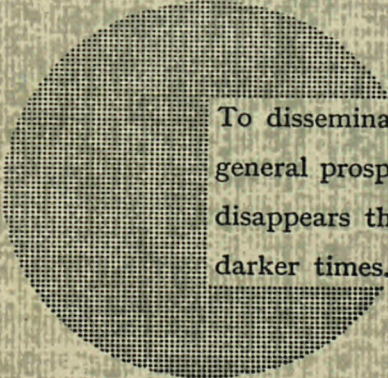
## NOTICE TO THE READER

All Euratom reports are announced, as and when they are issued, in the monthly periodical **EURATOM INFORMATION**, edited by the Centre for Information and Documentation (CID). For subscription (1 year : US\$ 15, £ 5.7) or free specimen copies please write to :

**Handelsblatt GmbH**  
**"Euratom Information"**  
**Postfach 1102**  
**D-4 Düsseldorf (Germany)**

or

**Office de vente des publications**  
**des Communautés européennes**  
**2, Place de Metz**  
**Luxembourg**



To disseminate knowledge is to disseminate prosperity — I mean general prosperity and not individual riches — and with prosperity disappears the greater part of the evil which is our heritage from darker times.

Alfred Nobel

## SALES OFFICES

All Euratom reports are on sale at the offices listed below, at the prices given on the back of the front cover (when ordering, specify clearly the EUR number and the title of the report, which are shown on the front cover).

### PRESSES ACADEMIQUES EUROPEENNES

98, Chaussée de Charleroi, Bruxelles 6

Banque de la Société Générale - Bruxelles  
compte N° 964.558,

Banque Belgo Congolaise - Bruxelles  
compte N° 2444.141,

Compte chèque postal - Bruxelles - N° 167.37,

Belgian American Bank and Trust Company - New York  
compte No. 22.186,

Lloyds Bank (Europe) Ltd. - 10 Moorgate, London E.C.2,

Postscheckkonto - Köln - Nr. 160.861.

### OFFICE CENTRAL DE VENTE DES PUBLICATIONS DES COMMUNAUTES EUROPEENNES

2 place de Metz, Luxembourg (Compte chèque postal N° 191-90)

#### BELGIQUE — BELGIË

MONITEUR BELGE  
40-42, rue de Louvain - Bruxelles  
BELGISCH STAATSBLAD  
Leuvenseweg 40-42 - Brussel

#### LUXEMBOURG

OFFICE CENTRAL DE VENTE  
DES PUBLICATIONS DES  
COMMUNAUTES EUROPEENNES  
9, rue Goethe - Luxembourg

#### DEUTSCHLAND

BUNDESANZEIGER  
Postfach - Köln 1

#### NEDERLAND

STAATSDRUKKERIJ  
Christoffel Plantijnstraat - Den Haag

#### FRANCE

SERVICE DE VENTE EN FRANCE  
DES PUBLICATIONS DES  
COMMUNAUTES EUROPEENNES  
26, rue Desaix - Paris 15<sup>e</sup>

#### ITALIA

LIBRERIA DELLO STATO  
Piazza G. Verdi, 10 - Roma

#### UNITED KINGDOM

H. M. STATIONERY OFFICE  
P. O. Box 569 - London S.E.1

EURATOM — C.I.D.  
51-53, rue Belliard  
Bruxelles (Belgique)

CDNA02842ENC